ABSTRACT

YANILMAZ, MELTEM. Novel Nanofiber-based Membrane Separators for Lithium-ion Batteries. (Under the direction of Professor Xiangwu Zhang).

Lithium-ion batteries have been widely used in electronic devices including mobile phones, laptop computers, and cameras due to their high specific energy, high energy density, long cycling lifetime, and low self-discharge rate. Nowadays, lithium-ion batteries are finding new applications in electric/hybrid vehicles and energy storage for smart grids. To be used in these new applications, novel battery components are needed so that lithium-ion batteries with higher cell performance, better safety, and lower cost can be developed.

A separator is an important component to obtain safe batteries and its primary function is to prevent electronic contact between electrodes while regulating cell kinetics and ionic flow. Currently, microporous membranes are the most commonly used separator type and they have good mechanical properties and chemical stability. However, their wettability and thermal stabilities are not sufficient for applications that require high operating temperature and high performance.

Due to the superior properties such as large specific surface area, small pore size and high porosity, electrospun nanofiber membranes can be good separator candidate for high-performance lithium-ion batteries. In this work, we focus our research on fabricating nanofiber-based membranes to design new high-performance separators with good thermal stability, as well as superior electrochemical performance compared to microporous polyolefin membranes. To combine the good mechanical strength of PP nonwovens with the excellent electrochemical properties of SiO_2/polyvinylidene fluoride (PVDF) composite nanofibers, SiO_2/PVDF composite nanofiber-coated PP nonwoven membranes were

prepared. It was found that the addition of SiO_2 nanoparticles played an important role in improving the overall performance of these nanofiber-coated nonwoven membranes.

Although ceramic/polymer composites can be prepared by encapsulating ceramic particles directly into polymer nanofibers, the performance of the resultant composite membranes is restricted because these nanoparticles are not exposed to liquid electrolytes and have limited effect on improving the cell performance. Hence, we introduced new nanoparticle-on-nanofiber hybrid membrane separators by combining electrospraying with electrospinning techniques. Electrochemical properties were enhanced due to the increased surface area caused by the unique hybrid structure of SiO_2 nanoparticles and PVDF nanofibers.

To design a high-performance separator with enhanced mechanical properties and good thermal stability, electrospun SiO_2/nylon 6,6 nanofiber membranes were fabricated. It was found that SiO_2/nylon 6,6 nanofiber membranes had superior thermal stability and mechanical strength.

Electrospinning has serious drawbacks such as low spinning rate and high production cost. Centrifugal spinning is a fast, cost-effective and safe alternative to the electrospinning. SiO_2/polyacrylonitrile (PAN) membranes were produced by using centrifugal spinning. Compared with commercial microporous polyolefin membranes, SiO_2/PAN membranes had larger liquid electrolyte uptake, higher electrochemical oxidation limit, and lower interfacial resistance with lithium. SiO_2/PAN membrane separators were assembled into lithium/lithium iron phosphate cells and these cells exhibited good cycling and C-rate performance.

PAN-based separators show promising properties including high ionic conductivity, good thermal stability and good compatibility with Li metal. Polymethylmethacrylate (PMMA) has also been used as a separator due to its good compatibility with Li and high affinity to liquid electrolyte. Blending PAN and PMMA can potentially lead to new separators with enhanced microstructure, porosity and electrochemical properties. Hence, PMMA/PAN membranes were produced via centrifugal spinning. Compared with commercial microporous polyolefin membrane, centrifugally-spun PMMA/PAN membranes had larger ionic conductivity, higher electrochemical oxidation limit, and lower interfacial resistance with lithium. Centrifugally-spun PMMA/PAN membrane separators were assembled into Li/$LiFePO_4$ cells and these cells delivered high capacities and exhibited good cycling and C-rate performance.

In summary, different nanofiber production techniques and various polymers were employed to produce high-performance nanofiber separators for lithium-ion batteries. In order to improve electrochemical properties, different approaches were utilized, including nanofiber-coating on nonwoven membranes, electrospraying of nanoparticles on nanofibers, fabrication of ceramic nanoparticle-incorporated nanofibers, and blending of different polymers.

Novel Nanofiber-based Membrane Separators for Lithium-Ion Batteries

by
Meltem Yanilmaz

A dissertation submitted to the Graduate Faculty of
North Carolina State University
in partial fulfillment of the
requirements for the Degree of
Doctor of Philosophy

Fiber and Polymer Science

Raleigh, North Carolina

2015

APPROVED BY:

_____	_____
Xiangwu Zhang Committee Chair	Richard Kotek
_____	_____
Subhashish Bhattacharya	Philip D. Bradford

DEDICATION

To my husband Ayhan Yanilmaz

for his support, encouragement, and love.

BIOGRAPHY

Meltem Yanilmaz was born in Turkey on May 18, 1985. She began her undergraduate study in Textile Engineering at Istanbul Technical University in 2003. She graduated with a Bachelor of Science degree in Textile Engineering in 2007. She began working as a research assistant at Istanbul Technical University in 2010. She received her Master of Science degree in Textile Engineering from Istanbul Technical University in 2010. In 2012, she enrolled in North Carolina State University to pursue her doctorate degree in Fiber and Polymer Science. Her dissertation research was done under the direction of Professor Xiangwu Zhang at North Carolina State University. Her research focused on design and characterization of membrane separators for lithium-ion batteries.

ACKNOWLEDGMENTS

I would like to express my sincere gratitude to my advisor Dr. Xiangwu Zhang for his guidance, encouragement and support throughout the course of this research. I sincerely appreciate his help and advice. My experience of working with him had a profound impact on me as an individual as well as a scientist. I also would like to thank Prof. Richard Kotek, Prof. Philip D. Bradford, and Prof. Subhashish Bhattacharya for serving on my advisory committee and their guidance.

I would like to acknowledge the Council of Higher Education and the Scientific and Technological Research Council of Turkey for financially supporting me through my Ph.D. studies.

I am thankful to all my lab fellows and colleagues at Dr. Zhang's group. I am especially grateful to Yao Lu, Dr. Ying Li, Chen Chen, and Dr. Shu Zhang for their co-operation and support during my research.

Finally, I would like to thank all those people who gave me emotional support during this work and throughout my life; my family and friends. I am grateful to my husband and my family for always standing by me and for giving me the freedom and support to pursue my dreams.

TABLE OF CONTENTS

LIST OF TABLES

LIST OF FIGURES

CHAPTER 1. Introduction

1.1 Overview on batteries

1.1.1 Introduction on batteries

World economy is highly dependent on fossil fuel and it has a severe impact on world ecology. Air quality and global climate impact are two major concerns about fossil fuel. In addition, heavily populated developing countries are enlarging their economies and energy consumption is increasing dramatically. Therefore, electrochemical energy production has received great attention as an alternative energy/power source due to its sustainability and environmentally friendly properties [1-5].

Batteries, fuel cells and supercapacitors are systems for electrochemical energy storage and conversion [1, 3, 6, 7]. Electrical energy is generated by redox reactions at the electrodes in batteries and fuel cells. In supercapacitors, energy-delivering processes occur by forming and releasing electrical double layers, which is orientation of electrolyte ions at the interface between electrodes and electrolyte. Although energy storage and conversion mechanisms are different in each system, all systems include two electrodes and electrolyte between them [6].

Batteries store chemical energy by converting it into electrical energy. There are two types of batteries: primary and secondary batteries. Primary batteries have high energy density and long self-life. However, they cannot be electrically charged. Examples of primary cells are lithium-manganese dioxide, carbon-zinc, alkaline-manganese and zinc-air, etc. Secondary batteries can electrically be charged and used again. Lithium-ion, nickel-cadmium and lead-acid, etc are some examples of secondary cells [8].

Each battery has two electrodes, anode and cathode, electrolyte and separators (Figure 1.1). The anode is the negative electrode and oxidation occurs at the anode. The cathode is the positive electrode and it gains electron from external circuit. An electrolyte provides ionic conductivity between negative and positive electrodes. A separator is a physical barrier between electrodes to prevent short circuit while allowing ionic flow [6].

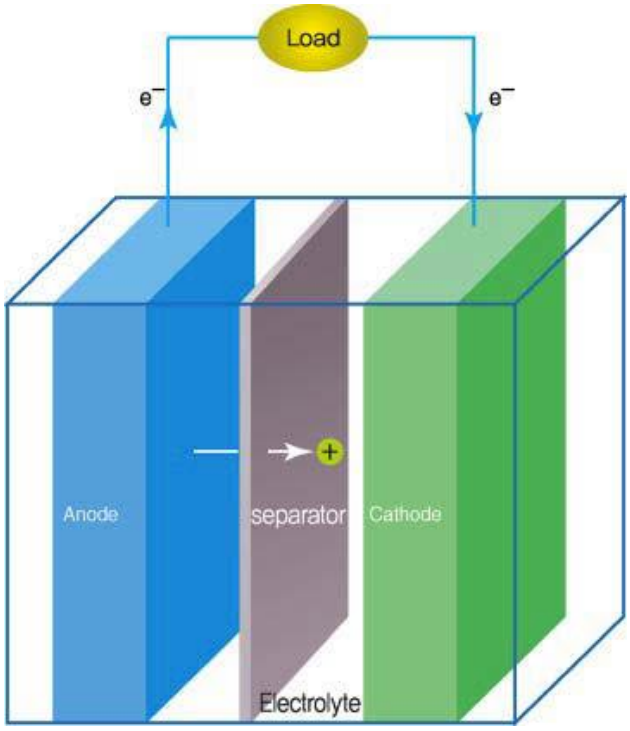

Figure 1.1 The components of a battery or electrochemical cell (during discharging) [9].

1.1.2 Working principle of batteries

In batteries, electronic current is produced by electrochemical reactions. When two electrodes with different electric potentials are immersed in the electrolyte, a potential difference (electromotive force) is created between the electrodes. Figure 1.2 shows a

voltaic cell which consists of silver electrode immersed in a solution of silver nitrate and a copper electrode in a solution of copper nitrate. The two solutions are joined by a salt bridge which consists of a tube filled with electrolyte. The two ends of the tube are fitted with porous plugs which permits the flow of ions but prevent siphoning of liquid from one electrolyte to the other. Isolation is necessary to prevent reaction between silver ions and the copper electrode. When high impedance meter is replaced with a low resistance wire, the circuit is completed and charge flows. Electrons move from the copper electrode through the external wire to the silver electrode. In the cell, the voltage is a measure of the tendency for the cell reactions to proceed toward equilibrium [10]. The electrode processes are described by the reactions:

$$Cu(s) \text{ <--> } Cu^{+2}(aq) + 2e^{-} \quad (1.1)$$

$$Ag^{+}(aq) + e^{-} \text{ <--> } Ag(s) \quad (1.2)$$

Electric potential is the potential energy of a unit charge within an electric field. Electric potential and electromotive force drive current in an electric circuit. This force induces redox reactions which occur at each electrode and the electrons generated by redox reactions pass through the external circuit [9]. During discharge, reduction and oxidation occur at the cathode and the anode, respectively. Electrochemically active material is oxidized and electrons are released at the anode and they move from anode to cathode through external circuit during discharging. At the cathode, active materials are reduced by receiving electrons. During charging, ions are reduced at the anode and oxidation occurs at the cathode.

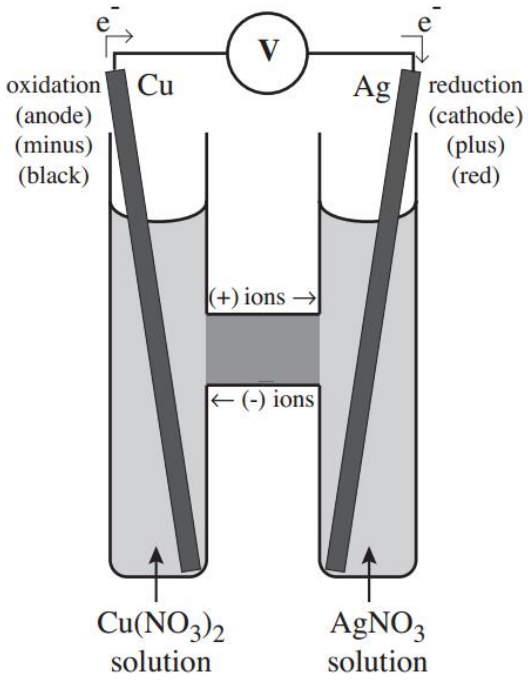

Figure 1.2 A voltaic cell [11].

1.1.3 Types of batteries

Batteries are divided into two subgroups: primary and secondary batteries, based on the reversibility of the electrode reactions. Due to irreversibility of cell reactions, primary batteries are used once and disposed while secondary batteries can be used many times. Carbon-zinc, mercury oxide, silver oxide and Li-CuS are some examples of primary batteries. For example, in Li-CuS batteries, Cu is replaced by Li during discharging while Li_2S and Cu are products of irreversible oxidation reactions. Secondary or rechargeable batteries have lower energy storage capability than primary batteries. Lead acid, nickel-cadmium (Ni-Cd), nickel metal hybride (Ni-MH) and lithium-ion (Li-ion) batteries are major rechargeable battery systems. Some characteristics of secondary batteries are listed in Table 1.1.

Table 1.1 Characteristics of secondary batteries

Battery type	Size	Rechargeable	Voltage	Energy density (Wh/kg)	Power density (W/kg)	Cycle life	Memory	Self-Disharge
Lead acid	Large	Yes	2 V	25-30	75-130	200-400	No	Medium (3%-20%)
Ni-Cd	All sizes	Yes	1.2 V	35-57	50-200	1000-2000	Yes	Low (10%)
Ni-MH	All sizes	Yes	1.2 V	50-80	150-250	600-1500	No	High (30%)
Lithium-ion	Small to large	Yes	3.6 V	100-150	300	400-1200	No	Low (5%-10%)

Lead acid batteries were invented in 1859. Lead acid batteries have lead peroxide as the anode, lead as the cathode, and weak sulfuric acid as the electrolyte. The electromotive force is 2V per cell for lead acid batteries and they are used as storage batteries in motor vehicles.

Nickel-cadmium batteries (1.2 V) were commercialized in 1984 and they have replaced primary batteries. However, Nickel-cadmium batteries are not very common nowadays because of harmful environmental effects of these batteries [9].

Nickel-cadmium batteries have been replaced by Ni-MH batteries since 1990s. Ni-MH batteries have some advantages such as eco-friendliness, high rates, very prolonged cycle life and excellent safety. However, energy density is low for these cells.

Lithium-ion batteries have been commonly used in electronic devices such as mobile phones, laptop computers, and digital cameras. Furthermore, lithium-ion batteries can be used in electric vehicles [12, 13] due to higher power and energy density compared to other

batteries (Figure 1.3). Energy densities of rechargeable lithium-ion batteries are 2-3 times higher than Ni-Cd and Ni-MH batteries and rechargeable lithium-ion batteries offer power densities 5-6 times higher than Ni-Cd and Ni-MH batteries. Lithium-ion batteries have also other advantages such as high Coulombic efficiency, low self-discharge, high operating voltage and no memory effect [7].

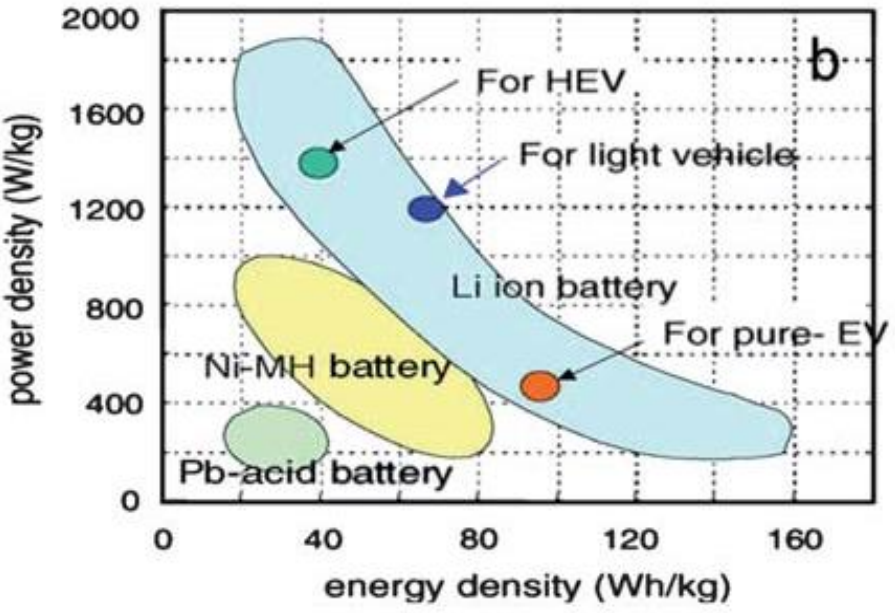

Figure 1.3 Ragone plot for rechargeable batteries [12].

1.1.4 Introduction on lithium-ion batteries

Lithium-ion batteries have superior properties compared to other secondary batteries such as higher working voltage, higher energy density, lower gravimetric density and longer service life. Owing to these properties, lithium-ion batteries have been used in various devices such as eco-friendly transportation power storage, health care and defense [14-16]. In

addition, lithium-ion batteries use lithium ions as the main charge carrier and they not only maintain a high average discharge voltage of 3.7 V but also have the advantage of lightweight which result in high energy density [1].

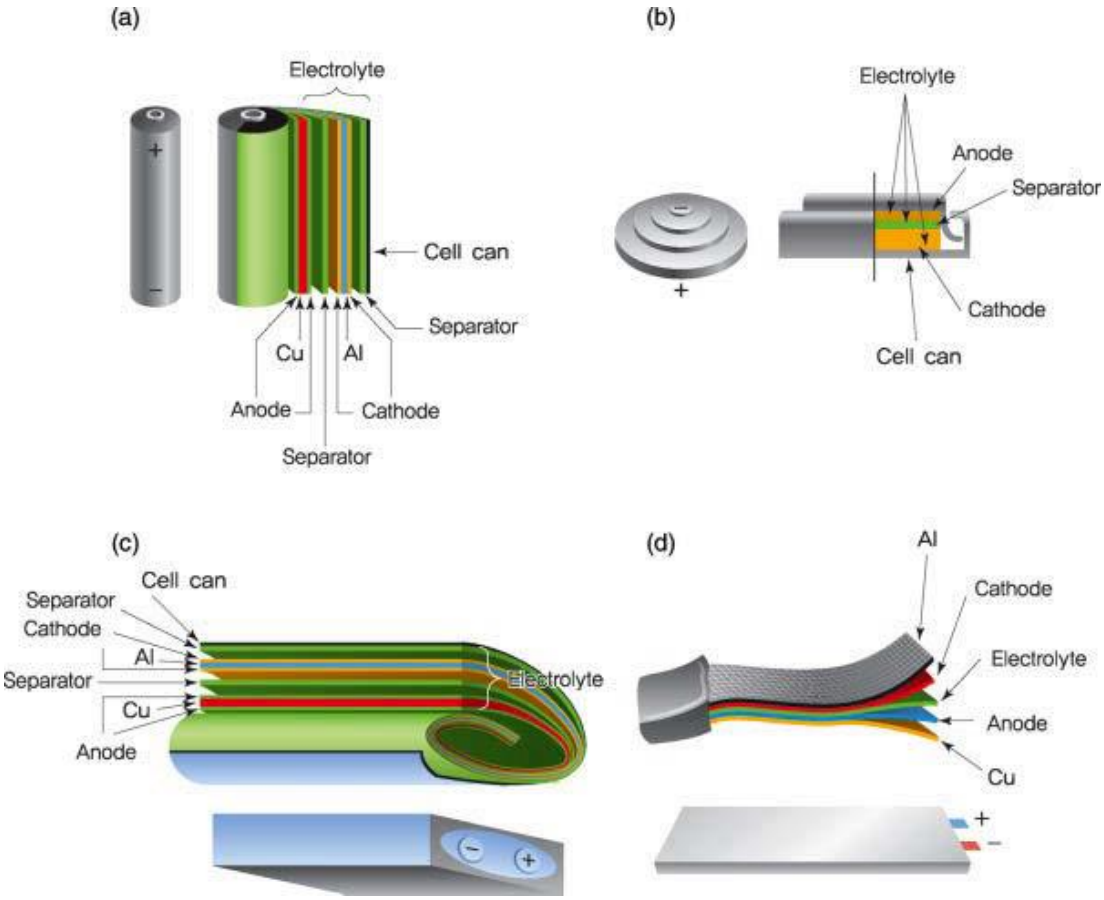

Figure 1.4 Different shapes of lithium-ion batteries: (a) cylindrical, (b) coin, (c) prismatic, (d) pouch [9].

Lithium-ion batteries can be designed in various shapes such as cylindrical, coin, prismatic, and pouch depending on devices and application areas (Figure 1.4). Cylindrical batteries are used in laptop computers, prismatic cells are common in portable devices, single-cell coin-shaped batteries are used in small electric appliances and portable IT devices,

and pouch-shaped cells cased in aluminum plastic composites are good for electric vehicle applications [9].

Lithium-ion batteries have been used since 1990s for portable electronic devices. Up to now, lithium-ion batteries have received great attention due to their high energy density, low gravimetric density, long cycle life and flexible design. The development of improved electrodes for lithium-ion batteries is critical to obtain high energy and power densities for electric and hybrid electric vehicles [17]. Fast charging and discharging at high power rates, energy density, power, cycling, life, charge/discharge rates, safety and cost must be addressed to design advanced lithium-ion batteries [18].

For the future applications of lithium-ion batteries, medium- and large sized cells gain great interest because they can store alternative energy such as solar, wind, and marine energy, which leads to designing next-generation smart grid technology. Microcells are also important due to their usage in RFID/USN, MEMS/NEMS, and embedded medical devices. Besides these, development of light weight, thin, flexible batteries gain great interest because of their potential applications in portable electronics such as interactive packaging, radio frequency sensing, roll up displays, smart electronics and electronic paper. Due to safety concerns, developing all-solid-state lithium-ion batteries is highly attractive as well. Replacing liquid electrolytes with solid electrolytes and design suitable electrode materials could solve the problems about the instability of existing liquid electrolytes which cause battery explosions [9, 19, 20].

1.1.5 Working principle of lithium-ion batteries

Lithium-ion batteries are secondary batteries. After they are discharged, applied electrical energy reverses the electrochemical reactions. The reactants turn into their original form and they can be used again to store electrical energy. In lithium-ion batteries, ions transport the charge between electrodes in the electrolyte. Lithium ions move between electrodes in the electrolyte and electrons move through external circuit. In the discharge process, electrochemically active material at the anode is oxidized and electrons are released and cathodic substances are reduced. Lithium ions move from anode to cathode. During charging, lithium ions are extracted from cathode to anode. Ions are reduced at the negative electrode and oxidation occurs at the positive electrode [7, 21].

Figure 1.5 shows the commonly used anode and cathode materials for lithium-ion batteries. Carbon based materials have been widely used as anode due to their good cycling stability and long cycle life. As a result of LiC_6 formation, graphite compounds deliver a theoretical capacity of 372 mAh/g. There are other materials to be used as anode such as tin (Sn), germanium (Ge), and silicon (Si). Even these materials have high capacity values they have some disadvantages. Tin suffers from poor cycling life caused by a volume expansion of about 300% during alloying de-alloying reactions while tin oxides can be considered as promising candidate due to high theoretical capacity (1491 mAh/g), good cycle ability, and high Coulombic efficiency. Theoretical capacity of germanium is 1600 mAh/g. However, it has a high electrical resistivity (1 Ω.m) which causes inefficient charge transfer during cycling. Silicon has a theoretical capacity of 4200 mAh/g corresponding to $Li_{22}Si_5$ formation;

$$22Li^+ + 5Si + 22e^- \rightarrow Li_{22}Si_5 \qquad (1.3)$$

However, it suffers from slow diffusion rate, low conductivity, and poor cycling performance due to great volume changes that is related to insertion and extraction of lithium ions [14, 15, 21].

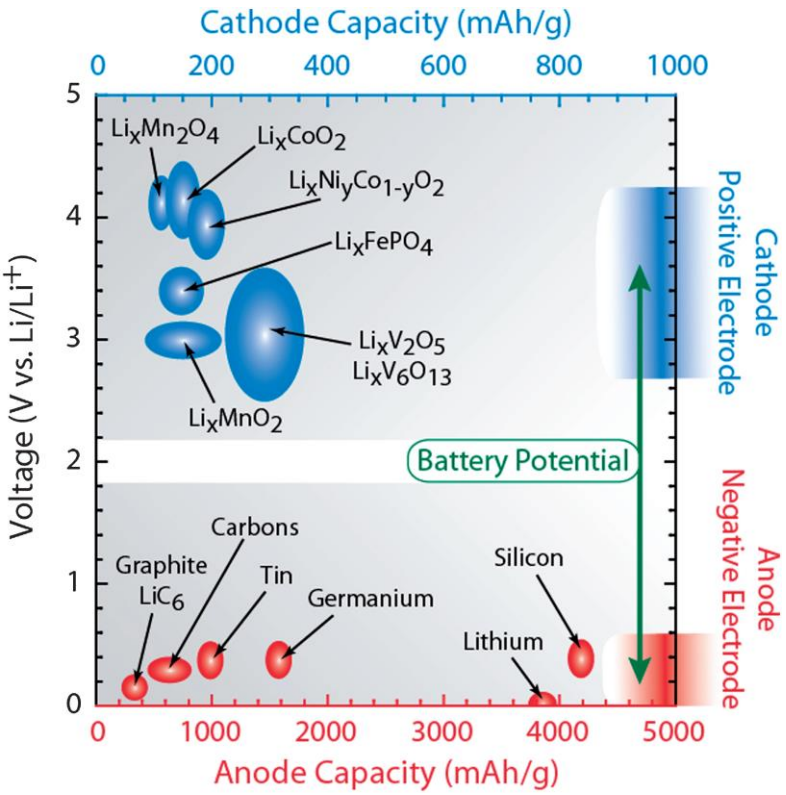

Figure 1.5 Diagram illustrating the lithium ion capacity and electrochemical reduction potentials with respect to lithium metal for conventional anode (red axis) and cathode materials (blue axis). The battery potential is the relative difference between the voltage of the selected positive electrode materials (blue ovals) and voltage of the corresponding negative electrode material (red ovals) [14].

Lithium metal oxides ($LiCoO_2$), spinels ($LiMn_2O_4$) and lithium metal phosphates ($LiV_2(PO_4)_3$, $LiFePO_4$) are the most common cathodes for lithium-ion batteries. Table 1.2 shows the characteristics of some cathode materials. Structural stability and conductivity affect the performance of cathode materials. Reversible intercalation and de-intercalation of lithium, lithium ion diffusivity, microstructure, morphology and inherent electrochemical

properties are also important [21, 22]. Lithiated transition metal phosphates ($LiFePO_4$, $LiNiPO_4$, $Li_3Fe_2(PO_4)_3$, $Li_3V_2(PO_4)_3$, $LiMnPO_4$, $LiCoPO_4$ and so on) have good lithium ion mobility, high reversible capacity, operative redox potentials and high safety. Lithium vanadium phosphate (LVP) shows an average intercalation voltage up to 4.0V and a theoretical capacity of 197 mAh/g. In addition, its low conductivity has been enhanced to some extent by metal doping, inducing particle size and coating the material with a carbon layer [23].

Table 1.2 Characteristics of some cathode materials [24].

Material	**Specific capacity, mAh/g**	**Midpoint V vs. Li C/20**	**Properties**
$LiCoO_2$	155	3.9	the most common, expensive
$LiNi_{1-x-y}Mn_xCo_yO_2$	140-180	3.8	capacity depends on upper voltage cut off, safer and less expensive than $LiCoO_2$
$LiNi_{0.8}Co_{0.15}Al_{0.05}O_2$	200	3.73	High capacity, about as safe as $LiCoO_2$
$LiMn_2O_4$ (spinel)	100-120	4.05	Poor high temperature stability, safer and less expensive than $LiCoO_2$
$LiFePO_4$	160	3.45	Synthesis in inert gas leads to process cost, very safe, low volumetric energy
$Li(Li_{1/9}Ni_{1/3}Mn_{5/9})O_2$	275	3.8	High specific capacity, R&D sale, low rate capability
$LiNi_{0.5}Mn_{1.5}O_2$	130	4.6	Requires an electrolyte that is stable at high voltages

$LiFePO_4$ has some advantages over cobalt oxides or spinels. It has low cost, low toxicity, and long cycle life with a theoretical capacity of 170 mAh/g. But, its low conductivity restricts its uses in high power batteries. Charging and discharging mechanisms of $LiFePO_4$ are below [21];

$$LiFePO_4 - xLi^+ - xe^- \text{ --> } xFePO_4 + (1-x)LiFePO_4 \quad (1.4)$$

$$FePO_4 + xLi^+ + xe^- \text{ --> } xLiFePO_4 + (1-x)FePO_4 \quad (1.5)$$

An electrolyte serves as a medium for the transfer of lithium ions and it consists of a solvent and salt. In general, lithium secondary batteries use organic electrolytes. Alkyl carbonates, ethylene carbonate, dimethyl carbonate, ethyl methyl carbonate or diethyl carbonate are used as solvents in the electrolyte. Combination of binary solvent mixtures and lithium salt, generally lithium hexafluorophosphate, is the common electrolyte for lithium-ion batteries. The electrolyte with high ionic conductivity (higher than 10^{-3} S/cm) is essential for high-performance batteries. In addition to ionic conductivity, there are some other requirements for liquid electrolyte to be used in lithium-ion batteries; chemical and electrochemical stability in the temperature ranging from -20 ^{0}C to 60^{0}C, high ignition or flash points, no flammability, low toxicity and low cost [9].

Figure 1.6 shows the schematic presentation of the most commonly used lithium-ion batteries based on graphite anodes and $LiCoO_2$ cathodes. Graphite- $LiCoO_2$ is used in portable electronic devices, cellular phones, laptops, digital cameras, etc. The main cell reactions in lithium-ion batteries are lithium ion intercalation and de-intercalation cycles. The cathode reactions are

$$LiCoO_2 \text{ <=> } \tfrac{1}{2} Li^+ + \tfrac{1}{2} e^- + Li_{0.5}CoO_2 \quad (1.6)$$

The lithium source of the cells is $LiCoO_2$ and the first step is charging, oxidation and delithiation of $LiCoO_2$ at the cathode. At the same time the reduction and lithiation of graphite occur at the anode. LiC_6 is formed as a result of intercalation reaction of graphite with lithium [25]. During discharging, the reactions reverse: oxidation and delithiation occur at the anode and reduction and lithiation take place at the cathode.

$$C_6 + Li^+ + e^- \quad <=> \quad LiC_6 \qquad (1.7)$$

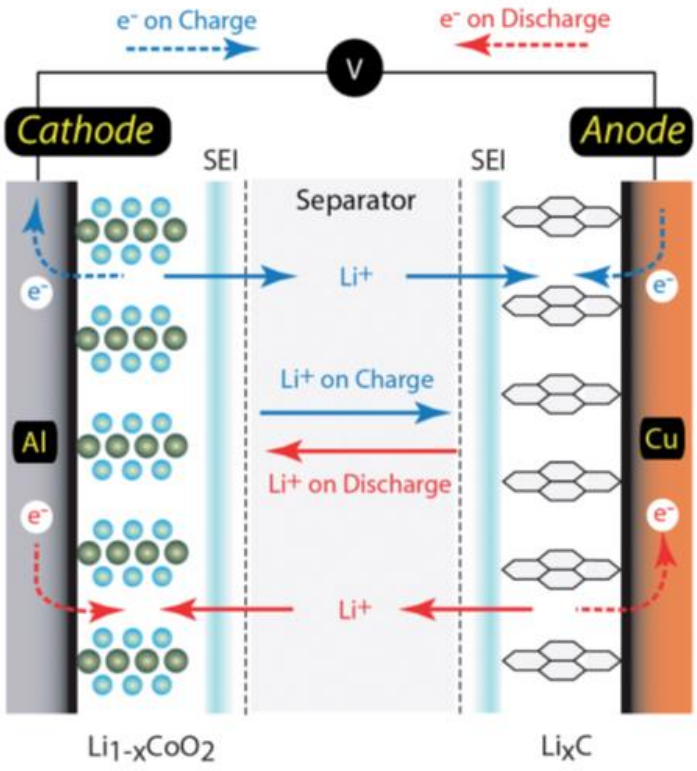

Figure 1.6 Schematic illustrating the mechanism of operation for a lithium-ion battery including the movement of ions between electrodes (solid lines) and the electron transport through the complete electrical circuit (dashed lines) during charge (blue) and discharge (red) states.[14].

Voltage: the electrical driving force and it is equal to the electric potential difference between two points in an electric circuit.

Active mass: the materials that create electrical current as a result of chemical reaction.

Open-circuit voltage: is the voltage of the cell when no external current flows.

Current: the rate of flow of electric charge.

Discharge: process in which battery delivers electrical energy to an external load.

Cutoff voltage: the battery voltage at the point at which discharge is complete.

Charge: process in which current flow reversed and battery is restored to its original charged condition.

Capacity: the product of the total amount of charge or a total number of ampere hours that can be obtained in discharging.

Energy density: the amount of energy stored per unit mass or volume.

Power: the energy that can be derived from battery per unit time.

Cycle life: the number of charge and discharge cycles that a battery can achieve before its capacity is consumed.

C-rate: Charge/discharge rate, the speed at which the batteries charge and discharge.

Polarization: a lack or excess of electrode potential at equilibrium.

Overpotential: the potential difference between the actual potential and the equilibrium potential. It is used as a measure of the extent of polarization.

Internal resistance: resistance or impedance that battery offers to current flow.

Thermal runaway: event that occurs when the battery electrode's reaction with the electrolyte becomes self-sustaining and this may cause safety incidents and fires [6, 9].

1.2 Overview on separators

1.2.1 Introduction on the separators

As shown Figure 1.7, a lithium-ion battery includes cathode, anode, electrolyte and separator. Separator is a critical component of lithium-ion batteries which is placed between two electrodes to provide a physical barrier while it serves as a medium for the transport of ions during the charging and discharging cycles.

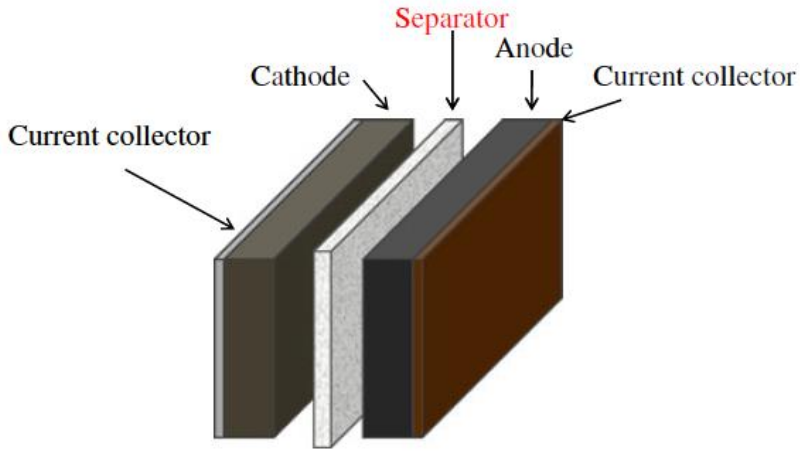

Figure 1.7 Schematic illustration of a typical lithium-ion battery [26].

Even though separators do not involve in any cell reactions, the structure and materials of the separators affect the performance of lithium-ion batteries. The separator influences internal cell resistance and cell kinetics so that it affects the battery performance, including cycle life, safety, energy density, and power density.

There are four important types of membrane separators which are microporous membranes, modified microporous membranes, non-woven membranes, and composite membranes. Each separator type has inherent advantages and disadvantages and the selection

of the separators affects the performance of lithium-ion batteries. Many factors must be considered while selecting ideal separators for lithium-ion batteries. General requirements are summarized in Table 1.3 and discussed in detail in the following section.

Table 1.3 General requirements for separators used in lithium-ion batteries [27].

Parameter	Requirement
Chemical and electrochemical stabilities	stable for a long period of time
Wettability	wet out quickly and completely
Mechanical property	> 1000 kg/cm (98.06 MPa)
Thickness	20 – 25 μm
Pore size	< 1 μm
Porosity	40-60%
Permeability (Gurley)	< 0.025 sec/μm
Dimensional stability	no curl up and lay flat
Thermal stability	< 5% shrinkage after 60 min at 90 °C
Shutdown	effectively shut down the battery at elevated temperatures

1.2.2 Requirements for the separators

1.2.2.1 Chemical and electrochemical stability

Separators must have enough chemical and electrochemical stability to the electrolyte and electrode materials in lithium-ion batteries. They should not involve any chemical reactions during charging and discharging cycles. In addition, they should not cause any

interference by producing impurities. In some battery applications, separators should also be chemically stable and inert at elevated temperatures [28].

1.2.2.2 Wettability

Wettability is one of the most critical properties of the separators because wettability affects electrolyte absorption and high amount of electrolyte absorption is required to obtain low internal cell resistance.

1.2.2.3 Mechanical strength

The separators must withstand the tension of winding operation during battery assembly. The mechanical strength of separators can be characterized by the tensile strength and puncture strength. The minimum tensile strength for separators is 98.06 MPA according to ASTM D882 and D638. The puncture strength, defined by the maximum load required for a needle to penetrate a given separator, should be higher than 300 g/min according to ASTM D3763.

1.2.2.4 Thickness

Typically, separators in rechargeable batteries are 20 - 50 μm in thickness however commercial separators are 20 - 25 μm in thickness. Thin separators are favorable for lower internal cell resistance and batteries with thin separators exhibit high energy and power densities. However, thin separators may cause short circuit if the mechanical strength is not high enough. Hence, the separator should be as thin as possible while having required strength to maintain mechanical and electrical separation between electrodes [29] .

1.2.2.5 Pore size

The pore size is also critical for separators because it affects the performance of the cell and safety. When the pore sizes are too small, they restrict the lithium ion movement and increase internal resistance while large pore sizes may cause short circuit.

1.2.2.6 Porosity

High porosity is beneficial for separators in order to absorb high amount of electrolyte. In cells, the separator with low porosity cause high internal resistance due to the lack of electrolyte between electrodes. On the other hand, when the porosity is too high, it may cause short circuit by allowing the electrodes get connected. The porosity is defined by the ratio of void volume to apparent geometric volume and it can be measured by the weights of the separator before and after the absorption of a liquid by assuming the volume occupied by the liquid is equal to the porous volume of the separator as the following equation:

$$Porosity\ (\%) = \frac{W - W_0}{\rho_L V_0} \times 100 \qquad (1.8)$$

where W_0 and W represent the weights of the separator before and after immersing a liquid, respectively, ρ_L the density of the liquid, and V_0 the geometric volume of the separator.

1.2.2.7 Ionic conductivity

The presence of the separator increases the internal resistance of the cell. The MacMullin number, which is defined by the ratio of the resistance of the separator immersed with liquid electrolyte to the resistance of the electrolyte, can be used to characterize the increase in resistance due to the presence of the separator. The MacMullin number for lithium-ion batteries should be in the range from 5 to 15.

1.2.2.8 Permeability

Permeability is a measure of the ability of separator to transmit a liquid and it can be characterized by using Gurley number. The Gurley value is defined by the time needed for air to pass through unit area of the separator under a fixed pressure. The Gurley number depends on the porosity, the fraction of open pores and the tortuosity, which is the ratio of a mean effective capillary length to separator thickness.

1.2.2.9 Dimensional stability

Separators must keep their shape and sizes when they are immersed in liquid electrolyte. In addition, any shrinkage during storage or when the battery is in use cause safety problems.

1.2.2.10 Thermal stability

Separators must also have dimensional stability at high temperatures. Separators must not shrink or wrinkle when the temperature increases. If a battery overheats due to overcharging or other cell reactions, separators with a poor thermal stability can cause shortcircuit and thus safety problems. The requirement is less than 5 % shrinkage after 60 min at 90 ^{0}C.

1.2.3 Types of separators

Separators can be divided into four major types: microporous membrane separators, modified microporous membrane separators, non-woven membrane separators, and composite membrane separators. Microporous membrane separators are commonly used in lithium-ion batteries due to their high chemical and mechanical stability. However, they suffer from low wettability and high thermal shrinkage. In order to address the limitations of

microporous membranes, modified microporous membrane separators are introduced in recent years. Non-woven membranes have some advantages including high porosity and low cost. Composite membranes are fabricated by introducing inorganic materials to polymeric membranes. Composite membranes can be prepared by coating inorganic layers on polymeric membranes or directly filling them into the membrane materials. Due to the high thermal stability and superior wettability of inorganic materials, composite membranes offer high performance and high safety as a separator.

1.2.3.1 Microporous membrane separators

Dry and wet processes are two most commonly used techniques to produce microporous polymeric membranes. Both processes use an extruder, low-cost polyolefin materials (PP, PE, other polyolefins, their mixtures, copolymers) and have stretching process to increase porosity and improve mechanical strength.

Figure 1.8 shows the fabrication steps in dry process. In dry process, the polyolefin materials are melted and extruded to obtain polyolefin film. This film was then annealed at an elevated temperature to induce crystallite formation followed by uniaxial stretching at a low and a high temperature. The porous structure with slit-like pores is formed due to fracturing of the amorphous phase as shown in Figure 1.9a. Finally, heat treatment is applied to relax the residual stress. Good mechanical properties (higher than 150 MPa tensile strength) and high thermal shrinkage in the machine direction and low tensile strength in the transverse direction are the characteristics of the membrane separators prepared by the dry process [26, 28].

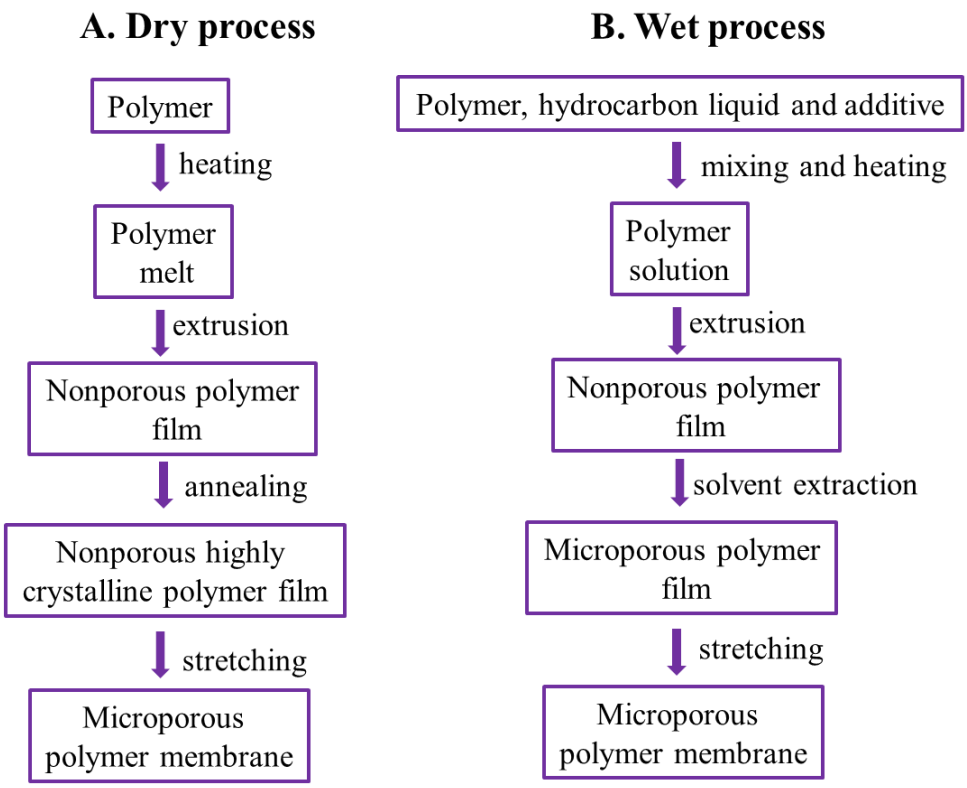

Figure 1.8 Fabrication processes of microporous membranes: (A) dry and (B) wet process.

As shown in Figure 1.8B, wet process includes the following steps: adding plasticizers into the polymer, extrusion, calendaring of the film, extraction of plasticizer with the solvent, and stretching. Round-like pores are obtained due to biaxially stretching (Figure 1.9b). Tensile strengths in both directions are comparable and about 100 MPa [26, 30]. Due to their open and straight pore structure, membranes fabricated by the dry process are ideal for high power density batteries while membranes made by wet process is suitable for long-cycle life batteries owing to tortuous structure and interconnected pores.

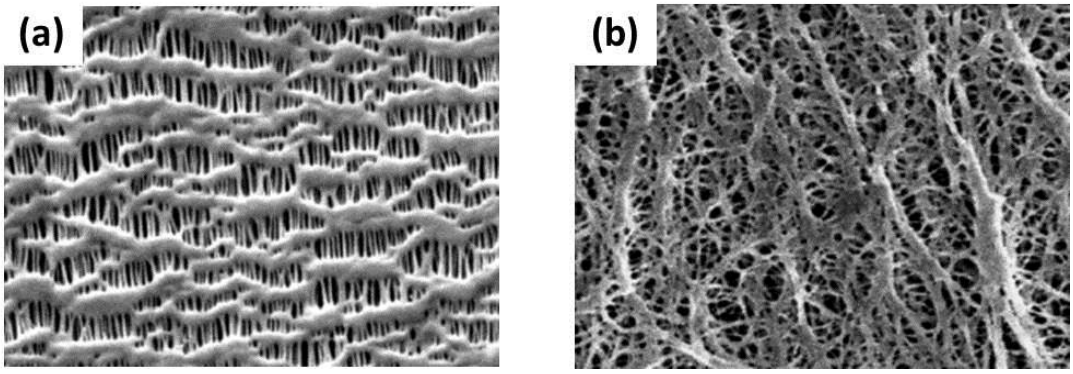

Figure 1.9 SEM images of polyolefin microporous membrane separators made by (a) dry process and (b) wet process [26].

Most polyolefin membranes have thermal shutdown capability at various temperatures (around 160 ^{0}C for PP, around 120-150 ^{0}C for PE) by closing the pores. Shutdown refers to a large increase in impedance with temperature. If two layers of separators have different melting temperatures, the component with lower melting temperature closes the pores of the other component and stops the ion transport when the temperature is increased (Figure 1.10). However, the cell temperature may keep increasing after thermal shutdown and the separator may shrink, melt and cause short circuit. Large enough temperature difference between shutdown temperature and melting temperature may prevent the shortcircuiting [26]. In addition, mechanical integrity must be high enough to prevent short circuit at high temperatures.

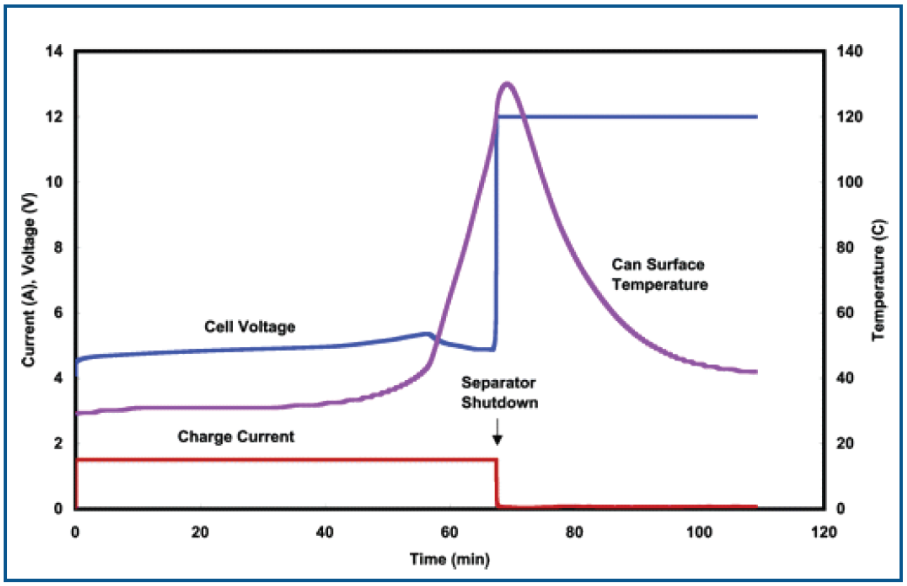

Figure 1.10 Ideal separator shutdown function for a $LiCoO_2$ 18650 cell during a 1C-rate overcharge test [31].

Venugopal et al. [32] characterized some commercial microporous membranes with different compositions, including PP, PE, PP/PP, PP/PE/PP. Many properties of the separators such as pore size, porosity, permeability, thermal properties were studied and it was found that the porosity values were between 40 and 50% and average pore sizes were less than 0.1 µm. Prasanna et al. [33] prepared stretched PE separators by dry process. Separators with 300% stretching showed better physical properties (porosity and Gurley value) and cell performance (ionic conductivity and cycling performance) than those with 180% stretching.

In addition to dry and wet processes, polymer membranes can be prepared by nonsolvent-induced phase separation (NIPS) process, such as phase inversion process, immersion precipitation technique, liquid extraction/activation, evaporation phase inversion and solvent–solvent extraction process [34]. Phase inversion is one of the most commonly

used techniques to produce microporous membranes. Phase inversion technique includes two main steps: casting a thin film and soaking it in a non-solvent coagulation bath. In this technique, the micro pores are formed through solvent exchange when a thin polymer solution is immersed into a non-solvent coagulation bath. Solvent, non-solvent, compositions of polymer solution and bath temperature affect the morphology.

Polyolefin microporous membranes, such as polypropylene and polyethylene, exhibit poor miscibility with polar electrolytes because of their very low polarity. To overcome the limitations of polyolefin microporous membranes, PAN and PVDF microporous membranes are presented as alternative separator materials for lithium-ion batteries. PAN and PVDF have excellent miscibility with the liquid electrolyte. PAN has high electrochemical stability to both anode and cathode of lithium and lithium-ion batteries [35]. Huai et al. [35] prepared PAN based membranes and reported good cycling performance, high coulombic efficiency, and high capacity retention ratio for the cell containing PAN membranes.

PVDF exhibits appealing properties for use as a separator in lithium ion cell applications. PVDF is semi-crystalline polymer with a degree of crystallinity ranging from 40% to 60%. It shows high dielectric constant due to its strong electron-withdrawing functional groups (–C–F) which help obtain better dissolution of lithium salts to support higher concentration of charge carriers. The ionic conductivity of PVDF is associated to the total solution uptake, which depends on the porosity, pore size and crystalline of the separators. Boudin et al. [36] prepared PVDF membranes by phase inversion and a good rate capability was reported for the cells containing microporous PVDF membranes. Han et al. [37] investigated the effect of polymer types, concentrations of solution, amounts of additive, and non-solvent ratios of water/ethanol on the morphology of PVDF membranes. It was

found that the morphology of membranes was affected significantly by the ratio of a coagulation bath and a low molecular weight additive.

Even though PVDF is one of the most commonly used polymers for separators, it has some disadvantages. It is a semi-crystalline polymer and hard to absorb more liquid electrolyte into the polymer network. In addition, the affinity between PVDF matrix and liquid electrolyte is not strong enough to hold on the entrapped liquid electrolyte [9]. They are potentially instable to the negative electrode of lithium and lithium-ion batteries. The F–C bonds may react with lithium and lithiated graphite to form more stable LiF and >C=CF– unsaturated bonds, which deteriorates battery performance and cause safety concerns. In addition, PVdF-based polymers are soluble in liquid electrolytes, which leads to a loss in the mechanical strength of the separator [38]. In order to decrease the crystallinity and increase the affinity with the liquid electrolyte, suitable polymers can be blended with PVDF [39]. To decrease the crystallinity and increase the affinity with the liquid electrolyte, Li et al. [39] fabricated microporous PVDF/P(MMA-co-PEGMA) blend membranes by using phase inversion process. As a result of blending, crystallinity decreased from 46 % to 38 % and electrolyte uptake increased. The maximum conductivity value of 3.01×10^{-3} S/cm was reached in blended samples at 25^{0}C. Hwang et al. [40] prepared PVdF-HFP/PEG blend and it was reported that the porosity, electrolyte uptake, and ionic conductivity increased by increasing the content of PEG. Ma et al. [41] prepared PVDF/PMMA blend microporous membranes via thermally induced phase separation which is one of phase inversion methods. The addition of PMMA increased porosity, decreased crystallinity, enhanced electrolyte uptake and enhanced the ionic conductivity of resulting membranes. Figure 1.11 shows the changes in morphology by increasing PMMA content. Some other examples of blend

membranes are PVDF/PEO-PPO-PEO blend microporous membranes [34], PVDF/polysulfone blend membrane [42], and PVDF-HFP/PS [43].

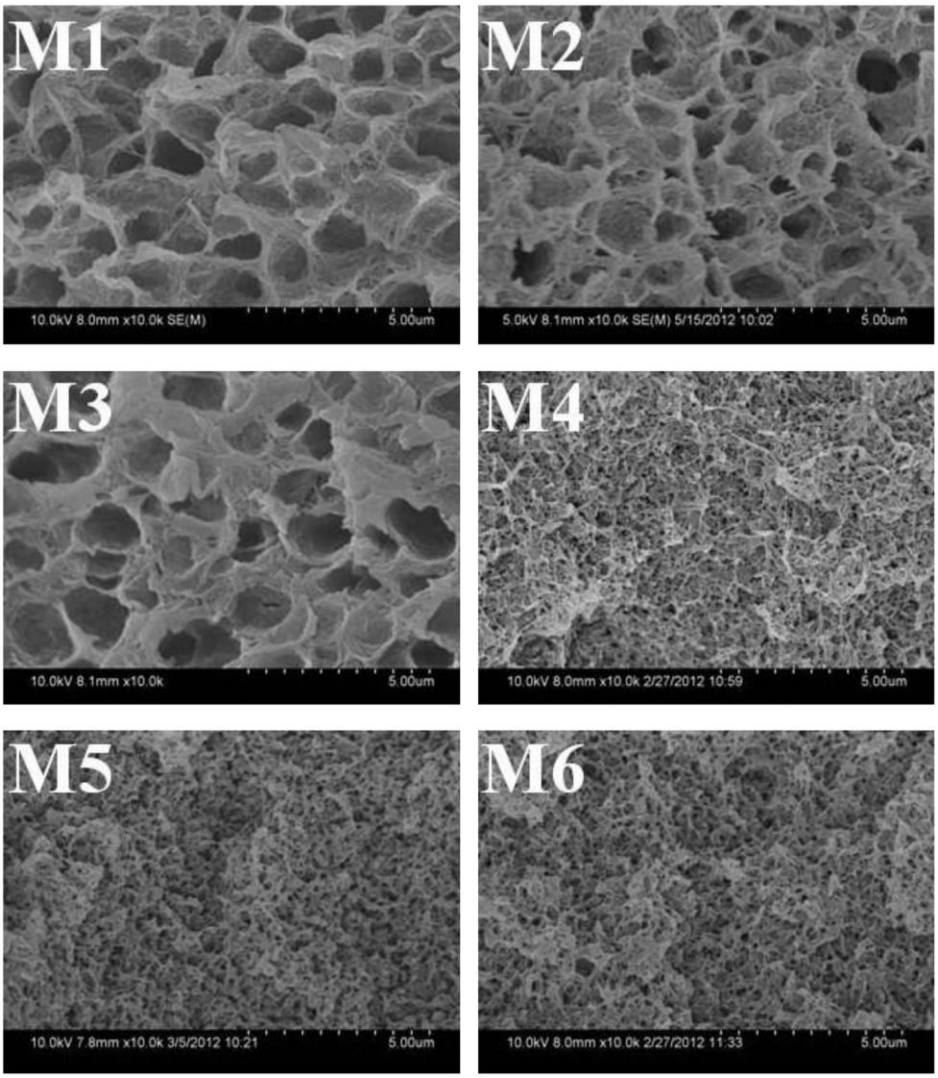

Figure 1.11 Cross-section SEM micrographs of blend membranes with different weight ratios of PMMA/PVDF [41].

Copolymer structures can also be used to decrease crystallinity of polymer matrix. Costa et al. [44] prepared poly(vinylidene fluoride-trifluoroethylene) membrane by solvent evaporation. Zhang et al. [38] prepared microporous poly(acrylonitrile-methyl methacrylate)

membrane by the phase inversion method with N,N-dimethylformamide as the solvent and water as the non-solvent and it was found that morphology of the membrane was affected by the concentration of polymer solution. Finger-like pores with dense skin on two surfaces of the membrane were observed when low concentration was used, while high concentration produced open voids with dense layer on the other surface of the membrane. In addition, high ionic conductivity, good compatibility with lithium metal, excellent cycle performance was reported for the resulting membranes. In another study, P(AN–MMA) membranes with the pore sizes of 1–5 μm showed the ionic conductivity of 2.52×10^{-3} S/cm at room temperature when immersed into 1M $LiPF_6$/EC-DMC (1:1 vol.%) electrolyte solution [45]. Compared with PVDF, PVDF–HFP has relatively lower crystallinity. Therefore, PVDF–HFP contains more amorphous domains capable of trapping large amounts of liquid electrolytes. The amorphous HFP phase serves as an ionic conductor while the crystalline PVdF phase acts as a mechanical support. Pu et al. [46] prepared PVDF–HFP microporous membrane by phase inversion techniques using water as the non-solvent. Polymer was first dissolved in acetone and water and then solution was cast onto a plate and the microporous membranes were obtained after the evaporation of the solvent. Subramania et al. [47] improved the ionic conductivity of PVDF-co-HFP microporous membranes by adding PAN.

1.2.3.2 Modified microporous membrane separators

The most common separators for lithium-ion batteries are microporous PP and PE membranes. However, the disadvantages including poor wettability, low electrolyte retention and unsatisfactory thermal stability are needed to be improved. In order to enhance wettability and thermal properties of polyolefin separators different approaches have been reported.

It has been known that the thermal stability of PE has been improved by high-energy irradiation and thermal shrinkage has been effectively reduced when the PE was treated by an electron beam irradiation. Kim et al. [48] investigated the effects of gamma-ray irradiation on the thermal stability of the PE separator under the high temperature environments. After the gamma-ray irradiation, thermal stability improved, pore structure and ionic conductivity remained same and the cells prepared by using gamma-ray irradiated separators showed better rate-capability and cyclic performance due to carbonyl bands.

Even though significant improvements have been reported with Gamma-ray irradiation, it has some drawbacks including long processing time and high equipment cost. Therefore, electron-beam irradiation can be presented as another method with many advantages such as short process time, in-line process, low equipment cost, and short release time [49]. Kim et al. [49] prepared electron-beam-irradiated polyethylene membrane and the electron-beam irradiation enabled installation of carbonyl group on the bare PE separator. Therefore, resulting separators had improved the electrolyte affinity of the PE separator, resulting in better ionic conductivity and rate discharge capability. In addition to electrochemical properties, the electronbeam-irradiated PE separators exhibited a lower thermal shrinkage ratio at 120 ºC compared to the bare PE separator.

One of the most common approaches is grafting. The surface of the separator can be made hydrophilic by means of a radiochemical grafting of vinyl monomers. Several methods including UV radiation, decomposition of chemical initiator, plasma treatment, and high energy radiation (c-rays, ion beams, or electron beams) can be used for graft polymerization. Gineste et al. [50] grafted acrylic acid and diethyleneglycol-dimethacrylate onto polypropylene films. First, separator was irradiated in air by electron beams and the

irradiated film was then immersed in a grafting solution composed of monomers. Resulting membranes showed improved cycling performance due to enhanced wettability. Gwon et al. [51] used radiation grafting of methyl methacrylate onto polyethylene separators. Electrolyte uptake and ionic conductivity of the resulting separators increased significantly. In addition to improved electrochemical properties, the thermal stability of the PE-g-PMMA separators was also improved compared with the PE separator [52]. In another study, poly(ethylene glycol) borate acrylate was grafted onto polyethylene (PE) separator by means of electron beam irradiation and improved cycling and C-rate performance was reported for grafted separators owing to their higher ionic conductivity compared to bare separators [53]. In another study, siloxane grafted on PE separator by electron beam irradiation [54]. Fang et al. [55] grafted PEG chains on PP membrane and introduction of PEG chains improved the ionic conductivity and decreased interfacial resistance, and thus resulting separators showed improved cycling performance.

Even though, the radiation process is a promising method due to its advantages including the rapid formation of active sites for initiating the reaction through the polymer matrix and the uniformity of polymers over the specimens, the plasma process is a preferred and convenient technique when considering a large scale production or commercialization of the membrane. In addition, plasma is an effective and green process for modifying the surface of the separators by introducing functional groups onto the surface of the polymeric materials. The general reactions are; cleaning to remove organic contamination from the surfaces, etching to remove a weak boundary layer and increase surface roughness, crosslinking of near-surface molecules to cohesively strengthen the surface layers activation by creating reactive sites, grafting of functional groups to modify chemical structure,

polymerized deposition of thin polymeric film [56]. Figure 1.12 shows the schematic drawing of surface modification of microporous PP membranes via plasma-induced graft polymerization of PAA onto PP membrane and membrane morphologies. First PP membranes were modified by argon plasma treatment to create grafting sites; UV irradiation was then used to covalently bond acrylic acid to the surface of PP membranes. As can be seen from SEM images, the holes on the surface were covered by polyacryic acid [56].

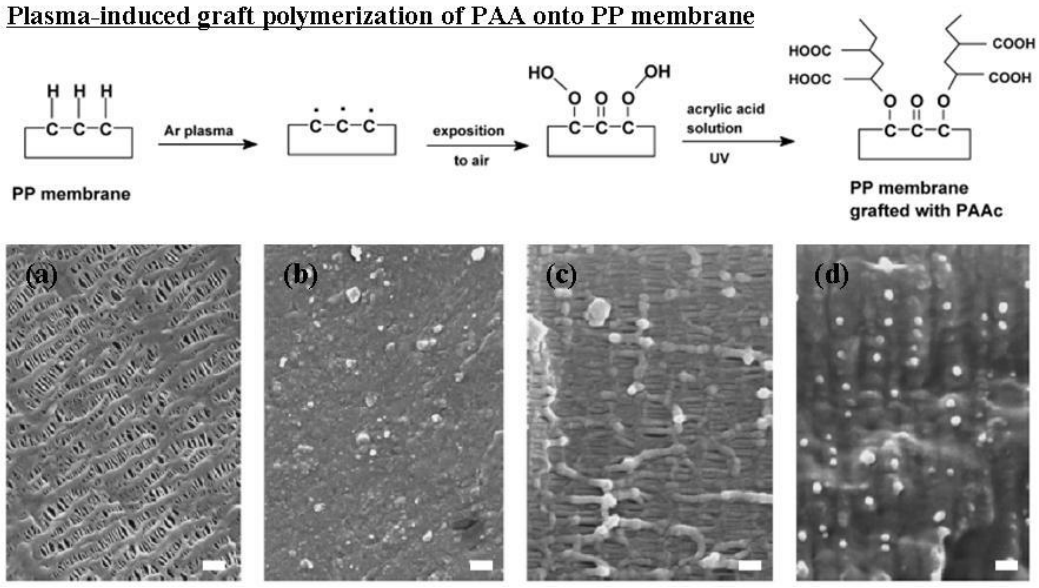

Figure 1.12 (Top) Schematic drawing of surface modification of microporous PP membranes via plasma-induced graft polymerization of PAA onto PP membrane. (Bottom) SEM images of surfaces [(a) and (b)] and cross-sections [(c) and (d)] of PP [(a) and (c)] and surface-modified PP membrane (b) and (d)] (Scale bar: 1 μm) [56].

Kim et al. [57] modified the surface of PE membranes with acrylonitrile using the plasma technology. Plasma-modified polyethylene membranes exhibited increased ionic conductivity, good wettability, and enhanced interfacial adhesion between the electrodes and the separators so that cycling performance was improved compared to bare separator. In another study, PP/PE/PP trilayer separators were modified by cyclonic atmospheric-pressure

plasma and resulting separators exhibited improved wettability and cycling stability [58]. Li et al. [59] also used plasma technique to graft MMA and SO_3Li functional groups into the PP separator.

Coating is also commonly applied to polyolefin membranes to improve the performance of the separators. Sohn et al. [60] used dip coating technique to prepare modified PE membrane. PVDF-HFP was chosen considering its excellent mechanical and chemical stability and PMMA was used due to its high affinity with liquid electrolyte. Resulting PVDF-HFP/PMMA-coated PE separators showed higher porosity and conductivity values compared to bare PE separators. In addition, better rate capability and cycle stability was reported for coated PE separators. Xiong et al. [61] reported ethylcellulose-coated polyolefin separators (PE and PP/PE/PP) with improved thermal stability. Ethylcellulose was chosen due to its high thermal stability and polarity so that improved thermal stability and cycling performance was reported for the resulting separators. In this study PVP was used to create pores on the surface of the separators as shown in Figure 1.13.

Lee at al. [62] used electrospinning technique to coat PVDF-co-CTFE on polyolefin membranes. Resulting membranes showed higher ionic conductivity and better cycling performance compared to bare separators. Improvements were contributed to the nanofiber layer and the polymer used. Nanofiber coating provided a 3-D interlaced network of nanoscale fibers which could entrap more liquid electrolyte and the affinity of the PVDF-co-CTFE polymer for the liquid electrolyte also led to maintain full wetting of the coated membrane and so that better cell performance was obtained. Some other studies about coated polyolefin separators are poly(acrylonitrile - methyl methacrylate) copolymer coated PE separators [63], porous PVDF coated PE separators [64], diethylene glycol dimethacrylate

coated PE separators [65], PEO-coated PE separators [66], and co-polyimide coated PE separator [67].

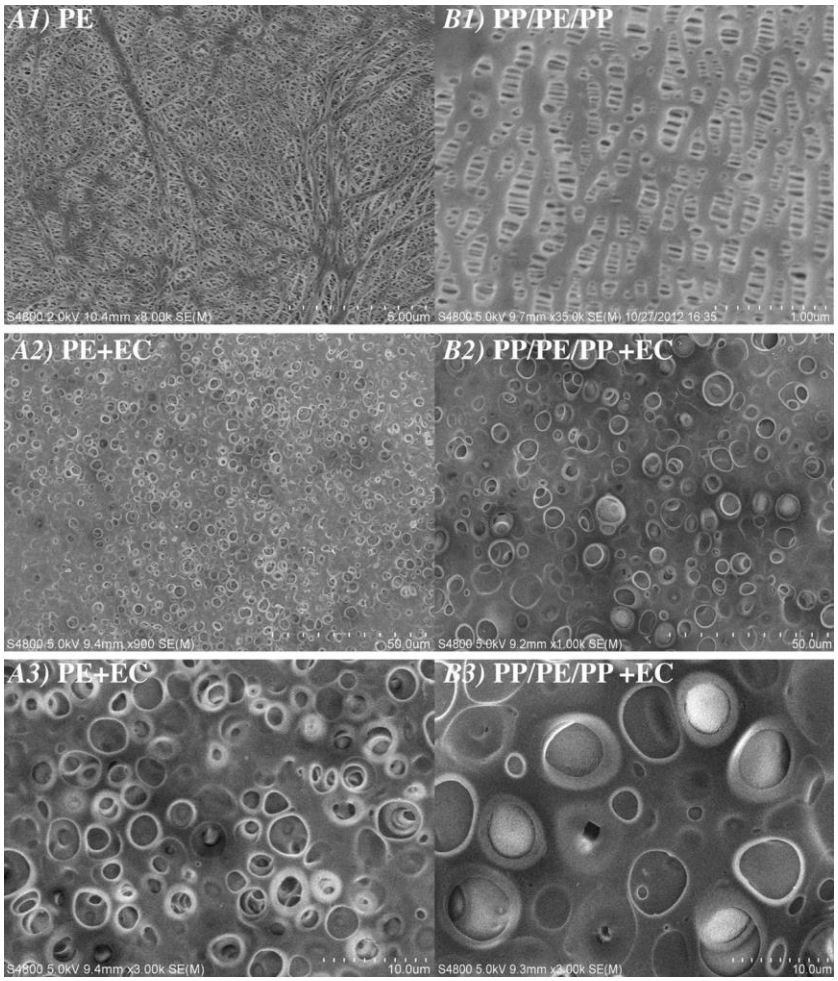

Figure 1.13 FE-SEM photographs for separators: (A1) PE separator; (A2)–(A3) PE + EC coated separator; (B1) PP/PE/PP separator; (B2)–(B3) PP/PE/PP + EC coated separator [61].

Besides commonly used polymers including PAN, PVDF, different polymeric structures was also applied onto polyolefin materials to modify the wettability of the separators. Wang et al. [68] used polydopamine to coat PP separators and the cells prepared by using modified separators showed improved C-rate performance due to the increase in

wettability. Figure 1.14 shows the effect of modification on contact angle. In another study, PE separators was modified by polydopamine coating and enhanced cycling and C-rate performance was reported owing to hydrophilic surface properties of the coated separators [69]. Shi et al. [70] modified PE separators by means of polydopamine treatment and subsequent PMMA coating.

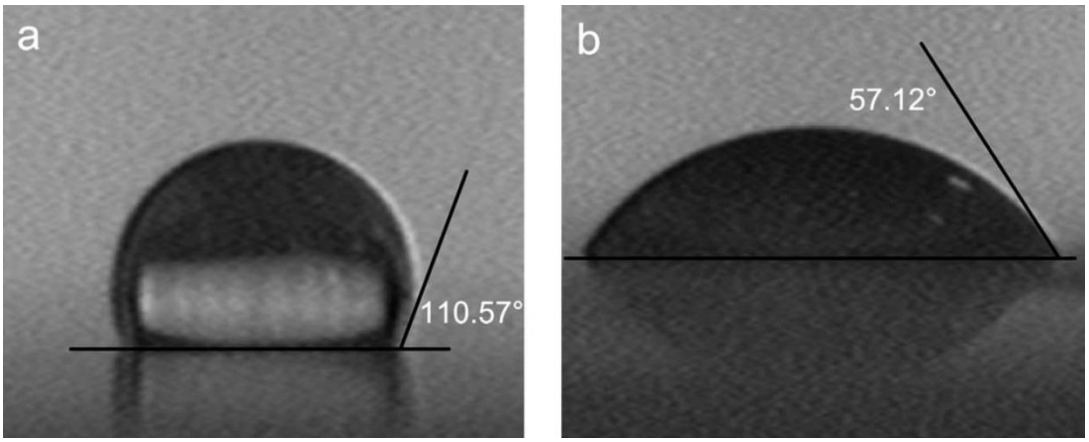

Figure 1.14 Water contact angle of PP separators with/without dopamine modification. (a) PP (110.57º ± 3.74º), (b) modified PP (57.12º ± 4.27º) [68]

In summary, the modification of microporous membrane separators has resulted in improvements in wettability, ionic conductivity, and electrochemical performance.

1.2.3.3 Non-woven membrane separators

Non-woven membranes are made by bonding randomly oriented fibers through chemical and mechanical methods. Melt-blown method, wet laid method and paper making method are some techniques to prepare non-woven membranes. In melt-blown method, melted polymer is extruded through a spinneret in order to form a polymer web and the fibers then are stretched and cooled by high-velocity hot air. In final step; the resulting web is collected into rolls and bonded by calendaring at high temperature and pressure. In the wet

process, a fibrous web is formed and a resin is sprayed onto the web to bond the base fibers with heat and pressure [26, 28]. Structure and properties of non-woven mats change depending on materials and process parameters including polymer type, polymer composition, temperature, and pressure. Even non-woven separator can be used in lead acid batteries, their pore sizes are too large to be used in lithium-ion batteries.

As an alternative to conventional methods, electrospinning has been presented to produce highly porous non-woven mats. Electrospun membranes have many advantages as battery separators such as high porosity, interconnected pore structure, small pore size and large surface area.

Electrospun PVDF membranes have been commonly used as separators due to their good electrochemical stability, and excellent affinity to electrolyte. Hwang et al. [71] prepared PVDF separators and higher thermal stability and electrolyte uptake were reported compared to commercial PE membranes. In addition, the effect of different parameters including spinning conditions, after post treatment and sheet forming on pore properties of PVDF membranes were investigated. Gao et al. [72] also compared cycling performance of the cells prepared by using commercial membranes and PVDF membranes. PVDF membranes showed less capacity fading owing to their high porosity. Costa et al. [73] investigated the effect of fiber orientation for electrospun PVDF membranes and mechanical properties improved with fiber alignment. However, ionic conductivity was higher for random fibers due to lower tortuosity. Yang et al. [74] used an electrospinning system with spherical hat target type collector to obtain PVDF membranes with uniform thicknesses. Liang et al. [75] reported electrospun PVDF membranes with high oxidation limit, low interfacial resistance and good cycling performance. In addition, heat treatment was also

employed to improve the mechanical properties. Cao et al. [76] used polydopamine coating to further improve electrochemical performance of PVDF nanofiber-based membranes. Better cycling and C-rate performance was reported due to hydrophilic structure of polydopamine.

Considering the drawbacks of PVDF, some studies reported PVDF copolymers including PVDF-HFP. Raghavan et al. [77] compared the physical and electrochemical properties of PVDF-HFP membranes prepared by using two different methods; electrospinning and phase inversion. Electrospun PVDF-HFP membrane showed superior electrochemical performance due to higher porosity compared to microporous membrane.

PAN is also commonly used as separators owing to its good mechanical and thermal stability, compatibility with electrodes, avoiding dendrite growth and fast lithium ion transport. Cho et al. [78] reported electrochemical properties of electrospun PAN separators. PAN membranes with two different thicknesses were fabricated and their electrochemical performance including C-rate and cycling performance was evaluated. Results showed that PAN membranes delivered higher capacity at high C-rates compared to PE and PP membranes as shown in Figure 1.15. In addition, PAN membranes showed less capacity fading after 200 cycles.

In another study Cho et al. [79] performed hot oven tests for the charged cells up to 4.2V and they reported that the PAN separator was thermally stable at 120 ˚C, but showed shrinkage of about 26% isotropically after the test at 150 ◦C for 1 h (Figure 1.16). The Celgard membrane showed uniaxial shrinkage of about 30% along the machine direction at 150 ◦C for 1 h.

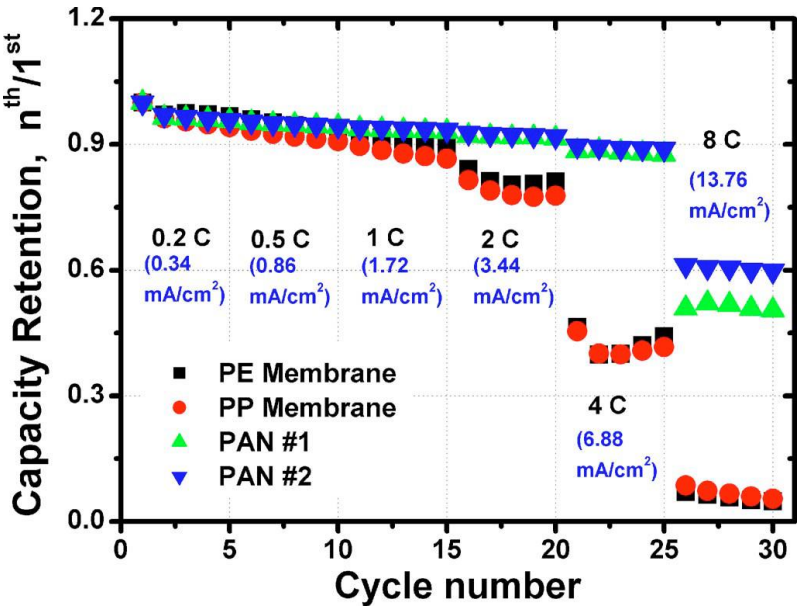

Figure 1.15 Results of rate capability test for the cells with PE, PP, and PAN separators with different thicknesses, PAN no. 1(33 μm) and PAN no. 2. (35 μm) [78].

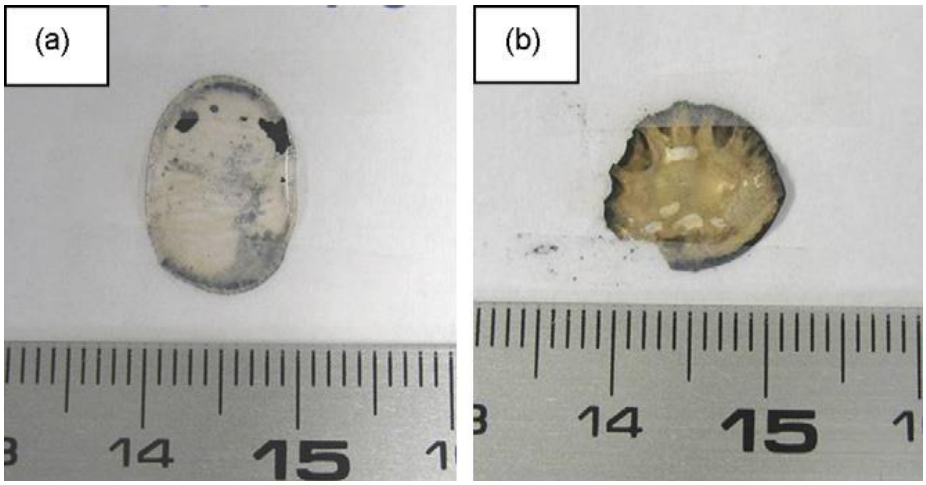

Figure 1.16 Photographs of the (a) Celgard membrane and the (b) PAN nonwoven after the hot oven test at 150 ◦C [79].

In order to improve physical and electrochemical properties of separators, different separators which composed of polymer blends have been reported. Gopalan et al. [80]

reported electrospun PVDF-PAN membranes. PVDF-PAN membranes with 25% PAN showed the best results in terms of ionic conductivity and cycling performance due to the high porosity and electrolyte uptake. In another study, polydiphenylamine was introduced into PVDF matrix and resultant blend electrospun membranes showed improved ionic conductivity compared to PVDF membrane [81]. Li et al. [82] prepared electrospun PVDF/PMMA membranes considering amorphous structure of PMMA. By introducing PMMA into PVDF matrix crystallinity decreased (from 39% to 32%) and porosity increased from 57% to 60%. In another study, PVdF-HFP/PVC/PVdF-HFP based- trilayer separators with enhanced electrolyte uptake, mechanical integrity and thermal stability were reported [83]. Zhong et al. [84] used PVC to suppress the crystallinity of PVDF and the crystallinity decreased from 38 to 30% and ionic conductivity increased from 1.47 to 2.25 mS/cm for the resultant PVDF-PVC membranes. Increase in ionic conductivity was explained by decreased crystallinity, decrease in fiber diameter and increased porosity (Figure 1.17). Some other blend electrospun membranes are PVDF-co-HFP/poly(ethylene glycol) dimethacrylate [85], and PVDF-HFP/PMMA [86].

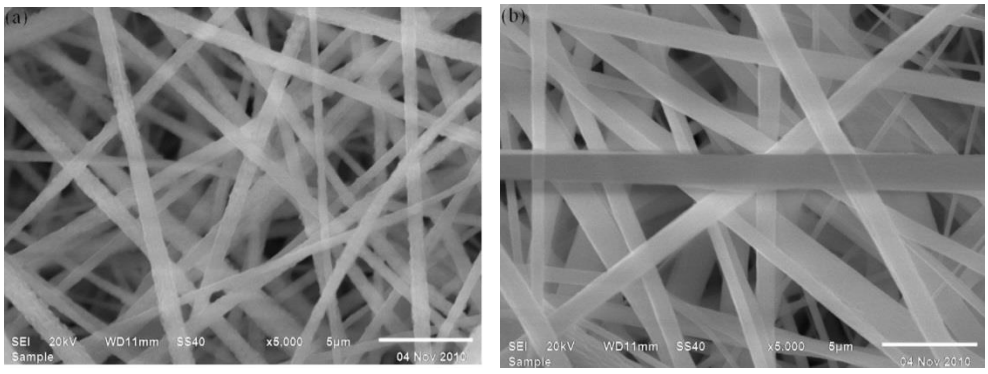

Figure 1.17 SEM photographs of (a) PVdF–PVC and (b) PVdF membranes [84].

In recent years, besides commonly-used separator materials such as PVDF, PAN and PMMA, new polymers such as polyimide, nylon, polysulfonamide, polyethylene terephthalate, etc., have been utilized to prepare separators with improved thermal stability. Jiang et al. [87] reported polyimide-based non-woven membranes by using electrospinning, followed by subsequent thermal imidization and mechanical pressing. Superior electrochemical performance was reported at room temperature and 120 ^{o}C due to the high thermal stability of polyimide and the highly porous structure of the non-woven membranes. Other non-woven mat separators with improved thermal stability include, but are not limited to polysulfonamide [88], polyester [89-94], polyphthalazinone ether sulfone ketone (PPESK) [95], PPESK/PVDF/PPESK [96], cellulose/PVDF-HFP [97], cellulose/polysulfonamide [98], polysulfonamide/polypropylene [99] and cellulose/PDA based non-woven membranes [100]. These membranes not only showed high thermal stability but also exhibited good electrochemical performance.

As discussed above, electrospun membranes show desirable electrochemical properties owing to their physical properties such as high porosity, interconnected pore structure, small pore size and large surface area.

1.2.3.4 Composite membrane separators

It has been well established that introducing inorganic particles can enhance physical and chemical properties of separators. Inorganic particles lead to excellent wettability due to their high hydrophilicity and high surface area. Inorganic nanoparticles like ZrO_2, Al_2O_3, TiO_2, and SiO_2 have been used to fabricate composite membranes. These particles reduce the crystallinity of polymer matrix and introduce Lewis acid-base interaction between polar groups of the inorganic particles and the electrolyte ionic species, and thus improve ionic

conductivity. In addition, in most cases mechanical and thermal properties are also improved by introducing inorganic particles [101]. Composite membrane separators can be divided into three subgroups: inorganic particle-coated composite membranes, inorganic particle-filled composite membranes and inorganic particle-filled non-woven membranes.

1.2.3.4.1 Inorganic particle-coated composite membrane separators

Very thin layer of inorganic particles can be applied onto microporous polyolefin membranes to improve wettability and thermal properties. Jeong et al. [102] introduced SiO_2/PVDF-HFP coating layer onto both sides of PE separators to improve thermal stability of the separators and thermal shrinkage reduced to 77 % (thermal shrinkage was 94% for the pristine separator) for the resulting membranes. Fu et al. [103] used SiO_2 to coat PP membranes (Figure 1.18). Resultant separators showed improved electrochemical performance including C-rate and cycling performance and enhanced thermal stability.

In another study electrospun PVDF-CTFE/Al_2O_3 was coated on PE separators to improve thermal stability and wettability and thus resultant separators showed enhanced C-rate and cycling performance with less thermal shrinkage [104]. Park et al. [105] coated SiO_2/PMMA onto PE separators. Inorganic particle coating led to improvement in thermal shrinkage and ionic conductivity. Kim et al. [106] used chemical vapor deposition method to coat a very thin layer of SiO_2 on PE separators. Chen et al. [107] combined plasma activation and atomic layer deposition of TiO_2 to improve the performance of PP separators. By plasma activation, active groups were generated on the separators, and ultra-thin TiO_2 films were deposited on the separators at only 20 cycles. The thermal shrinkage was suppressed

significantly by the TiO_2 layer. Kim et al. [108] coated ZrO_2/(PVdF-HFP) copolymer on a polyethylene separator and it was found that when the moisture content increased, the

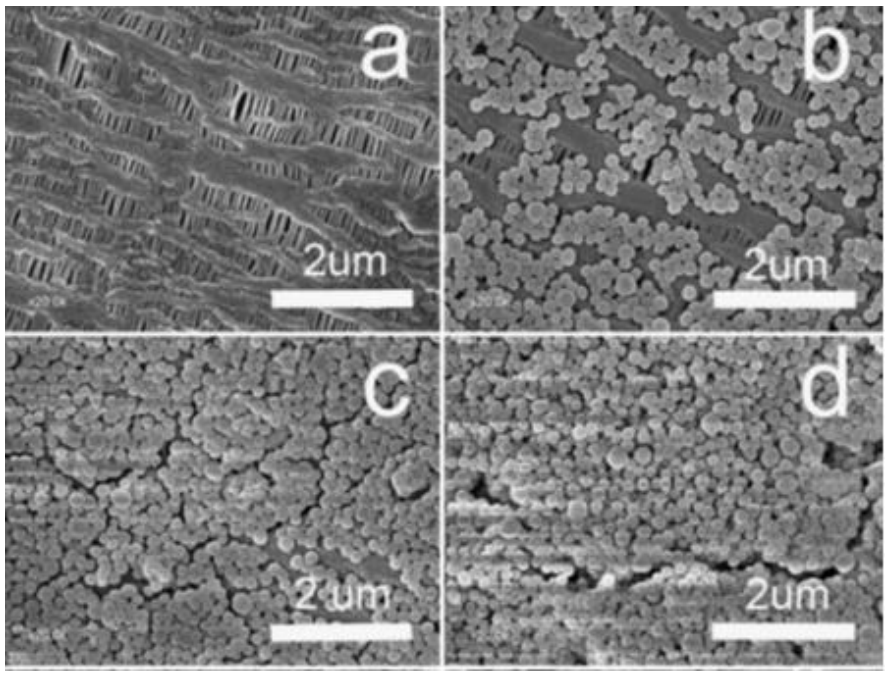

Figure 1.18 SEM images of PP separator surface with and without SiO_2 particles coating. (a) Without coating, (b) 8%, (c) 20%, (d) 27% [103].

number of micro-pores increased, resulting in improved electrochemical properties of the separators. Lee et al. [104] used electrospinning to coat PVDF/Al_2O_3 onto both sides of PE membranes and interfacial resistance, cycling and C-rate performance improved compared to bare PE membrane.

Some other studies which reported inorganic particle coating on polyolefin separators are SiO_2/PVDF-HFP coating on PE separators [109], $SiO_2(Li^+)$/PVDF-HFP coated- PE separators [110], Al_2O_3/PVDF-HFP on PE separators [111], SiO_2 nanoparticle coated PP/PE/PP [112], Al_2O_3/carboxymethyl cellulose/styrene butadiene rubber coated PE

separator [113], P(AN-co-MMA)/nano-Al_2O_3 coated PE membrane [114] and, SiO_2 coated PE and PP separators [115, 116].

1.2.3.4.2 Inorganic particle-filled composite membrane separators

Besides coating inorganic particles onto microporous membranes, inorganic particles can be incorporated into polymer matrices. Takemura et al. [117] fabricated Al_2O_3 containing PVDF microporous membranes to improve thermal stability of the separators. Addition of inorganic particles improved not only thermal resistance but also cycling performance. Prosini et al. [118] introduced $LiAlO_2$, Al_2O_3, and MgO into PVDF-HFP polymer matrix and MgO containing separator showed the best anode and cathode compatibilities. In another study, Al_2O_3 containing membranes with high ionic conductivity of 3.1×10^{-3} S/cm, and wide electrochemical stability (above 4.5 V) was reported [119].

Huang et al. [120] combined microporous PVDF and ceramic layer to produce composite membrane with good thermal stability and better C-rate performance was obtained compared to commercial separators. Wang et al. [121] prepared Al_2O_3/PVDF composite by dispersing Al_2O_3 particle in PVDF matrix and using casting method and improved thermal stability reported due to high amount of inorganic particle loading.

Kim et al. [101] introduced SiO_2 particles in PVDF membranes and ionic conductivity increased due to Lewis acid–base type interactions between the inorganic particles and the electrolyte polar groups.

1.2.3.4.3 Inorganic particle-filled non-woven membrane separators

In addition to microporous membranes, inorganic particles can also be incorporated into the electrospun membranes. Adding inorganic particles improves electrolyte uptake and

ionic conductivity, and thus improves the electrochemical performance. In addition, inorganic materials improve thermal stability resulting in improvement in safety of the separators [122].

Sethupathy et al. [123] prepared PVDF/SiO_2 membranes and adding SiO_2 particles led to improved electrolyte uptake and conductivity of the resultant membranes. In another study, SiO_2 nanoparticles improved ionic conductivity, and mechanical properties while decreasing crystallinity of electrospun PVDF membranes [101]. Ding et al. [124] used TiO_2 particles and electrospun PVDF/TiO_2 membranes exhibited less capacity fade due to higher ionic conductivity compared to PVDF membranes.

Jung et al. [125] prepared electrospun SiO_2/PAN separators and investigated the effect of SiO_2 on the physical properties and electrochemical performance of the separators. 12 wt.% SiO_2 containing membranes showed the best performance in terms of interfacial resistance, ionic conductivity and cycling performance. Liang et al. [126, 127] used two different inorganic particles, lithium lanthanum titanate oxide and lithium aluminum titanium phosphate to prepare PAN based composite separators and improved performance was reported as a result of introducing inorganic particles. Kim et al. [128] produced PVDF/SiO_2 nanofibrous membranes by the electrospinning and the thermal treatment. Average fiber diameter reduced and porosity increased by increasing SiO_2 content. In addition thermal treatment led to an improvement in mechanical properties owing to crosslinking structure between polymer chains and inorganic network.

Cho et al. [129] reported different approach to enhance physical and electrochemical properties of the separator. They combined ceramic containing polyolefin nonwoven and PAN nanofiber nonwoven. Figure 1.19 shows SEM image of cross-section of the separator.

Improved cycling and C-rate performance with high thermal stability was reported compared to commercial separators owing to ceramic layer and novel structure.

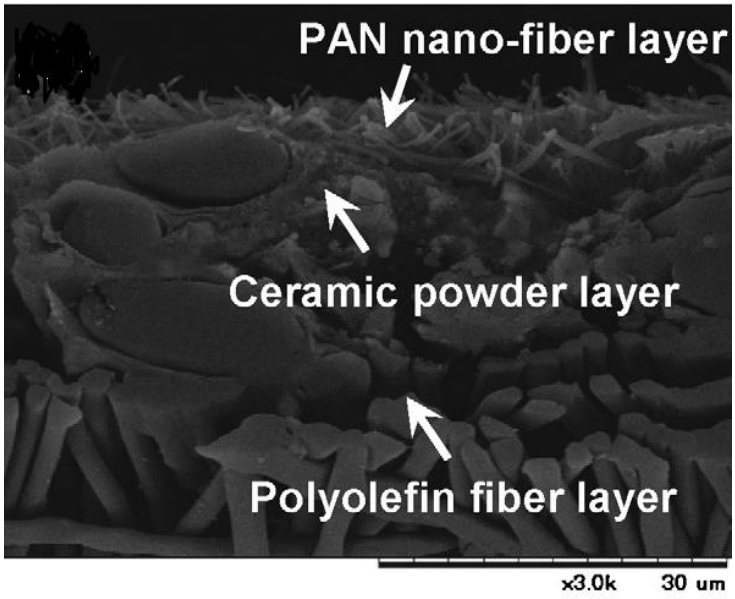

Figure 1.19 SEM image of cross-section of the ceramic powder containing polyolefin nonwoven and PAN nanofiber separator [129].

In another study composite nonwoven separators were produced by mixing SiO_2 particles and PE-PP fibers and then heat bonding and roll press was used to obtain nonwoven mat. Improved C-rate performance was reported for composite separator compared to bare commercial membrane [130].

Besides PVDF and PAN membranes, nylon 6,6 [131], polysulfonamide [132], polyimide [133, 134] and polyethylene terephthalate [135-139] membranes were used to fabricate high-performance membranes by incorporating inorganic particles into the nonwoven structure. Cells using these membranes exhibited good C-rate performance and high cycling stability, which were attributed to improved interfacial resistances and higher ionic conductivities due to the effect of inorganic particles in the membranes.

1.3 Overview on electrospinning

1.3.1 Introduction on electrospinning

Nanostructured materials have received great attention due to their superior properties such as unusual mechanical, electrical and optical properties [140]. Among nanostructured materials, nanofibers have found application in many fields and there are different methods to produce nanofibers such as centrifugal spinning, meltblowing, bicomponent spinning, phase separation, template synthesis and electrospinning [141, 142]. In centrifugal spinning, centrifugal forces are used to obtain nanofibers and main variables for this technique are rotational speed of the spinneret, collector type and the shape and size of the nozzles. Figure 1.20 shows the schematic of the meltblowing process, phase separation, template synthesis, and self-assembly. In meltblowing, a polymer melt is extruded through the orifice of a die. Fibers are produced by elongating polymer by using air drag. Throughput rate, melt viscosity, melt temperature, air temperature and air velocity affect diameters of fibers in this method. Bicomponent spinning includes two steps: spinning of the polymers together and removal of one polymer. [143, 144]. Figure 1.20b shows the different cross section shapes of bicomponent fibers. Phase separation technique includes polymer dissolution, gelation, phase separation, solvent removal, and drying. In template synthesis, hollow channels are used as templates. Polymer nanofibers are synthesized from their monomers in templates and then templates are dissolved or etched to obtain separated nanofibers. Polymer solution can also be fed to the hollow templates and nanofibers are obtained by removing the solvent. In self-assembly, nanofibers are produced by intermolecular interactions between molecules and different mechanism can be employed depending on the chemical structure of molecules [145].

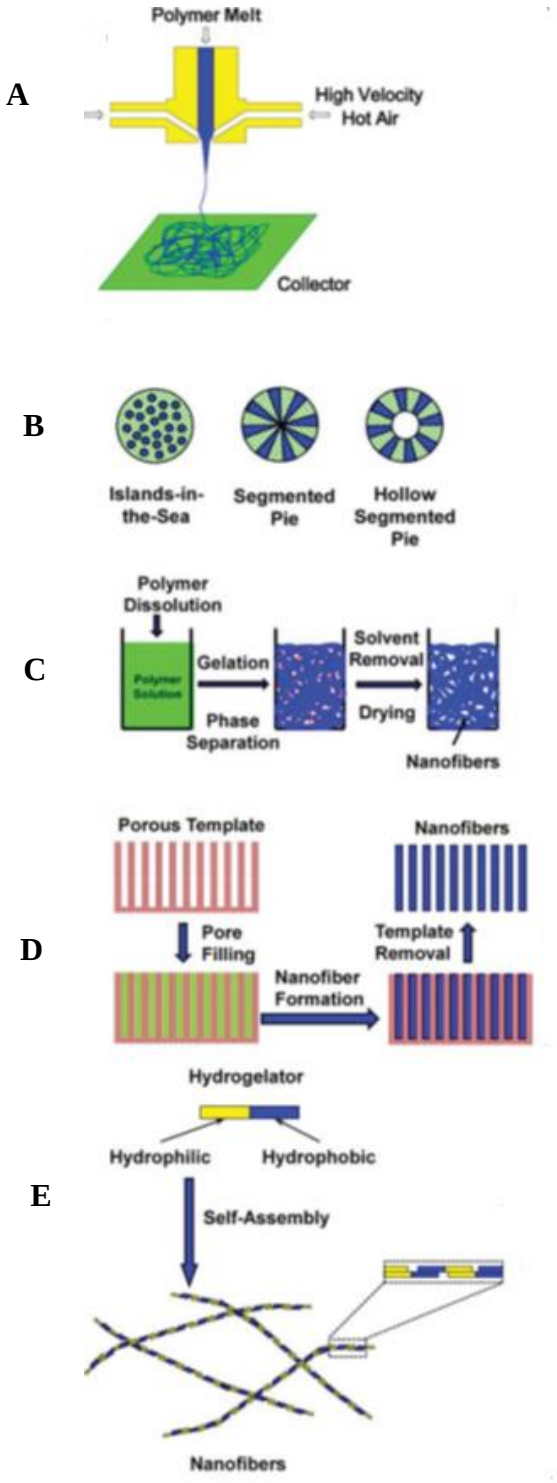

Figure 1.20 The schematic and of the meltblowing process, phase separation, template synthesis, and self assembly [145].

Compared to other techniques, the electrospinning is the most common process to fabricate nanofibers. In the electrospinning technique, polymer nanofibers can be obtained by applying electrical force at the surface of a polymer solution. Nanofibers, which have diameters from several nanometers to hundreds of nanometers, can be obtained in the form of nonwoven fiber mats. The small diameters lead to a large surface area to mass ratio, a porous structure with excellent pore-interconnectivity and extremely small pore dimensions [143, 146].

Electrospinning has been patented in 1934 for fabricating small-sized fibers. A jet forming process was developed by Taylor and the relationship between electrospinning parameters and fiber structure/properties was investigated by using polyethylene and polypropylene fibers by 1969. Until 1990s there was not many works about electrospinning. After that, electrospinning has been using to obtain nanofibers by using broad range of polymers for different applications [147].

1.3.2 Working principle of electrospinning

Electrospinning technique is used to produce continuous polymer fibers with the fiber diameter on nanometer scales or submicron scales in the form of nonwoven mats. In electrospinning technique, electric charge is used to transform viscoelastic liquids into nano-sized filaments. The typical electrospinning set up consists of pump, nozzle, polymer solution, power supply and collector (Figure 1.21).

In a typical electrospinning set up, viscoelastic liquids is ejected at the tip of the needle which is at high positive potential. When electric charge is applied on liquid droplet, the solution becomes highly charged, charges accumulate at the surface of the droplet and

thus it causes instability of the liquid. Coulomb repulsion of like charges tries to distort the droplet and surface tension opposes droplet division. When a critical voltage is reached, electrostatic forces deform the droplet and droplet turns into a conical shape. This cone is called Taylor cone. Under the electric field, jet thins and accelerates from Taylor cone through the collector. Jet experiences whipping instabilities and solvent evaporation. Finally, filaments accumulate on the collector. In order to get continuous filaments, polymer solution must be above the critical concentration for chain overlap [147-149].

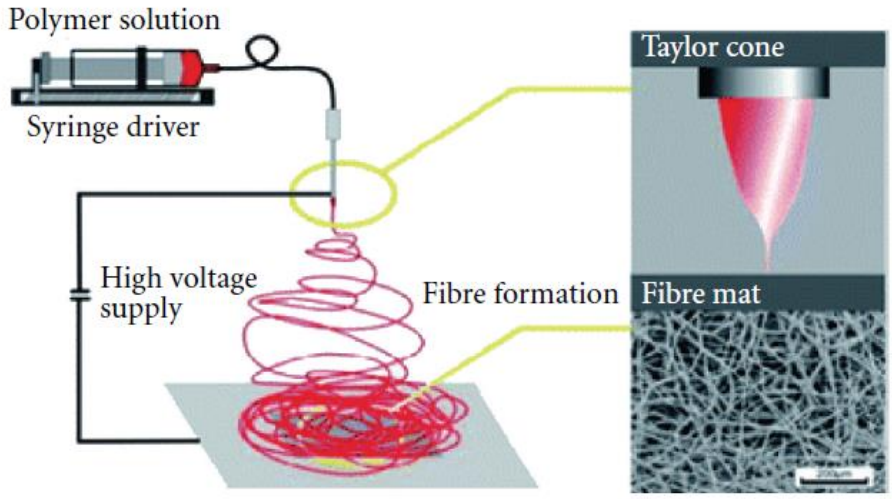

Figure 1.21 Schematic of typical electrospinning set up showing Taylor cone and SEM image of electrospun nanofibers [150].

1.3.3 Parameters

The electrospun nanofibers generally have threadlike structure or ribbonlike fibrous morphology. Defects or beads can be seen depending on process parameters and material properties [148]. In the electrospinning technique, there are mainly two types of parameters: system and process parameters (Table 1.4). Viscosity, concentration, surface tension, molecular weight, conductivity and dielectric of polymer solution are system parameters.

Applied voltage, feeding rate, tip-to-collector distance, heat of the solution and ambient parameters are process parameters. The fiber morphology also depends on the polymer type, and conformation of the polymer chain [151].

Table 1.4 Electrospinning parameters.

Electrospinning parameters	
System parameters	Process parameters
Viscosity Concentration Surface tension Conductivity and Dielectric of polymer solution	Applied voltage Feeding rate Tip-to-collector distance Heat of solution Ambient parameters (temperature, humidity, etc.)

One of the most significant parameters influencing the fiber diameter is the solution viscosity. The viscosity of a polymer solution must be high enough to cause polymer entanglements and fiber formation. However, too high viscosity prevents polymer motion under the electric field and too low viscosity means that fibers cannot form but instead beads are formed. Polymer concentration has also a big effect on fiber diameter. Increasing concentration cause an increase in fiber diameter. Figure 1.22 shows the effect of concentration on the fiber morphology for PVA fibers. Too low polymer concentration

causes defects in the structure such as beads because viscoelastic force is too small to hold the fibrous structure. Concentration also affects other solution properties such as viscosity, surface tension and conductivity. In addition, the diameters of nanofibers increase with increasing concentration according to the power law relationship. The relationship between polymer concentration and fiber diameter is not linear because viscosity is affected by concentration and material properties such as intermolecular interactions. The solution must also have a surface tension low enough, and a charge density high enough to form fibers [151].

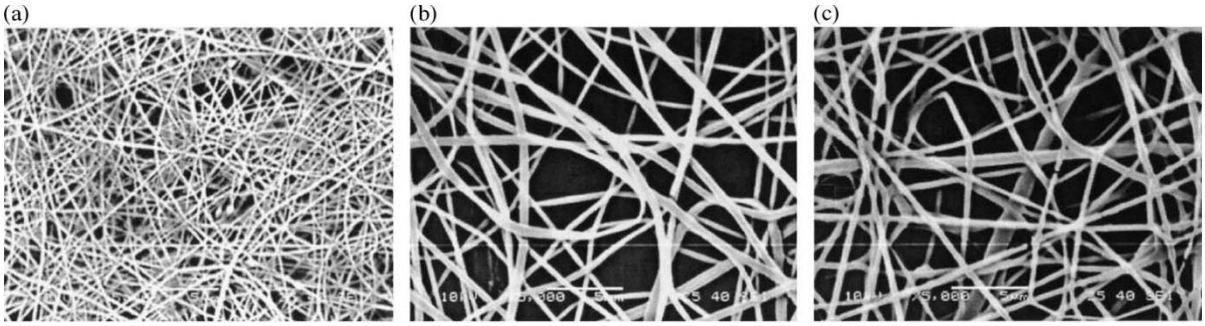

Figure 1.22 Photographs showing the effect of solution concentration on the structure of electrospun PVA nanofibers. Molecular weight = 13,000– 23,000 g/mol; (a) 21 wt.%; (b) 27 wt.%; and (c) 31 wt.% [152].

Polymer molecular weight is also very effective on the morphology. Koski et al. [152] studied the effect of polymer molecular weight on the morphology of PVA nanofibers. Figure 1.23 shows the morphology of PVA nanofibers prepared by using PVA with different molecular weight. At low molecular weight, the jets are not stabilized and this cause beaded structure. As the molecular weight increases to 13,000–23,000 g/mol, a fibrous structure is stabilized resulting in bead-free structure. Further increase in molecular weight causes an increase in diameters.

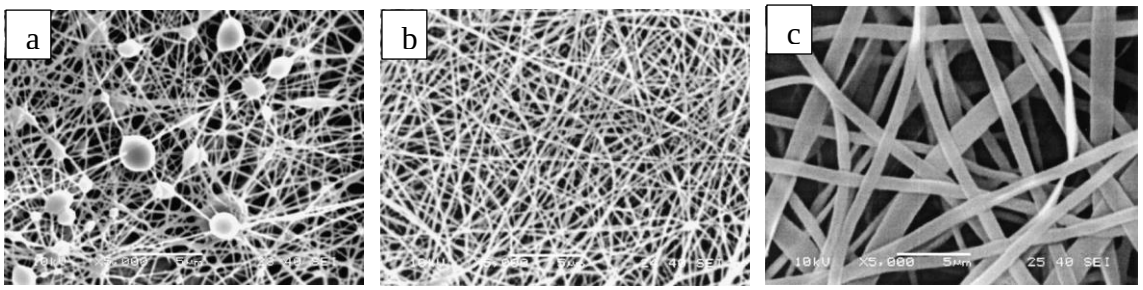

Figure 1.23 Photographs showing the typical structure in electrospun PVA nanofibers for various molecular weights. (a) 9000–10,000 g/mol; (b) 13,000–23,000 g/mol; and (c) 31,000–50,000 g/mol (solution concentration: 25 wt.%) [152].

In addition to system parameters, process parameters are also important. The applied voltage influences fiber diameter and morphology, but the significance and the direction of the effect may vary with other factors, such as tip-to-collector distance and solution properties [143]. Li et al. [153] reported slight decrease in diameter with increasing the voltage and needle tip-to-collector distance for nylon nanofibers. In general, the diameter of the nanofibers decreases, and the diameter distribution narrows when the applied voltage increases. Increasing flow rate leads to thicker fibers. With an increase in tip-to-collector distance, a reduction in diameter size and distribution is observed. Thinner fiber diameters can be obtained by using nozzle with smaller diameter. The solvent also affects surface tension and evaporation process. [143].

Heikkila et al. [154] investigated the effect of system and process parameters on the diameter of polyamide 6. In Figure 1.24, the effect of different parameters on diameter can be seen. The fiber diameter was directly proportional to the nozzle size, the viscosity, the salt content and the acid grade. The dependency curves of the fiber diameter on the voltage, the distance and the electric field strength were concave in shape. Decreasing fiber diameter due

to the higher voltage was attributed to higher electrostatic forces. The higher voltage induced higher electrostatic forces on the jet, and the higher repulsive forces favoured the formation of the thinner fibers. Increasing diameter can also easily be explained, since the higher field can cause a higher mass flow leading to thicker fibers.

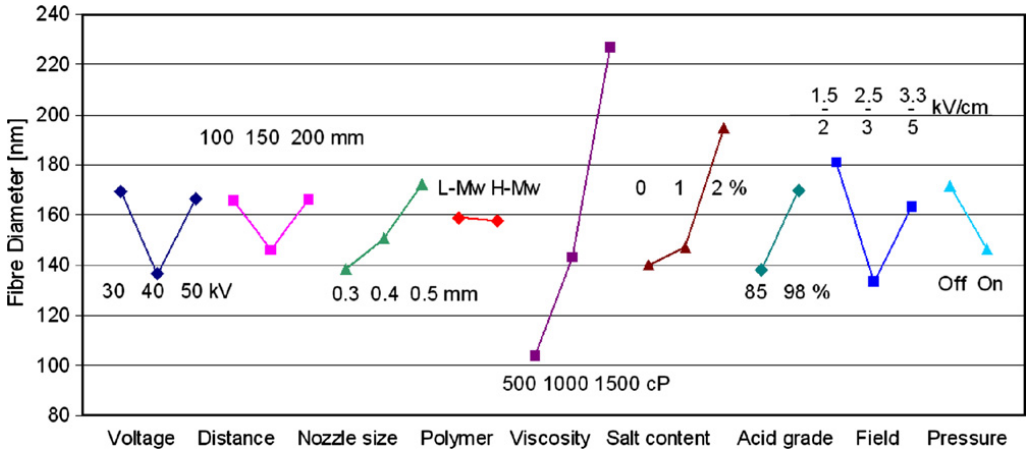

Figure 1.24 Mean effects of the parameters on polyamide 6 nanofibers [154].

Fiber morphology can be varied depending on electrospinning parameters. Smooth, porous or rough surface can be obtained by controlling parameters. For example, higher applied voltage leads to rougher surface. Rapid solvent evaporation and condensation of moisture leads pores on fiber surface. Surface morphology can also be controlled by polymer used, applied voltage, solvent, humidity, and other environmental conditions. Bead formation can be prevented by increasing viscosity. In addition, solution conductivity has also effect on bead formation. Solution conductivity can be increased by adding surfactant into polymer solution [148, 151, 155].

1.3.4 Applications on energy devices

The electrospun fibers have been used in filtration, protective clothing, tissue engineering scaffolds, sensors, energy storage, battery separators, composite materials and biomedical applications, such as wound dressing and drug delivery systems etc. Fundamental requirements for all cases are controlled pore sizes, small diameters with enhanced specific surface area and permeation properties [156-159]. Figure 1.25 shows the applications of nanofibers.

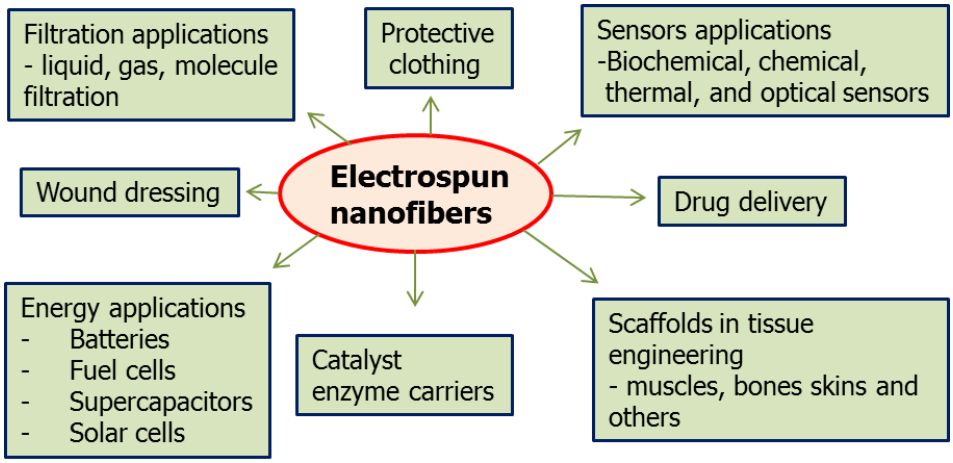

Figure 1.25 Applications of electrospun nanofibers, adopted from REFs [158, 159].

Nanofibers are very attractive in biomedical applications. The reasons are high surface area, which allows enhanced adhesion of cells, proteins, and drugs, and a wide range of polymer selection for different applications. In addition, nanofibers can be fabricated into different hierarchical structures that mimic those in animals and human [160].

Nanofiber mats for filter media provide advantages of high filtration efficiency and low air resistance because the very high surface area to volume ratio and high surface cohesion. Tiny particles of the order of < 0.5 μm can be easily trapped in the electrospun nanofibrous structured filters and hence the filtration efficiency can be improved [161].

Electrospun nanofibers are advantageous for use as electrode and separator materials in battery and supercapacitor applications. Electrospun nanofibers have shorter diffusion path relative to the commonly employed powder materials and faster intercalation kinetics is expected due to their high area/mass ratio in lithium-ion batteries. Electrospun nanofibers also offer relatively large number of lithium insertion sites, and therefore the charge-transfer resistance at the interface between the electrolyte and active electrode materials is decreased. In addition, electrospun nanofiber separators are enable high-rate charge/discharge of batteries because of their high porosity and desirable pathways for ion transport [7].

Similar to lithium-ion batteries, fuel cells can also benefit from electrospun based cell components. Electrospun anodes [162, 163], cathodes [164], and electrolyte membranes [165-170] have been reported. The nanofiber electrodes have several advantages including high porosity, high percolation, continuous pathway for charge transport; good thermal stability at the operating temperature; and excellent scaffold for infiltration. Moreover, nanofibers have not only large surface-to-volume ratio and high catalytic activity, but also high charge mobility [162-164]. Electrospun membranes have many unique properties such as a large specific surface area, unique three dimensional network structures with fully interconnected pores, high porosity, high solvent uptake, and superior mechanical properties [167, 169-171]. Furthermore, carbon nanofibers have attracted interest as catalytic support owing to their high electronic conductivity at a lower cost compared to similar nanostructures like carbon nanotubes, high specific surface area, high electrochemical and chemical stability, and easier electron transfer over carbon particles [5, 17, 172, 173].

High electrical conductivity, high surface area, sufficient pore size, and good pore connectivity is required for high performance supercapacitor electrodes. Therefore, 1D

nanostructured electrodes including nanofibers are beneficial in terms of electrochemical performance due to their high accessible surface area, shorten diffusion length, structural integrity and conducting pathways [174-177]. Recently, electrospun continuous carbon nanofibers (CNFs) nonwoven mats have been introduced as high performance supercapacitor electrodes due to their high porosity and large surface area [178, 179]. For carbon electrochemical double-layer capacitors (EDLC), which are able to store and release electrical energy through ion adsorption and desorption on electrode surface, the maximum capacitance is limited by the active electrode surface area and the pore size distribution. To increase the energy density, conductive polymer including polyaniline, polypyrrole, polythiophene or transitional metal oxides such as NiO, RuO_2 and MnO_2 have been introduced for the pseudocapacitance, in which energy storage and retrieval is achieved by charge transfer at the interface between electrode and electrolyte via reversible redox or Faradaic reactions [180-182]. However, conductive polymers suffer from capacity decay due to swelling during cycling and metal oxides have low electrical conductivity that limits its rate capability [180, 183-186]. Hence, composite structures are beneficial to combine the benefits of carbon materials including stable cycling performance and high-capacitance. There are many studies on carbon composites as supercapacitor electrodes such as PANI/C nanofibers [187-189], graphene/C nanofibers [190, 191] vanadium pentoxide/C [192], tin oxide (SnO_2)/C nanofibers [186], MnO_2/C [180], Fe_3O_4/C [179] V–O–C composite nanofibers [185], NiO/RuO_2/C .

In solar cell applications, nanofiber based semiconducting metal oxides photoelectrodes, and nanofiber counter electrodes enhance energy conversion efficiencies and nanofiber electrolyte can replace liquid electrolyte due to their unique pore structure,

high surface area, and high porosity. Nanostructured metal oxides act as a scaffold for dyes and a transfer media for photogenerated electrons to the transparent conductive oxide layer in DSSCs [193]. TiO_2, SnO_2 and ZnO based anodes are used in DSSCs and these anode films are generally composed of nanoparticles. However, in nanoparticle-based DSSCs, efficiencies are limited due to their disordered geometrical structures and interfacial interference in electron transport [194, 195]. Nanofibers can be offered in order to avoid these drawbacks because of their unique morphologies, enhanced surface activity and improved electron transfer leading to enhanced electron collection efficiencies [196, 197]. Photoanodes with large surface area and high porosity can anchor the maximum amount of dye sensitisers so nanofibers are promising candidates as photoanodes [12]. There are many studies that have reported TiO_2 nanofiber based electrodes [193-195, 198-208]. In addition to electrodes, nanofiber electrolyte was also studied in DSSCs with the aim of suppressing the limitations of liquid electrolyte including the lack of long term stability, liquid leakage, electrode corrosion, dye degradation and volatility [209, 210]. Some examples of gel electrolytes which have been studied in DSSCs are PVDF-HFP nanofibers [210], PVDF–HFP/polystyrene blend nanofibers [211], poly(2,6-dimethyl-1,4-phenylene oxide) electrospun nanofiber mat [212], liquid crystal embedded electrospun PVDF-HFP nanofibers [213], PVDF-HFP [214].

1.3.4.1 Lithium-ion batteries

Lithium-ion batteries include three main components: a cathode, an anode, and an electrolyte-soaked separator. When electrospun fiber mats are employed as a battery component, they can improve battery performance due to their superior properties such as nano-sized structure, high specific surface area, large pore volume and light weight [147].

Electrospun mats based electrodes show enhanced electrochemical properties such as high reversibility, small impedance growth, and better cycle performance [147]. Also, highly porous structure makes them good separators [7, 15].

Using nanostructured electrodes are advantageous in many aspects. Firstly, high surface area allows high electrode electrolyte contact area which enhances the rate capability of the electrodes. Secondly, strain associated with insertion extraction is better accommodated in nanostructured electrodes which leads to improved cycle life [17]. Moreover, increase in the rate of Li^+ insertion/extraction because of short diffusion length for lithium ion transport within the particles enhances the rate capability and power density. For instance, electrospun $LiCoO_2$ nanofiber cathode has shown improved diffusion and increased migration of Li^+ cation [147].

Transition metal oxides show good electrochemical behavior, however they suffer from poor cycling performance due to their agglomeration and volume changes during cycling. In order to solve this problem carbon nanofibers (CNFs) could be used as matrix for incorporating nano-sized active materials. Decreased lithium ion diffusion distance, increased electron transport rate could be achieved by using CNFs which have high surface area, large porosity, and long fiber lengths [147] Also, dispersing active cathode particles into the carbon nanofiber matrix can prevent large agglomeration of particles [215]. $LiFePO_4$/C [216] $LiFe_{1-y}Mn_yPO_4$/C [217], $Li[Fe_{0.9}Mn_{0.1}]PO_4$/C [218] and Li_2MnSiO_4/C [215] composite nanofibers are some examples of the cathodes that have been reported with 1D nanostructured morphology, improved electrochemical kinetics for the extraction/insertion of the lithium ion, fast ion transport and charge transfer, and improved the overall conductivity due to the presence of CNFs.

Electrical storage capacities of anode materials depend on how much lithium can be stored in the anode. Carbon is commonly used as anodes since it has the merits of low cost, good safety and great cycle life. However, it suffers from low cell voltage, low capacity (theoretical capacity of 372 mAh/g) and low rate capability [17]. CNFs loaded with metal or oxides (MnO_2, Fe_2O_3, Fe_3O4, Co_3O_4, *etc*.) nanoparticles could be used as anodes in which CNFs acts as a structural buffer, particle stabilizer and also electroactive materials while it eliminates binder and conductive additives in the anode materials [4, 17, 219-221]. Figure 1.26A and B show the SEM images of Si/PAN and Si/C nanofiber electrodes. Figure 1.26C and D show the schematic of Si/C nanofiber and capacity of Si/C electrodes.

In addition, CNFs improves distribution of active nanoparticles in the structure that leads to the increase of electrochemically active sites by increasing the specific surface area with highly porous structure and prevents the aggregation of active materials, maintains the structure integrity and thus enhances the electronic conductivity during lithium insertion and extraction (Figure 1.26C) [220-222]. In addition to metal oxides, alloy anode material, silicon (Si), germanium (Ge) and tin (Sn) also suffer from large volume changes and nanoparticle aggregations during lithium insertion and extraction. This problem cause rapid pulverization and capacity loss. Carbon nanofibers have the ability to keep alloy materials in the structure and provide stable cycling performance [2, 18, 219, 222-230]. Shorter distance for lithium ion transport leads to improved reversible capacity while reduced diffusion length and alleviated mechanical stress during the charging/discharging cycles enhance cycling performance in nanostructured anode materials [3, 219, 222, 223, 229].

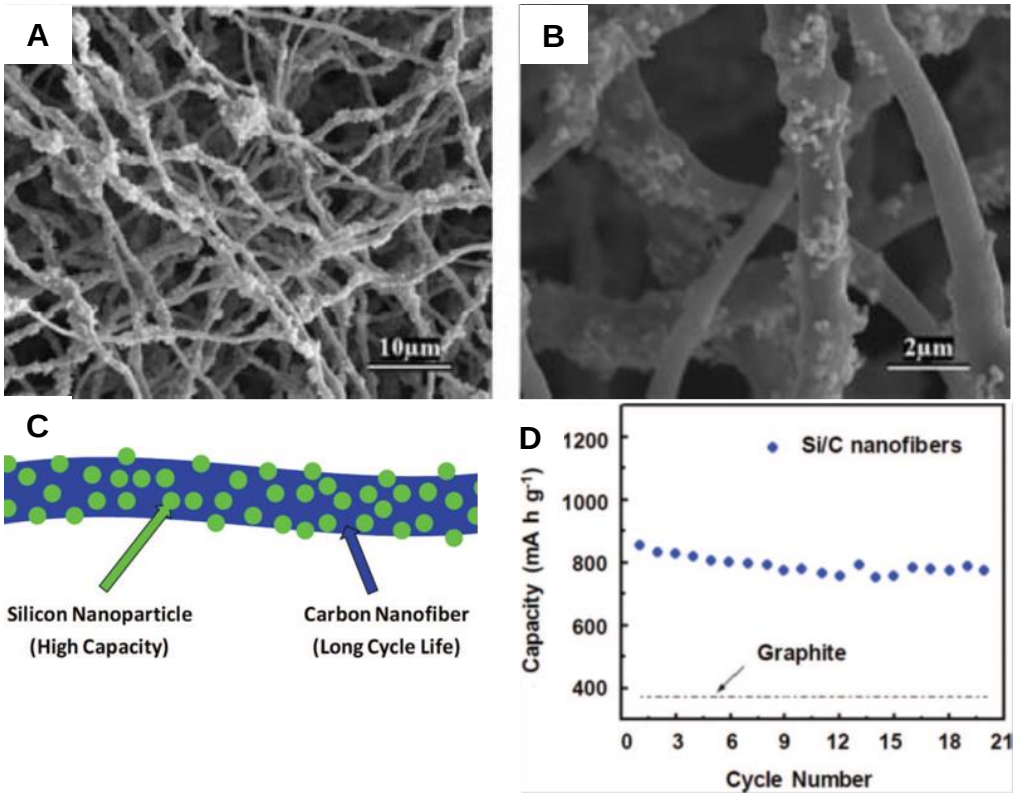

Figure 1.26 SEM images of Si/C nanofibers (A, B), Schematic of a Si/C nanofiber (C), Cycling performance of Si/C nanofiber anode (D) [7].

Electrospun membrane separators show excellent affinity for liquid electrolytes, increase ionic conductivity and enhance the battery performance, so that nanofiber structures are also attractive for designing high-performance separator and electrolyte membranes [7, 15]. There are many studies on membrane separators [13, 75, 125-127, 131, 231] and polymer electrolyte [80, 149, 232-237] which report good battery performance in terms of ionic conductivity, C-rate and cycling performance.

1.4 Overview on centrifugal spinning

1.4.1 Introduction on centrifugal spinning

In recent years, centrifugal spinning has been presented as an alternative to electrospinning due to its high production rate, safety and ease to scale features. In centrifugal spinning technique, nanofibers are obtained by using high-speed rotary and perforated spinneret. Moreover, this technique does not require high-voltage electric field which addresses safety concerns. In addition, high rotational speed gives the opportunity of obtaining fast, 500 times faster than electrospinning, and scalable fiber production [146, 238, 239].

Up to now, many nanofiber mats have been produced by centrifugal spinning such as PAN [146], PVDF [240], silica [238, 241], carbon nanotube reinforced PMMA [242], nylon 6 [243, 244], polypropylene [243, 245], polycaprolactone-polyvinyl pyrrolidone PCL-PVP [246], barium titanate [247], CNT [248], alumina [249] polyhydroxybutyrate [250], PCL, PCL-collagen and PCL-gelatin fibers [251], poly-lactic-co-glycolic acid (PLGA) and PS [252], TiO_2 [253, 254], PEO [255, 256], poly(2,5-bis(20-ethyl-hexyl)-1,4-phenylenevinylene) (BEH-PPV) [257], PCL [258], polyvinylpyrrolidone (PVP) polylactic acid (PLA) [256], poly(acrylic acid) [256] and poly(L-lactic acid) (PLLA) composite fibers [259].

1.4.2 Working principle of centrifugal spinning

The centrifugal spinning system consists of a spinneret, a DC motor, a speed controller, rod collectors, and flexible air foils (Figure 1.27). The spinneret is placed in the center of the spinning platform and contains two small nozzles to extrude polymer solutions.

The DC motor rotates the spinneret and rotational speed is controlled by the speed controller. Air foils help nanofibers travel to the rod collectors [146].

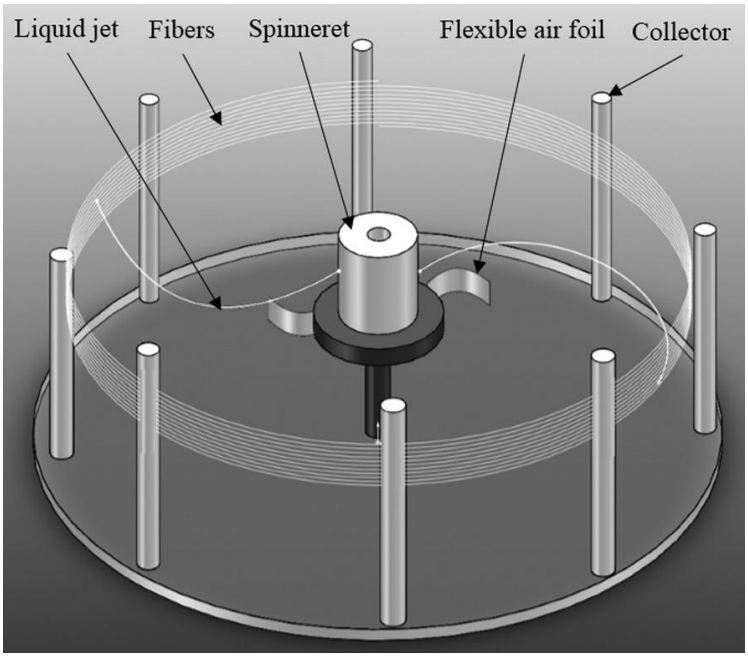

Figure 1.27 Schematic of centrifugal spinning process [146].

The fiber production process includes three steps: jet-initiation to induce flow of the polymer solution through the nozzle, jet-extension to increase surface area of the propelled polymer jet, and solvent evaporation to solidify and shrink the polymer jet [256]. Figure 1.28 shows the mechanism of fiber formation. During spinning, the spinneret which includes the polymer solution rotates and polymer solutions are pushed through the nozzles by applying centrifugal force. When the critical speed is reached, centrifugal force overcomes the surface tension of the solution and ejects a liquid solution from each nozzle. After stretching and rapid solvent evaporation, fibers deposit on rod collectors and forms nonwoven mats [146].

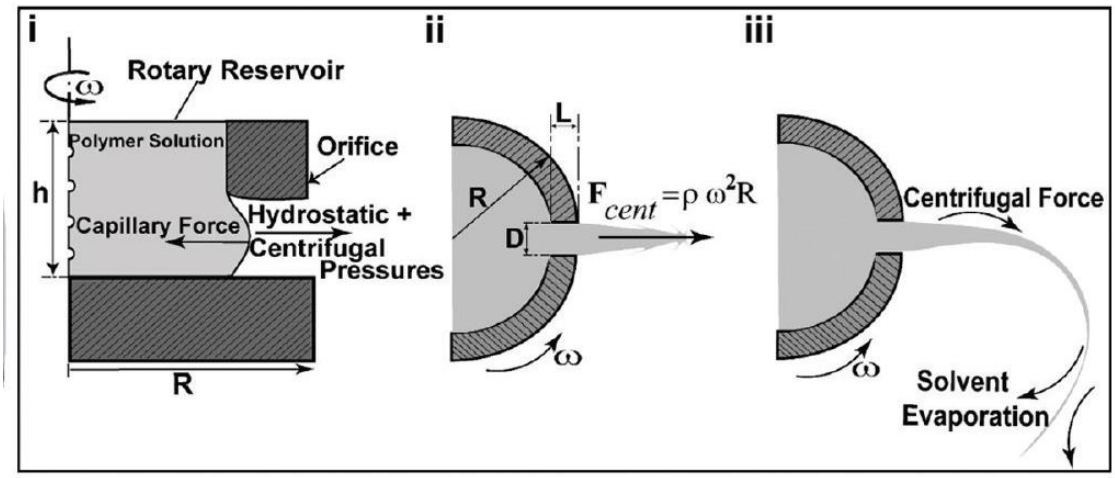

Figure 1.28 Fiber formation mechanism of centrifugal spinning [256].

1.4.3 Parameters of centrifugal spinning

In centrifugal spinning, solution properties (viscosity, surface tension, polymer molecular weight, and solution concentration), solvent type, rotational speed, nozzle diameter, nozzle-collector distance, temperature, collector type, fluid fill level, and solvent evaporation rate are the parameters which affect the morphology of centrifugally-spun fibers [242, 260]. Table 1.5 shows the system and process parameters of centrifugal spinning.

Solution intrinsic properties are important to determine the morphology of fibers. Polymer molecular weight, solvent type, solution concentration, and additives change the rheological behavior and surface tension of the solution as well as the morphology of fibers. In general, too high viscosity prevents jet formation while low viscosity causes bead formation.

Table 1.5 Centrifugal spinning parameters

Centrifugal spinning parameters	
System parameters	Process parameters
Viscosity	Rotational speed
Concentration	Nozzle diameter
Surface tension	Nozzle-collector distance
Polymer molecular weight	Temperature
Solvent type	Collector type

During spinning, rotational forces must be enough to overcome surface tension, however too high forces break jets and cause bead formation. The surface tension causes jet instability and bead formation while the centrifugal force accelerates a slender liquid stream where solvent evaporation and polymer chain elongation occur simultaneously. Therefore, higher centrifugal force induces greater extension and thinning of the polymer jet which results in thinner fiber diameters. If the solvent evaporation rate is too low, fibers may convert into a thin film on the collector due to merging of wet fibers. If the evaporation rate is high, thick fibers are formed. Also, short collector nozzle distance leads to larger fiber diameters [256, 260].

The effect of different parameters on fiber morphology was investigated by Lu et al. [146]. In order to investigate the effect of solution properties, polymer solutions with different concentrations were prepared and spun at constant operational parameters including

rotational speed, nozzle diameter, and nozzle-collector distance. It was found that increasing concentration led to increase in fiber diameter. In addition to solution properties, operational parameters such as rotational speed, nozzle diameter, nozzle-collector distance were also studied. Increasing rotational speed caused to decrease in average fiber diameter and decrease in nozzle diameter led to thinner fiber. Also, longer distance between nozzle and collector caused slightly thinner fibers. Vazquez et al. [240] also investigated the effect of concentration on the morphology of PVDF nanofibers and found similar results with Lu et al. Weng et al. [242] studied carbon nanotube reinforced PMMA nonwoven mats by centrifugal spinning and the most influential parameters were found as viscosity of the solution and angular velocity. McEachin et al.[258] studied PCL fibers and showed the effect of speed on the morphology and fiber diameter. As can be seen from Figure 1.29, fibers spun at 9000 rpm have the least amount of beading.

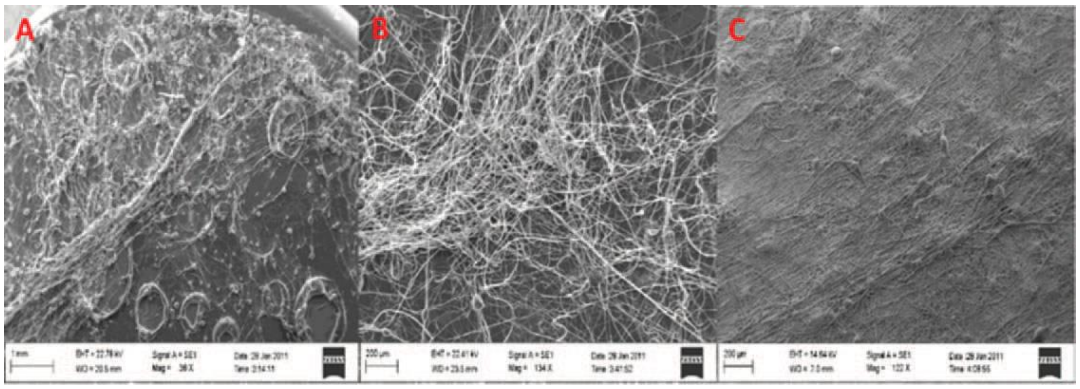

Figure 1.29 Effects of spinneret speed on beading of PCL fiber mats. A: 3000 rpm. B: 6000 rpm. C: 9000 rpm.[258].

Hammami et al. [244] also investigated effect of parameters on fiber morphology by using three different concentrations, three levels of spinneret rotation speed, and two spinneret needle gages for PA6 fibers. Viscosity was found as a major effect on the diameter

and diameter distribution. Krifa et al. [261] studied morphology and frequency of bead-on-string occurrences on centrifugally-spun nano- and sub-micron PA6 fibers. The effect of the spinning solution concentration was significant at all speeds; the number of beads decreased significantly with increased solution viscosity (Figure 1.30). Overall, the smaller diameter needles yielded fibers with fewer beads; however, the difference was less noticeable at high concentrations. Solution concentration and needle size had a significant effect on the bead formation however the spinneret rotation speed did not appear to have any effect on the bead counts.

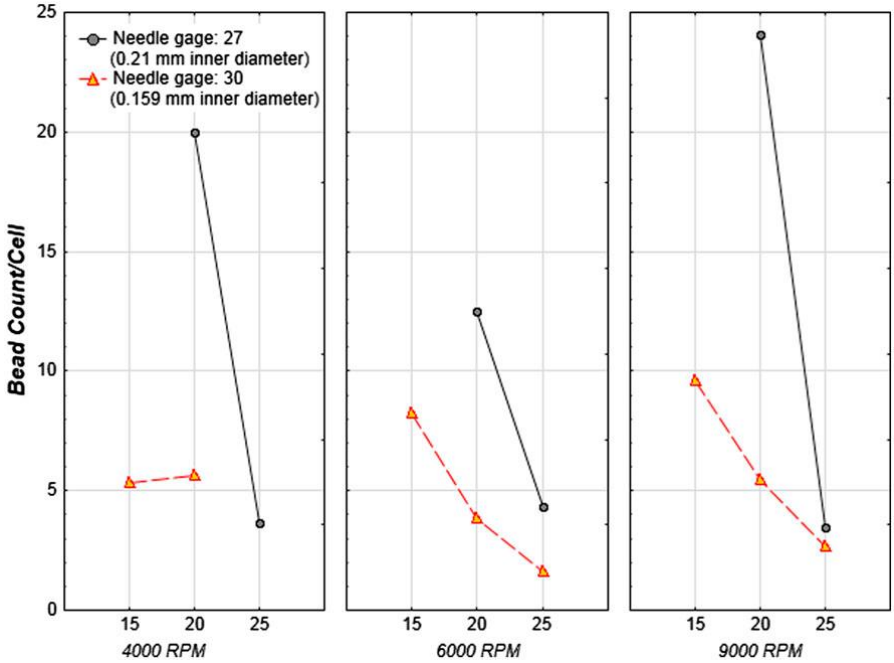

Figure 1.30 Variation of the number of bead-on-string structures as a function of spinning solution concentration, spinneret speed, and needle gage for PA6 fibers [261].

1.4.4 Applications of centrifugal spinning

Centrifugally-spun fibrous webs show high surface area to volume ratio, high degree of alignment, high porosity, and interconnected pores. In addition, fast production and low cost

are the other advantages of centrifugal spinning. Due to these features, centrifugally-spun fibers can be used in tissue engineering, drug delivery, and energy applications [146, 240, 246].

For example, Badrossamay et al. [251] reported the fabrication of centrifugally-spun biohybrid PCL/gelatin and PCL/collagen highly-aligned nanofibers as a scaffold material for a wide variety of biological tissues and organs, and it was found that highly anisotropic fibers were able to support cellular alignment, maturation and self-organization. In another study, Ren et al. [259] fabricated PVP–PLLA composite fiber assemblies for tissue engineering scaffolds and the application of the PLLA fiber assemblies as dermal tissue scaffolds was successfully demonstrated with robust fibroblast cell attachment and proliferation.

Carbon nanofibers can also be prepared by centrifugal spinning of precursor polymers followed by heat treatment of the precursor fibers. The resultant carbon fibers are appropriate for use in energy conversion and storage, semiconductors, aerospace etc [145].

In conclusion, centrifugal spinning is an effective nanofiber fabrication technique which uses high-speed mechanical rotation of polymeric solutions through a rotary spinnneret. It has several advantages in comparison with other nanofiber fabrication methods such as no high-voltage electric fields, simple to implement, and fast production. In addition, an aligned 3D structure can be obtained by varying the collector geometry and fiber morphology (beaded, textured, or smooth), fiber diameters, and web porosity can be manipulated by changing the process variables.

REFERENCES

[1] Z. Lin, L. Ji, M.D. Woodroof, X. Zhang, Electrodeposited MnO< i> x</i>/carbon nanofiber composites for use as anode materials in rechargeable lithium-ion batteries, Journal of Power Sources, 195 (2010) 5025-5031.

[2] Y. Li, B. Guo, L. Ji, Z. Lin, G. Xu, Y. Liang, S. Zhang, O. Toprakci, Y. Hu, M. Alcoutlabi, Structure control and performance improvement of carbon nanofibers containing a dispersion of silicon nanoparticles for energy storage, Carbon, 51 (2013) 185-194.

[3] L. Ji, X. Zhang, Evaluation of Si/carbon composite nanofiber-based insertion anodes for new-generation rechargeable lithium-ion batteries, Energy & Environmental Science, 3 (2010) 124-129.

[4] Y. Wu, P. Zhu, M.V. Reddy, B.V.R. Chowdari, S. Ramakrishna, Maghemite Nanoparticles on Electrospun CNFs Template as Prospective Lithium-Ion Battery Anode, ACS applied materials & interfaces, 6 (2014) 1951-1958.

[5] C. Lai, P. Kolla, Y. Zhao, H. Fong, A.L. Smirnova, Lignin-derived electrospun carbon nanofiber mats with supercritically deposited Ag nanoparticles for oxygen reduction reaction in alkaline fuel cells, Electrochimica Acta, 130 (2014) 431-438.

[6] M. Winter, R.J. Brodd, What are batteries, fuel cells, and supercapacitors?, Chemical reviews, 104 (2004) 4245-4270.

[7] X. Zhang, L. Ji, O. Toprakci, Y. Liang, M. Alcoutlabi, Electrospun nanofiber-based anodes, cathodes, and separators for advanced lithium-ion batteries, Polymer Reviews, 51 (2011) 239-264.

[8] J.O. Besenhard, Handbook of Battery Materials, Second Edition, 2011.

[9] J.-K. Park, Principles and applications of lithium secondary batteries, John Wiley & Sons2012.

[10] D.A. Skoog, Principles of Instrumental Analysis.

[11] http://www2.ohlone.edu/people/jklent/labs/101B_labs/Voltaic%20Cells.pdf.

[12] V. Etacheri, R. Marom, R. Elazari, G. Salitra, D. Aurbach, Challenges in the development of advanced Li-ion batteries: a review, Energy & Environmental Science, 4 (2011) 3243-3262.

[13] M. Yanilmaz, Y. Lu, M. Dirican, K. Fu, X. Zhang, Nanoparticle-on-Nanofiber Hybrid Membrane Separators for Lithium-ion Batteries via Combining Electrospraying and Electrospinning Techniques, Journal of Membrane Science, (2014).

[14] B.J. Landi, M.J. Ganter, C.D. Cress, R.A. DiLeo, R.P. Raffaelle, Carbon nanotubes for lithium ion batteries, Energy & Environmental Science, 2 (2009) 638-654.

[15] L. Ji, Z. Lin, M. Alcoutlabi, X. Zhang, Recent developments in nanostructured anode materials for rechargeable lithium-ion batteries, Energy & Environmental Science, 4 (2011) 2682-2699.

[16] P. Verma, P. Maire, P. Novák, A review of the features and analyses of the solid electrolyte interphase in Li-ion batteries, Electrochimica Acta, 55 (2010) 6332-6341.

[17] S. Cavaliere, S. Subianto, I. Savych, D.J. Jones, J. Rozière, Electrospinning: designed architectures for energy conversion and storage devices, Energy & Environmental Science, 4 (2011) 4761-4785.

[18] L. Ji, X. Zhang, Electrospun carbon nanofibers containing silicon particles as an energy-storage medium, Carbon, 47 (2009) 3219-3226.

[19] X. Jia, C. Yan, Z. Chen, R. Wang, Q. Zhang, L. Guo, F. Wei, Y. Lu, Direct growth of flexible LiMn 2 O 4/CNT lithium-ion cathodes, Chemical Communications, 47 (2011) 9669-9671.

[20] L. Jabbour, C. Gerbaldi, D. Chaussy, E. Zeno, S. Bodoardo, D. Beneventi, Microfibrillated cellulose–graphite nanocomposites for highly flexible paper-like Li-ion battery electrodes, Journal of Materials Chemistry, 20 (2010) 7344-7347.

[21] R. Mukherjee, R. Krishnan, T.-M. Lu, N. Koratkar, Nanostructured electrodes for high-power lithium ion batteries, Nano Energy, 1 (2012) 518-533.

[22] J.W. Fergus, Recent developments in cathode materials for lithium ion batteries, Journal of Power Sources, 195 (2010) 939-954.

[23] C. Chang, J. Xiang, X. Shi, X. Han, L. Yuan, J. Sun, Rheological phase reaction synthesis and electrochemical performance of Li3V2 (PO4)(3)/carbon cathode for lithium ion batteries, Electrochimica Acta, 53 (2008) 2232-2237.

[24] D. Doughty, E.P. Roth, A general discussion of Li ion battery safety, Electrochemical Society Interface, 21 (2012) 37-44.

[25] L. Fu, H. Liu, C. Li, Y. Wu, E. Rahm, R. Holze, H. Wu, Surface modifications of electrode materials for lithium ion batteries, Solid State Sciences, 8 (2006) 113-128.

[26] X. Huang, Separator technologies for lithium-ion batteries, Journal of Solid State Electrochemistry, 15 (2011) 649-662.

[27] H. Lee, M. Yanilmaz, O. Toprakci, K. Fu, X. Zhang, A Review and Recent Developments in Membrane Separators for Rechargeable Lithium-ion Batteries, Energy & Environmental Science, (2014).

[28] S.S. Zhang, A review on the separators of liquid electrolyte Li-ion batteries, Journal of Power Sources, 164 (2007) 351-364.

[29] R.S. Baldwin, A review of state-of-the-art separator materials for advanced lithium-based batteries for future aerospace missions, National Aeronautics and Space Administration, Glenn Research Center, Cleveland, Ohio, 2009.

[30] M. Yang, J. Hou, Membranes in lithium ion batteries, Membranes, 2 (2012) 367-383.

[31] C.J. Orendorff, The role of separators in lithium-ion cell safety, Electrochemical Society Interface, 21 (2012) 61-65.

[32] G. Venugopal, J. Moore, J. Howard, S. Pendalwar, Characterization of microporous separators for lithium-ion batteries, Journal of Power Sources, 77 (1999) 34-41.

[33] K. Prasanna, C.W. Lee, Physical, thermal, and electrochemical characterization of stretched polyethylene separators for application in lithium-ion batteries, Journal of Solid State Electrochemistry, 17 (2013) 1377-1382.

[34] Z.-Y. Cui, Y.-Y. Xu, L.-P. Zhu, J.-Y. Wang, Z.-Y. Xi, B.-K. Zhu, Preparation of PVDF/PEO-PPO-PEO blend microporous membranes for lithium ion batteries via thermally induced phase separation process, Journal of Membrane Science, 325 (2008) 957-963.

[35] Y. Huai, J. Gao, Z. Deng, J. Suo, Preparation and characterization of a special structural poly (acrylonitrile)-based microporous membrane for lithium-ion batteries, Ionics, 16 (2010) 603-611.

[36] F. Boudin, X. Andrieu, C. Jehoulet, I. Olsen, Microporous PVdF gel for lithium-ion batteries, Journal of Power Sources, 81 (1999) 804-807.

[37] J.Y. Han, H.H. Oh, K. Jun Choi, B.R. Min, Characterization of poly (vinylidene fluoride) flat sheet membranes prepared in various ratios of water/ethanol for separator of li-

ion batteries: Morphology and other properties, Journal of Applied Polymer Science, 122 (2011) 2653-2665.

[38] S. Zhang, M. Ervin, K. Xu, T. Jow, Microporous poly (acrylonitrile-methyl methacrylate) membrane as a separator of rechargeable lithium battery, Electrochimica Acta, 49 (2004) 3339-3345.

[39] H. Li, C.-E. Lin, J.-L. Shi, X.-T. Ma, B.-K. Zhu, L.-P. Zhu, Preparation and characterization of safety PVDF/P (MMA-co-PEGMA) active separators by studying the liquid electrolyte distribution in this kind of membrane, Electrochimica Acta, 115 (2014) 317-325.

[40] Y.J. Hwang, K.S. Nahm, T.P. Kumar, A.M. Stephan, Poly (vinylidene fluoride-hexafluoropropylene)-based membranes for lithium batteries, Journal of Membrane Science, 310 (2008) 349-355.

[41] T. Ma, Z. Cui, Y. Wu, S. Qin, H. Wang, F. Yan, N. Han, J. Li, Preparation of PVDF based blend microporous membranes for lithium ion batteries by thermally induced phase separation: I. Effect of PMMA on the membrane formation process and the properties, Journal of Membrane Science, 444 (2013) 213-222.

[42] Q. Cheng, Z. Cui, J. Li, S. Qin, F. Yan, J. Li, Preparation and performance of polymer electrolyte based on poly (vinylidene fluoride)/polysulfone blend membrane via thermally induced phase separation process for lithium ion battery, Journal of Power Sources, 266 (2014) 401-413.

[43] H. Huang, S.L. Wunder, Ionic conductivity of microporous PVDF-HFP/PS polymer blends, journal of the Electrochemical Society, 148 (2001) A279-A283.

[44] C. Costa, L. Rodrigues, V. Sencadas, M. Silva, J. Rocha, S. Lanceros-Méndez, Effect of degree of porosity on the properties of poly (vinylidene fluoride–trifluorethylene) for Li-ion battery separators, Journal of Membrane Science, 407 (2012) 193-201.

[45] W. Pu, X. He, L. Wang, Z. Tian, C. Jiang, C. Wan, Preparation of P (AN–MMA) microporous membrane for Li-ion batteries by phase inversion, Journal of Membrane Science, 280 (2006) 6-9.

[46] W. Pu, X. He, L. Wang, C. Jiang, C. Wan, Preparation of PVDF–HFP microporous membrane for Li-ion batteries by phase inversion, Journal of Membrane Science, 272 (2006) 11-14.

[47] A. Subramania, N. Sundaram, G.V. Kumar, Structural and electrochemical properties of micro-porous polymer blend electrolytes based on PVdF-< i> co</i>-HFP-PAN for Li-ion battery applications, Journal of Power Sources, 153 (2006) 177-182.

[48] K.J. Kim, M.-S. Park, H. Kim, Y.-J. Kim, Thermal Stability Enhancement of Polyethylene Separators by Gamma-ray Irradiation for Lithium Ion Batteries, Japanese Journal of Applied Physics, 51 (2012) 09MB03.

[49] K.J. Kim, M.-S. Park, T. Yim, J.-S. Yu, Y.-J. Kim, Electron-beam-irradiated polyethylene membrane with improved electrochemical and thermal properties for lithium-ion batteries, Journal of Applied Electrochemistry, 44 (2014) 345-352.

[50] J.L. Gineste, Polypropylene separator grafted with hydrophilic monomers for lithium batteries, Journal of Membrane Science, 107 (1995) 155-164.

[51] S.-J. Gwon, J.-H. Choi, J.-Y. Sohn, S.-J. An, Y.-E. Ihm, Y.-C. Nho, Radiation grafting of methyl methacrylate onto polyethylene separators for lithium secondary batteries, Nuclear

Instruments and Methods in Physics Research Section B: Beam Interactions with Materials and Atoms, 266 (2008) 3387-3391.

[52] S.-J. Gwon, J.-H. Choi, J.-Y. Sohn, Y.-M. Lim, Y.-C. Nho, Y.-E. Ihm, Battery performance of PMMA-grafted PE separators prepared by pre-irradiation grafting technique, Journal of Industrial and Engineering Chemistry, 15 (2009) 748-751.

[53] J.Y. Lee, B. Bhattacharya, Y.-C. Nho, J.-K. Park, New separator prepared by electron beam irradiation for high voltage lithium secondary batteries, Nuclear Instruments and Methods in Physics Research Section B: Beam Interactions with Materials and Atoms, 267 (2009) 2390-2394.

[54] J.Y. Lee, Y.M. Lee, B. Bhattacharya, Y.-C. Nho, J.-K. Park, Separator grafted with siloxane by electron beam irradiation for lithium secondary batteries, Electrochimica Acta, 54 (2009) 4312-4315.

[55] L.-F. Fang, J.-L. Shi, B.-K. Zhu, L.-P. Zhu, Facile introduction of polyether chains onto polypropylene separators and its application in lithium ion batteries, Journal of Membrane Science, 448 (2013) 143-150.

[56] J.Y. Kim, D.Y. Lim, Surface-modified membrane as a separator for lithium-ion polymer battery, Energies, 3 (2010) 866-885.

[57] J.Y. Kim, Y. Lee, D.Y. Lim, Plasma-modified polyethylene membrane as a separator for lithium-ion polymer battery, Electrochimica Acta, 54 (2009) 3714-3719.

[58] C. Huang, C.C. Lin, C.Y. Tsai, R.S. Juang, Tailoring Surface Properties of Polymeric Separators for Lithium-Ion Batteries by Cyclonic Atmospheric-Pressure Plasma, Plasma Processes and Polymers, 10 (2013) 407-415.

[59] Z. Li, L. Ju, D. Li, J. Zheng, Y. Xu, The MMA and SO3Li-grafted polypropylene separator used in Li ion batteries, Ionics, 18 (2012) 673-677.

[60] J.-Y. Sohn, J.-S. Im, J. Shin, Y.-C. Nho, PVDF-HFP/PMMA-coated PE separator for lithium ion battery, Journal of Solid State Electrochemistry, 16 (2012) 551-556.

[61] M. Xiong, H. Tang, Y. Wang, M. Pan, Ethylcellulose-coated polyolefin separators for lithium-ion batteries with improved safety performance, Carbohydrate polymers, 101 (2014) 1140-1146.

[62] H. Lee, M. Alcoutlabi, O. Toprakci, G. Xu, J.V. Watson, X. Zhang, Preparation and characterization of electrospun nanofiber-coated membrane separators for lithium-ion batteries, Journal of Solid State Electrochemistry, (2014) 1-8.

[63] Y.-B. Jeong, D.-W. Kim, Effect of thickness of coating layer on polymer-coated separator on cycling performance of lithium-ion polymer cells, Journal of Power Sources, 128 (2004) 256-262.

[64] L.-F. Fang, J.-L. Shi, H. Li, B.-K. Zhu, L.-P. Zhu, Construction of porous coating layer and electrochemical performances of the corresponding modified polyethylene separators for lithium ion batteries, Journal of Applied Polymer Science, 131 (2014) n/a-n/a.

[65] Y. Chung, S. Yoo, C. Kim, Enhancement of meltdown temperature of the polyethylene lithium-ion battery separator via surface coating with polymers having high thermal resistance, Industrial & Engineering Chemistry Research, 48 (2009) 4346-4351.

[66] D.-W. Kim, J.-M. Ko, J.-H. Chun, S.-H. Kim, J.-K. Park, Electrochemical performances of lithium-ion cells prepared with polyethylene oxide-coated separators, Electrochemistry Communications, 3 (2001) 535-538.

[67] J. Song, M.-H. Ryou, B. Son, J.-N. Lee, D.J. Lee, Y.M. Lee, J.W. Choi, J.-K. Park, Co-polyimide-coated polyethylene separators for enhanced thermal stability of lithium ion batteries, Electrochimica Acta, (2012).

[68] D. Wang, Z. Zhao, L. Yu, K. Zhang, H. Na, S. Ying, D. Xu, G. Zhang, Polydopamine hydrophilic modification of polypropylene separator for lithium ion battery, Journal of Applied Polymer Science, 131 (2014).

[69] Y. Lee, M.-H. Ryou, M. Seo, J.W. Choi, Y.M. Lee, Effect of polydopamine surface coating on polyethylene separators as a function of their porosity for high-power Li-ion batteries, Electrochimica Acta, 113 (2013) 433-438.

[70] J.-L. Shi, L.-F. Fang, H. Li, H. Zhang, B.-K. Zhu, L.-P. Zhu, Improved thermal and electrochemical performances of PMMA modified PE separator skeleton prepared via dopamine-initiated ATRP for lithium ion batteries, Journal of Membrane Science, 437 (2013) 160-168.

[71] K. Hwang, B. Kwon, H. Byun, Preparation of PVdF nanofiber membranes by electrospinning and their use as secondary battery separators, Journal of Membrane Science, 378 (2011) 111-116.

[72] K. Gao, X. Hu, C. Dai, T. Yi, Crystal structures of electrospun PVDF membranes and its separator application for rechargeable lithium metal cells, Materials Science and Engineering: B, 131 (2006) 100-105.

[73] C. Costa, J. Nunes-Pereira, V. Sencadas, M. Silva, S. Lanceros-Méndez, Effect of fiber orientation in gelled poly (vinylidene fluoride) electrospun membranes for Li-ion battery applications, Journal of Materials Science, 48 (2013) 6833-6840.

[74] C. Yang, Z. Jia, Z. Guan, L. Wang, Polyvinylidene fluoride membrane by novel electrospinning system for separator of Li-ion batteries, Journal of Power Sources, 189 (2009) 716-720.

[75] Y. Liang, S. Cheng, J. Zhao, C. Zhang, S. Sun, N. Zhou, Y. Qiu, X. Zhang, Heat treatment of electrospun PVDF fibrous membrane separators for rechargeable lithium-ion batteries, Journal of Power Sources, (2013).

[76] C. Cao, L. Tan, W. Liu, J. Ma, L. Li, Polydopamine coated electrospun poly (vinyldiene fluoride) nanofibrous membrane as separator for lithium-ion batteries, Journal of Power Sources, 248 (2014) 224-229.

[77] P. Raghavan, X. Zhao, J. Manuel, C. Shin, M.-Y. Heo, J.-H. Ahn, H.-S. Ryu, H.-J. Ahn, J.-P. Noh, G.-B. Cho, Electrochemical studies on polymer electrolytes based on poly (vinylidene fluoride-< i> co</i>-hexafluoropropylene) membranes prepared by electrospinning and phase inversion—A comparative study, Materials Research Bulletin, 45 (2010) 362-366.

[78] T. Cho, T. Sakai, S. Tanase, K. Kimura, Y. Kondo, T. Tarao, M. Tanaka, Electrochemical performances of polyacrylonitrile nanofiber-based nonwoven separator for lithium-ion battery, Electrochemical and Solid-State Letters, 10 (2007) A159-A162.

[79] T.-H. Cho, M. Tanaka, H. Onishi, Y. Kondo, T. Nakamura, H. Yamazaki, S. Tanase, T. Sakai, Battery performances and thermal stability of polyacrylonitrile nano-fiber-based nonwoven separators for Li-ion battery, Journal of Power Sources, 181 (2008) 155-160.

[80] A.I. Gopalan, P. Santhosh, K.M. Manesh, J.H. Nho, S.H. Kim, C.-G. Hwang, K.-P. Lee, Development of electrospun PVdF–PAN membrane-based polymer electrolytes for lithium batteries, Journal of Membrane Science, 325 (2008) 683-690.

[81] A.I. Gopalan, K.-P. Lee, K.M. Manesh, P. Santhosh, Poly (vinylidene fluoride)–polydiphenylamine composite electrospun membrane as high-performance polymer electrolyte for lithium batteries, Journal of Membrane Science, 318 (2008) 422-428.

[82] X. Li, Q. Cao, X. Wang, S. Jiang, H. Deng, N. Wu, Preparation of poly (vinylidene fluoride)/poly (methyl methacrylate) membranes by novel electrospinning system for lithium ion batteries, Journal of Applied Polymer Science, 122 (2011) 2616-2620.

[83] N. Angulakshmi, A.M. Stephan, Electrospun Trilayer Polymeric Membranes as Separator for Lithium–ion Batteries, Electrochimica Acta, 127 (2014) 167-172.

[84] Z. Zhong, Q. Cao, B. Jing, X. Wang, X. Li, H. Deng, Electrospun PVdF–PVC nanofibrous polymer electrolytes for polymer lithium-ion batteries, Materials Science and Engineering: B, 177 (2012) 86-91.

[85] L. Zhao, H. Zhang, X. Li, J. Zhao, C. Zhao, X. Yuan, Modification of electrospun poly (vinylidene fluoride-co-hexafluoropropylene) membranes through the introduction of poly (ethylene glycol) dimethacrylate, Journal of Applied Polymer Science, 111 (2009) 3104-3112.

[86] Y. Ding, P. Zhang, Z. Long, Y. Jiang, F. Xu, W. Di, The ionic conductivity and mechanical property of electrospun P (VdF-HFP)/PMMA membranes for lithium ion batteries, Journal of Membrane Science, 329 (2009) 56-59.

[87] W. Jiang, Z. Liu, Q. Kong, J. Yao, C. Zhang, P. Han, G. Cui, A high temperature operating nanofibrous polyimide separator in Li-ion battery, Solid State Ionics, 232 (2013) 44-48.

[88] X. Zhou, L. Yue, J. Zhang, Q. Kong, Z. Liu, J. Yao, G. Cui, A core-shell structured polysulfonamide-based composite nonwoven towards high power lithium ion battery separator, journal of the Electrochemical Society, 160 (2013) A1341-A1347.

[89] J. Hao, G. Lei, Z. Li, L. Wu, Q. Xiao, L. Wang, A novel polyethylene terephthalate nonwoven separator based on electrospinning technique for lithium ion battery, Journal of Membrane Science, 428 (2013) 11-16.

[90] C.J. Orendorff, T.N. Lambert, C.A. Chavez, M. Bencomo, K.R. Fenton, Polyester Separators for Lithium-Ion Cells: Improving Thermal Stability and Abuse Tolerance, Advanced Energy Materials, (2012).

[91] J.-H. Cho, J.-H. Park, J.H. Kim, S.-Y. Lee, Facile fabrication of nanoporous composite separator membranes for lithium-ion batteries: poly(methyl methacrylate) colloidal particles-embedded nonwoven poly(ethylene terephthalate), Journal of Materials Chemistry, 21 (2011) 8192-8198.

[92] H.-S. Jeong, J.H. Kim, S.-Y. Lee, A novel poly(vinylidene fluoride-hexafluoropropylene)/poly(ethylene terephthalate) composite nonwoven separator with phase inversion-controlled microporous structure for a lithium-ion battery, Journal of Materials Chemistry, 20 (2010) 9180-9186.

[93] J. Hao, G. Lei, Z. Li, L. Wu, Q. Xiao, L. Wang, A novel polyethylene terephthalate nonwoven separator based on electrospinning technique for lithium ion battery, Journal of Membrane Science, 428 (2013) 11-16.

[94] H.-S. Jeong, E.-S. Choi, J.H. Kim, S.-Y. Lee, Potential application of microporous structured poly(vinylidene fluoride-hexafluoropropylene)/poly(ethylene terephthalate)

composite nonwoven separators to high-voltage and high-power lithium-ion batteries, Electrochimica Acta, 56 (2011) 5201-5204.

[95] W. Qi, C. Lu, P. Chen, L. Han, Q. Yu, R. Xu, Electrochemical performances and thermal properties of electrospun Poly (phthalazinone ether sulfone ketone) membrane for lithium-ion battery, Materials Letters, 66 (2012) 239-241.

[96] C. Lu, W. Qi, L. Li, J. Xu, P. Chen, R. Xu, L. Han, Q. Yu, Electrochemical performance and thermal property of electrospun PPESK/PVDF/PPESK composite separator for lithium-ion battery, Journal of Applied Electrochemistry, 43 (2013) 711-720.

[97] J. Zhang, Z. Liu, Q. Kong, C. Zhang, S. Pang, L. Yue, X. Wang, J. Yao, G. Cui, Renewable and superior thermal-resistant cellulose-based composite nonwoven as lithium-ion battery separator, ACS applied materials & interfaces, 5 (2012) 128-134.

[98] Q. Xu, Q. Kong, Z. Liu, X. Wang, R. Liu, J. Zhang, L. Yue, Y. Duan, G. Cui, Cellulose/Polysulfonamide Composite Membrane as a High Performance Lithium-Ion Battery Separator, ACS Sustainable Chemistry & Engineering, 2 (2013) 194-199.

[99] L. Yue, J. Zhang, Z. Liu, Q. Kong, X. Zhou, Q. Xu, J. Yao, G. Cui, A Heat Resistant and Flame-Retardant Polysulfonamide/Polypropylene Composite Nonwoven for High Performance Lithium Ion Battery Separator, journal of the Electrochemical Society, 161 (2014) A1032-A1038.

[100] Q. Xu, Q. Kong, Z. Liu, J. Zhang, X. Wang, R. Liu, L. Yue, G. Cui, Polydopamine-coated cellulose microfibrillated membrane as high performance lithium-ion battery separator, RSC Advances, 4 (2014) 7845-7850.

[101] Y.-J. Kim, C.H. Ahn, M.B. Lee, M.-S. Choi, Characteristics of electrospun PVDF/SiO< sub> 2</sub> composite nanofiber membranes as polymer electrolyte, Materials Chemistry and Physics, 127 (2011) 137-142.

[102] H.S. Jeong, J.H. Noh, C.G. Hwang, S.H. Kim, S.Y. Lee, Effect of Solvent–Nonsolvent Miscibility on Morphology and Electrochemical Performance of SiO2/PVdF-HFP-Based Composite Separator Membranes for Safer Lithium-Ion Batteries, Macromolecular Chemistry and Physics, 211 (2010) 420-425.

[103] D. Fu, B. Luan, S. Argue, M.N. Bureau, I.J. Davidson, Nano SiO< sub> 2</sub> particle formation and deposition on polypropylene separators for lithium-ion batteries, Journal of Power Sources, 206 (2012) 325-333.

[104] Y.-S. Lee, Y.B. Jeong, D.-W. Kim, Cycling performance of lithium-ion batteries assembled with a hybrid composite membrane prepared by an electrospinning method, Journal of Power Sources, 195 (2010) 6197-6201.

[105] J.-H. Park, J.-H. Cho, W. Park, D. Ryoo, S.-J. Yoon, J.H. Kim, Y.U. Jeong, S.-Y. Lee, Close-packed SiO< sub> 2</sub>/poly (methyl methacrylate) binary nanoparticles-coated polyethylene separators for lithium-ion batteries, Journal of Power Sources, 195 (2010) 8306-8310.

[106] M. Kim, J.H. Park, Inorganic thin layer coated porous separator with high thermal stability for safety reinforced Li-ion battery, Journal of Power Sources, 212 (2012) 22-27.

[107] H. Chen, Q. Lin, Q. Xu, Y. Yang, Z. Shao, Y. Wang, Plasma activation and atomic layer deposition of TiO2 on polypropylene membranes for improved performances of lithium-ion batteries, Journal of Membrane Science, 458 (2014) 217-224.

[108] K.J. Kim, H.K. Kwon, M.-S. Park, T. Yim, J.-S. Yu, Y.-J. Kim, Ceramic composite separators coated with moisturized ZrO 2 nanoparticles for improving the electrochemical performance and thermal stability of lithium ion batteries, Physical Chemistry Chemical Physics, 16 (2014) 9337-9343.

[109] H.-S. Jeong, S.-Y. Lee, Closely packed SiO2 nanoparticles/poly(vinylidene fluoride-hexafluoropropylene) layers-coated polyethylene separators for lithium-ion batteries, Journal of Power Sources, 196 (2011) 6716-6722.

[110] W.-K. Shin, D.-W. Kim, High performance ceramic-coated separators prepared with lithium ion-containing SiO< sub> 2</sub> particles for lithium-ion batteries, Journal of Power Sources, 226 (2013) 54-60.

[111] H.-S. Jeong, S.C. Hong, S.-Y. Lee, Effect of microporous structure on thermal shrinkage and electrochemical performance of Al< sub> 2</sub> O< sub> 3</sub>/poly (vinylidene fluoride-hexafluoropropylene) composite separators for lithium-ion batteries, Journal of Membrane Science, 364 (2010) 177-182.

[112] J. Fang, A. Kelarakis, Y.-W. Lin, C.-Y. Kang, M.-H. Yang, C.-L. Cheng, Y. Wang, E.P. Giannelis, L.-D. Tsai, Nanoparticle-coated separators for lithium-ion batteries with advanced electrochemical performance, Physical Chemistry Chemical Physics, 13 (2011) 14457-14461.

[113] C. Shi, P. Zhang, L. Chen, P. Yang, J. Zhao, Effect of a thin ceramic-coating layer on thermal and electrochemical properties of polyethylene separator for lithium-ion batteries, Journal of Power Sources, (2014).

[114] M. Rao, J. Liu, W. Li, Y. Liao, Y. Liang, L. Zhao, Polyethylene-supported poly (acrylonitrile-co-methyl methacrylate)/nano-Al2O3 microporous composite polymer

electrolyte for lithium ion battery, Journal of Solid State Electrochemistry, 14 (2010) 255-261.

[115] K. Prasanna, C.-S. Kim, C.W. Lee, Effect of SiO2 coating on polyethylene separator with different stretching ratios for application in lithium ion batteries, Materials Chemistry and Physics, 146 (2014) 545-550.

[116] H. Liu, J. Xu, B. Guo, X. He, Preparation and performance of silica/polypropylene composite separator for lithium-ion batteries, Journal of Materials Science, 49 (2014) 6961-6966.

[117] D. Takemura, S. Aihara, K. Hamano, M. Kise, T. Nishimura, H. Urushibata, H. Yoshiyasu, A powder particle size effect on ceramic powder based separator for lithium rechargeable battery, Journal of Power Sources, 146 (2005) 779-783.

[118] P.P. Prosini, P. Villano, M. Carewska, A novel intrinsically porous separator for self-standing lithium-ion batteries, Electrochimica Acta, 48 (2002) 227-233.

[119] G.B. Appetecchi, P. Romagnoli, B. Scrosati, Composite gel membranes: a new class of improved polymer electrolytes for lithium batteries, Electrochemistry Communications, 3 (2001) 281-284.

[120] X. Huang, Development and characterization of a bilayer separator for lithium ion batteries, Journal of Power Sources, 196 (2011) 8125-8128.

[121] H. Wang, H. Li, L. Yu, Y. Jiang, K. Wang, Synthesis of porous Al2O3-PVDF composite separators and their application in lithium-ion batteries, Journal of Applied Polymer Science, 130 (2013) 2886-2890.

[122] F. Zhang, X. Ma, C. Cao, J. Li, Y. Zhu, Poly(vinylidene fluoride)/SiO2 composite membranes prepared by electrospinning and their excellent properties for nonwoven separators for lithium-ion batteries, Journal of Power Sources, 251 (2014) 423-431.

[123] M. Sethupathy, V. Sethuraman, P. Manisankar, Preparation of PVDF/SiO2 Composite Nanofiber Membrane Using Electrospinning for Polymer Electrolyte Analysis, Soft Nanoscience Letters, 3 (2013) 37.

[124] Y. Ding, P. Zhang, Z. Long, Y. Jiang, F. Xu, W. Di, Preparation of PVdF-based electrospun membranes and their application as separators, Science and Technology of Advanced Materials, 9 (2008) 015005.

[125] H.-R. Jung, D.-H. Ju, W.-J. Lee, X. Zhang, R. Kotek, Electrospun hydrophilic fumed silica/polyacrylonitrile nanofiber-based composite electrolyte membranes, Electrochimica Acta, 54 (2009) 3630-3637.

[126] Y. Liang, L. Ji, B. Guo, Z. Lin, Y. Yao, Y. Li, M. Alcoutlabi, Y. Qiu, X. Zhang, Preparation and electrochemical characterization of ionic-conducting lithium lanthanum titanate oxide/polyacrylonitrile submicron composite fiber-based lithium-ion battery separators, Journal of Power Sources, 196 (2011) 436-441.

[127] Y. Liang, Z. Lin, Y. Qiu, X. Zhang, Fabrication and characterization of LATP/PAN composite fiber-based lithium-ion battery separators, Electrochimica Acta, 56 (2011) 6474-6480.

[128] Y.-J. Kim, C.H. Ahn, M.O. Choi, Effect of thermal treatment on the characteristics of electrospun PVDF− silica composite nanofibrous membrane, European Polymer Journal, 46 (2010) 1957-1965.

[129] T.-H. Cho, M. Tanaka, H. Ohnishi, Y. Kondo, M. Yoshikazu, T. Nakamura, T. Sakai, Composite nonwoven separator for lithium-ion battery: Development and characterization, Journal of Power Sources, 195 (2010) 4272-4277.

[130] T.-H. Cho, M. Tanaka, H. Onishi, Y. Kondo, T. Nakamura, H. Yamazaki, S. Tanase, T. Sakai, Silica-composite nonwoven separators for lithium-ion battery: Development and characterization, journal of the Electrochemical Society, 155 (2008) A699-A703.

[131] M. Yanilmaz, M. Dirican, X. Zhang, Evaluation of electrospun SiO< sub> 2</sub>/nylon 6, 6 nanofiber membranes as a thermally-stable separator for lithium-ion batteries, Electrochimica Acta, (2014).

[132] J. Zhang, L. Yue, Q. Kong, Z. Liu, X. Zhou, C. Zhang, S. Pang, X. Wang, J. Yao, G. Cui, A Heat-Resistant Silica Nanoparticle Enhanced Polysulfonamide Nonwoven Separator for High-Performance Lithium Ion Battery, journal of the Electrochemical Society, 160 (2013) A769-A774.

[133] J. Lee, C.-L. Lee, K. Park, I.-D. Kim, Synthesis of an Al2O3-coated polyimide nanofiber mat and its electrochemical characteristics as a separator for lithium ion batteries, Journal of Power Sources, 248 (2014) 1211-1217.

[134] J.-R. Lee, N.-Y. Kim, M.-S. Lee, S.-Y. Lee, SiO2-coated polyimide nonwoven/Nafion composite membranes for proton exchange membrane fuel cells, Journal of Membrane Science, 367 (2011) 265-272.

[135] E.-S. Choi, S.-Y. Lee, Particle size-dependent, tunable porous structure of a SiO2/poly(vinylidene fluoride-hexafluoropropylene)-coated poly(ethylene terephthalate) nonwoven composite separator for a lithium-ion battery, Journal of Materials Chemistry, 21 (2011) 14747-14754.

[136] H.-S. Jeong, E.-S. Choi, S.-Y. Lee, Composition ratio-dependent structural evolution of SiO2/poly(vinylidene fluoride-hexafluoropropylene)-coated poly(ethylene terephthalate) nonwoven composite separators for lithium-ion batteries, Electrochimica Acta, 86 (2012) 317-322.

[137] J.-R. Lee, J.-H. Won, S.-Y. Lee, SiO2/styrene butadiene rubber-coated poly (ethylene terephthalate) nonwoven composite separators for safer lithium-ion batteries, Journal of Electrochemical Science and Technology, 2 (2011) 51-56.

[138] J.-R. Lee, J.-H. Won, J.H. Kim, K.J. Kim, S.-Y. Lee, Evaporation-induced self-assembled silica colloidal particle-assisted nanoporous structural evolution of poly(ethylene terephthalate) nonwoven composite separators for high-safety/high-rate lithium-ion batteries, Journal of Power Sources, 216 (2012) 42-47.

[139] H.-S. Jeong, E.-S. Choi, S.-Y. Lee, J.H. Kim, Evaporation-induced, close-packed silica nanoparticle-embedded nonwoven composite separator membranes for high-voltage/high-rate lithium-ion batteries: Advantageous effect of highly percolated, electrolyte-philic microporous architecture, Journal of Membrane Science, 415 (2012) 513-519.

[140] A.S. Aricò, P. Bruce, B. Scrosati, J.-M. Tarascon, W. Van Schalkwijk, Nanostructured materials for advanced energy conversion and storage devices, Nature materials, 4 (2005) 366-377.

[141] J. Fang, H. Niu, T. Lin, X. Wang, Applications of electrospun nanofibers, Chinese Science Bulletin, 53 (2008) 2265-2286.

[142] A.N. Aleshin, Polymer nanofibers and nanotubes: Charge transport and device applications, Advanced Materials, 18 (2006) 17-27.

[143] M. Yanilmaz, A.S. Sarac, A review: effect of conductive polymers on the conductivities of electrospun mats, Textile Research Journal, (2014) 0040517513495943.

[144] R. Nayak, R. Padhye, I.L. Kyratzis, Y.B. Truong, L. Arnold, Recent advances in nanofibre fabrication techniques, Textile Research Journal, 82 (2012) 129-147.

[145] X. Zhang, Y. Lu, Centrifugal Spinning: An Alternative Approach to Fabricate Nanofibers at High Speed and Low Cost, Polymer Reviews, 54 (2014) 677-701.

[146] Y. Lu, Y. Li, S. Zhang, G. Xu, K. Fu, H. Lee, X. Zhang, Parameter study and characterization for polyacrylonitrile nanofibers fabricated via centrifugal spinning process, European Polymer Journal, 49 (2013) 3834-3845.

[147] J. Miao, M. Miyauchi, T.J. Simmons, J.S. Dordick, R.J. Linhardt, Electrospinning of nanomaterials and applications in electronic components and devices, Journal of nanoscience and nanotechnology, 10 (2010) 5507-5519.

[148] P.J. Brown, Nanofibers and nanotechnology in textiles, (2007).

[149] J. Kim, S. Choi, S. Jo, W. Lee, B.C. Kim, Characterization and properties of P (VdF-HFP)-based fibrous polymer electrolyte membrane prepared by electrospinning, journal of the Electrochemical Society, 152 (2005) A295-A300.

[150] V. Pillay, C. Dott, Y.E. Choonara, C. Tyagi, L. Tomar, P. Kumar, L.C. du Toit, V.M. Ndesendo, A review of the effect of processing variables on the fabrication of electrospun nanofibers for drug delivery applications, Journal of Nanomaterials, 2013 (2013).

[151] M. Yanilmaz, F. Kalaoglu, H. Karakas, Investigation on the Effect of Process Variables on Polyurethane Nanofibre Diameter Using a Factorial Design, FIBRES & TEXTILES IN EASTERN EUROPE, 21 (2013) 19-21.

[152] A. Koski, K. Yim, S. Shivkumar, Effect of molecular weight on fibrous PVA produced by electrospinning, Materials Letters, 58 (2004) 493-497.

[153] Y. Li, Z. Huang, Y. Lǔ, Electrospinning of nylon-6, 66, 1010 terpolymer, European Polymer Journal, 42 (2006) 1696-1704.

[154] P. Heikkilä, A. Harlin, Parameter study of electrospinning of polyamide-6, European Polymer Journal, 44 (2008) 3067-3079.

[155] D. Li, Y. Xia, Electrospinning of nanofibers: reinventing the wheel?, Advanced Materials, 16 (2004) 1151-1170.

[156] D. Hussain, F. Loyal, A. Greiner, J. Wendorff, Structure property correlations for electrospun nanofiber nonwovens, Polymer, 51 (2010) 3989-3997.

[157] L. Ji, Z. Lin, Y. Li, S. Li, Y. Liang, O. Toprakci, Q. Shi, X. Zhang, Formation and characterization of core-sheath nanofibers through electrospinning and surface-initiated polymerization, Polymer, 51 (2010) 4368-4374.

[158] N. Bhardwaj, S.C. Kundu, Electrospinning: a fascinating fiber fabrication technique, Biotechnology advances, 28 (2010) 325-347.

[159] J.-S. Park, Electrospinning and its applications, Advances in Natural Sciences: Nanoscience and Nanotechnology, 1 (2010) 043002.

[160] V. Leung, F. Ko, Biomedical applications of nanofibers, Polymers for Advanced Technologies, 22 (2011) 350-365.

[161] X.H. Qin, S.Y. Wang, Filtration properties of electrospinning nanofibers, Journal of Applied Polymer Science, 102 (2006) 1285-1290.

[162] P. Schechner, E. Kroll, E. Bubis, S. Chervinsky, E. Zussman, Silver-plated electrospun fibrous anode for glucose alkaline fuel cells, journal of the Electrochemical Society, 154 (2007) B942-B948.

[163] S. Chen, G. He, A.A. Carmona-Martinez, S. Agarwal, A. Greiner, H. Hou, U. Schröder, Electrospun carbon fiber mat with layered architecture for anode in microbial fuel cells, Electrochemistry Communications, 13 (2011) 1026-1029.

[164] M. Zhi, S. Lee, N. Miller, N.H. Menzler, N. Wu, An intermediate-temperature solid oxide fuel cell with electrospun nanofiber cathode, Energy & Environmental Science, 5 (2012) 7066-7071.

[165] A. Park, P. Pintauro, Alkaline fuel cell membranes from electrospun fiber mats, Electrochemical and Solid-State Letters, 15 (2011) B27-B30.

[166] J.B. Ballengee, P.N. Pintauro, Composite fuel cell membranes from dual-nanofiber electrospun mats, Macromolecules, 44 (2011) 7307-7314.

[167] H.-Y. Li, Y.-Y. Lee, J.-Y. Lai, Y.-L. Liu, Composite membranes of Nafion and poly (styrene sulfonic acid)-grafted poly (vinylidene fluoride) electrospun nanofiber mats for fuel cells, Journal of Membrane Science, 466 (2014) 238-245.

[168] S.-H. Yun, J.-J. Woo, S.-J. Seo, L. Wu, D. Wu, T. Xu, S.-H. Moon, Sulfonated poly (2, 6-dimethyl-1, 4-phenylene oxide)(SPPO) electrolyte membranes reinforced by electrospun nanofiber porous substrates for fuel cells, Journal of Membrane Science, 367 (2011) 296-305.

[169] S. Choi, Y.-Z. Fu, Y. Ahn, S. Jo, A. Manthiram, Nafion-impregnated electrospun polyvinylidene fluoride composite membranes for direct methanol fuel cells, Journal of Power Sources, 180 (2008) 167-171.

[170] R. Takemori, H. Kawakami, Electrospun nanofibrous blend membranes for fuel cell electrolytes, Journal of Power Sources, 195 (2010) 5957-5961.

[171] H.-Y. Li, Y.-L. Liu, Polyelectrolyte composite membranes of polybenzimidazole and crosslinked polybenzimidazole-polybenzoxazine electrospun nanofibers for proton exchange membrane fuel cells, Journal of Materials Chemistry A, 1 (2013) 1171-1178.

[172] R. Padmavathi, D. Sangeetha, Synthesis and characterization of electrospun carbon nanofiber supported Pt catalyst for fuel cells, Electrochimica Acta, 112 (2013) 1-13.

[173] M.J. Laudenslager, R.H. Scheffler, W.M. Sigmund, Electrospun materials for energy harvesting, conversion, and storage: A review, Pure and Applied Chemistry, 82 (2010) 2137-2156.

[174] S. Chaudhari, Y. Sharma, P.S. Archana, R. Jose, S. Ramakrishna, S. Mhaisalkar, M. Srinivasan, Electrospun polyaniline nanofibers web electrodes for supercapacitors, Journal of Applied Polymer Science, 129 (2013) 1660-1668.

[175] B.-H. Kim, K.S. Yang, H.-G. Woo, Thin, bendable electrodes consisting of porous carbon nanofibers via the electrospinning of polyacrylonitrile containing tetraethoxy orthosilicate for supercapacitor, Electrochemistry Communications, 13 (2011) 1042-1046.

[176] C. Kim, K. Yang, Electrochemical properties of carbon nanofiber web as an electrode for supercapacitor prepared by electrospinning, Applied Physics Letters, 83 (2003) 1216-1218.

[177] C. Ma, Y. Song, J. Shi, D. Zhang, M. Zhong, Q. Guo, L. Liu, Phenolic-based carbon nanofiber webs prepared by electrospinning for supercapacitors, Materials Letters, 76 (2012) 211-214.

[178] K. Jia, X. Zhuang, B. Cheng, S. Shi, Z. Shi, B. Zhang, Solution blown aligned carbon nanofiber yarn as supercapacitor electrode, Journal of Materials Science: Materials in Electronics, 24 (2013) 4769-4773.

[179] J. Mu, B. Chen, Z. Guo, M. Zhang, Z. Zhang, P. Zhang, C. Shao, Y. Liu, Highly dispersed Fe3O4 nanosheets on one-dimensional carbon nanofibers: Synthesis, formation mechanism, and electrochemical performance as supercapacitor electrode materials, Nanoscale, 3 (2011) 5034-5040.

[180] M. Zhi, A. Manivannan, F. Meng, N. Wu, Highly conductive electrospun carbon nanofiber/MnO< sub> 2</sub> coaxial nano-cables for high energy and power density supercapacitors, Journal of Power Sources, 208 (2012) 345-353.

[181] C. Lai, Z. Zhou, L. Zhang, X. Wang, Q. Zhou, Y. Zhao, Y. Wang, X.-F. Wu, Z. Zhu, H. Fong, Free-standing and mechanically flexible mats consisting of electrospun carbon nanofibers made from a natural product of alkali lignin as binder-free electrodes for high-performance supercapacitors, Journal of Power Sources, 247 (2014) 134-141.

[182] Y.-E. Miao, W. Fan, D. Chen, T. Liu, High-performance supercapacitors based on hollow polyaniline nanofibers by electrospinning, ACS applied materials & interfaces, 5 (2013) 4423-4428.

[183] G.A. Snook, P. Kao, A.S. Best, Conducting-polymer-based supercapacitor devices and electrodes, Journal of Power Sources, 196 (2011) 1-12.

[184] L.L. Zhang, X. Zhao, Carbon-based materials as supercapacitor electrodes, Chemical Society Reviews, 38 (2009) 2520-2531.

[185] X. Chen, B. Zhao, Y. Cai, M.O. Tadé, Z. Shao, Amorphous V–O–C composite nanofibers electrospun from solution precursors as binder-and conductive additive-free

electrodes for supercapacitors with outstanding performance, Nanoscale, 5 (2013) 12589-12597.

[186] J. Mu, B. Chen, Z. Guo, M. Zhang, Z. Zhang, C. Shao, Y. Liu, Tin oxide (SnO< sub> 2</sub>) nanoparticles/electrospun carbon nanofibers (CNFs) heterostructures: Controlled fabrication and high capacitive behavior, Journal of colloid and interface science, 356 (2011) 706-712.

[187] K. Sujith, A. Asha, P. Anjali, N. Sivakumar, K. Subramanian, S.V. Nair, A. Balakrishnan, Fabrication of highly porous conducting PANI-C composite fiber mats via electrospinning, Materials Letters, 67 (2012) 376-378.

[188] J.E. Yang, I. Jang, M. Kim, S.H. Baeck, S. Hwang, S.E. Shim, Electrochemically polymerized vine-like nanostructured polyaniline on activated carbon nanofibers for supercapacitor, Electrochimica Acta, 111 (2013) 136-143.

[189] X. Yan, Z. Tai, J. Chen, Q. Xue, Fabrication of carbon nanofiber–polyaniline composite flexible paper for supercapacitor, Nanoscale, 3 (2011) 212-216.

[190] B.-H. Kim, K.S. Yang, Structure and electrochemical properties of electrospun carbon fiber composites containing graphene, Journal of Industrial and Engineering Chemistry, (2013).

[191] Q. Dong, G. Wang, H. Hu, J. Yang, B. Qian, Z. Ling, J. Qiu, Ultrasound-assisted preparation of electrospun carbon nanofiber/graphene composite electrode for supercapacitors, Journal of Power Sources, 243 (2013) 350-353.

[192] B.-H. Kim, C.H. Kim, K.S. Yang, A. Rahy, D.J. Yang, Electrospun vanadium pentoxide/carbon nanofiber composites for supercapacitor electrodes, Electrochimica Acta, 83 (2012) 335-340.

[193] X. Li, C. Gao, J. Wang, B. Lu, W. Chen, J. Song, S. Zhang, Z. Zhang, X. Pan, E. Xie, TiO< sub> 2</sub> films with rich bulk oxygen vacancies prepared by electrospinning for dye-sensitized solar cells, Journal of Power Sources, 214 (2012) 244-250.

[194] S. Chuangchote, T. Sagawa, S. Yoshikawa, Efficient dye-sensitized solar cells using electrospun TiO 2 nanofibers as a light harvesting layer, Applied Physics Letters, 93 (2008) 033310-033310-033313.

[195] D. Sabba, N. Mathews, J. Chua, S.S. Pramana, H.K. Mulmudi, Q. Wang, S.G. Mhaisalkar, High-surface-area, interconnected, nanofibrillar TiO< sub> 2</sub> structures as photoanodes in dye-sensitized solar cells, Scripta Materialia, 68 (2013) 487-490.

[196] I.-D. Kim, J.-M. Hong, B.H. Lee, D.Y. Kim, E.-K. Jeon, D.-K. Choi, D.-J. Yang, Dye-sensitized solar cells using network structure of electrospun ZnO nanofiber mats, Applied Physics Letters, 91 (2007) 163109.

[197] J. Li, X. Chen, N. Ai, J. Hao, Q. Chen, S. Strauf, Y. Shi, Silver nanoparticle doped TiO< sub> 2</sub> nanofiber dye sensitized solar cells, Chemical Physics Letters, 514 (2011) 141-145.

[198] P. Du, L. Song, J. Xiong, N. Li, Z. Xi, L. Wang, D. Jin, S. Guo, Y. Yuan, Coaxial electrospun TiO< sub> 2</sub>/ZnO core–sheath nanofibers film: Novel structure for photoanode of dye-sensitized solar cells, Electrochimica Acta, 78 (2012) 392-397.

[199] M.Y. Song, D.K. Kim, K.J. Ihn, S.M. Jo, D.Y. Kim, New application of electrospun TiO2 electrode to solid-state dye-sensitized solar cells, Synthetic metals, 153 (2005) 77-80.

[200] M.Y. Song, D.K. Kim, S.M. Jo, D.Y. Kim, Enhancement of the photocurrent generation in dye-sensitized solar cell based on electrospun TiO< sub> 2</sub> electrode by surface treatment, Synthetic metals, 155 (2005) 635-638.

[201] N.T. Hieu, S.J. Baik, O.H. Chung, J.S. Park, Fabrication and characterization of electrospun carbon nanotubes/titanium dioxide nanofibers used in anodes of dye-sensitized solar cells, Synthetic metals, 193 (2014) 125-131.

[202] H. Krysova, J. Trckova-Barakova, J. Prochazka, A. Zukal, J. Maixner, L. Kavan, Titania nanofiber photoanodes for dye-sensitized solar cells, Catalysis Today, 230 (2014) 234-239.

[203] Z. Peining, A.S. Nair, Y. Shengyuan, P. Shengjie, N.K. Elumalai, S. Ramakrishna, Rice grain-shaped TiO< sub> 2</sub>–CNT composite—A functional material with a novel morphology for dye-sensitized solar cells, Journal of Photochemistry and Photobiology A: Chemistry, 231 (2012) 9-18.

[204] Z. Wei, Y. Li, S. Luo, C. Liu, D. Meng, M. Ding, G. Zeng, Hierarchical heterostructure of CdS nanoparticles sensitized electrospun TiO2 nanofibers with enhanced photocatalytic activity, Separation and Purification Technology, 122 (2014) 60-66.

[205] M. Hamadanian, V. Jabbari, Fabrication and characterization of dye-sensitized solar cells using electrospun TiO2 nanofibre as a solar light harvesting layer, International Journal of Sustainable Energy, 31 (2012) 277-289.

[206] Y. Chan, C. Wang, C. Chen, Electrospun TiO2-MWCNTs nanofibers as photoanode in dye-sensitized solar cell (DSSC), Journal of Materials Science, 48 (2013) 5261-5272.

[207] J. Ding, Y. Li, H. Hu, L. Bai, S. Zhang, N. Yuan, The influence of anatase-rutile mixed phase and ZnO blocking layer on dye-sensitized solar cells based on TiO2nanofiberphotoanodes, Nanoscale research letters, 8 (2013) 1-9.

[208] D. Sabba, S. Agarwala, S.S. Pramana, S. Mhaisalkar, A maskless synthesis of TiO2-nanofiber-based hierarchical structures for solid-state dye-sensitized solar cells with improved performance, Nanoscale research letters, 9 (2014) 1-9.

[209] M. Dissanayake, H. Divarathne, C. Thotawatthage, C. Dissanayake, G. Senadeera, B. Bandara, Dye-sensitized solar cells based on electrospun polyacrylonitrile (PAN) nanofibre membrane gel electrolyte, Electrochimica Acta, 130 (2014) 76-81.

[210] J.-U. Kim, S.-H. Park, H.-J. Choi, W.-K. Lee, J.-K. Lee, M.-R. Kim, Effect of electrolyte in electrospun poly(vinylidene fluoride-co-hexafluoropropylene) nanofibers on dye-sensitized solar cells, Solar Energy Materials and Solar Cells, 93 (2009) 803-807.

[211] S.-H. Park, D.-H. Won, H.-J. Choi, W.-P. Hwang, S.-i. Jang, J.-H. Kim, S.-H. Jeong, J.-U. Kim, J.-K. Lee, M.-R. Kim, Dye-sensitized solar cells based on electrospun polymer blends as electrolytes, Solar Energy Materials and Solar Cells, 95 (2011) 296-300.

[212] S.-J. Seo, S.-H. Yun, J.-J. Woo, D.-W. Park, M.-S. Kang, A. Hinsch, S.-H. Moon, Preparation and characterization of quasi-solid-state electrolytes using a brominated poly (2, 6-dimethyl-1, 4-phenylene oxide) electrospun nanofiber mat for dye-sensitized solar cells, Electrochemistry Communications, 13 (2011) 1391-1394.

[213] S.K. Ahn, T. Ban, P. Sakthivel, J.W. Lee, Y.-S. Gal, J.-K. Lee, M.-R. Kim, S.-H. Jin, Development of dye-sensitized solar cells composed of liquid crystal embedded, electrospun poly (vinylidene fluoride-co-hexafluoropropylene) nanofibers as polymer gel electrolytes, ACS applied materials & interfaces, 4 (2012) 2096-2100.

[214] J.-Y. Park, J.-W. Lee, K.H. Park, T.-Y. Kim, S.-H. Yim, X.G. Zhao, H.-B. Gu, E.M. Jin, Dye-sensitized solar cells based on electrospun poly (vinylidenefluoride-co-hexafluoropropylene) nanofibers, Polymer bulletin, 70 (2013) 507-515.

[215] S. Zhang, Z. Lin, L. Ji, Y. Li, G. Xu, L. Xue, S. Li, Y. Lu, O. Toprakci, X. Zhang, Cr-doped Li 2 MnSiO 4/carbon composite nanofibers as high-energy cathodes for Li-ion batteries, Journal of Materials Chemistry, 22 (2012) 14661-14666.

[216] O. Toprakci, H.A. Toprakci, L. Ji, X. Zhang, Fabrication and electrochemical characteristics of LiFePO 4 powders for lithium-ion batteries, KONA Powder and Particle Journal, 28 (2010) 50-73.

[217] R. von Hagen, H. Lorrmann, K.C. Möller, S. Mathur, Electrospun LiFe1− yMnyPO4/C Nanofiber Composites as Self-Supporting Cathodes in Li-Ion Batteries, Advanced Energy Materials, 2 (2012) 553-559.

[218] C. Kim, S.H. Kang, H.J. Jeon, J.T. Son, Electrochemical properties of nanostructured Li [Fe0. 9Mn0. 1] PO4/C as a cathode material for lithium ion batteries prepared by electrospinning method, Journal of Electroceramics, 31 (2013) 204-209.

[219] C.A. Bonino, L. Ji, Z. Lin, O. Toprakci, X. Zhang, S.A. Khan, Electrospun carbon-tin oxide composite nanofibers for use as lithium ion battery anodes, ACS applied materials & interfaces, 3 (2011) 2534-2542.

[220] B.-O. Jang, S.-H. Park, W.-J. Lee, Electrospun Co–Sn alloy/carbon nanofibers composite anode for lithium ion batteries, Journal of Alloys and Compounds, 574 (2013) 325-330.

[221] X. Zhang, H. Liu, S. Petnikota, S. Ramakrishna, H.J. Fan, Electrospun Fe 2 O 3–carbon composite nanofibers as durable anode materials for lithium ion batteries, Journal of Materials Chemistry A, (2014).

[222] B. Liu, X. Hu, H. Xu, W. Luo, Y. Sun, Y. Huang, Encapsulation of MnO Nanocrystals in Electrospun Carbon Nanofibers as High-Performance Anode Materials for Lithium-Ion Batteries, Scientific reports, 4 (2014).

[223] S. Li, C. Chen, K. Fu, L. Xue, C. Zhao, S. Zhang, Y. Hu, L. Zhou, X. Zhang, Comparison of Si/C, Ge/C and Sn/C composite nanofiber anodes used in advanced lithium-ion batteries, Solid State Ionics, 254 (2014) 17-26.

[224] M. Dirican, M. Yanilmaz, K. Fu, Y. Lu, H. Kizil, X. Zhang, Carbon-enhanced electrodeposited SnO< sub> 2</sub>/carbon nanofiber composites as anode for lithium-ion batteries, Journal of Power Sources, (2014).

[225] L. Ji, X. Zhang, Manganese oxide nanoparticle-loaded porous carbon nanofibers as anode materials for high-performance lithium-ion batteries, Electrochemistry Communications, 11 (2009) 795-798.

[226] K. Fu, Y. Lu, M. Dirican, C. Chen, M. Yanilmaz, Q. Shi, P.D. Bradford, X. Zhang, Chamber-Confined Silicon-Carbon Nanofiber Composites for Prolonged Cycling Life of Li-Ion Battery, Nanoscale, (2014).

[227] L. Xue, K. Fu, Y. Li, G. Xu, Y. Lu, S. Zhang, O. Toprakci, X. Zhang, Si/C composite nanofibers with stable electric conductive network for use as durable lithium-ion battery anode, Nano Energy, 2 (2013) 361-367.

[228] L. Ji, X. Zhang, Fabrication of porous carbon nanofibers and their application as anode materials for rechargeable lithium-ion batteries, Nanotechnology, 20 (2009) 155705.

[229] D. Kim, D. Lee, J. Kim, J. Moon, Electrospun Ni-Added SnO2–Carbon Nanofiber Composite Anode for High-Performance Lithium-Ion Batteries, ACS applied materials & interfaces, 4 (2012) 5408-5415.

[230] Z. Fu, X. Li, G. Xu, Novel electrospun SnO2@ carbon nanofibers as high performance anodes for lithium-ion batteries, Crystal Research and Technology, 49 (2014) 441-445.

[231] M. Yanilmaz, C. Chen, X. Zhang, Fabrication and characterization of SiO2/PVDF composite nanofiber-coated PP nonwoven separators for lithium-ion batteries, Journal of Polymer Science Part B: Polymer Physics, (2013).

[232] J.R. Kim, S.W. Choi, S.M. Jo, W.S. Lee, B.C. Kim, Electrospun PVdF-based fibrous polymer electrolytes for lithium ion polymer batteries, Electrochimica Acta, 50 (2004) 69-75.

[233] P. Raghavan, X. Zhao, J.-K. Kim, J. Manuel, G.S. Chauhan, J.-H. Ahn, C. Nah, Ionic conductivity and electrochemical properties of nanocomposite polymer electrolytes based on electrospun poly(vinylidene fluoride-co-hexafluoropropylene) with nano-sized ceramic fillers, Electrochimica Acta, 54 (2008) 228-234.

[234] Y. Zhu, S. Xiao, Y. Shi, Y. Yang, Y. Hou, Y. Wu, A Composite Gel Polymer Electrolyte with High Performance Based on Poly (Vinylidene Fluoride) and Polyborate for Lithium Ion Batteries, Advanced Energy Materials, 4 (2014) 1-9.

[235] H.-R. Jung, W.-J. Lee, Electrochemical characteristics of electrospun poly (methyl methacrylate)/polyvinyl chloride as gel polymer electrolytes for lithium ion battery, Electrochimica Acta, 58 (2011) 674-680.

[236] Z. Zhong, Q. Cao, B. Jing, S. Li, X. Wang, Novel electrospun PAN–PVC composite fibrous membranes as polymer electrolytes for polymer lithium-ion batteries, Ionics, 18 (2012) 853-859.

[237] S.W. Choi, J.R. Kim, Y.R. Ahn, S.M. Jo, E.J. Cairns, Characterization of electrospun PVDF fiber-based polymer electrolytes, Chemistry of materials, 19 (2007) 104-115.

[238] L. Ren, R. Ozisik, S.P. Kotha, Rapid and efficient fabrication of multilevel structured silica micro-/nanofibers by centrifugal jet spinning, Journal of colloid and interface science, 425 (2014) 136-142.

[239] R. Weitz, L. Harnau, S. Rauschenbach, M. Burghard, K. Kern, Polymer nanofibers via nozzle-free centrifugal spinning, Nano letters, 8 (2008) 1187-1191.

[240] B. Vazquez, H. Vasquez, K. Lozano, Preparation and characterization of polyvinylidene fluoride nanofibrous membranes by forcespinning™, Polymer Engineering & Science, 52 (2012) 2260-2265.

[241] L. Ren, T.J. Simmons, F. Lu, O. Rahmi, S.P. Kotha, Template Free and Large-Scale Fabrication of Silica Nanotubes with Centrifugal Jet Spinning, Chemical Engineering Journal, (2014).

[242] B. Weng, F. Xu, A. Salinas, K. Lozano, Mass production of carbon nanotube reinforced poly(methyl methacrylate) nonwoven nanofiber mats, Carbon, 75 (2014) 217-226.

[243] B. Raghavan, Y. Ner, E. Peno, C. Gomez, K. Lozano, Forcespinning TM: An important advancement in nanofibers production, TAPPI Innovative Nonwovens Conference, Atlanta, GA, 2011.

[244] M.A. Hammami, M. Krifa, O. Harzallah, Centrifugal force spinning of PA6 nanofibers–processability and morphology of solution-spun fibers, The Journal of The Textile Institute, 105 (2014) 637-647.

[245] B. Raghavan, H. Soto, K. Lozano, Fabrication of Melt Spun Polypropylene Nanofibers by Forcespinning, Journal of Engineered Fabrics & Fibers (JEFF), 8 (2013).

[246] L.A. Mary, T. Senthilram, S. Suganya, L. Nagarajan, J. Venugopal, S. Ramakrishna, V. Dev, Centrifugal spun ultrafine fibrous web as a potential drug delivery vehicle, EXPRESS POLYMER LETTERS, 7 (2013) 238-248.

[247] L. Ren, S.P. Kotha, Centrifugal jet spinning for highly efficient and large-scale fabrication of barium titanate nanofibers, Materials Letters, 117 (2014) 153-157.

[248] T. Sandou, A. Oya, Preparation of carbon nanotubes by centrifugal spinning of coreshell polymer particles, Carbon, 43 (2005) 2015-2017.

[249] A. Sedaghat, E. Taheri-Nassaj, R. Naghizadeh, An alumina mat with a nano microstructure prepared by centrifugal spinning method, Journal of non-crystalline solids, 352 (2006) 2818-2828.

[250] L. Foster, B. Tighe, Centrifugally spun polyhydroxybutyrate fibres: accelerated hydrolytic degradation studies, Polymer degradation and stability, 87 (2005) 1-10.

[251] M.R. Badrossamay, K. Balachandran, A.K. Capulli, H.M. Golecki, A. Agarwal, J.A. Goss, H. Kim, K. Shin, K.K. Parker, Engineering hybrid polymer-protein super-aligned nanofibers via rotary jet spinning, Biomaterials, 35 (2014) 3188-3197.

[252] L. Wang, J. Shi, L. Liu, E. Secret, Y. Chen, Fabrication of polymer fiber scaffolds by centrifugal spinning for cell culture studies, Microelectronic Engineering, 88 (2011) 1718-1721.

[253] N. Bao, Z. Wei, Z. Ma, F. Liu, G. Yin, Si-doped mesoporous TiO< sub> 2</sub> continuous fibers: Preparation by centrifugal spinning and photocatalytic properties, Journal of hazardous materials, 174 (2010) 129-136.

[254] H. Liu, Y. Chen, S. Pei, G. Liu, J. Liu, Preparation of nanocrystalline titanium dioxide fibers using sol–gel method and centrifugal spinning, Journal of sol-gel science and technology, 65 (2013) 443-451.

[255] S. Mahalingam, M. Edirisinghe, Forming of polymer nanofibers by a pressurised gyration process, Macromolecular rapid communications, 34 (2013) 1134-1139.

[256] M.R. Badrossamay, H.A. McIlwee, J.A. Goss, K.K. Parker, Nanofiber assembly by rotary jet-spinning, Nano letters, 10 (2010) 2257-2261.

[257] S. Padron, R. Patlan, J. Gutierrez, N. Santos, T. Eubanks, K. Lozano, Production and characterization of hybrid BEH-PPV/PEO conjugated polymer nanofibers by forcespinning™, Journal of Applied Polymer Science, 125 (2012) 3610-3616.

[258] Z. McEachin, K. Lozano, Production and characterization of polycaprolactone nanofibers via forcespinning™ technology, Journal of Applied Polymer Science, 126 (2012) 473-479.

[259] L. Ren, V. Pandit, J. Elkin, T. Denman, J.A. Cooper, S.P. Kotha, Large-scale and highly efficient synthesis of micro-and nano-fibers with controlled fiber morphology by centrifugal jet spinning for tissue regeneration, Nanoscale, 5 (2013) 2337-2345.

[260] S. Padron, A. Fuentes, D. Caruntu, K. Lozano, Experimental study of nanofiber production through forcespinning, Journal of Applied Physics, 113 (2013) 024318.

[261] M. Krifa, M.A. Hammami, H. Wu, Occurrence and morphology of bead-on-string structures in centrifugal forcespun PA6 fibers, The Journal of The Textile Institute, (2014) 1-11.

CHAPTER 2. RESEARCH OBJECTIVES

A separator provides a physical barrier between the positive and negative electrodes in order to prevent electrical short circuits. The separator also serves as the electrolyte reservoir for the transport of ions during the charging and discharging cycles of a battery. Although they do not participate in electrochemical reactions, separators play a vital role in preventing short circuit, allowing lithium ion transfer, and regulating cell kinetics. As a result, the physical properties of separators can affect the cell capacity, cell resistance, rate performance, and long-term cycling capability of lithium-ion batteries. Currently, microporous membranes are the most commonly used separator type and they are polyolefin-based materials with good mechanical properties and chemical stability. However, their wettability and thermal stabilities are not sufficient for applications that require high operating temperature and high performance such as fast charge/discharge rate. Low affinity of these membranes to liquid electrolyte also leads to high cell resistance that affects the cycling performance and rate performance negatively.

Electrospinning technique is used to produce continuous polymer fibers with the fiber diameter on nanometer or submicron scales in the form of nonwoven mats. In electrospinning technique, electric charge is used to transform viscoelastic liquids into nano-sized filaments. Due to the superior properties such as large specific surface area, small pore size and high porosity, electrospun nanofiber membranes can be good separator candidate for high-performance lithium-ion batteries. Moreover, the performance of nanofiber membranes can be further improved by introducing ceramic fillers which form Lewis acid/base interactions with the ionic species in the liquid electrolyte.

Centrifugal spinning technique can also be used as a fast, cost-effective and safe technique to fabricate high-performance fiber-based separators. In this technique, a high speed rotary and perforated spinneret is used to fabricate nanofibers from polymer solutions. The diameters of fibers can vary from several nanometers to micrometers and the production rate of the centrifugal spinning process could be more than 500 times faster than conventional electrospinning technique

The objective of this work is to fabricate nanofiber-based membrane separators with enhanced electrochemical performance and high thermal stability for high-performance rechargeable lithium-ion batteries. In this research, novel approaches are proposed to fabricate high-performance membrane separators. The resultant membranes have the potential to combine the advantages of both nanofiber-based membranes and inorganic nanoparticles. Nanofiber-based membranes serve as highly porous membrane separators and inorganic nanoparticles improve thermal stability and electrochemical performance.

(I) SiO_2/PVDF Composite Nanofiber-Coated PP Nonwoven Membranes as Separator for Lithium-Ion Batteries

SiO_2/PVDF composite nanofiber-coated PP nonwoven membranes were prepared by electrospinning of SiO_2/PVDF dispersions onto both sides of PP nonwovens. The goal of this study was to combine the good mechanical strength of PP nonwoven with excellent electrochemical properties of SiO_2/PVDF composite nanofibers to obtain a new high-performance separator. The results of this work are discussed in Chapter 3.

(II) Nanoparticle-on-Nanofiber Hybrid Membranes as Separator for Lithium-ion Batteries via Combining Electrospraying and Electrospinning Techniques

Nanoparticle-on-nanofiber hybrid membranes were prepared by electrospraying of SiO_2 dispersions and electrospinning of polyvinylidene fluoride (PVDF) solution *simultaneously*. The aim of this study was to design new high-performance separators with superior electrochemical properties such as high C-rate performance and good thermal stability compared to polyolefin based membranes. The results of this work are discussed in Chapter 4.

(III) Electrospun SiO_2/Nylon 6,6 Nanofiber Membranes as Thermally-Stable Separator for Lithium-Ion Batteries

Electrospun nanofiber mats with enhanced mechanical properties and thermal stability can be obtained by using polymeric materials with higher mechanical strength and melting temperature such as nylon 6,6. In this study, nylon 6,6 was used to prepare novel electrospun membranes with high thermal stability, superior mechanical strength, and enhanced electrochemical properties. Inorganic SiO_2 nanoparticles were also introduced to further improve the mechanical and electrochemical properties. The results of this work are discussed in Chapter 5.

(IV) SiO_2/Polyacrylonitrile Nanofiber Membranes via Centrifugal Spinning as Separator for Li-Ion Batteries

Centrifugal spinning is a fast, cost-effective and safe alternative to the electrospinning technique, which is commonly used for making fiber-based separator membranes. In this work, SiO_2/polyacrylonitrile (PAN) membranes were produced by using centrifugal spinning and they were characterized by using different electrochemical

techniques for use as separators in Li-ion batteries. The results of this work are discussed in Chapter 6.

(V) Polymethylmethacrylate/Polyacrylonitrile Blend Nanofiber Membranes via Centrifugal Spinning as Separator for Li-Ion Batteries

PAN-based separators show promising properties including high ionic conductivity, good thermal stability, high electrolyte uptake and good compatibility with Li metal. Polymethylmethacrylate (PMMA) has also been used as a separator material due to its good compatibility with Li and high affinity to liquid electrolyte. Blending PAN and PMMA can potentially lead to new separators with enhanced microstructure, porosity and electrochemical properties that cannot be achieved by single-component polymer membranes. In this work, centrifugal spinning was utilized to produce PAN/PMMA blend nanofiber membranes for use as high-performance separator for Li-ion batteries. The results of this work are discussed in Chapter 7.

CHAPTER 3. SIO_2/PVDF COMPOSITE NANOFIBER-COATED PP NONWOVEN MEMBRANES AS SEPARATOR FOR LITHIUM-ION BATTERIES

ABSTRACT

SiO_2/Polyvinylidene fluoride (PVDF) composite nanofiber-coated polypropylene (PP) nonwoven membranes were prepared by electrospinning of SiO_2/PVDF dispersions onto both sides of PP nonwovens. The goal of this study was to combine the good mechanical strength of PP nonwoven with the excellent electrochemical properties of SiO_2/PVDF composite nanofibers to obtain a new high-performance separator. It was found that the addition of SiO_2 nanoparticles played an important role in improving the overall performance of these nanofiber-coated nonwoven membranes. Among the membranes with various SiO_2 contents, 15% SiO_2/PVDF composite nanofiber-coated PP nonwoven membranes provided the highest ionic conductivity of 2.6×10^{-3} S/cm after being immersed in a liquid electrolyte, 1 mol/L lithium hexafluorophosphate in ethylene carbonate, dimethyl carbonate and diethyl carbonate. Compared with pure PVDF nanofiber-coated PP nonwoven membranes, SiO_2/PVDF composite fiber-coated PP nonwoven membranes had greater liquid electrolyte uptake, higher electrochemical oxidation limit, and lower interfacial resistance with lithium. SiO_2/PVDF composite fiber-coated PP nonwoven membrane separators were assembled into lithium/lithium iron phosphate cells and demonstrated high cell capacities and good cycling performance at room temperature.

3.1. Introduction

Lithium-ion batteries have been widely used in electronic devices such as mobile phones, laptop computers, and digital cameras due to their high specific energy (~150 Wh/kg), high energy density (~400 Wh/L), high operational voltages (2.5 - 4.2 V), long cycling lifetime (>1000 cycles), and low self-discharge rate (2-8 %/month). Other advantages of lithium-ion batteries include high coulombic efficiency and no memory effect [1-6]. Nowadays, lithium-ion batteries are finding new applications in electric/hybrid vehicles and energy storage of smart grids. To be used in these new applications, new battery components are needed so that lithium-ion batteries with higher cell performance, better safety, and lower cost can be developed.

Separators are an important component in order to obtain safe batteries and their primary function is to prevent electronic contact between electrodes while regulating cell kinetics and ionic flow [7,8]. Separators must be porous, thin, mechanically strong, chemically and dimensionally stable with minimum shrinkage and high wettability [9]. Although the capacities of lithium-ion batteries are determined by the electrode materials, it is well known that the separators influence the battery performance, e.g., charge/discharge capacity and cycle life [8,10]. Conventional microporous polyolefin separators have appropriate chemical stability, suitable thickness and sufficient mechanical strength, but they have low melting temperature, low porosity, poor wettability, and high dielectric constant. These disadvantages lead to some performance issues such as relatively high cell resistance and short lifetime [8,9,11].

Because of the superior properties such as large specific surface area, small pore size and high porosity, electrospun nanofiber membranes have attracted much attention for used

as battery separators [11,12]. Large porosities with fully interconnected pore structures and high surface areas lead to high electrolyte uptakes and facile transport of ions [13]. It is reported that increased rate capability can also be achieved in lithium-ion batteries by using nanofiber membrane separators with high porosities and large air permeabilities [14]. Various polymer materials, including polyvinylidene fluoride (PVDF), polyvinyl chloride (PVC), polyacrylonitrile (PAN), polyphthalazinone ether sulfone ketone, and polyvinylidenefluoride-hexafluoropropylene (PVDF-HFP), have been used to prepare nanofiber membrane separators [10,15-22]. Among them, PVDF has been extensively studied for making separators due to its excellent chemical resistance, high mechanical strength, good thermal stability, and high affinity to electrolyte solution [15].

The performance of nanofiber membranes can be improved by introducing ceramic fillers [2,13,23-26]. Raghavan et al. [13] reported that nanosized ceramic fillers, such as TiO_2 and AlO_2, reduced polymer crystallinity and improved the ionic conductivity of nanofiber membrane membranes due to Lewis acid/base interactions between the polar surface groups on the filler surface and the ionic species in the liquid electrolyte. Jung et al. [20] reported that SiO_2 fillers also decreased the fiber diameter and improved the ionic conductivity of electrospun hydrophilic fumed SiO_2/polyacrylonitrile nanofiber membranes by introducing Lewis acid/base interactions.

One major disadvantage of electrospun nanofiber membrane separators is their poor mechanical stability. Electrospun nanofiber membranes are inherently weak and cannot withstand the large tension developed by the winding operation used during battery assembly. In this study, SiO_2/PVDF composite nanofibers were directly electrospun onto both sides of polypropylene (PP) nonwoven membranes to obtain new nanofiber-coated

nonwoven membrane separators. In these separators, PP nonwovens serve as the mechanical support and SiO_2/PVDF composite nanofibers help provide excellent separator properties, such as good wettability, high ionic conductivity, high oxidation limit, low interfacial resistance, and good cycling performance. Results demonstrated that SiO_2/PVDF nanofiber-coated PP nonwoven membranes are promising separator candidate for high-performance lithium-ion batteries.

3.2. Experimental

3.2.1 Chemicals

Hydrophilic pyrogenic SiO_2 (Aerosil 380, particle size = 7 nm) was purchased from Evonic industries. PVDF polymer (M_w = 30×10^4 - 50×10^4) and PP nonwoven membranes (11 g/m^2) were obtained from Shanghai Ofluorine Chemical Technology and Zhejiang Dongyang Sanxing Industry, respectively. N,N-dimethylformamide (DMF), acetone and n-butanol were purchased from Sigma Aldrich. Lithium hexafluorophosphate ($LiPF_6$), ethylene carbonate and ethyl methyl carbonate were supplied from Ferro Corp. for liquid electrolyte uptake tests. The electrolyte, 1 mol/L Lithium hexafluorophosphate ($LiPF_6$) in ethylene carbonate, dimethyl carbonate and diethyl carbonate (EC+DMC+DEC, 1:1:1 in volume), was purchased from MTI corporation. $LiFePO_4$ was obtained from Hydro-Qubec. All chemicals were used as received without further purification.

3.2.2 Separator preparation

SiO_2/PVDF composite nanofiber-coated PP nonwoven separators were prepared by electrospinning of SiO_2/PVDF dispersions onto both sides of PP nonwoven membranes (Figure 3.1). The dispersions were prepared by adding different amounts of SiO_2

nanoparticles (0, 5, 10 and 15 wt% with respect to PVDF) into 10 wt% PVDF solution in DMF/acetone (7/3: v/v). The dispersions were stirred at 60 ^{o}C for at least 8 hours to ensure the uniformity.

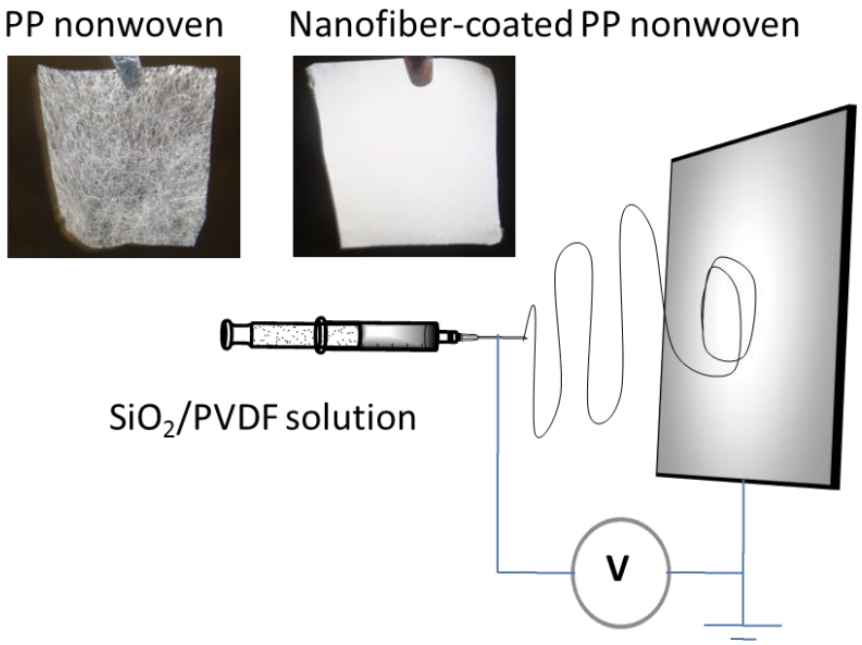

Figure 3.1 Preparation of SiO_2/PVDF nanofiber-coated PP nonwoven separators.

During electrospinning, a variable high voltage power supply (Gamma) was used to provide a high voltage of 15 kV. The feeding rate used was 1 ml/h and the tip-to-collector-distance was 15 cm. Electrospun SiO_2/PVDF composite nanofibers were accumulated on the PP nonwoven placed on the collector. After the deposition of nanofibers on one side, the PP nonwoven was flipped to deposit nanofibers on the other side. The resultant SiO_2/PVDF nanofiber-coated PP nonwoven membranes were dried at 80 $^{\circ}$C for at least 24 hours to remove residual solvents.

3.2.3 Structure Characterization

The morphology of SiO_2/PVDF nanofiber-coated PP nonwoven membranes was studied by using Hitachi S3200 scanning electron microscopy. The fiber diameters were calculated by measuring 100 randomly-selected nanofibers in SEM images using Revolution 1.6 software for each sample.

The porosities of the membranes were determined by using n-butanol uptake tests. In an uptake test, the porosity was calculated by using the following equation:

$$Porosity\ (\%) = \frac{w_w - w_d}{\rho_b \times V} \quad (1)$$

where w_w and w_d are the weights of wet and dry membranes, respectively, ρ_b the density of n-butanol, and V the geometric volume of the membrane.

The mechanical properties of the membranes were determined by using a universal tensile tester (Instron 5544) with 100 N capacity load cell. The dimensions of test specimens were 10 mm wide, 60 μm thick and 60 mm long. For each membrane, ten specimens were tested to obtain the average moduli, strengths, and strains-at-break.

3.2.4 Performance evaluation

Liquid electrolyte uptakes were measured by soaking weighed membranes in the liquid electrolyte of 1M $LiPF_6$ in EC+EMC (1:1 in volume) for two hours at room temperature. The electrolyte uptake (EU) was calculated by:

$$EU\ (\%) = \frac{w_1 - w_0}{w_0} \times 100 \quad (2)$$

where w_0 and w_1 are the weights of dry and wet membranes, respectively.

The ionic conductivities of liquid electrolyte-soaked membranes were measured by electrochemical impedance spectroscopy (EIS) using Reference 600

Potentiostat/Galvanostat/ZRA (GAMRY). The impedance measurements were performed on liquid electrolyte-soaked membranes sandwiched between two stainless steel electrodes over a frequency range of 1 MHz to 1 Hz with AC amplitude of 10 mV and within a temperature range of 25 to 85 ^{o}C. The ionic conductivity was calculated by:

$$\sigma = \frac{d}{R_b \times S} \tag{3}$$

where d is the membrane thickness, S the cross-sectional area, and R_b the bulk resistance obtained at the high frequency intercept of the Nyquist plot on the real axis.

The electrochemical oxidation limits of liquid electrolyte-soaked membranes were determined by linear sweep voltammetry at room temperature. In these tests, electrochemical cells consisting of stainless steel working electrode and lithium metal counter electrode were used. The scan rate used was 10 mVs^{-1} and the potential range was 2.5 to 6.0 V.

The interfacial resistances between the liquid electrolyte-soaked membranes and lithium metal were investigated by measuring the impedance of symmetrical lithium cells. The frequency range used was 100 kHz to 0.1 Hz.

The cycling performance of Li/$LiFePO_4$ cells containing liquid electrolyte-soaked membranes was evaluated using coin-type cells. The $LiFePO_4$ cathode was prepared by blending $LiFePO_4$ powder (80 wt%), carbon black conductor (10 wt%) and PVDF binder (10 wt%). Arbin automatic battery cycler was used in a potential range of 4.2 - 2.5 V at a current density of 0.2 C to evaluate the cycling performance.

3.3 Results and Discussions

3.3.1 Separator morphology

Figure 3.2 shows SEM images and diameter distributions of SiO_2/PVDF nanofiber-coated PP nonwoven membranes with various SiO_2 contents (0, 5, 10 and 15%). Pure PVDF nanofibers (*i.e.*, SiO_2 content = 0%) are straight and have an average diameter of 381 nm.

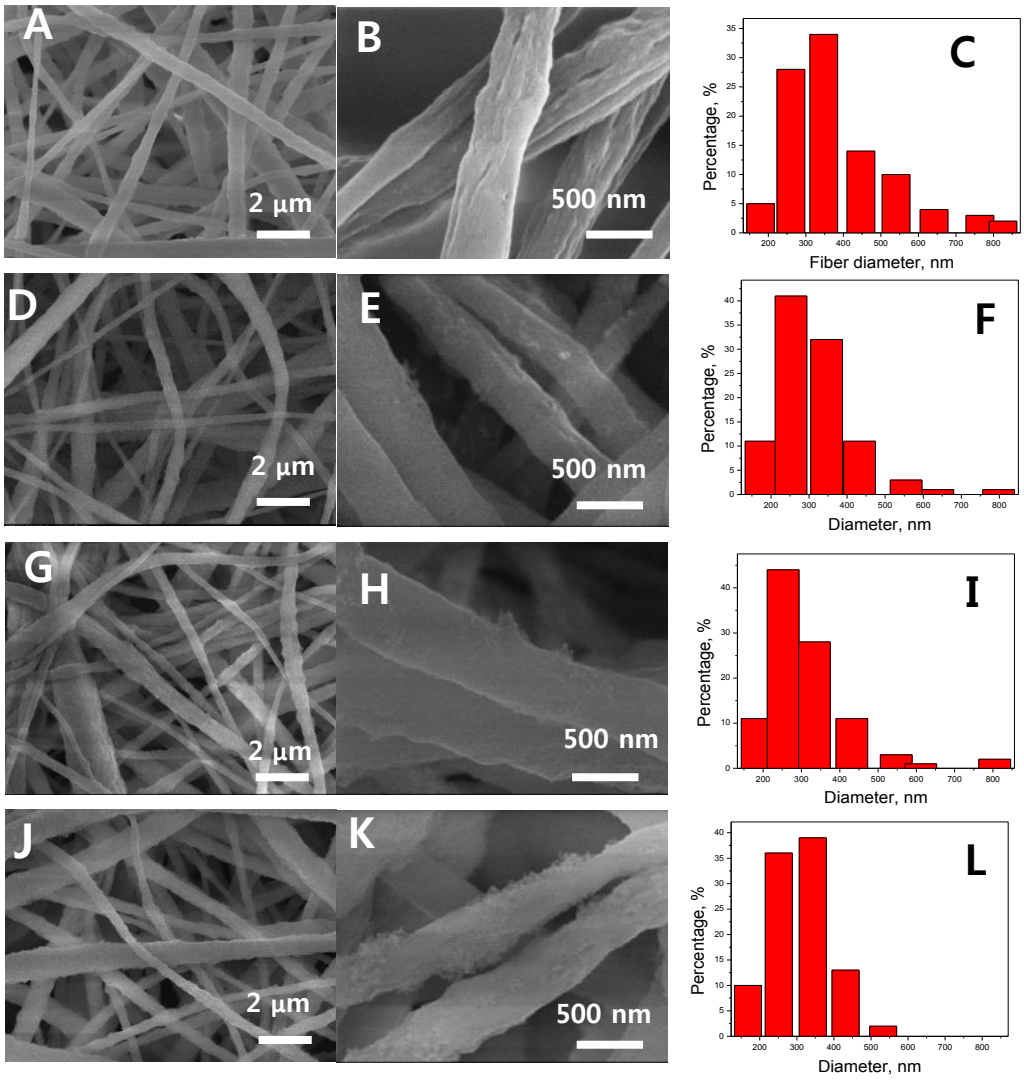

Figure 3.2 SEM images and diameter distributions of SiO_2/PVDF nanofiber-coated PP nonwoven membranes with different SiO_2 contents: (A-C) 0%, (D-F) 5%, (G-I) 10%, (J-L) 15%.

The addition of 5, 10, and 15% SiO_2 nanoparticles slightly decreases the average fiber diameter to 312, 310, and 307 nm, respectively. Similar results were reported on SiO_2/PAN nanofibers and decreased diameters at high filler contents were attributed to the repulsive force of SiO_2 that minimizes the entanglement of polymer chains [20,27]. From Figure 3.2, it is also seen that, with increase in SiO_2 content, the fiber surfaces become rougher probably because of the aggregation of nanoparticles.

Figure 3.3 shows the porosities of SiO_2/PVDF nanofiber-coated PP nonwoven membranes. It is seen that the membrane porosity increases with increase in SiO_2 content. The porosities are 53, 60, 63 and 73%, respectively, for membranes containing 0, 5, 10, and 15% SiO_2 nanoparticles. The increase in porosity can be explained by the decreased fiber diameter and increased roughness as a result of increasing SiO_2 content (Figure 3.2). In general, smaller fiber diameter leads to higher porosity since more void space is available between thin fibers. Increased surface roughness also contributes to the higher porosity value because the extra surface area can help trap more liquid n-butanol during the porosity measurement. Several research groups have reported that the addition of SiO_2 particles can increase the surface roughness of electrospun nanofibers [20,32]. The reduced fiber diameter, increased surface roughness and enhanced porosity affect the properties of the composite membranes and lithium-ion cells, as discussed below.

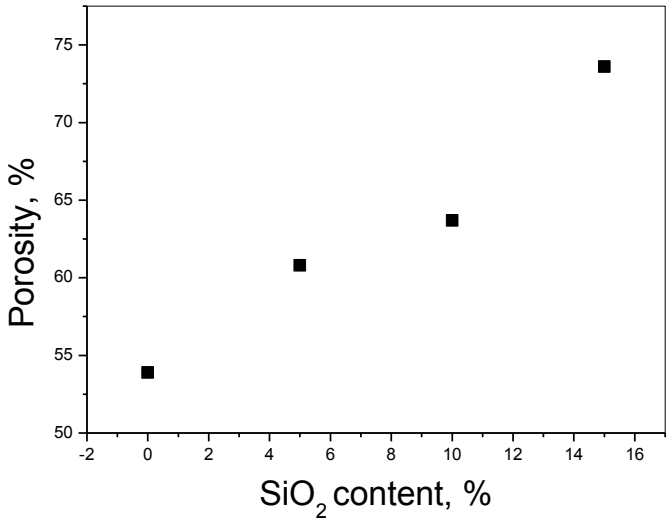

Figure 3.3 Porosities of SiO_2/PVDF nanofiber-coated PP nonwoven membranes.

3.3.2 Mechanical properties

One main purpose to prepare SiO_2/PVDF nanofiber-coated PP nonwoven membranes is to improve the mechanical properties of electrospun nanofiber membrane separators. Electrospun nanofiber membranes are inherently weak and cannot withstand the large tension developed by the winding operation used during battery assembly. Coating electrospun SiO_2/PVDF nanofibers onto both sides of PP nonwovens leads to new SiO_2/PVDF nanofiber-coated PP nonwoven separators with improved mechanical properties.

The tensile properties of SiO_2/PVDF nanofiber-coated PP nonwoven membranes are shown in Table 3.1. For comparison, the properties of free-standing PVDF nanofiber mat and un-coated PP nonwoven are also shown. The free-standing PVDF nanofiber mat has a Young` s modulus of 26 MPa, a tensile strength of 2.2 MPa, and a strain-at-break of 40%. Compared with PVDF nanofiber mat, the PP nonwoven has higher modulus (46 MPa),

strength (2.7 MPa) and strain-at-break (190%). Coating SiO_2/PVDF nanofibers onto the both sides of the PP nonwoven leads to new membrane separators that have greater moduli and strengths than both the nanofiber mat and the PP nonwoven.

From Table 3.1, it is also seen that the introduction of SiO_2 increases both modulus and tensile strength of nanofiber-coated membranes. For example, the modulus and tensile strength of the 15% SiO_2/PVDF nanofiber-coated PP nonwoven membrane are 109.2 MPa and 3.9 MPa, respectively, which are 322% and 77% times higher than those of the free-standing nanofiber mat. The strains-at-break of SiO_2/PVDF nanofiber-coated PP nonwoven membranes are also greater than that of the nanofiber mat although they are slightly lower than that of the PP nonwoven.

Table 3.1 Mechanical properties of SiO_2/PVDF nanofiber-coated PP nonwoven membranes.

	Young Modulus (MPa)	**Strength (MPa)**	**Strain-at-Break (%)**
PVDF nanofiber mat	25.9	2.2	40%
PP nonwoven	46.4	2.7	190%
0% SiO_2/PVDF nanofiber-coated PP nonwoven	85.3	2.8	180%
5% SiO_2/PVDF nanofiber-coated PP nonwoven	88.0	3.0	170%
10% SiO_2/PVDF nanofiber-coated PP nonwoven	91.3	3.2	160%
15% SiO_2/PVDF nanofiber-coated PP nonwoven	109.2	3.9	150%

3.3.3 Liquid electrolyte uptake

Rapid and high amount of electrolyte absorption is important for battery application because it can reduce the electrolyte filling time and improve the cell performance [2]. On the other hand, low electrolyte uptake leads to increased internal ionic resistance and hinders the performance of cells. Figure 3.4 shows the uptake capacities of SiO_2/PVDF nanofiber-coated PP nonwoven membranes as a function of SiO_2 content. All membranes show good wettability for the liquid electrolyte solution because of the high surface area of nanofibers and good affinity of PVDF. From Figure 3.4, it is also seen that with increase in SiO_2 content, the electrolyte uptake capacity increases. The electrolyte uptake capacities are 226, 237, 246, and 291%, respectively, for 0, 5, 10, and 15% SiO_2/PVDF nanofiber-coated PP nonwoven membranes. The electrolyte uptake is dependent on the membrane morphology. As discussed in section 3.1, with the SiO_2 content increasing from 0 to 5%, the average fiber diameter decreases from 381 to 312 nm. In this case, the decrease in fiber diameter is the main reason for the electrolyte uptake capacity to increase from 226 to 237%. When the SiO_2 content increases from 5 to 10%, the fiber diameter only decreases slightly from 312 to 310 nm, but the fiber surface roughness increases significantly, as shown in Figure 3.2. As a result of the increased surface roughness, the electrolyte uptake increases from 237 to 246%. When the SiO_2 content continues to increase from 10 to 15%, the fiber surface roughness even increases faster although the fiber diameter only decreases from 310 to 307 nm. This leads to a rapid increase in electrolyte uptake from 246 to 291%. Therefore, both fiber diameter and surface roughness play important roles in determining the electrolyte uptake. These results indicate that SiO_2 particles help sustain tunneling structures and hold more liquid electrolyte when they are used as the filler for battery separators. Similar relationship

between the fiber structure and electrolyte uptake capacity has also been reported by Sethupathy et al [32] on PVDF/SiO_2 composite polymer electrolytes.

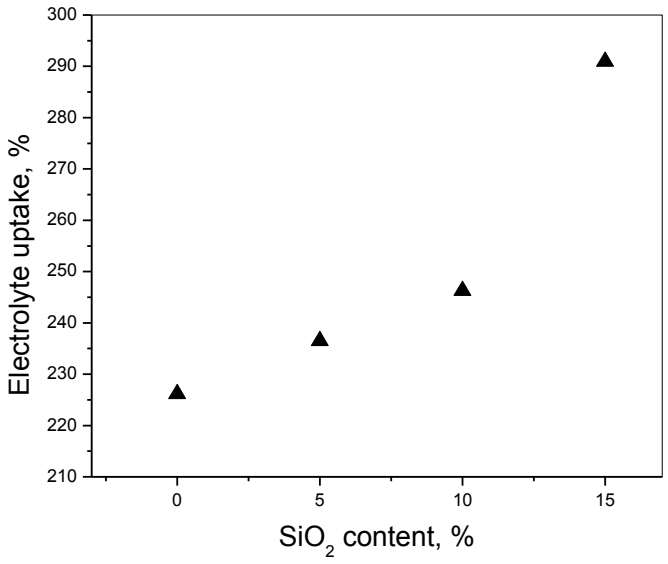

Figure 3.4 Electrolyte uptake capacities of SiO_2/PVDF nanofiber-coated PP nonwoven membranes.

3.3.4 Ionic conductivity

In a lithium-ion cell, the cell conductivity mainly depends on the electrolyte. However, the separator can affect the electrochemical performance of a lithium-ion cell since its porous structure determines the ionic pathways and the inorganic nanoparticle fillers could form intermolecular interactions with electrolyte components [13,20,30,33]. Figure 3.5 shows the conductivities of liquid electrolyte-soaked SiO_2/PVDF nanofiber-coated PP nonwoven membranes at room temperature. It is seen that adding SiO_2 nanoparticles increases the ionic conductivity. The room-temperature conductivity is 8.4×10^{-4}, 2.1×10^{-3},

2.3×10^{-3}, and 2.6×10^{-3} S/cm, respectively, for liquid electrolyte-soaked membranes that contain 0, 5, 10, and 15% SiO_2 nanoparticles.

For SiO_2/PVDF nanofiber-coated PP nonwoven membranes, the presence of SiO_2 nanoparticles decreases the fiber diameter and increases the surface roughness of SiO_2/PVDF nanofibers, which can help the membranes entrap more liquid electrolyte. This may be the main reason for the increased conductivities at high SiO_2 contents. Comparing Figures 3.2 and 3.5, it is seen that the conductivity and average fiber diameter are inversely correlated, *i.e.*, the conductivity increases with decrease in fiber diameter. Jung et al [20] studied polyacrylonitrile nanofiber-based composite membranes and found that both electrolyte uptake and conductivity increased after adding 12% SiO_2 particles due to the fact that these nanoparticles elevated the surface area by introducing Lewis acid/base interaction. Improved ionic conductivities of nanofiber membranes due to Lewis acid/base interactions between the polar surface groups on the filler surface and the ionic species in the liquid electrolyte have also been reported in other earlier studies [13,20,30,33].

The temperature dependence of ionic conductivity of liquid electrolyte-soaked SiO_2/PVDF nanofiber-coated PP nonwoven membranes is shown in Figure 3.6. It is seen that for all membranes, the ionic conductivity increases with increase in temperature. Ionic conductivity of the electrolyte is dependent on the number of charge carriers and their mobility. Increasing temperatures elevates the motilities of charge carriers, which in turn lead to increased conductivities [13,18,19,28].

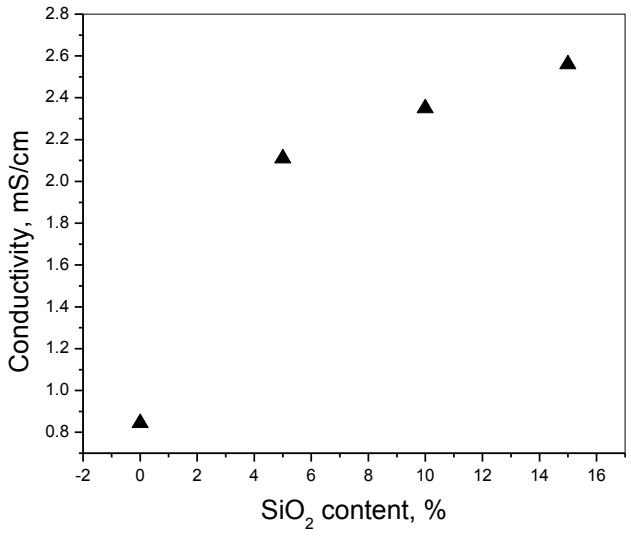

Figure 3.5 Ionic conductivities of SiO_2/PVDF nanofiber-coated PP nonwoven membranes at 25 ^oC.

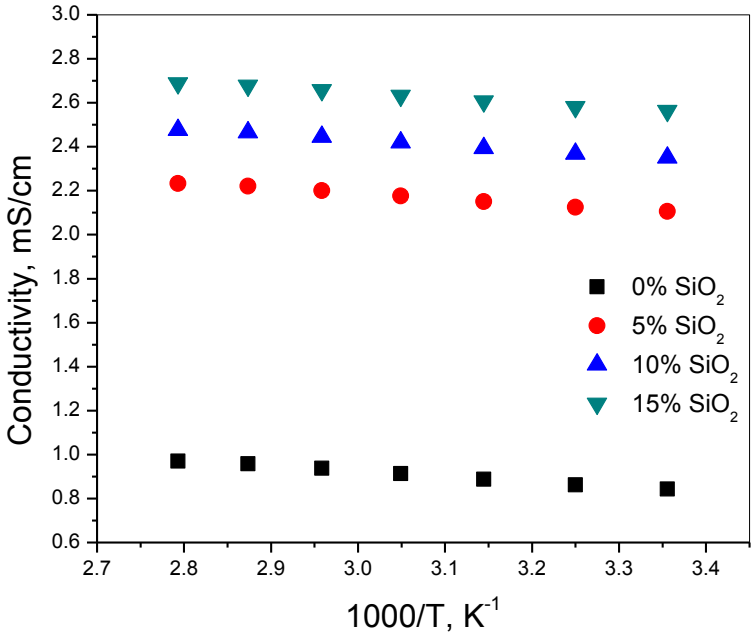

Figure 3.6 Ionic conductivities of SiO_2/PVDF nanofiber-coated PP nonwoven membranes as a function of temperature.

3.3.5 Electrochemical oxidation limit

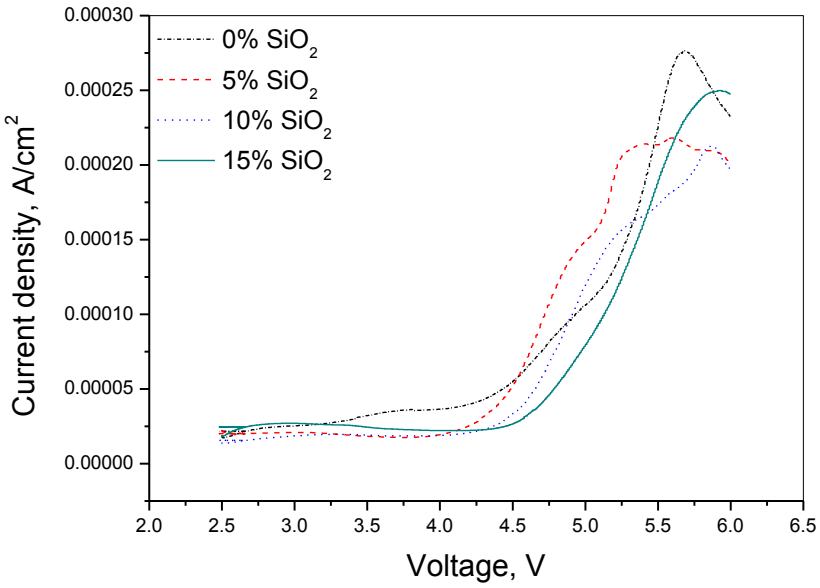

Figure 3.7 Electrochemical oxidation limits of SiO_2/PVDF nanofiber-coated PP nonwoven membranes.

Electrochemical oxidation limit is an important parameter for characterizing battery separators. The electrochemical oxidation limits of liquid electrolyte-soaked SiO_2/PVDF nanofiber-coated PP nonwoven membranes were evaluated by linear sweep voltammetry measurements (Figure 3.7). In these measurements, the electrochemical oxidation limit can be identified by the rapid increase of the current observed when the electrolyte starts to decompose. The working potential range of practical lithium-ion rechargeable batteries are generally between 1.8 V to 3.5 V vs. Li. From Figure 3.7, it is seen that all membranes show sufficient electrochemical stabilities. In addition, the addition of SiO_2 nanoparticles increases the electrochemical oxidation limit. For example, pure PVDF nanofiber-coated PP nonwoven membranes exhibit an electrochemical oxidation limit of around 4.5 V, while the

15% SiO_2/PVDF nanofiber-coated membranes have an increased oxidation limit of about 4.7 V. This indicates that SiO_2 nanoparticles act as a stabilizer by absorbing electrolyte impurities and enhance the electrochemical oxidization stability of liquid electrolyte-soaked membranes. The stabilizing effect of SiO_2 nanoparticles have also been observed by several research groups [20,28,34-36].

3.3.6 Interfacial resistance

The compatibility of liquid electrolyte-soaked SiO_2/PVDF nanofiber-coated PP nonwoven membranes with lithium metal was investigated by measuring electrochemical impedance spectra of Li/liquid electrolyte-soaked membrane/Li cells, and the results are shown in Figure 3.8. The intermediate-frequency semicircle corresponds to the charge transfer process and its diameter is related to the impedance of the passivation layer formed on the surface of lithium metal. It is seen in Figure 3.8 that with increase in SiO_2 content, the interfacial resistance decreases. This result is in a good agreement with earlier studies on filler-containing separator systems [20,24,29,31]. For example, it has been reported by Stephan et al. [29] and Liao et al. [31] that adding ceramic fillers can improve the interfacial properties with the lithium electrode because the nanoparticles with high surface areas can trap impurities by capillary force. In general, higher filler content and smaller particle size are more effective in increasing the interfacial properties [20,30].

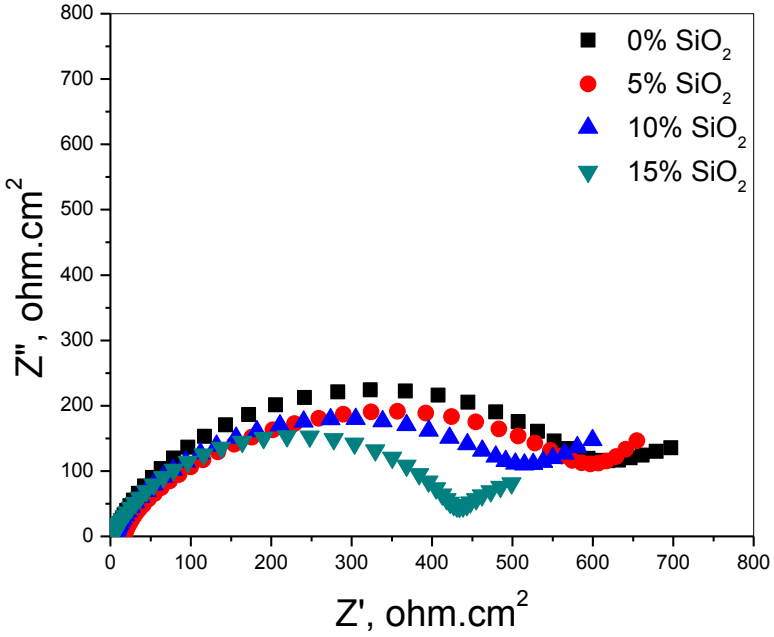

Figure 3.8 Electrochemical impedance spectra of SiO_2/PVDF nanofiber-coated PP nonwoven membranes.

3.3.7 Cycling performance

In order to further examine the feasibility of using SiO_2/PVDF nanofiber-coated PP nonwoven membranes as separators in rechargeable lithium-ion batteries, coin-type cells were fabricated with $LiFePO_4$ as the cathode and lithium metal as the counter electrode. The first-cycle charge and discharge curves of the cells are shown in Figure 3.9. All curves show stable platforms for both charging and discharging. For cells containing 0, 5, 10, and 15% SiO_2/PVDF nanofiber-coated PP nonwoven membranes, the first-cycle discharge capacities are 153, 159, 159, and 159 mAh/g, respectively.

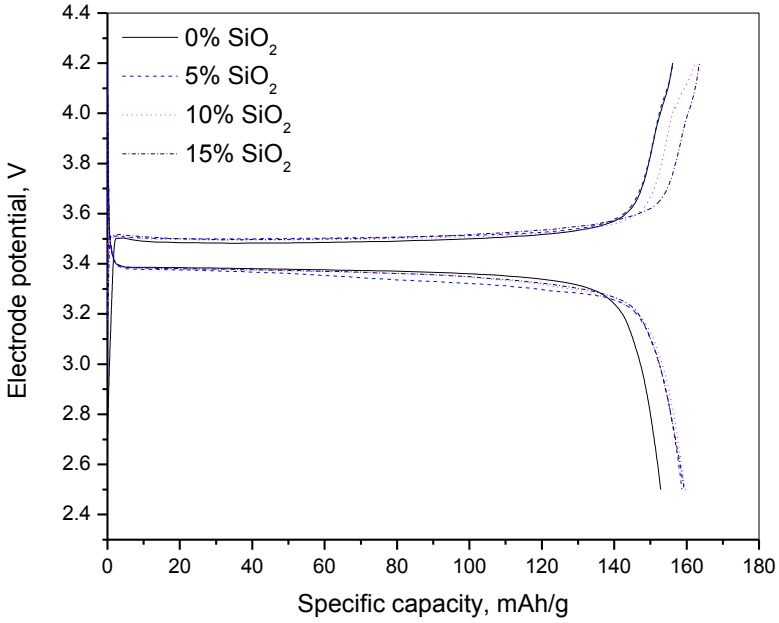

Figure 3.9 First cycle charge and discharge curves of Li/$LiFePO_4$ cells containing SiO_2/PVDF nanofiber-coated PP nonwoven membranes.

The cycling performance of the cells is shown in Figure 3.10. For cells containing 0, 5, 10, and 15% SiO_2/PVDF nanofiber-coated PP nonwoven membranes, the capacities after 50 cycles are 152,152, 159 ,163 mAh/g, respectively. The corresponding capacity retentions in the first 50 cycles are 88%, 90%, 93% and 96%, respectively. Here, the capacity retentions were calculated based on the theoretical capacity (170 mAh/g) of $LiFePO_4$. Therefore, increasing SiO_2 content improves the discharge capacity and leads to better cycling performance. As discussed in previous sections, the addition of SiO_2 nanoparticles leads to reduced fiber diameter, increased surface area, improved liquid electrolyte uptake, and lower interfacial resistance. It is well known that SiO_2 nanoparticles can enhance the electrochemical performance by increasing surface area, enhancing ionic conductivity and

promoting better membrane-electrode contact [20]. Therefore, the improved cycling performance shown in Figure 3.10 could be attributed to the unique porous structure, high liquid electrolyte uptake, and low interfacial resistance of SiO_2/PVDF nanofiber-coated PP nonwoven membranes at high SiO_2 contents. These results confirm that SiO_2/PVDF nanofiber-coated PP nonwoven membranes are promising separator candidate for rechargeable lithium-ion batteries.

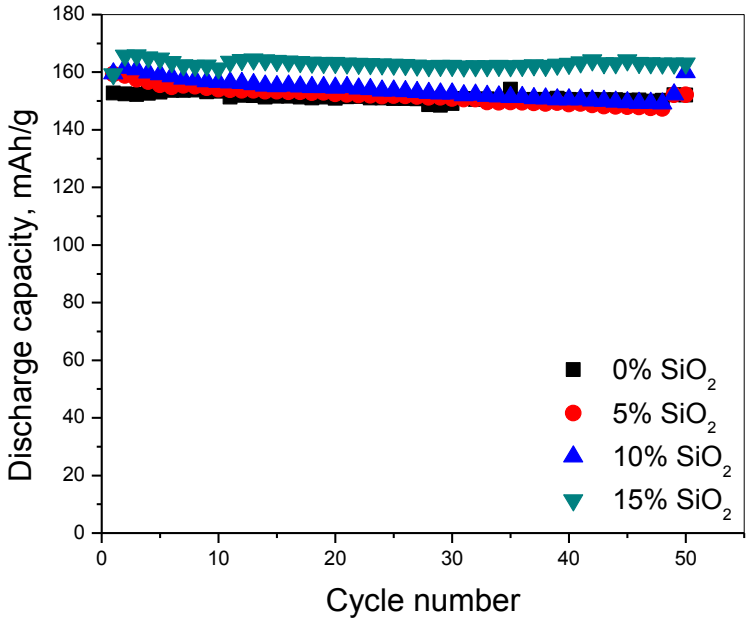

Figure 3.10 Cycling performance of Li/$LiFePO_4$ cells containing SiO_2/PVDF nanofiber-coated PP nonwoven membranes.

3.4 Conclusion

SiO_2/PVDF nanofiber-coated PP nonwoven membranes were prepared by using electrospinning technique. The physical and electrochemical properties, such as porosity, mechanical strength, uptake capacity, lithium-ion conductivity, electrochemical oxidation

limit, interfacial resistance and cycling performance, were investigated. Results show these novel composite separators possess good wettability, high ionic conductivity, sufficient electrochemical stability, low interfacial resistance and good cycling performance. Improved mechanical strengths, ionic conductivities, electrochemical stabilities and interfacial resistances were observed at high SiO_2 contents. The cells containing SiO_2/PVDF nanofiber-coated PP nonwoven separators with high SiO_2 contents also showed excellent cycling performance. SiO_2/PVDF nanofiber-coated PP nonwoven membranes are promising separator candidate for rechargeable lithium-ion batteries.

REFERENCES

[1] D. Saikia, H. Y. Wu, Y. C. Pan, C. P. Lin, K. P. Huang, K. N. Chen, G. T. K. Fey, H. M. Kao, J Power Sources, 196 (2011) 2826–2834.

[2] X. Huang, J Solid State Chem, 15 (2011) 649–662.

[3] Xiang, J. Chen, Z. Li, H.Wang, , J Power Sources, 196 (2011) 8651-8655.

[4] D. Fu, B. Luan, S. Argueb, M. N. Bureau, I. J. Davidson, J Power Sources,206 (2012) 325–333.

[5] S. H. Yoo and C. K. Kim, Ind. Eng. Chem. Res. 48 (2009) 9936–9941.

[6] X. Zhang, L. Ji, O. Toprakci, Y. Liang, and M. Alcoutlabi, Polym Rev,51 (2011) 239–264.

[7] J. H. Cho, J. H. Park, J. H. Kim, S. Y. Lee, J Mater Chem, 21 (2011) 8192.

[8] K.Gao, X. Hu, C. Dai, T. Yi, Mat Sci Eng B-Solid, 131 (2006) 100–105.

[9] J. Fang, A. Kelarakis, Y. W. Lin, C.Y. Kang, M. H. Yang, C. L. Cheng, Y. Wang, E. P. Giannelis, L. D. Tsai, Phys Chem Chem Phys 13 (2011) 14457-61.

[10] J. R. Kim, S. W. Choi, S. M. Jo, W. S. Lee, and B. C. Kim, J Electrochem Soc 152 (2005) A295-A300.

[11] C. Yang, Z. Jia, Z. Guan, L. Wang, J Power Sources, 189 (2009) 716–720.

[12] L. Zhao, H. Zhang, X. Li, J. Zhao, C. Zhao, X. Yuan, J Appl Polym Sci 111 (2009) 3104–3112.

[13] P. Raghavan, X. Zhao, J. K. Kim, J. Manuel, G. S. Chauhan, J. H. Ahn, C.Nah, Electrochim Acta 54 (2008) 228–234.

[14] T. H. Cho, M. Tanaka, H. Onishi, Y. Kondob,T. Nakamura, H. Yamazaki, S. Tanase, T. Sakai, J Power Sources, 181 (2008) 155–160.

[15] M.Alcoutlabi, H. Lee, J.V. Watson, and X. Zhang, J Mater Sci 48 (2013) 2690-2700.

[16] S. S. Choi, Y. S. Lee, C. W. Joo, S. G. Lee, J. K. Park, K. S. Han, Electrochim Acta 50 (2004) 339–343.

[17] Z. Zhong, Q. Cao, B. Jing, X. Wang, X. Li, H. Deng Mater Sci Eng B Solid, 177 (2012) 86–91.

[18] Y. Liang, Z. Lin, Y. Qiu, and X. Zhang, Electrochim Acta, 56 (2011) 6474-6480.

[19] Y. Liang, L.Ji, B. Guo, Z. Lin, Y. Yao, Y. Li, M. Alcoutlabi, Y. Qiu, and X. Zhang, J Power Sources, 196 (2011) 436-441.

[20] H. R. Jung, D. H. Ju, W. J. Lee, X. Zhang, and R. Kotek, Electrochim Acta, 54 (2009) 3630-3637.

[21] W. Qi , C.Lu , P. Chen , L. Han , Q. Yu , R. Xu, Mater Lett, 66 (2012) 239–241.

[22] S. W. Lee , S. W. Choi , S. M. Jo , B. D. Chin ,D. Y. Kim, K. Y. Lee, J Power Sources, 163 (2006) 41–46.

[23] A. I. Gopalan, P. Santhosh, K. M. Manesh, J. H. Nho, S. H. Kim, C. G. Hwang, K. P. Lee, J Membrane Sci, 325 (2008) 683–690.

[24] X. Zhang, Y. Li, S.A. Khan and P. S. Fedkiw, J. Electrochem. Soc. 151 (2004) A1257-A1263.

[25] K. M. Kim, N. G. Park, K. S. Ryua, S. H. Chang Electrochim Acta , 51 (2006) 5636–5644.

[26] J. K. Kim, G. Cheruvally, X. Li, J. H. Ahna, K. W. Kim, H. J. Ahn, J Power Sources 178 (2008) 815–820.

[27] L. Ji, X. Zhang, Mater Lett 62 (2008) 2161–2164.

[28] P. Raghavan, J.W. Choi, J.-H. Ahn, Gouri Cheruvalla,G.S. Chauhan, H.J. Ahn, C.Nah, J Power Sources 184 (2008) 437–443.

[29] A. Manuel Stephan, K.S. Nahm, Polymer 47 (2006) 5952-5964

[30] C. Nan, L. Fan, Y. Lin, Q. Cai, Physical Review Letters, 91 (2003) 266104-1.

[31] Y. Liao, C Sun, S. Hu, W Li, Electrochimica Acta, 89 (2013) 461-468.

[32] M. Sethupathy, V. Sethuraman, P. Manisankar, Soft Nanoscience Letters,3 (2013) 73,37-43.

[33] Y. J. Kim, C. H. Ahn, M. B.Lee, M.S. Choi, Materials Chemistry and Physics, 127 (2011) 137-142.

[34] W. L. Li, J. J. Tang, B.T. Li, J Organomet Polym, 23 (2013) 831-834.

[35] Y.H. Liao, M. M. Rao, W. S. Li, L. T. Yang, B. K. Zhu, R. Xu, C. H. Fu, , J of Membrane Sci, 352 (2010) 95-99.

[36] Y. Liao, S. Sun, S. Hu, W. Li, Electrochimica Acta (2013) 461-468.

CHAPTER 4. NANOPARTICLE-ON-NANOFIBER HYBRID MEMBRANES AS SEPARATOR FOR LITHIUM-ION BATTERIES VIA COMBINING ELECTROSPRAYING AND ELECTROSPINNING TECHNIQUES

ABSTRACT

Nanoparticle-on-nanofiber hybrid membranes were prepared by electrospraying of SiO_2 dispersions and electrospinning of polyvinylidene fluoride (PVDF) solution *simultaneously*. The aim of this study was to design new high-performance separator membranes with superior electrochemical properties such as high C-rate performance and good thermal stability compared to polyolefin based membranes. Uniform, bead-free fibrous structure with high amount of SiO_2 nanoparticles exposed on PVDF nanofiber surfaces was observed. It was found that wettability and ionic conductivity were improved by dispersing SiO_2 nanoparticles onto PVDF nanofiber surfaces. Electrochemical properties were enhanced due to the increased surface area caused by the unique hybrid structure of SiO_2 nanoparticles and PVDF nanofibers. Compared with commercial microporous polyolefin membranes, SiO_2/PVDF hybrid membranes had larger liquid electrolyte uptake, higher electrochemical oxidation limit, and lower interfacial resistance with lithium. SiO_2/PVDF hybrid membrane separators were assembled into lithium/lithium iron phosphate cells and demonstrated high cell capacities and good cycling performance at room temperature. In addition, cells using SiO_2/PVDF hybrid membrane separators showed superior C-rate performance compared to those using commercial microporous PP membrane.

4.1. Introduction

Li-ion batteries are important power sources with high energy density, high operational voltage, long cycle life, and low self-discharge rate, and hence they have been widely used to power many portable devices such as cellular phone, laptops, digital cameras, etc. Although current Li-ion batteries have the highest energy density compared to other commercial rechargeable batteries, significant improvements are still needed in energy density, safety, durability and cost to meet the long-term performance targets for plug-in hybrid electric vehicles and all electric vehicles [1-3].

Presently available Li-ion batteries utilize liquid electrolyte which makes them prone to catching fire and explosion. There are two ways to overcome this problem: firstly, by using solid state electrolytes [4, 5], and secondly, by using thermally-stable separators [6]. Separators are placed between the positive and negative electrodes in Li-ion batteries. They must be electronic insulators to prevent electron transfer between two electrodes and, at the same time, they must be highly porous to allow Li-ions to travel. Although they do not participate in electrochemical reactions, separators play a vital role in preventing short circuit, allowing Li-ion transfer, and regulating cell kinetics. As a result, the physical properties of separators can affect the cell capacity, cell resistance, rate performance, and long-term cycling capability of Li-ion batteries [7-10]. There are many requirements for separator materials such as good mechanical, dimensional, chemical stabilities, low ionic resistance, high wettability, and excellent structural uniformity to obtain safe batteries with high performance. Among them, low resistance, low shrinkage, and uniform pore structure are essential for separators. Currently, microporous membranes are the most commonly used separator types and they are polyolefin-based materials with good mechanical properties and

chemical stability [11-14]. However, their wettability and thermal stabilities are not sufficient for applications that require high operating temperature and high performance such as higher charge/discharge rate. Low affinity of these membranes to liquid electrolyte also leads to high cell resistance that affects the cycling performance and rate performance negatively [15].

Due to the superior properties such as large specific surface area, small pore size and high porosity, electrospun nanofiber membranes can be good separator candidates for high-performance lithium-ion batteries [8]. Polyvinylidene fluoride (PVDF) and its copolymers are the most studied materials for nanofiber separators due to their high polarity, good thermal and mechanical properties, high affinity to electrolyte solutions, good chemical stability, and excellent compatibility with electrodes [16].

Moreover, the performance of nanofiber membranes can be further improved by introducing ceramic fillers which form Lewis acid/base interactions with the ionic species in the liquid electrolyte [17-19]. Although ceramic/polymer composites can be prepared by encapsulating ceramic particles directly into polymer nanofibers, the performance of the resultant composite membranes are restricted because these nanoparticles are not exposed to liquid electrolytes and have limited effect on improving the cell performance.

Here, we introduce new nanoparticle-on-nanofiber hybrid membrane separators by combining electrospraying with electrospinning. Both techniques utilize electric forces to draw jets from charged liquids and deposit them onto grounded collector. In electrospraying, when the electric force is higher than surface tension of the liquid, the jets are atomized into fine droplets. In electrospinning, the electric repulsion force cannot overcome the intermolecular forces in the liquid, and hence the jets are not broken and they extend, bend

and eventually reach the collector forming a nonwoven mat of nanofibers [20-22]. In this study, SiO_2/PVDF nanoparticle/nanofiber hybrid membranes were prepared by *simultaneously* electrospraying of SiO_2 dispersion and electrospinning of PVDF solution (Figure 4.1A). By using this electrospraying-electrospinning combined process, SiO_2 nanoparticles were attached on the nanofiber surfaces (Figure 4.1B) and are more effective to improve the separator properties since they are not encapsulated and separated from liquid electrolytes. Experimental results showed that these novel hybrid membranes had higher conductivities, lower interfacial resistances and better C-rate performance compared to pure PVDF nanofiber membrane and microporous PP membrane. It is, therefore, demonstrated that SiO_2/PVDF nanoparticle/nanofiber hybrid membranes prepared by the electrospraying-electrospinning combined process are promising separator candidate for high-performance Li-ion batteries.

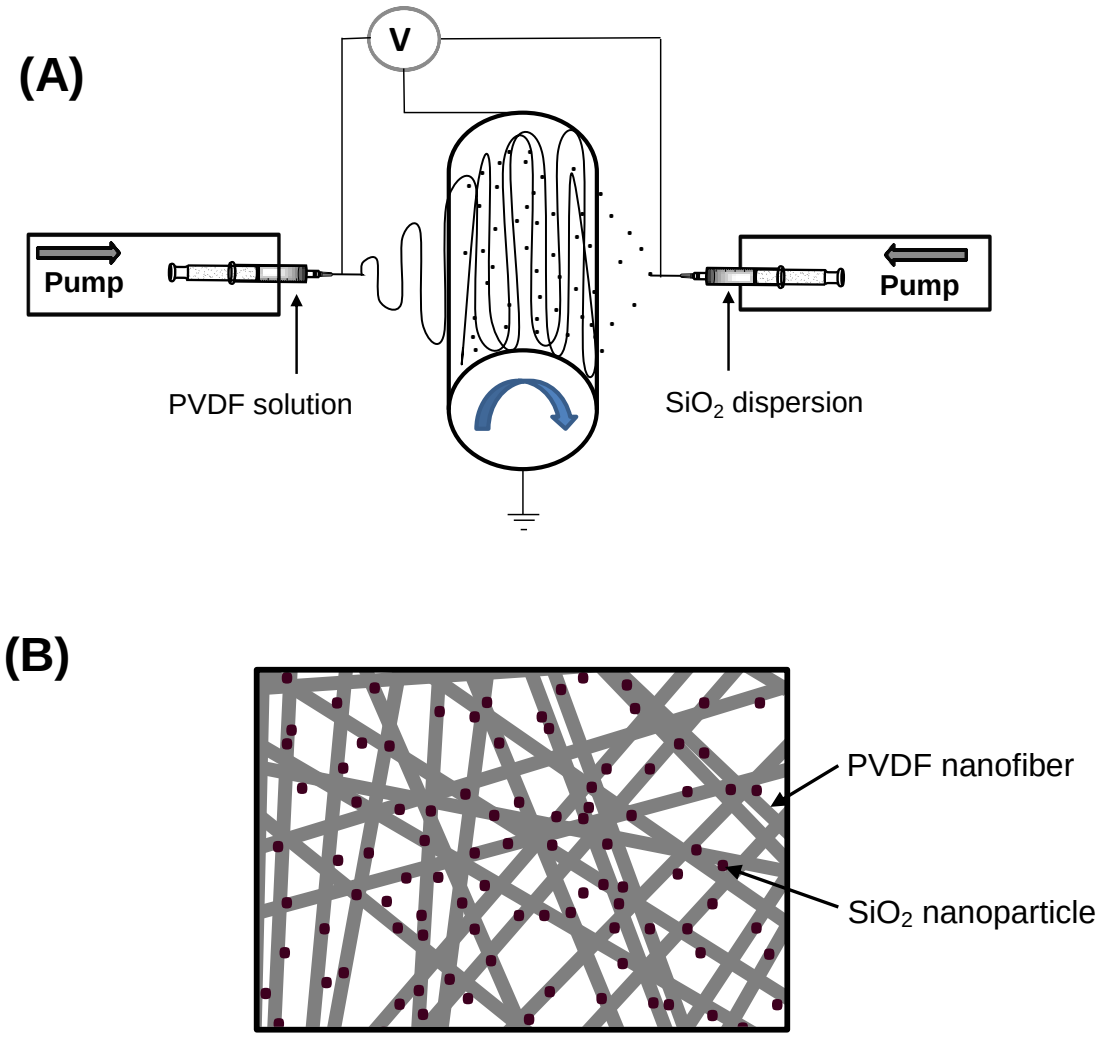

Figure 4.1 (A) Preparation and (B) schematic view of SiO_2/PVDF nanoparticle/nanofiber hybrid separators.

4.2 Experimental

4.2.1 Chemicals

Hydrophilic pyrogenic SiO_2 (Aerosil 380, particle size = 7 nm, surface area = 380 m^2/g) was supplied from Evonic industries. Polyvinylidene fluoride (PVDF, M_w = 30×10^4 - 50×10^4) was obtained from Shanghai Ofluorine Chemical Technology. N,N-

dimethylformamide (DMF), acetone, methanol and n-butanol were purchased from Sigma Aldrich. Liquid electrolyte, 1 M lithium hexafluorophosphate ($LiPF_6$) in ethylene carbonate and ethyl methyl carbonate (EC+EMC, 1:1 by volume), was supplied from Ferro Corp. Celgard 2400 microporous polypropylene was used for comparison. $LiFePO_4$ was obtained from Hydro-Qubec. All chemicals were used as received without further purification.

4.2.2 Separator preparation

SiO_2/PVDF nanoparticle/nanofiber hybrid membranes were prepared by electrospraying of SiO_2 dispersions and electrospinning of PVDF solution *simultaneously*. SiO_2 dispersions were prepared by dispersing different amounts of SiO_2 nanoparticles (0, 1, 3 and 5 wt%) into methanol. The dispersions were stirred at room temperature overnight and ultrasonificated before electrospraying to ensure the uniformity. PVDF solution was prepared by dissolving 10 wt% PVDF in DMF/acetone (7:3 by volume), which was stirred at 60 ^{o}C for at least 8 hours to ensure dissolution of the polymer.

During the preparation of SiO_2/PVDF hybrid membranes, a variable high voltage power supply (Gamma) was used to provide a high voltage of 20 kV. For both SiO_2 dispersions and PVDF solution, the feeding rate used was 1.5 ml/h and the tip-to-collector-distance was 17 cm. Electrosprayed nanoparticles and electrospun PVDF nanofibers were accumulated on the collector *simultaneously* to form nanoparticle/nanofiber hybrid membranes. The resultant membranes were dried at 80 $^{\circ}$C for at least 24 hours to remove residual solvents.

4.2.3 Structure Characterization

The morphology of SiO_2/PVDF hybrid membranes was studied by using a JEOL JSM-6400F field-emission scanning electron microscope (FESEM). The SiO_2 contents in SiO_2/PVDF hybrid membranes were analyzed on a Perkin Elmer 2000 DV ICP-Optical emission spectrometer after acid digestion.

The porosities of the membranes were determined by using n-butanol uptake tests. In a uptake test, the porosity was calculated by using the following equation:

$$Porosity\ (\%) = \frac{w_w - w_d}{\rho_b \times V} \quad (1)$$

where w_w and w_d are the weights of wet and dry membranes, respectively, ρ_b the density of n-butanol, and V the geometric volume of the membrane.

4.2.4 Performance evaluation

The dimensional stability of the membranes were determined by thermal shrinkage tests at 150 ^oC for 30 minutes. The mechanical properties of the membranes were determined by using a universal tensile tester (Instron 5544) with 100 N capacity load cell. The dimensions of test specimens were 10 mm wide, 60 μm thick, and 60 mm long.

Liquid electrolyte uptakes were measured by soaking weighed membranes in the liquid electrolyte of 1M $LiPF_6$ in EC+EMC (1:1 in volume) for two hours at room temperature. The electrolyte uptake (*EU*) was calculated by:

$$EU\ (\%) = \frac{w_1 - w_0}{w_0} \times 100 \quad (2)$$

where w_0 and w_1 are the weights of dry and wet membranes, respectively.

The ionic conductivities of liquid electrolyte-soaked membranes were measured by electrochemical impedance spectroscopy (EIS) using Reference 600

Potentiostat/Galvanostat/ZRA (GAMRY). The impedance measurements were performed on liquid electrolyte-soaked membranes sandwiched between two stainless steel electrodes over a frequency range of 1 MHz to 10^{-2} Hz with AC amplitude of 10 mV and within a temperature range of 25 to 85 ^{o}C. The ionic conductivity was calculated by:

$$\sigma = \frac{d}{R_b \times S} \tag{3}$$

where d is the membrane thickness, S the cross-sectional area, and R_b the bulk resistance obtained at the high frequency intercept of the Nyquist plot on the real axis.

The electrochemical oxidation limits of liquid electrolyte-soaked membranes were determined by linear sweep voltammetry at room temperature. In these tests, electrochemical cells consisting of stainless steel working electrode and lithium metal counter electrode were used. The scan rate used was 10 mVs^{-1} and the potential range was 2.5 to 6.0 V.

The interfacial resistances between the liquid electrolyte-soaked membranes and lithium metal were investigated by measuring the impedances of symmetrical lithium cells. The frequency range used was 1 MHz to 10^{-2} Hz.

The charge-discharge tests of Li/$LiFePO_4$ cells containing liquid electrolyte-soaked membranes were conducted by using coin-type cells. The $LiFePO_4$ cathode was prepared by blending $LiFePO_4$ powder (80 wt%), carbon black conductor (10 wt%) and PVDF binder (10 wt%). Arbin automatic battery cycler was used in a potential range of 4.2 - 2.5 V at a current density of 0.2 C and 1C to evaluate the cycling performance. In order to evaluate C-rate performance, different C-rates (0.2C, 0.5C, 1C, 2C, 4C, and 8C) were applied to cells.

4.3 Results and Discussion

4.3.1 Separator composition

The SiO_2 contents in SiO_2/PVDF hybrid membranes were analyzed by using ICP-Optical emission spectrometer. After the digesting process, samples were diluted with DI water and run against a Si calibration curve. The resultant ICP-OES spectra were used to determine SiO_2 contents in the hybrid membranes. Figure 4.2 shows the Si peak at approximately 251.611 nm for three SiO_2/PVDF hybrid membranes. The average SiO_2 contents in three hybrid membranes were calculated to be 7, 14 and 24 wt.%, respectively.

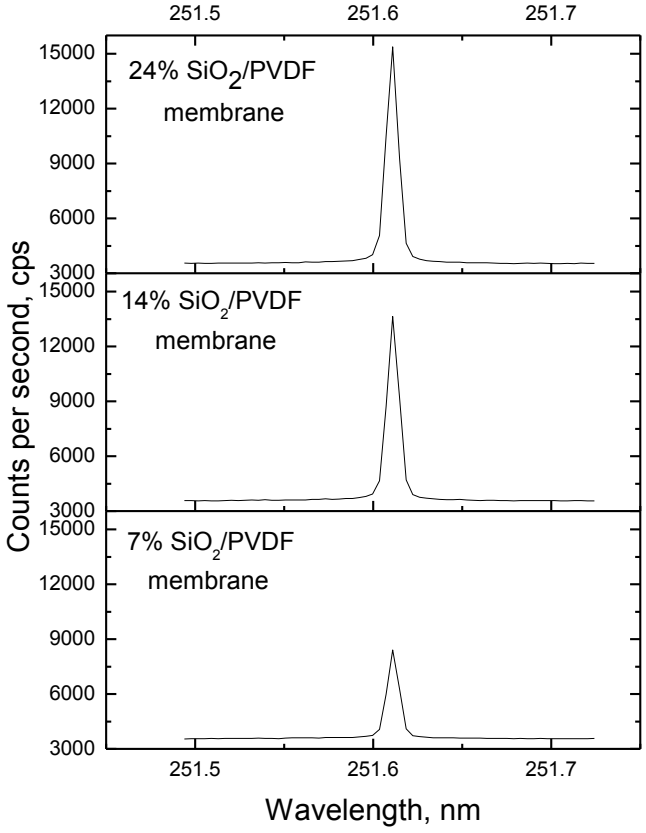

Figure 4.2 ICP-OES spectra of SiO_2/PVDF nanoparticle/nanofiber hybrid membranes with different SiO_2 contents.

4.3.2 Separator morphology

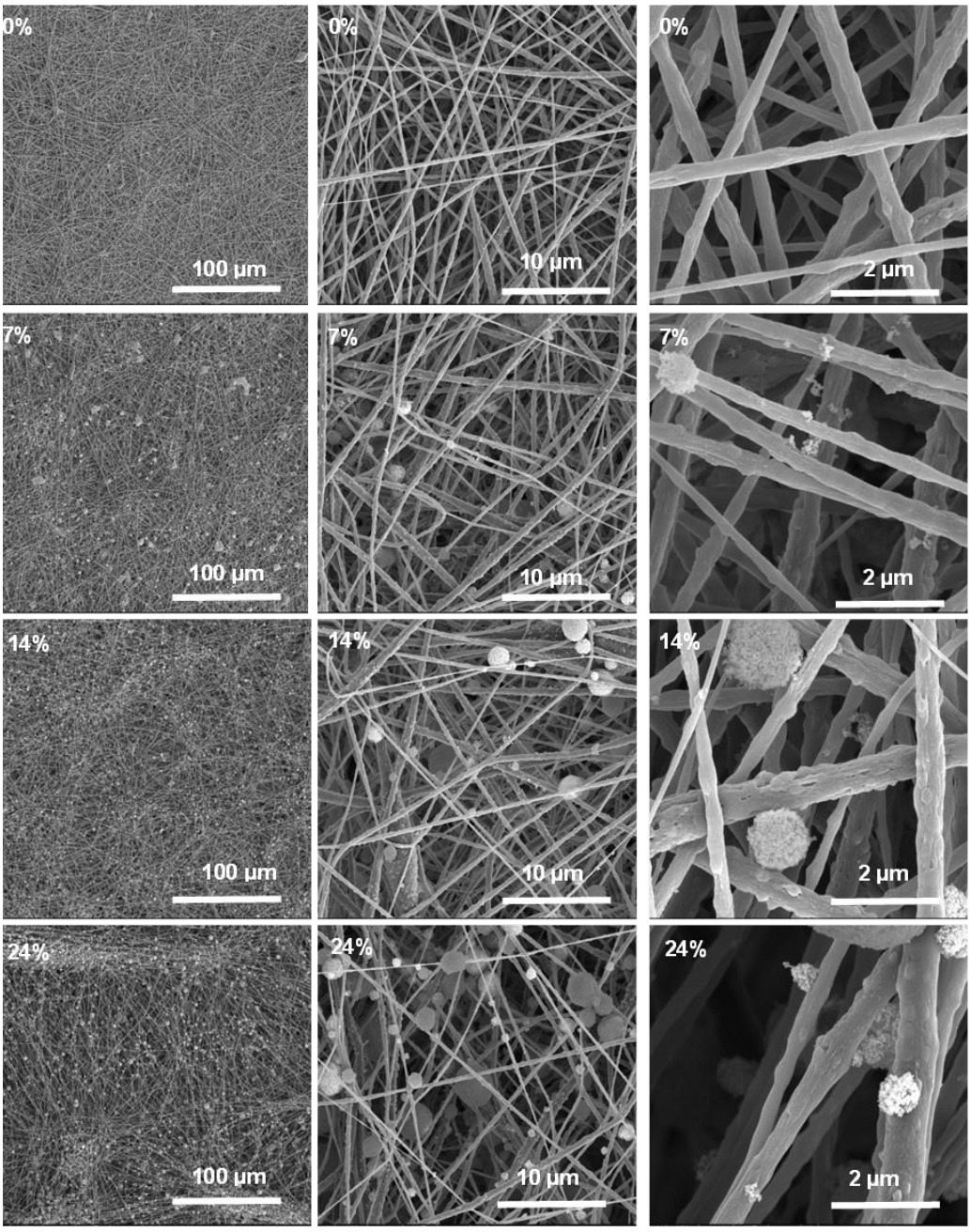

Figure 4.3 SEM images of SiO_2/PVDF nanoparticle/nanofiber hybrid membranes with different SiO_2 contents.

Figure 4.3 shows SEM images of SiO_2/PVDF hybrid membranes with various SiO_2 contents (0, 7, 14, and 24 wt%). Pure PVDF nanofiber membrane (*i.e.*, SiO_2 content = 0 wt%) shows an uniform and bead free morphology. The introduction of 7, 14, and 24 wt% SiO_2 does not change the morphology of electrospun PVDF nanofibers. However, SiO_2 nanoparticles have branched structure with primary partcile size of 7 nm [23, 24], and hence they form agglomerates easily and are dispersed on fiber surfaces. The exposure of SiO_2 nanoparticles on fiber surfaces allow them to increase accessable surface area and form extensive Lewis acid/base interactions with the ionic species in the liquid electrolyte.

Table 4.1 Porosities, electrolyte uptakes and ionic conductivities of SiO_2/PVDF nanoparticle/nanofiber hybrid membranes at room temperature.

	Porosity (%)	**Electrolyte uptake (%)**	**Ionic conductivity (mS/cm)**
0 wt% SiO_2/PVDF hybrid membrane	59 ± 9	289 ± 14	1.7 ± 0.3
7 wt% SiO_2/PVDF hybrid membrane	60 ± 6	352 ± 14	2.1 ± 0.3
14 wt% SiO_2/PVDF hybrid membrane	66 ± 6	357 ± 12	2.3 ± 0.3
24 wt% SiO_2/PVDF hybrid membrane	70 ± 6	370 ± 9	2.6 ± 0.3
Microporous PP membrane	41 ± 4	158 ± 19	0.8 ± 0.1

For battery separator application, high membrane porosity is needed for allowing fast ion transportation between two electrodes. Table 4.1 shows the porosities of SiO_2/PVDF hybrid membranes. For comparison, the porosity of a commercial polypropylene (PP) membrane separator (Celgard 2400) is also shown. It is seen that the porosities of 0, 7, 14, and 24 wt% SiO_2/PVDF hybrid membranes are 59, 60, 66 and 70%, respectively, which are significantly greater than that (41 %) of microporous PP membrane. The PVDF nanofibers form free-standing nonwoven membranes that have relatively high porosities. The introduction of SiO_2 nanoparticles further increases the porosity values since the extra surface area of nanoparticles can help trap more liquid n-butanol during the porosity measurement.

4.3.3 Thermal dimensional stability

Microporous membranes often shrink at elevated temperatures, which could lead to serious safety concern when they are used as battery separators. No or minimal thermal shrinkage is required for preventing internal short circuit failures. Figure 4.4 compares the photographs of SiO_2/PVDF hybrid membranes and microporous PP membrane before and after thermal exposure at 150 ^oC for 30 minutes. The microporous PP membrane could not maintain its shape at 150 ^oC and significant dimensional change was observed. The PVDF nanofiber membrane (SiO_2 content = 0 wt%) is able to maintain its shape, but the sample area reduces by about 3%. On the other hand, 7, 14, and 24 wt% SiO_2/PVDF hybrid membranes not only maintain their shape, but also show no apparent dimensional change. Therefore, SiO_2/PVDF hybrid membranes have excellent thermal dimensional stability.

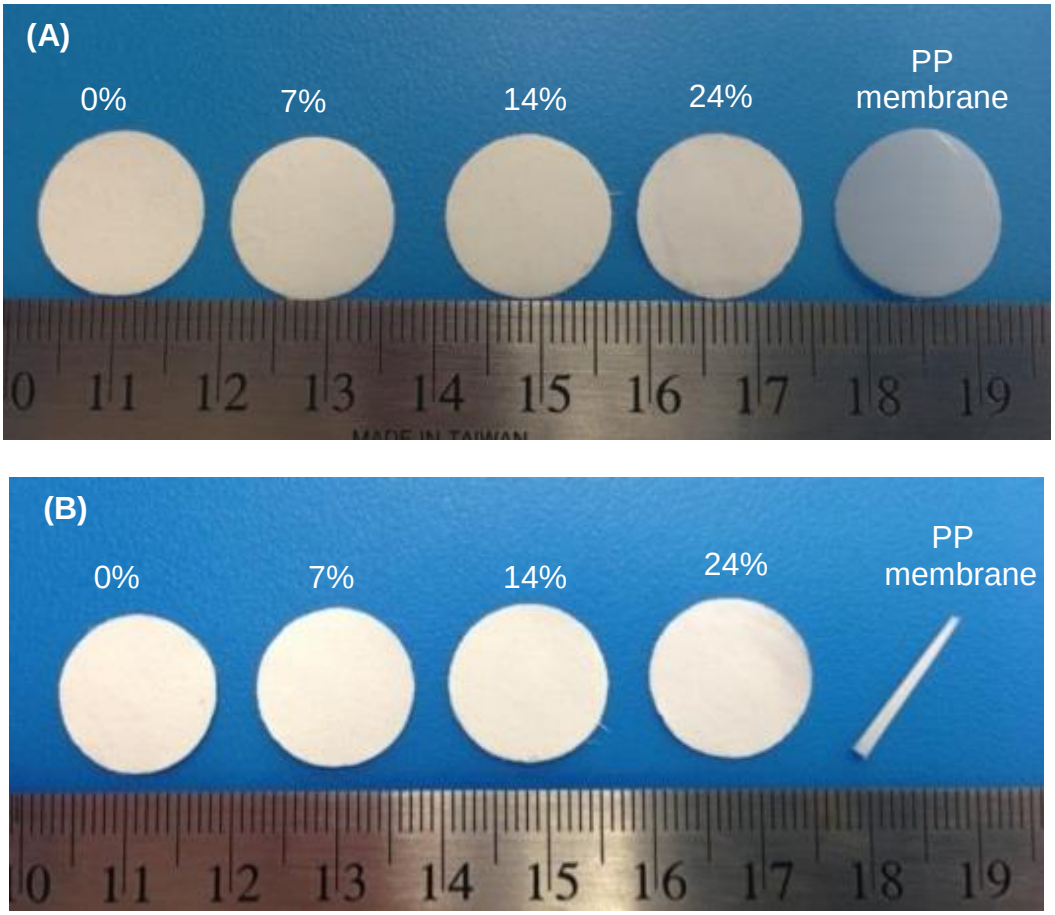

Figure 4.4 Photographs of SiO_2/PVDF nanoparticle/nanofiber hybrid membranes and microporous PP membrane (A) before and (B) after thermal exposure at 150 ^{o}C for 30 minutes.

4.3.4 Mechanical properties

Mechanical properties of SiO_2/PVDF hybrid membranes are important in separator applications. Figure 4.5 shows the typical stress strain curves of the SiO_2/PVDF hybrid membranes and PVDF membrane. All four membranes show comparable mechanical strengths and the strength values are around 13 MPa. These mechanical properties are considered sufficient for most conventional winding machines used in cylindrical battery fabrication [25].

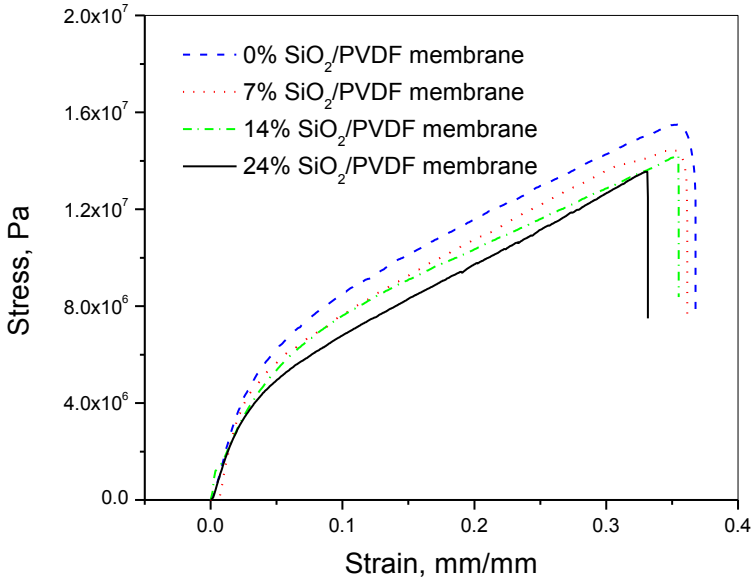

Figure 4.5 Stress strain curves of SiO_2/PVDF nanoparticle/nanofiber hybrid membranes and PVDF membrane.

4.3.5 Liquid electrolyte uptake

The ability of a membrane separator to uptake liquid electrolyte is vital for battery application because high electrolyte update is needed for reducing the internal ionic resistance of the cell [3]. Good separator material should absorb and retain large amount of liquid electrolyte when the cell is assembled. Table 4.1 shows the electrolyte uptake capacities of SiO_2/PVDF hybrid membranes as a function of SiO_2 content. The electrolyte uptake capacity for microporous PP membrane is 158%. The relatively low uptake capacity of this membrane can be explained by its low porosity value (41%). The electrolyte uptake capacity of PVDF nanofiber membrane is 289%, which is almost twice higher than that of the microporous PP membrane. This indicates that the 3-dimentional network formed by the nanofibers is able to uptake a large amount of liquid electrolyte, which has been

demonstrated by other researchers [21, 26]. From Table 4.1, it is also seen that when the SiO_2 content increases from 0 to 7, 14 and 24 wt%, the electrolyte uptake further increases from 289 to 352, 357 and 370%. This is because the SiO_2 nanoparticles can help sustain tunneling structures and hold more liquid electrolyte due to their large surface area [17].

4.3.6 Ionic conductivity

The ionic conductivity of the separator after uptaking liquid electrolyte is an important performance indicator and it depends on the porosity, tortuosity, and thickness of the separator and the resistivity of the electrolyte [12]. In this work, SiO_2/PVDF hybrid membranes were soaked in the liquid electrolyte and placed between two stainless steel electrodes to measure the conductivities. Table 4.1 shows the ionic conductivities of liquid electrolyte-soaked SiO_2/PVDF hybrid membranes and microporous PP membrane at room temperature. It is seen that the room-temperature conductivity (1.7×10^{-3} S/cm) of liquid electrolyte-soaked PVDF nanofiber membrane is significantly greater than that (0.8×10^{-3} S/cm) of liquid electrolyte-soaked microporous PP membrane since the nanofiber membrane has higher electrolyte uptake. Adding SiO_2 nanoparticles into PVDF nanofiber membrane leads to even greater conductivities. The room-temperature conductivities are 2.1×10^{-3}, 2.3×10^{-3}, and 2.6×10^{-3} S/cm, respectively, for liquid electrolyte-soaked hybrid membranes that contain 7, 14, and 24 wt% SiO_2 nanoparticles. For SiO_2/PVDF hybrid membranes, the presence of SiO_2 nanoparticles helps entrap more liquid electrolyte due to their large surface area [17, 27, 28].

The temperature dependence of ionic conductivities of liquid electrolyte-soaked membranes is shown in Figure 4.6. It is seen from the Arrhenius plots that the ionic

conductivities of all membranes increase with increase in temperature. Ionic conductivity is dependent on the number of charge carriers and their mobility, and increasing temperature elevates the mobility of charge carriers, which in turn lead to increased conductivities [27]. From Figure 4.6, it is also seen that after soaking liquid electrolyte, SiO_2/PVDF hybrid membranes exhibit higher ionic conductivities than microporous PP membrane at all temperatures, and higher SiO_2 content always leads to higher ionic conductivities for SiO_2/PVDF hybrid membranes.

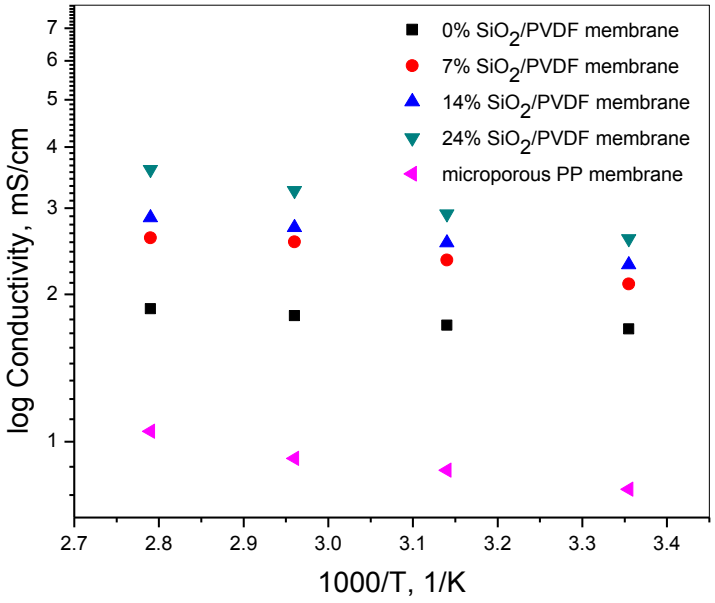

Figure 4.6 Ionic conductivities of SiO_2/PVDF nanoparticle/nanofiber hybrid membranes and microporous PP membrane as a function of temperature.

4.3.7 Electrochemical oxidation limit

The electrochemical oxidation limits of liquid electrolyte-soaked membranes were evaluated by linear sweep voltammetry measurements (Figure 4.7). In these measurements,

the electrochemical oxidation limit can be identified by the rapid increase of the current observed when the electrolyte starts to decompose.

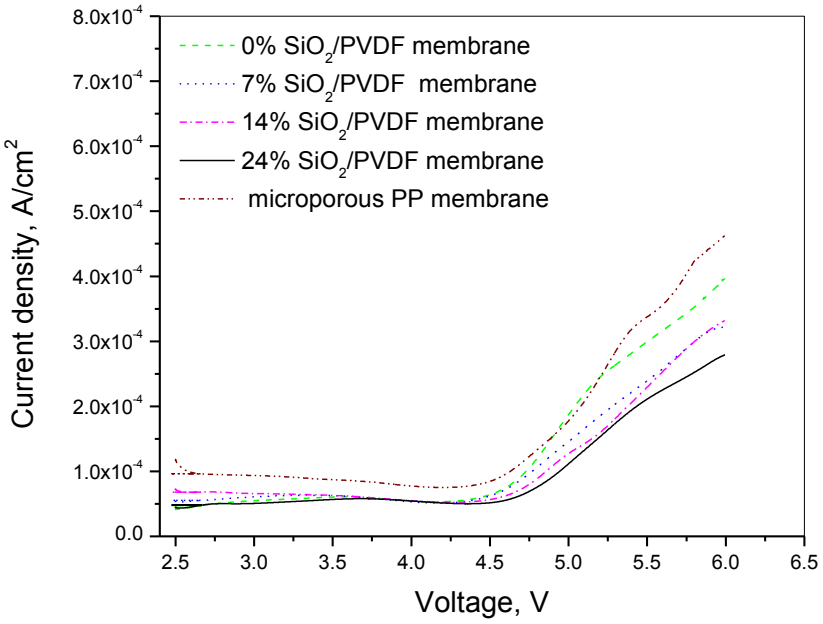

Figure 4.7 Electrochemical oxidation limits of SiO_2/PVDF nanoparticle/nanofiber hybrid membranes and microporous PP membrane.

The working potential range of practical lithium-ion rechargeable batteries are generally between 1.8 V to 3.5 V vs. Li^+/Li. From Figure 4.7, it is seen that all membranes show sufficient electrochemical stabilities. In addition, as compared to microporous PP membrane, SiO_2/PVDF hybrid membranes show slightly higher electrochemical oxidation limit. The improved electrochemical oxidation limit might be due to the stabilization effect of SiO_2 nanoparticles [29, 30]. It is believed by some researchers that SiO_2 nanoparticles can absorb impurities in the electrolyte and hence can stabilize the liquid electrolyte at high voltages [17, 29, 31, 32]. Another possible reason is that SiO_2 nanoparticles may affect the

decomposed reaction activity of solvents and/or salts since the electrochemical oxidation limit depends on the species in the electrolyte and their electrochemical reaction activities. For example, Zhang et al. reported that adding SiO_2 affected electrolyte properties not only by absorbing some impurities such as H_2O and O_2, but also through reducing side reactions between the electrolyte components and the electrode, which was supported by the fact that the interfacial resistance was reduced due to the formation of thinner solid electrolyte interphase (SEI) film [24]. Liao et al. also found that SiO_2 nanoparticles can improve the electrochemical stability window of poly(butyl methacrylate-styrene) based electrolytes form 4.7 to 5.2 V by stabilizing electrolyte species and reducing their reaction activities [33].

4.3.8 Interfacial resistance

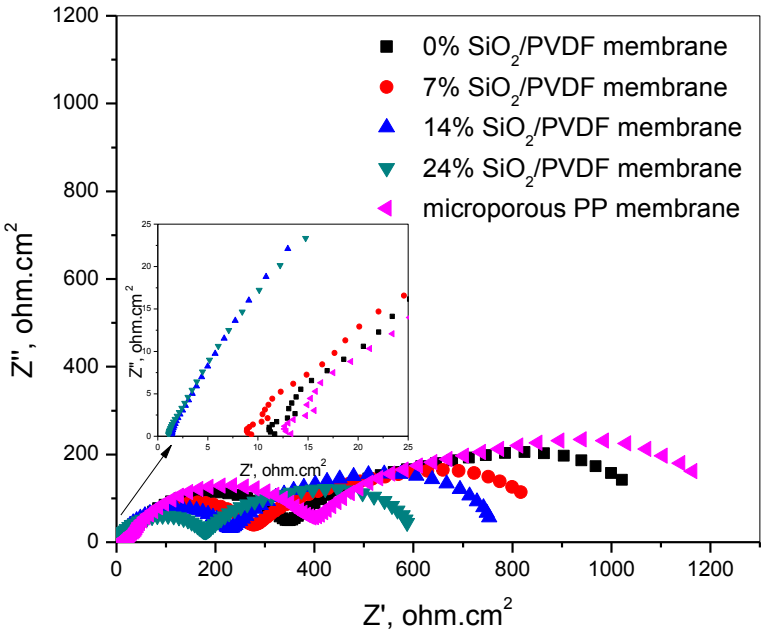

Figure 4.8 Electrochemical impedance spectra of SiO_2/PVDF nanoparticle/nanofiber hybrid membranes and micropous PP membrane. Inset shows the high frequency region.

The compatibility of liquid electrolyte-soaked membranes with lithium metal was investigated by measuring electrochemical impedance spectra of Li/liquid electrolyte-soaked membrane/Li cells, and the results are shown in Figure 4.8. A typical EIS spectrum contains an intercept with the x-axis in the high frequency region, referring to the ohmic resistance, one or more semi-circles in the intermediate frequency region, representing the resistance associated with the formation and charge transfer process of SEI, and a line in the low frequency region, showing the diffusion process in electrodes. In Figure 4.8, only high frequency and intermediate frequency regions are present. The lower frequency limit of the instrument used in this work is 10^{-2} Hz, which is not low enough for detecting the low-frequency diffusion process.

From the high-frequency region in Figure 4.8, it is seen that the ohmic resistances of liquid electrolyte-soaked 0 wt% SiO_2/PVDF hybrid membrane, 7 wt% SiO_2/PVDF hybrid membrane, 14 wt% SiO_2/PVDF membrane and 24 wt% SiO_2/PVDF membrane are around 12, 9.4, 1.4 and 1.0 ohm cm^2, respectively, which are lower than that (13 ohm cm^2) of liquid electrolyte-soaked microporous PP membrane. The lower resistances of liquid electrolyte-soaked hybrid membranes is simply because of their higher electrolyte uptakes. In the intermediate frequency region, all five spectra show two semi-circles, which represent the interfacial resistance associated with the formation and charge transfer process of SEI. The SEI film plays an important role in the electrochemical performance of Li-ion batteries. A thin SEI film with appropriate structure and composition could protect the lithium electrode from being intercalated in the solvated state and prevent the further reduction of the electrolyte by active lithium, and thus limits the degradation of the electrolyte [34]. From

Figure 4.8, it is seen that PVDF nanofiber membrane exhibits lower interfacial resistance than microporous PP membrane. The introduction of SiO_2 particles future reduces the interfacial resistance. Among all membranes studied, 24 wt% SiO_2/PVDF hybrid membrane has the lowest interfacial resistance of around 600 ohm·cm^2 when it is soaked with liquid electrolyte. The reduced interfacial resistances for SiO_2/PVDF hybrid membranes can be explained by the high surface area of SiO_2 nanoparticles. The presence of SiO_2 nanoparticles leads to thinner and more compact SEI due to the affinity of the particles to the ionic species in the liquid electrolyte. Furthermore, these particles prevent some unwanted reactions at the interface by trapping impurities [35].

4.3.9 Cycling performance

In order to investigate the feasibility of using SiO_2/PVDF hybrid membranes as separators in rechargeable Li-ion batteries, coin-type cells were fabricated with $LiFePO_4$ as the cathode and lithium metal as the counter electrode. The first-cycle charge-discharge curves of the cells are shown in Figure 4.9. For comparison, the charge-discharge curves of cells containing microporous PP membrane are also shown. In principle, the cell capacity mainly relies on the type and structure of the electrodes. However, many researchers have found that the structure of separators also play an important role in determining the measured cell performance since the separator structure affects the ion transporation between the electrodes, which is critically important in determining the cell kinetics [36, 37]. In this work, the first-cycle discharge capacity of the $LiFePO_4$/Li cell is 154 mAh/g when microporous PP membrane is used as the separator. The first-cycle discharge charge increases slight to 159 mAh/g when the separator used is changed to PVDF nanofiber

membrane. This is because that compared with microporous membrane, PVDF nanofiber membrane has higher porosity and exhibits larger ionic conductivity after uptaking liquid electrode, and as a result, the cell using PVDF nanofiber membrane has lower internal resistance and can better realize the performance potential, including first-cycle discharge capacity. From Figure 4.9, it is also seen that the first-cycle discharge capacity further increases when SiO_2 nanopartciles are introdued into the hybrid membranes. For cells contating 7, 14, and 24 wt% SiO_2/PVDF hybrid membranes, the first-cycle discharge capacities are 158, 162, and 162 mAh/g, respectively.

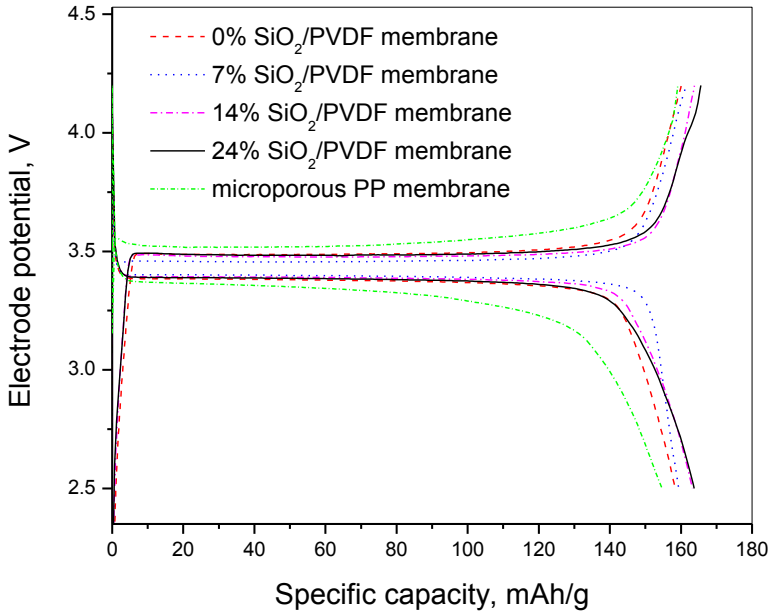

Figure 4.9 First-cycle charge-discharge curves of Li/$LiFePO_4$ cells containing SiO_2/PVDF nanoparticle/nanofiber hybrid membranes and micropous PP membrane at 0.2C.

The cycling performance of the cells at 0.2C is shown in Figure 4.10. For all five cells, no apparent capacity loss is observed in 50 cycles at 0.2C. Capacity loss during cycling

could be caused by unwanted side reactions due to electrolyte decomposition, active material dissolution, phase changes in the insertion electrode materials, and passive film formation over the electrode and current collector surfaces, and other phenomena [38].

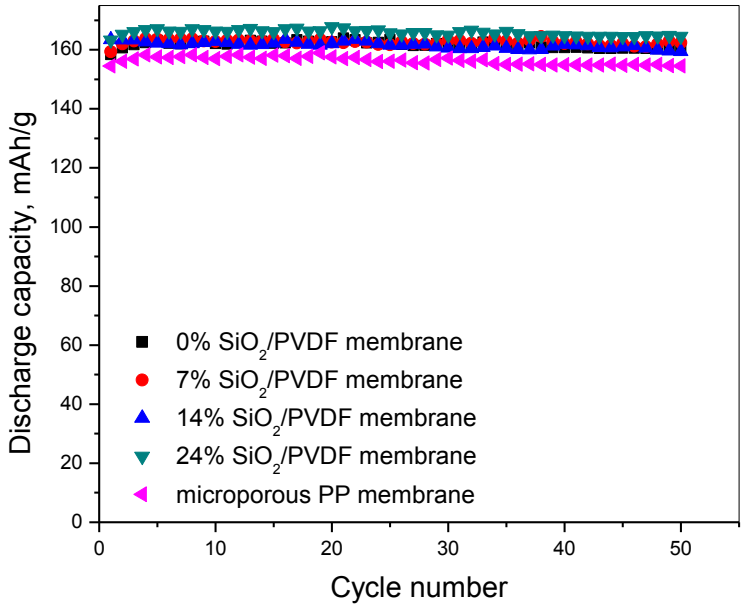

Figure 4.10 Cycling performance of Li/$LiFePO_4$ cells containing SiO_2/PVDF nanoparticle/nanofiber hybrid membranes and microporous PP membrane at 0.2C.

In many cases, the capacity loss is more significantly at high C rates than at low C rates [39]. Figure 4.11 shows the cycling performance of cells containg 24 wt% SiO_2/PVDF hybrid membrane and microporous PP membrane at a higher rate of 1C. Both cells show similiar discharge capacities in the first cycle. However, the cell containing SiO_2/PVDF hybrid membrane has higher discharge capacity (132 mAh/g vs. 125 mAh/g) than that containing micropous PP membrane at the 100th cycle. The capacity retensions are 78% and 74%, respectively, for cells containg 24 wt% SiO_2/PVDF hybrid membranes and

microporous PP membrane. This indidates that cells containg SiO_2/PVDF hybrid membranes can have high capacity rentention even at high C rates. In both Figures 4.10 and 4.11, the good capacity retension may be partially contributed to the low interfacial resistances and high ionic conductivities when SiO_2/PVDF hybrid membranes are used as separators, especially.

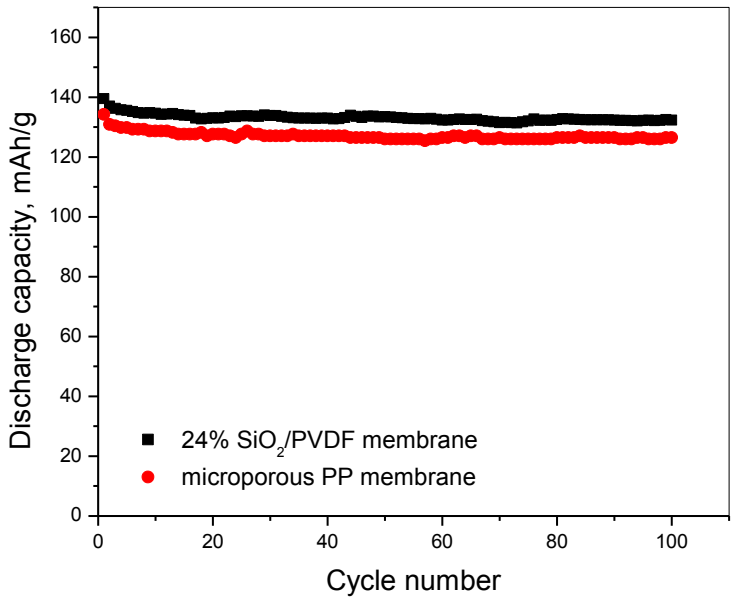

Figure 4.11 Cycling performance of Li/$LiFePO_4$ cells containing 24% SiO_2/PVDF nanoparticle/nanofiber hybrid membrane and micropous PP membrane at 1C.

4.3.10 C-rate performance

Figure 4.12 shows the C rate performance of the cells containing different membranes. The cells have slightly higher initial capacities compared to microporous PP membrane when SiO_2/PVDF hybrid membranes are used as separators. More importantly, cells containing SiO_2/PVDF hybrid nonwoven membranes exhibit less capacity fading when

the C rate increases. At 8C, the cell containing microporous PP membrane has the lowest discharge capacity of 67 mAh/g at the 30th cycle. The discharge capacity increases to 76 mAh/g when PVDF nanofiber membrane is used. The discharge capacity further increases to 80, 82, and 95 mAh/g for cells using 7, 14, and 24 wt% SiO_2/PVDF hybrid membranes. It is known that the rate performance is affected by the cell resistance [36].

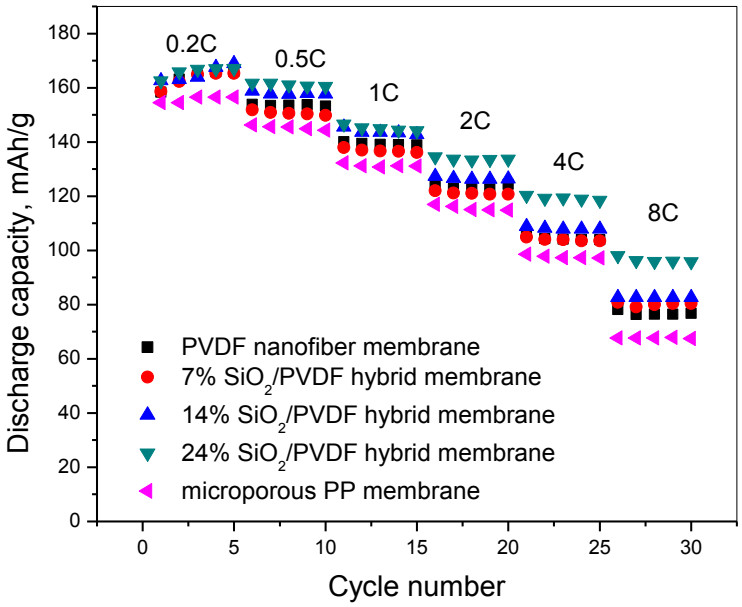

Figure 4.12 C-rate performance of Li/$LiFePO_4$ cells containing SiO_2/PVDF nanoparticle/nanofiber hybrid membranes and micropous PP membrane.

Figure 4.13 shows the cell resistances before and after the rate performance tests. Compared with cells containing microporous PP membrane, those containing SiO_2/PVDF hybrid membranes not only have lower resistance before cycling, but also exhibit less resistance increases after cycling. This trend becomes more apparent when the SiO_2 content increases from 0, 7, 14, to 24 wt%.

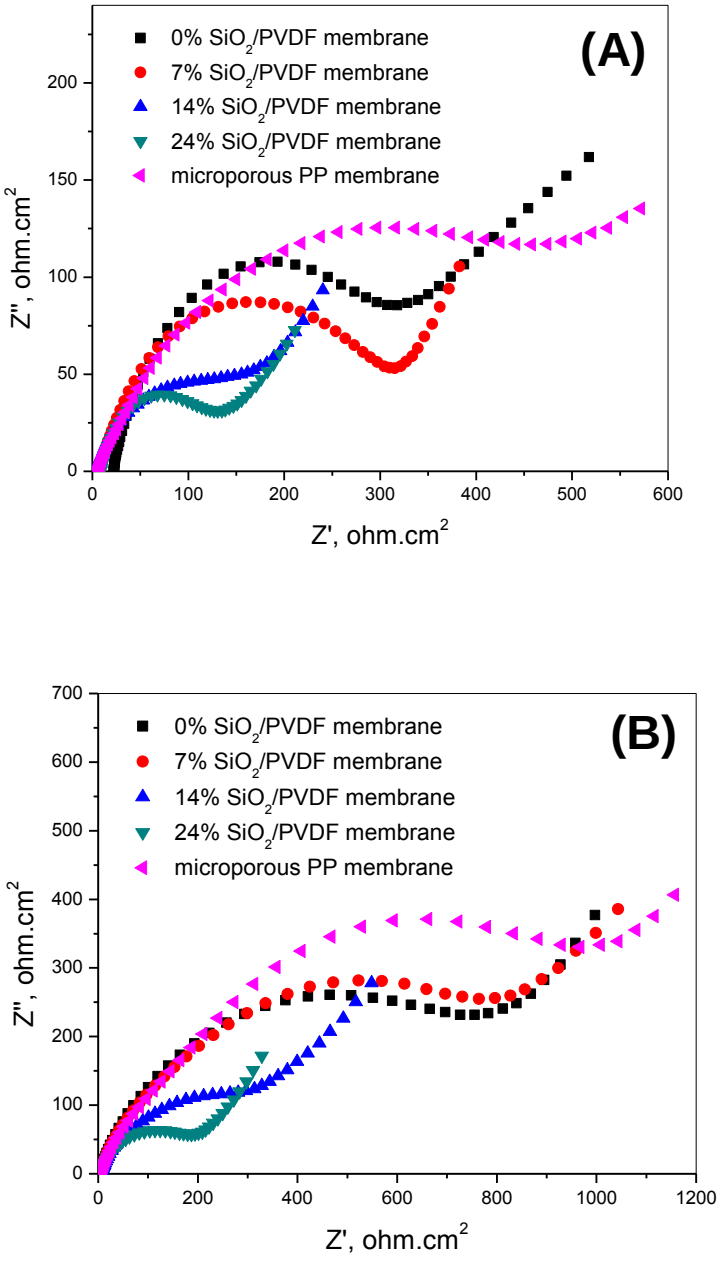

Figure 4.13 Comparison of resistance values of Li/$LiFePO_4$ cells containing SiO_2/PVDF nanoparticle/nanofiber hybrid membranes (A) before and (B) after cycling.

It can be concluded that the lower cell resistances are the main cause for the improved C rate performance when SiO_2/PVDF hybrid membranes are used as the separators in the cells. These results confirm that SiO_2/PVDF hybrid membranes are promising separator candidate for rechargeable Li-ion batteries.

4.3 Conclusion

SiO_2/PVDF nanoparticle/nanofiber hybrid membranes were prepared by combining electrospraying and electrospinning techniques. Three-dimentional PVDF nanofibrous structure loaded with high amounts of SiO_2 nanoparticles on fiber surfaces was observed from SEM images. The physical and electrochemical properties, such as porosity, thermal dimensional stability, electrolyte uptake capacity, ionic conductivity, electrochemical oxidation limit, interfacial resistance, cycling performance, and C-rate performance were investigated. Results show that these novel hybrid separators possessed better wettability, higher ionic conductivity, lower interfacial resistance and better cycling performance than both microporous PP membrane and pure PVDF nanofiber membrane. The cells containing SiO_2/PVDF hybrid separators with high SiO_2 contents also showed excellent cycling and C-rate performance.

REFERENCES

[1] J. Chen, Recent Progress in Advanced Materials for Lithium Ion Batteries, Materials, 6 (2013) 156-183.

[2] V. Etacheri, R. Marom, R. Elazari, G. Salitra, D. Aurbach, Challenges in the development of advanced Li-ion batteries: a review, Energy & Environmental Science, 4 (2011) 3243-3262.

[3] X. Huang, Separator technologies for lithium-ion batteries, Journal of Solid State Electrochemistry, 15 (2011) 649-662.

[4] J. Tan, A. Tiwari, Synthesis of Cubic Phase Li7La3Zr2O12 Electrolyte for Solid-State Lithium-Ion Batteries, Electrochemical and Solid-State Letters, 15 (2011) A37-A39.

[5] S. Teng, J. Tan, A. Tiwari, Recent developments in garnet based solid state electrolytes for thin film batteries, Current Opinion in Solid State and Materials Science, (2013).

[6] H.-S. Jeong, E.-S. Choi, S.-Y. Lee, J.H. Kim, Evaporation-induced, close-packed silica nanoparticle-embedded nonwoven composite separator membranes for high-voltage/high-rate lithium-ion batteries: Advantageous effect of highly percolated, electrolyte-philic microporous architecture, Journal of Membrane Science, 415 (2012) 513-519.

[7] Y. Liang, S. Cheng, J. Zhao, C. Zhang, S. Sun, N. Zhou, Y. Qiu, X. Zhang, Heat treatment of electrospun PVDF fibrous membrane separators for rechargeable lithium-ion batteries, Journal of Power Sources, 240 (2013) 204-211.

[8] X. Zhang, L. Ji, O. Toprakci, Y. Liang, M. Alcoutlabi, Electrospun nanofiber-based anodes, cathodes, and separators for advanced lithium-ion batteries, Polymer Reviews, 51 (2011) 239-264.

[9] Y. Liang, Z. Lin, Y. Qiu, X. Zhang, Fabrication and characterization of LATP/PAN composite fiber-based lithium-ion battery separators, Electrochimica Acta, 56 (2011) 6474-6480.

[10] H. Lee, M. Alcoutlabi, J.V. Watson, X. Zhang, Electrospun nanofiber-coated separator membranes for lithium-ion rechargeable batteries, Journal of Applied Polymer Science, 129 (2013) 1039-1951.

[11] S.S. Zhang, A review on the separators of liquid electrolyte Li-ion batteries, Journal of Power Sources, 164 (2007) 351-364.

[12] P. Arora, Z. Zhang, Battery separators, Chemical Reviews-Columbus, 104 (2004) 4419-4462.

[13] H. Lee, M. Alcoutlabi, J.V. Watson, X. Zhang, Polyvinylidene fluoride-co-chlorotrifluoroethylene and polyvinylidene fluoride-co-hexafluoropropylene nanofiber-coated polypropylene microporous battery separator membranes, Journal of Polymer Science Part B: Polymer Physics, 51 (2013) 349-357.

[14] M. Alcoutlabi, H. Lee, J.V. Watson, X. Zhang, Preparation and properties of nanofiber-coated composite membranes as battery separators via electrospinning, Journal of Materials Science, 48 (2013) 2690-2700.

[15] K. Gao, X. Hu, C. Dai, T. Yi, Crystal structures of electrospun PVDF membranes and its separator application for rechargeable lithium metal cells, Materials Science and Engineering: B, 131 (2006) 100-105.

[16] C.M. Costa, J.L. Gomez Ribelles, S. Lanceros-Méndez, G.B. Appetecchi, B. Scrosati, Poly(vinylidene fluoride)-based, co-polymer separator electrolyte membranes for lithium-ion battery systems, Journal of Power Sources, 245 (2014) 779-786.

[17] H.-R. Jung, D.-H. Ju, W.-J. Lee, X. Zhang, R. Kotek, Electrospun hydrophilic fumed silica/polyacrylonitrile nanofiber-based composite electrolyte membranes, Electrochimica Acta, 54 (2009) 3630-3637.

[18] Z. Li, G. Su, D. Gao, X. Wang, X. Li, Effect of Al2O3 nanoparticles on the electrochemical characteristics of P(VDF-HFP)-based polymer electrolyte, Electrochimica Acta, 49 (2004) 4633-4639.

[19] M. Yanilmaz, C. Chen, X. Zhang, Fabrication and characterization of SiO2/PVDF composite nanofiber-coated PP nonwoven separators for lithium-ion batteries, Journal of Polymer Science Part B: Polymer Physics, 51 (2013) 1719-1726.

[20] A. Jaworek, A. Krupa, M. Lackowski, A. Sobczyk, T. Czech, S. Ramakrishna, S. Sundarrajan, D. Pliszka, Nanocomposite fabric formation by electrospinning and electrospraying technologies, Journal of Electrostatics, 67 (2009) 435-438.

[21] J. Kim, S. Choi, S. Jo, W. Lee, B.C. Kim, Characterization and properties of P (VdF-HFP)-based fibrous polymer electrolyte membrane prepared by electrospinning, Journal of the Electrochemical Society, 152 (2005) A295-A300.

[22] M. Yanilmaz, F. Kalaoglu, H. Karakas, Investigation on the Effect of Process Variables on Polyurethane Nanofibre Diameter Using a Factorial Design, Fibres & Textiles in Eastern Europe, 21 (2013) 19-21.

[23] X.-W. Zhang, P.S. Fedkiw, Ionic transport and interfacial stability of sulfonate-modified fumed silicas as nanocomposite electrolytes, Journal of the Electrochemical Society, 152 (2005) A2413-A2420.

[24] X.-W. Zhang, Y. Li, S.A. Khan, P.S. Fedkiw, Inhibition of lithium dendrites by fumed silica-based composite electrolytes, Journal of the Electrochemical Society, 151 (2004) A1257-A1263.

[25] X. Huang, J. Hitt, Lithium ion battery separators: Development and performance characterization of a composite membrane, Journal of Membrane Science, 425-426 (2012) 163-168.

[26] J.R. Kim, S.W. Choi, S.M. Jo, W.S. Lee, B.C. Kim, Electrospun PVdF-based fibrous polymer electrolytes for lithium ion polymer batteries, Electrochimica Acta, 50 (2004) 69-75.

[27] P. Raghavan, X. Zhao, J.-K. Kim, J. Manuel, G.S. Chauhan, J.-H. Ahn, C. Nah, Ionic conductivity and electrochemical properties of nanocomposite polymer electrolytes based on electrospun poly(vinylidene fluoride-co-hexafluoropropylene) with nano-sized ceramic fillers, Electrochimica Acta, 54 (2008) 228-234.

[28] J.-K. Kim, G. Cheruvally, X. Li, J.-H. Ahn, K.-W. Kim, H.-J. Ahn, Preparation and electrochemical characterization of electrospun, microporous membrane-based composite polymer electrolytes for lithium batteries, Journal of Power Sources, 178 (2008) 815-820.

[29] Y. Liao, C. Sun, S. Hu, W. Li, Anti-thermal shrinkage nanoparticles/polymer and ionic liquid based gel polymer electrolyte for lithium ion battery, Electrochimica Acta, 89 (2012) 461-469.

[30] P. Raghavan, X. Zhao, J.-K. Kim, J. Manuel, G.S. Chauhan, J.-H. Ahn, C. Nah, Ionic conductivity and electrochemical properties of nanocomposite polymer electrolytes

based on electrospun poly (vinylidene fluoride-co-hexafluoropropylene) with nano-sized ceramic fillers, Electrochimica Acta, 54 (2008) 228-234.

[31] W.-l. Li, J.-j. Tang, B.-t. Li, Preparation and Characterization of Composite Microporous Gel Polymer Electrolytes Containing SiO2 (Li+), Journal of Inorganic and Organometallic Polymers and Materials, (2013) 1-8.

[32] M. Walkowiak, A. Zalewska, T. Jesionowski, M. Pokora, Stability of poly (vinylidene fluoride- co-hexafluoropropylene)-based composite gel electrolytes with functionalized silicas, Journal of Power Sources, 173 (2007) 721-728.

[33] Y. Liao, M. Rao, W. Li, L. Yang, B. Zhu, R. Xu, C. Fu, Fumed silica-doped poly (butyl methacrylate-styrene)-based gel polymer electrolyte for lithium ion battery, Journal of Membrane Science, 352 (2010) 95-99.

[34] Q.-C. Zhuang, S. Xu, X. Qiu, Y. Cui, L. Fang, S. Sun, Diagnosis of Electrochemical Impedance Spectroscopy in Lithium-Ion Batteries, Prog Chem, 22 (2010) 1044.

[35] K.-H. Lee, Y.-G. Lee, J.-K. Park, D.-Y. Seung, Effect of silica on the electrochemical characteristics of the plasticized polymer electrolytes based on the P (AN-co-MMA) copolymer, Solid State Ionics, 133 (2000) 257-263.

[36] E.-S. Choi, S.-Y. Lee, Particle size-dependent, tunable porous structure of a SiO2/poly (vinylidene fluoride-hexafluoropropylene)-coated poly (ethylene terephthalate) nonwoven composite separator for a lithium-ion battery, Journal of Materials Chemistry, 21 (2011) 14747-14754.

[37] Y. Liang, L. Ji, B. Guo, Z. Lin, Y. Yao, Y. Li, M. Alcoutlabi, Y. Qiu, X. Zhang, Preparation and electrochemical characterization of ionic-conducting lithium lanthanum

titanate oxide/polyacrylonitrile submicron composite fiber-based lithium-ion battery separators, Journal of Power Sources, 196 (2011) 436-441.

[38] P. Arora, R.E. White, M. Doyle, Capacity Fade Mechanisms and Side Reactions in Lithium-Ion Batteries, Journal of the Electrochemical Society, 145 (1998) 3647-3667.

[39] G. Ning, B. Haran, B.N. Popov, Capacity fade study of lithium-ion batteries cycled at high discharge rates, Journal of Power Sources, 117 (2003) 160-169.

CHAPTER 5. ELECTROSPUN SIO_2/NYLON 6,6 NANOFIBER MEMBRANES AS THERMALLY-STABLE SEPARATOR FOR LITHIUM-ION BATTERIES

ABSTRACT

Electrospun SiO_2/nylon 6,6 nanofiber membranes were fabricated and their electrochemical performance was evaluated for use as separators in Li-ion batteries. The aim of this study was to design new high-performance separator membranes with enhanced mechanical properties and good thermal stability, as well as superior electrochemical performance compared to microporous polyolefin membranes. It was found that SiO_2/nylon 6,6 nanofiber membranes had superior thermal stability and mechanical strength with highly porous structure. Enhanced electrochemical properties were also obtained for these nanofiber membranes due to their high porosity values. Compared with commercial microporous polyolefin membranes, SiO_2/nylon 6,6 nanofiber membranes had larger liquid electrolyte uptake, higher electrochemical oxidation limit, and lower interfacial resistance with lithium. SiO_2/nylon 6,6 nanofiber membranes with different SiO_2 contents (0, 3, 6, 9 and 12%) were assembled into lithium/lithium cobalt oxide and lithium/lithium iron phosphate cells. High cell capacities and good cycling performance were demonstrated at room temperature. In addition, cells using SiO_2/nylon 6,6 nanofiber membrane separators showed superior C-rate performance compared to those using commercial microporous polyolefin membrane.

5.1 Introduction

Li-ion batteries have been commonly used in electronic devices such as mobile phones, laptop computers, and digital cameras due to their superior characteristics such as high energy density, large operational voltage, long cycling life, and low self-discharge rate. Nowadays, Li-ion batteries have found new applications in electric/hybrid vehicles and energy storage for smart grids. Considering these new applications, improved battery components must be developed to obtain Li-ion batteries with higher cell performance, better safety, and lower cost [1, 2].

The separator plays a vital role in regulating cell kinetics and preventing electronic contact in Li-ion batteries. Microporous polyolefin membranes are the most commonly-used separators for Li-ion batteries. Polyolefin microporous membranes have good chemical stability and mechanical strength, but they suffer from low porosity and poor wettability with polar liquid electrolyte, which affects cell resistance, energy density, and rate capability of rechargeable Li-ion batteries [3-5]. Moreover, polyolefin-based separators exhibit large thermal shrinkage at high temperatures. This may cause internal short circuits, fire and even explosions in case of overcharge or overheating [6].

Electrospinning is a technique that produces continuous nanosized polymer fibers through the action of an external electric field imposed on a polymer solution [7-9]. Recently, it was found that electrospun nanofiber membranes can be used as separators in Li-ion batteries due to their large porosity and unique pore structure [10, 11]. There are several studies that reported on enhanced electrochemical properties such as higher C-rate capability, better cycling performance and lower cell resistances by using electrospun membranes [1-3, 12-14]. So far, the most commonly used electrospun nanofiber membranes are made from

polyvinylidenefluoride (PVDF), polyvinyl chloride (PVC), polyacrylonitrile (PAN), and polyvinylidenefluoride-hexafluoropropylene (PVDF-HFP). However, these membranes do not have good mechanical strength, and they cannot withstand the large tension developed by the winding operation used during battery assembly [1].

Electrospun nanofiber mats with enhanced mechanical properties and thermal stability can be obtained by using polymeric materials with higher mechanical strength and melting temperature such as nylon 6,6. In this study, nylon 6,6 was used to prepare novel electrospun membranes with high thermal stability, superior mechanical strength, and enhanced electrochemical properties. Inorganic SiO_2 nanoparticles were also introduced to further improve the mechanical and electrochemical properties. Experimental results showed that SiO_2/nylon 6,6 nanofiber membranes had higher ionic conductivities, lower interfacial resistances and superior C-rate performance compared to microporous polyolefin membrane. It is, therefore, demonstrated that SiO_2/nylon 6,6 nanofiber membranes with superior mechanical and thermal properties are promising separator candidate for high-performance Li-ion batteries.

5.2 Experimental

5.2.1 Chemicals

Nylon 6,6 (Mw = 262.35 g/mol) and formic acid were purchased from Sigma Aldrich. Hydrophilic pyrogenic SiO_2 (Aerosil 380, particle size = 20 nm, surface area = 90 m^2/g) was supplied from Evonic industries. Liquid electrolyte, 1 M lithium hexafluorophosphate ($LiPF_6$) in ethylene carbonate and ethyl methyl carbonate (EC+EMC, 1:1 by volume), was supplied from Ferro Corp. Celgard 2400 microporous polypropylene

(PP) membrane was used for comparison. $LiCoO_2$ was purchased from MTI Corporation. $LiFePO_4$ was obtained from Hydro-Qubec. All chemicals were used as received without further purification.

5.2.2 Separator preparation

In order to obtain nanofiber membranes, nylon 6,6 solution (18 wt.%) was prepared by dissolving the polymer in formic acid. SiO_2/nylon 6,6 solutions were prepared by adding different amounts of SiO_2 (3, 6, 9, and 12 wt.%) into the 18 wt.% nylon 6,6 solution. All solutions were stirred mechanically overnight prior to electrospinning.

During the electrospinning of nylon 6,6 and SiO_2/nylon 6,6 nanofibers, a variable high voltage power supply (Gamma) was used to provide a high voltage of 20 kV. The feeding rate used was 1 ml/h and the tip-to-collector-distance was 12 cm. Electrospun nylon 6,6 and SiO_2/nylon 6,6 nanofibers were accumulated on the collector to form free-standing membranes. The resultant nanofiber membranes were dried at 60 $^{\circ}$C for at least 24 hours to remove residual solvents. The thicknesses of the prepared nanofiber membranes were around 65 μm.

5.2.3 Structure Characterization

The morphology of nylon 6,6 and SiO_2/nylon 6,6 nanofiber membranes was studied by using a JEOL JSM-6400F field-emission scanning electron microscope (FESEM). The fiber diameters were calculated by measuring 50 randomly-selected nanofibers in SEM images using Revolution 1.6 software for each sample.

The porosities of the membranes were determined by using n-butanol uptake tests. In a uptake test, the porosity was calculated by using the following equation:

$$Porosity\ (\%) = \frac{w_w - w_d}{\rho_b \times V} \quad (1)$$

where w_w and w_d are the weights of wet and dry membranes, respectively, ρ_b the density of n-butanol, and V the geometric volume of the membrane.

5.2.4 Performance evaluation

The dimensional stability of the membranes was determined by thermal shrinkage tests at 150 ^{o}C for 30 minutes. The mechanical properties of the membranes were determined by using a universal tensile tester (Instron 5544) with 100 N capacity load cell. The dimensions of test specimens were 10 mm wide, 65 μm thick, and 60 mm long.

Liquid electrolyte uptakes were measured by soaking weighed membranes in the liquid electrolyte of 1M $LiPF_6$ in EC+EMC (1:1 in volume) for two hours at room temperature. The electrolyte uptake (*EU*) was calculated by:

$$EU\ (\%) = \frac{w_1 - w_0}{w_0} \times 100 \quad (2)$$

where w_0 and w_1 are the weights of dry and wet membranes, respectively.

The ionic conductivities of liquid electrolyte-soaked membranes were measured by electrochemical impedance spectroscopy (EIS) using Reference 600 Potentiostat/Galvanostat/ZRA (GAMRY). The impedance measurements were performed on liquid electrolyte-soaked membranes sandwiched between two stainless steel electrodes over a frequency range of 1 MHz to 1 Hz with AC amplitude of 10 mV at room temperature. The ionic conductivity was calculated by:

$$\sigma = \frac{d}{R_b \times S} \quad (3)$$

where d is the membrane thickness, S the cross-sectional area, and R_b the bulk resistance obtained at the high frequency intercept of the Nyquist plot on the real axis.

The electrochemical oxidation limits of liquid electrolyte-soaked membranes were determined by linear sweep voltammetry at room temperature. In these tests, electrochemical cells consisting of stainless steel working electrode and lithium metal counter electrode were used. The scan rate used was 10 mVs^{-1} and the potential range was 2.5 to 6.0 V.

The interfacial resistances between the liquid electrolyte-soaked membranes and lithium metal were investigated by measuring the impedances of symmetrical lithium cells. The frequency range used was 1 MHz to 1 Hz.

The charge-discharge tests of $Li/LiCoO_2$ and $Li/LiFePO_4$ cells containing liquid electrolyte-soaked membranes were conducted by using coin-type cells. The $LiCoO_2$ and $LiFePO_4$ cathodes were prepared by blending active material (80 wt.%), carbon black conductor (10 wt.%) and PVDF binder (10 wt.%). Arbin automatic battery cycler was used in a potential range of 4.2 - 2.5 V at 0.2 C and 1 C to evaluate the charge-discharge properties and cycling performance. Different C-rates (0.2 C, 0.5 C, 1 C, 2 C, 4 C, and 8 C) were also applied to the cells for evaluating the C-rate performance.

5.3 Results and Discussions

5.3.1 Separator morphology

Figure 5.1 shows SEM images of SiO_2/nylon 6,6 nanofiber membranes with various SiO_2 contents (0, 3, 6, 9, and 12 wt.%). Nanofibers in all five membranes form randomly-oriented, highly porous fibrous networks. The average fiber diameter is 463 nm for pure nylon 6,6 nanofibers (*i.e.*, SiO_2 content = 0 wt.%).

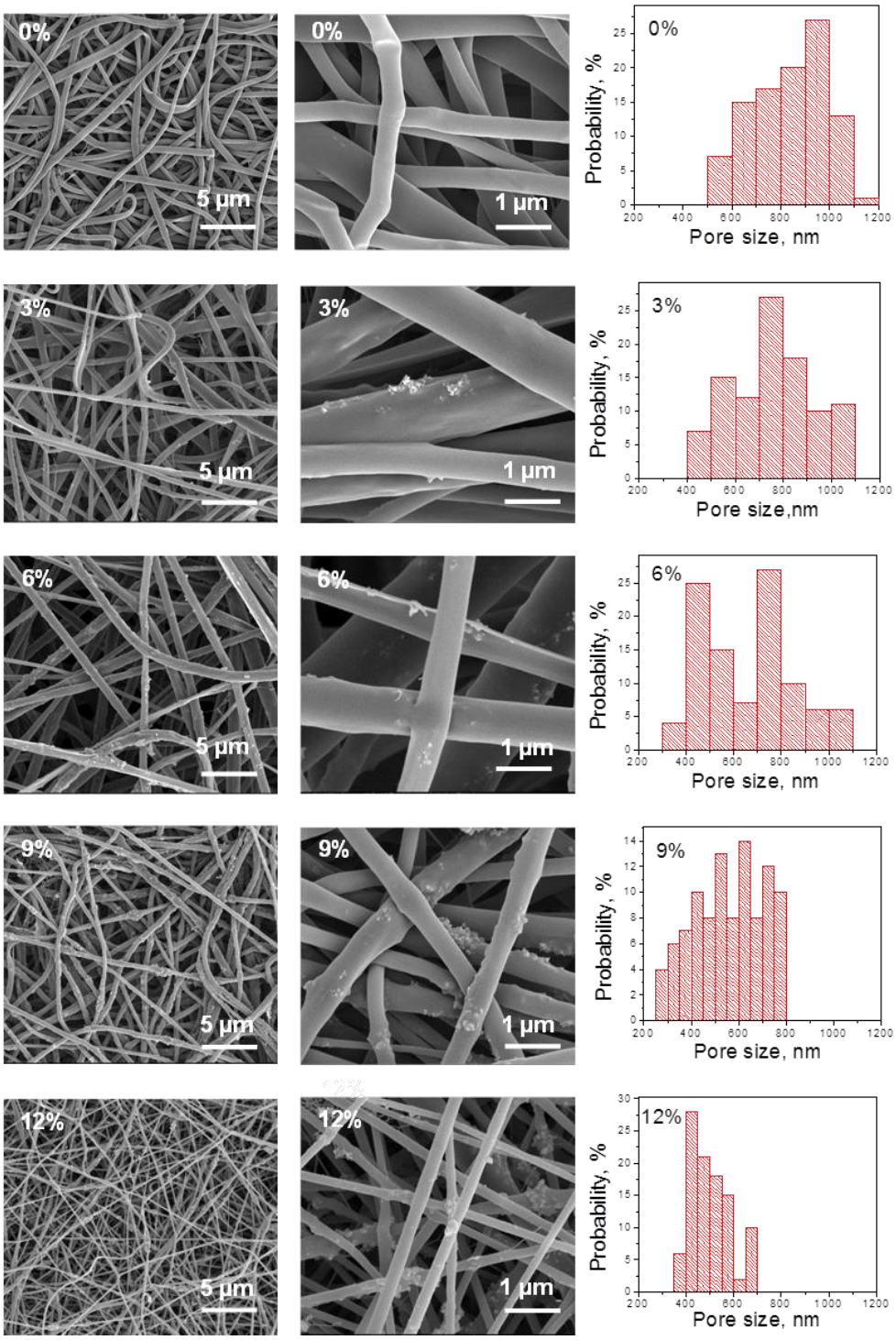

Figure 5.1 SEM images and pore size distributions of SiO_2/nylon 6,6 nanofiber membranes with different SiO_2 contents.

The addition of 3, 6, 9, and 12% SiO_2 nanoparticles decreases the average fiber diameter to 380, 326, 313 and 204 nm, respectively. Similar results were reported on SiO_2/PAN nanofibers and the decreases in fiber diameters at high filler contents were attributed to the repulsive force of SiO_2 particles that minimized the entanglement of polymer chains during electrospinning [1, 12].

Pore size distributions of the membranes are also shown in Figure 5.1. Pore sizes were measured by using an Image J image processing software. During the measurements, binary images were obtained by the thresholding method and the size of each pore was calculated in pixels, which was then converted into the nanometer scale. The average pore sizes were measured to be 837, 756, 660, 557 and 497 nm, respectively, for 0, 3, 6, 9 and 12 wt.% SiO_2/nylon 6,6 nanofiber membranes. Therefore, the addition of SiO_2 not only reduces the fiber diameters but also leads to smaller pore sizes in the resultant membranes. Similar trend was also reported by Zhang et al [15], who found the pore size of SiO_2/PVDF nanofiber separator membranes decreased with increase in SiO_2 content.

In order to further investigate the morphology of SiO_2/nylon 6,6 nanofiber membranes, cross-sectional SEM analysis was performed and the results are shown in Figure 5.2. The cross-sectional morphology indicates that SiO_2 nanoparticles are embedded mainly inside the fibers with a small amount dispersed on the fiber surfaces. A three-dimensional porous structure can also be seen in the cross-sectional SEM images.

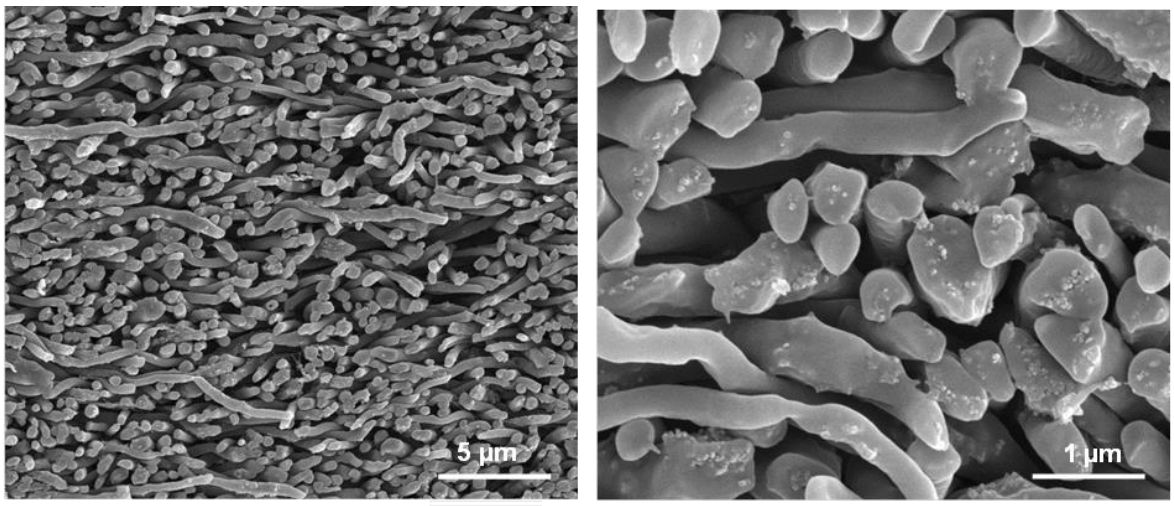

Figure 5.2 Cross sectional-SEM images of 12% SiO_2/nylon 6,6 nanofiber membranes.

For battery separators, high membrane porosity is beneficial for allowing fast ion transportation between two electrodes. Table 5.1 shows the porosities of SiO_2/nylon 6,6 nanofiber membranes with different SiO_2 contents (0, 3, 6, 9, and 12 wt.%).

For comparison, the porosity of a commercial microporous PP membrane separator (Celgard 2400) is also shown. It is seen that the porosities of 0, 3, 6, 9 and 12 wt.% SiO_2/nylon 6,6 nanofiber membranes are 67, 70, 72, 73 and 77%, respectively, which are significantly greater than that (41%) of microporous PP membrane. In general, smaller fiber diameter leads to higher porosity since more void space is available between thin fibers. Hence, the introduction of SiO_2 nanoparticles increases the porosity value by decreasing the fiber diameter.

Table 5.1 Porosities, electrolyte uptakes and ionic conductivities of SiO_2/nylon 6,6 nanofiber membranes with different SiO_2 contents at room temperature.

	Porosity (%)	**Electrolyte uptake (%)**	**Ionic conductivity (mS/cm)**
0 wt.% SiO_2/nylon 6,6 nanofiber membrane	67	260	2.8
3 wt.% SiO_2/nylon 6,6 nanofiber membrane	70	272	3.1
6 wt.% SiO_2/nylon 6,6 nanofiber membrane	72	289	3.4
9 wt.% SiO_2/nylon 6,6 nanofiber membrane	73	320	3.6
12 wt.% SiO_2/nylon 6,6 nanofiber membrane	77	360	3.8
Microporous PP membrane	41	158	0.8

5.3.2 Mechanical properties

Mechanical properties of electrospun nanofiber membranes are important in separator applications. Figure 5.3 shows typical stress-strain curves of SiO_2/nylon 6,6 nanofiber membranes with different SiO_2 contents. The tensile strength of the nylon 6,6 nanofiber membrane is about 18 MPa and the addition of SiO_2 nanoparticles slightly increases the strength up to about 22 MPa when SiO_2 content is 12 wt.%. It was reported that a tensile strength of 13 MPa was sufficient for most conventional winding machines used in cylindrical battery fabrication [16]. Therefore, SiO_2/nylon 6,6 nanofiber membranes have sufficient tensile strength for surviving the winding process of battery assembling.

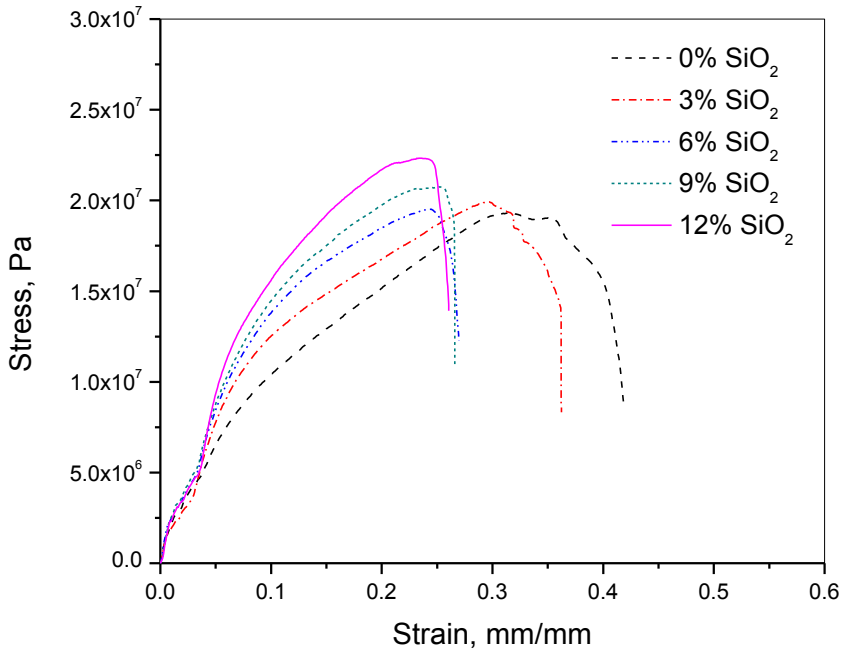

Figure 5.3 Stress-strain curves of SiO_2/nylon 6,6 nanofiber membranes with different SiO_2 contents.

5.3.3 Thermal dimensional stability

Microporous polyolefin membranes often shrink at elevated temperatures, which could lead to serious safety concern when they are used as battery separators. Figure 5.4 compares the photographs of SiO_2/nylon 6,6 nanofiber membranes and microporous PP membrane before and after thermal exposure at 150 ^oC for 30 minutes. The microporous PP membrane could not maintain its shape at 150 ^oC and significant dimensional change can be observed. On the other hand, SiO_2/nylon 6,6 nanofiber membranes with different SiO_2 contents not only maintain their shape, but also show no apparent dimensional change. Therefore, SiO_2/nylon 6,6 nanofiber membranes have excellent thermal dimensional stability.

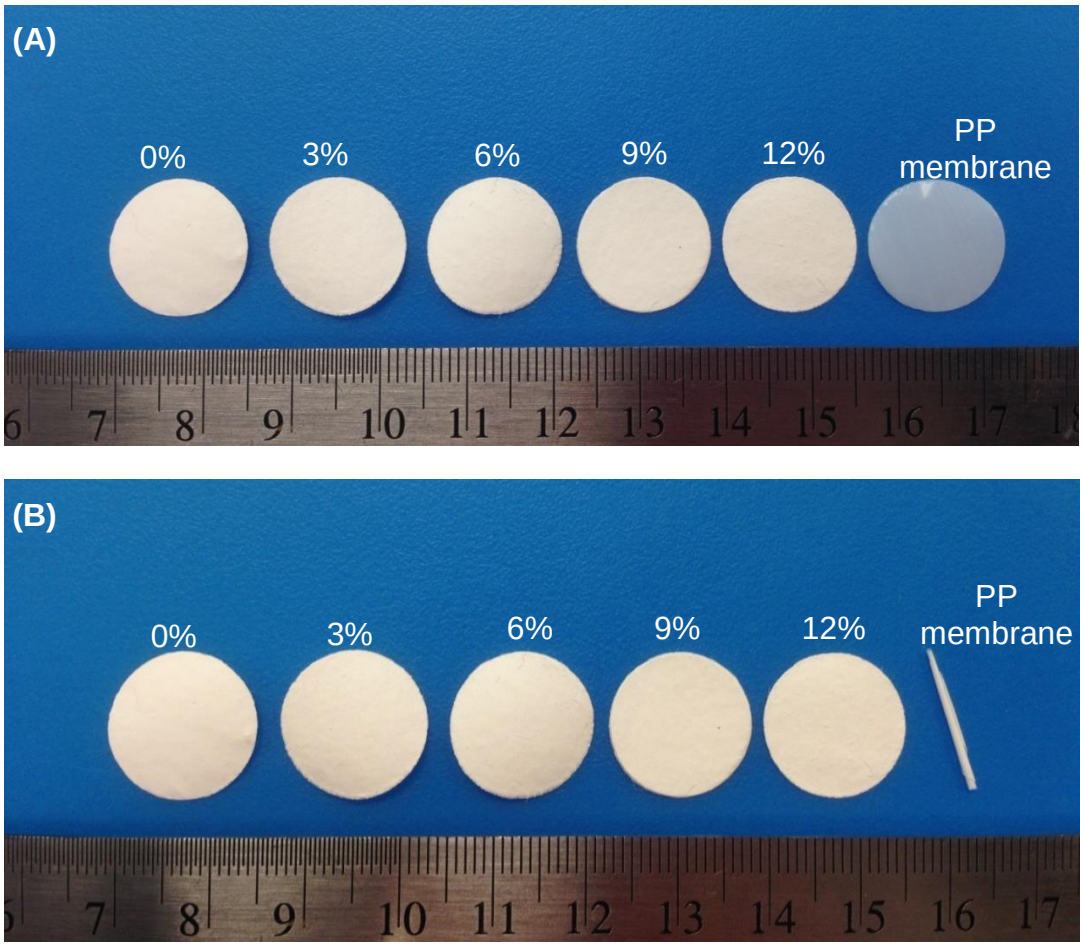

Figure 5.4 Photographs of SiO_2/nylon 6,6 nanofiber membranes with different SiO_2 contents and microporous PP membrane (A) before and (B) after thermal exposure at 150 ^{o}C for 30 minutes.

5.3.4 Liquid electrolyte uptake

The electrolyte uptake capacity of separators affects the performance of Li-ion batteries. Electrolyte uptake capacities of SiO_2/nylon 6,6 nanofiber membranes with different SiO_2 contents are shown in Table 5.1. The uptake capacity of nylon 6,6 nanofiber membrane is 260%, which is significantly higher than that (158%) of microporous PP membrane. The high uptake capacity of nylon 6,6 nanofiber membrane can be explained by its high porosity

value. Moreover, the introduction of SiO_2 nanoparticles further increases the electrolyte uptake capacity up to 360%. Such increase in electrolyte uptake capacity is mainly due to the reduced fiber diameter and increased porosity caused by the addition of SiO_2 nanoparticles.

5.3.5 Ionic conductivity

To realize the good performance of Li-ion batteries, it is important to have low ionic resistance between the two electrodes. The room-temperature ionic conductivities of liquid electrolyte-soaked SiO_2/nylon 6,6 nanofiber membranes are compared with that of liquid electrolyte-soaked microporous PP membrane in Table 5.1. The ionic conductivities are 2.8, 3.1, 3.4, 3.6, and 3.8 mS/cm, respectively, for liquid electrolyte-soaked SiO_2/nylon 6,6 nanofiber membranes that contain 0, 3, 6, 9, and 12 wt.% SiO_2 nanoparticles. These ionic conductivity values are significantly higher than that (0.8 mS/cm) of liquid electrolyte-soaked microporous PP membrane. This result can be explained by the higher porosities and larger electrolyte uptake capacities of SiO_2/nylon 6,6 nanofiber membranes. In addition, it is known that Lewis acid groups on the surfaces of SiO_2 nanoparticles can interact with polar groups of the polymer and ionic species of the electrolyte [17]. Jung et al. [12] reported that SiO_2 fillers could improve the ionic conductivity of electrospun SiO_2/PAN nanofiber membranes by introducing Lewis acid/base interactions. Therefore, the Lewis acid groups on SiO_2 nanoparticle surfaces may also play an role in increasing the ionic conductivity of liquid electrolyte-soaked SiO_2/nylon 6,6 nanofiber membranes.

5.3.6 Electrochemical oxidation limit

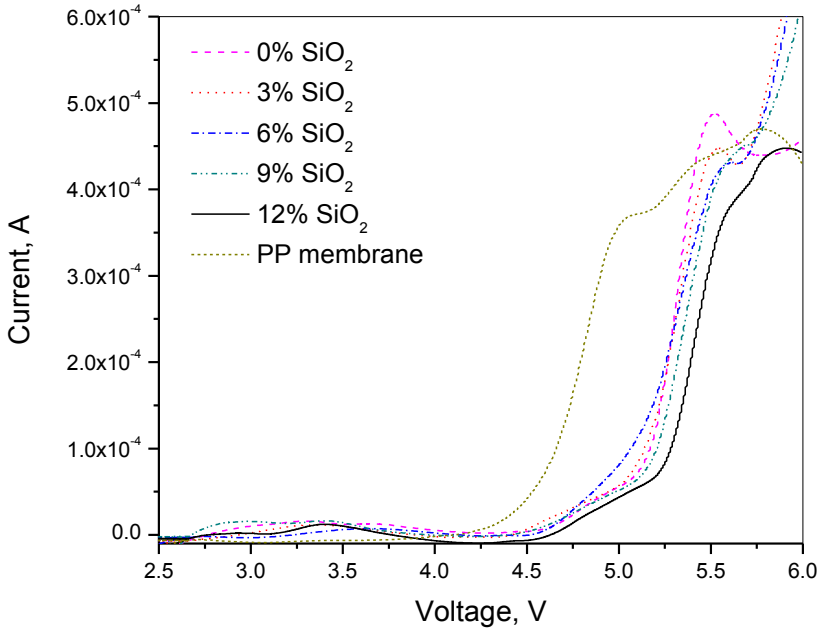

Figure 5.5 Electrochemical oxidation limits of SiO_2/nylon 6,6 nanofiber membranes with different SiO_2 contents and microporous PP membrane.

Linear sweep voltammetry measurements can be used to evaluate the electrochemical oxidation limits of liquid electrolyte-soaked membranes. Figure 5.5 shows the voltammetry curves of SiO_2/nylon 6,6 nanofiber membranes and microporous PP membrane. On these curves, the electrochemical oxidation limit can be identified by the rapid increase in the current, which indicates the starting point of electrolyte decomposition. From Figure 5.5, it is seen that the electrochemical oxidation limits of SiO_2/nylon 6,6 nanofiber membranes with different SiO_2 contents are all around 4.7 V, which is higher than that (4.3 V) of microporous PP membrane. Considering that the working potential range of Li-ion batteries is typically between 1.8 and 3.5 V, SiO_2/nylon 6,6 nanofiber membranes have sufficient electrochemical stabilities for Li-ion battery application.

5.3.7 Interfacial resistance

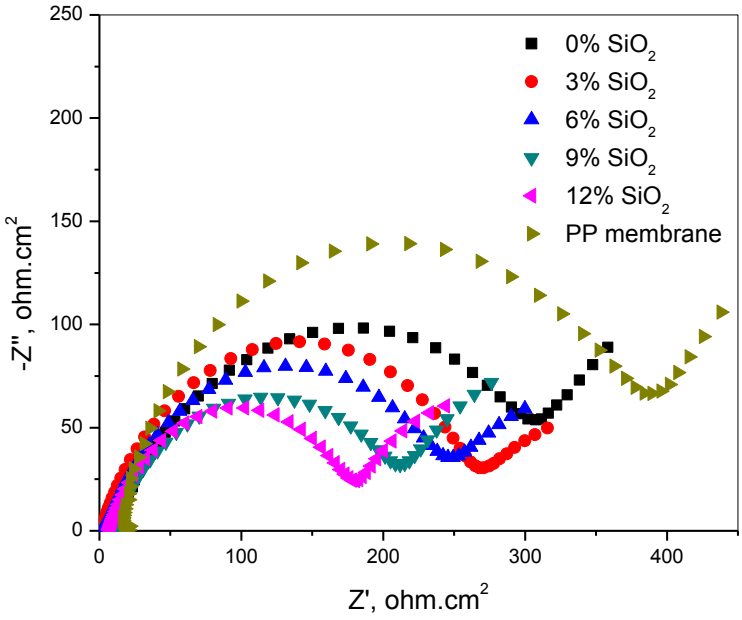

Figure 5.6 Electrochemical impedance spectra of SiO_2/nylon 6,6 nanofiber membranes with different SiO_2 contents and micropous PP membrane.

The compatibility of membrane separators with Li metal is another important aspect that influences cell performance. The interfacial properties of liquid electrolyte-soaked SiO_2/nylon 6,6 nanofiber membranes with Li metal were investigated by measuring the electrochemical impedance spectra of symmetric Li/Li cells containing these membranes (Figure 5.6). In the electrochemical impedance spectra, the diameters of semi-circles at the intermediate frequency region represent the interfacial resistances of liquid electrolyte-soaked membranes with Li metal. As shown in Figure 5.6, liquid electrolyte-soaked nylon 6,6 nanofiber membrane exhibits lower interfacial resistance (300 ohm·cm^2) than microporous PP membrane (400 ohm·cm^2), and the interfacial resistance further decreases to

260, 250, 210, and 180 ohm·cm^2, respectively, after introducing 3, 6, 9 and 12 wt.% SiO_2 nanoparticles. Lower interfacial resistances of SiO_2/nylon 6,6 nanofiber membranes compared to that of PP membrane can be explained by their higher uptake capacities. In addition, it has also been reported in previous studies [1, 5, 18] that adding ceramic fillers can improve the interfacial properties with the Li electrode because the nanoparticles with high surface areas can trap impurities and protect Li from corrosion.

5.3.8 First-cycle charge-discharge curves

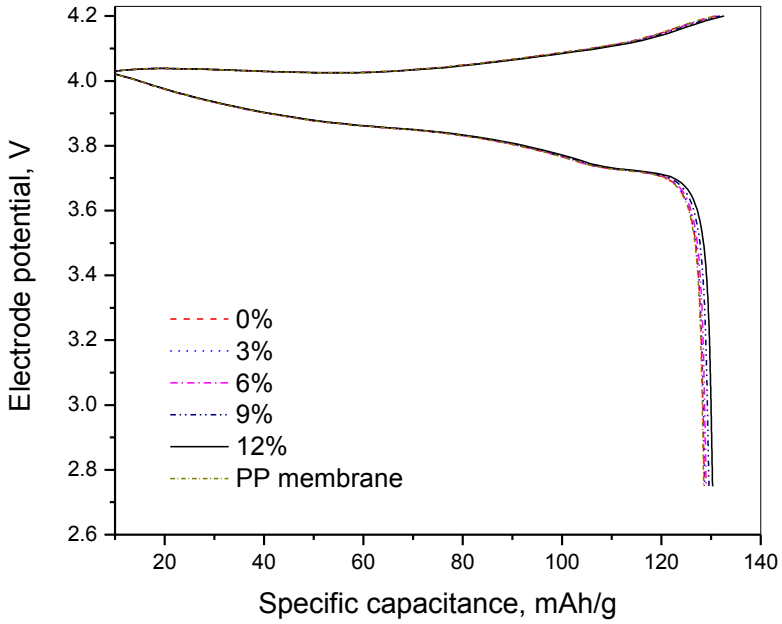

Figure 5.7 First-cycle charge-discharge curves of Li/$LiCoO_2$ cells containing SiO_2/nylon 6,6 nanofiber membranes with different SiO_2 contents and micropous PP membrane at 0.2 C.

In order to further investigate the performance of SiO_2/nylon 6,6 nanofiber membranes for use as separators in rechargeable Li-ion batteries, coin-type half cells were

fabricated by using two different cathode materials ($LiCoO_2$ and $LiFePO_4$). The first-cycle charge-discharge curves of Li/$LiCoO_2$ cells at 0.2 C are shown in Figure 5.7. In principle, the cell capacities are mainly determined by the type and structure of the electrodes. However, the separator material and structure also play an important role in determining the overall cell performance since separators can affect the ion transportation between the two electrodes, which is critically important in regulating the cell kinetics [2]. As shown in Figure 5.7, the discharge capacity of the cell using microporous PP membrane is 128 mAh/g. The discharge capacities of cells containing 0, 3, 6, 9, and 12 wt.% SiO_2/nylon 6,6 nanofiber membranes are 128, 128, 129, 129, and 130 mAh/g, respectively.

Figure 5.8 shows the first-cycle charge-discharge curves of Li/$LiFePO_4$ cells containing 0, 3, 6, 9, and 12 wt.% SiO_2/nylon 6,6 nanofiber membranes and PP membrane at 0.2 C. The first-cycle discharge capacity of the Li/$LiFePO_4$ cell is 154 mAh/g when microporous PP membrane is used. The discharge capacity increases to around 160 mAh/g when SiO_2/nylon 6,6 nanofiber membranes are used. Among all the cells studied, the cell containing 12 wt.% SiO_2/nylon 6,6 nanofiber membrane delivers the highest discharge capacity of 161 mAh/g. The high porosities and ionic conductivities of SiO_2/nylon 6,6 nanofiber membranes are the main reason for achieving improved capacity values in cells containing these membranes. Zhang et al [15] also found that the cells prepared by using SiO_2/PVDF nanofiber membranes have higher discharge capacities when a large amount of SiO_2 was used. They attributed this phenomenon to the increased porosities and improved electrolyte uptakes caused by the addition of SiO_2 particles.

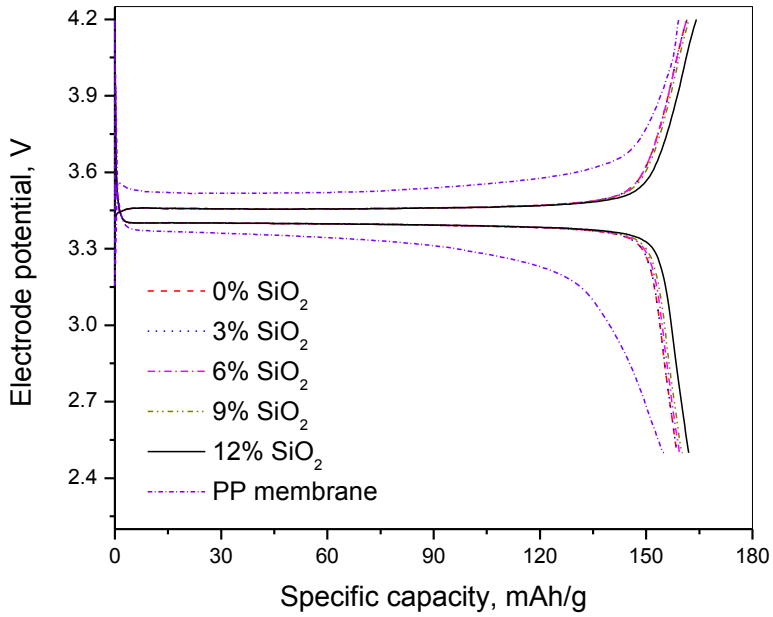

Figure 5.8 First-cycle charge-discharge curves of Li/$LiFePO_4$ cells containing SiO_2/nylon 6,6 nanofiber membranes with different SiO_2 contents and micropous PP membrane at 0.2 C.

5.3.9 Cycling performance

Figure 5.9 shows cycling performance of Li/$LiCoO_2$ cells at 0.2 C. It is seen that the cell containing microporous PP membrane shows the lowest capacity retention of 88% in 50 cycles. The capacity retentions are 90%, 91%, 92%, 93%, and 93%, respectively, for the cells containing 0, 3, 6, 9, and 12 wt.% SiO_2/nylon 6,6 nanofiber membranes. The improved cycling performance of the cells containing SiO_2/nylon 6,6 nanofiber membranes can be ascribed to the higher ionic conductivity and lower interfacial resistance of these membranes after uptaking liquid electrolyte. The remarkable improvement in the cyclability was also reported by Zhang et al [15], who compared highly porous SiO_2/PVDF nanofiber membranes with a commercial polyolefin membrane.

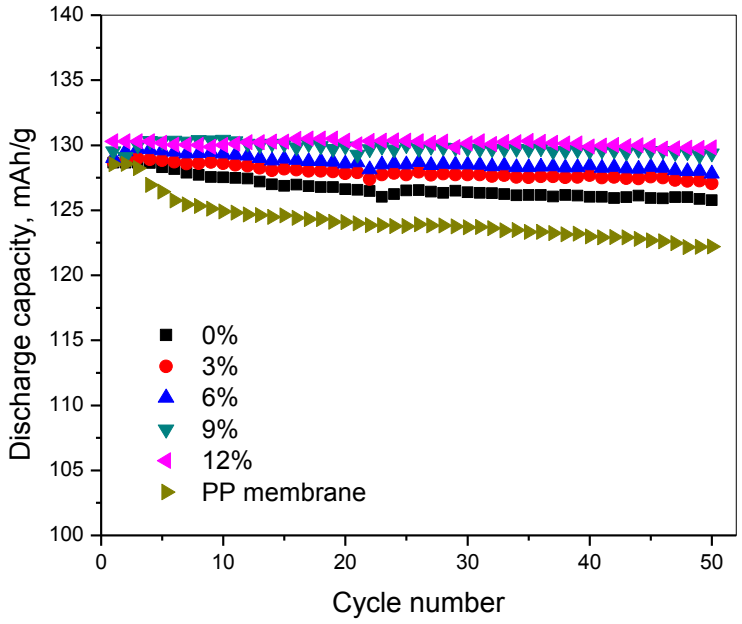

Figure 5.9 Cycling performance of Li/$LiCoO_2$ cells containing SiO_2/nylon 6,6 nanofiber membranes with different SiO_2 contents and microporous PP membrane at 0.2 C.

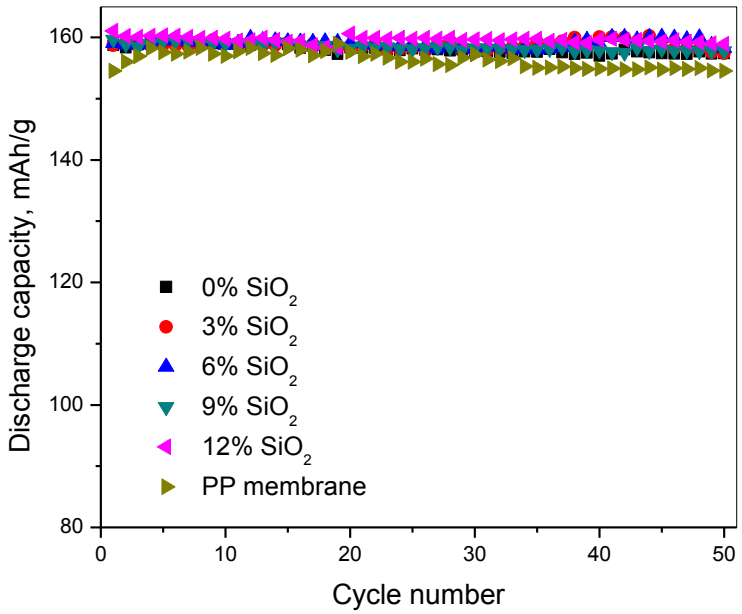

Figure 5.10 Cycling performance of Li/$LiFePO_4$ cells containing SiO_2/nylon 6,6 nanofiber membranes with different SiO_2 contents and microporous PP membrane at 0.2 C.

Figure 5.10 shows the cycling performance of Li/$LiFePO_4$ cells containing 0, 3, 6, 9, and 12 wt.% SiO_2/nylon 6,6 nanofiber membranes and microporous PP membrane at 0.2 C. For all six cells, no apparent capacity loss is observed in 50 cycles at a low rate of 0.2 C.

In order to investigate the cycling performance at a high C-rate, Li/$LiFePO_4$ cells were tested again at 1 C (Figure 5.11). The cells containing 0, 3, 6, 9, and 12 wt.% SiO_2/nylon 6,6 nanofiber membranes deliver similar discharge capacities of about 140 mAh/g and exhibit almost no capacity loss in 100 cycles. However, the cell containing microporous PP membrane delivers a lower discharge capacity of 134 mAh/g and exhibits apparent capacity loss during cycling. These results demonstrate that Li/$LiFePO_4$ cells containing SiO_2/nylon 6,6 nanofiber membranes also have superior cycling performance.

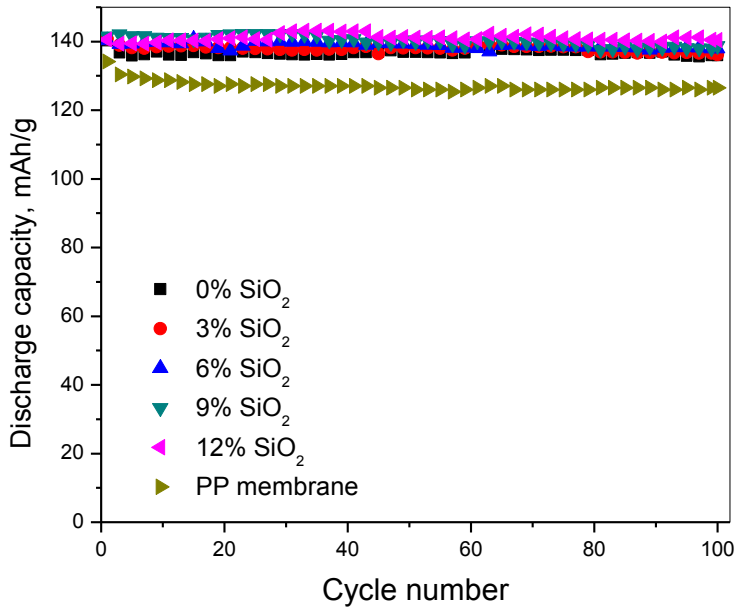

Figure 5.11 Cycling performance of Li/$LiFePO_4$ cells containing SiO_2/nylon 6,6 nanofiber membranes with different SiO_2 contents and micropous PP membrane at 1 C.

5.3.10 C-rate performance

Figure 5.12 shows the C-rate performance of Li/$LiFePO_4$ cells containing 0, 3, 6, 9, and 12 wt.% SiO_2/nylon 6,6 nanofiber membranes and microporous PP membrane. The cell containing microporous PP membrane has relatively a low discharge capacity of around 155 mAh/g at 0.2 C, which decreases to 67 mAh/g at 8 C. The cells containing SiO_2/nylon 6,6 nanofiber membranes have similar discharge capacities (about 160 mAh/g) at 0.2 C and they exhibit less capacity fading as the C rate increases. The capacities at 8 C are 71, 72, 73, 74 and 78 mAh/g, respectively, for the cells containing 0, 3, 6, 9, and 12 wt.% SiO_2/nylon 6,6 nanofiber membranes.

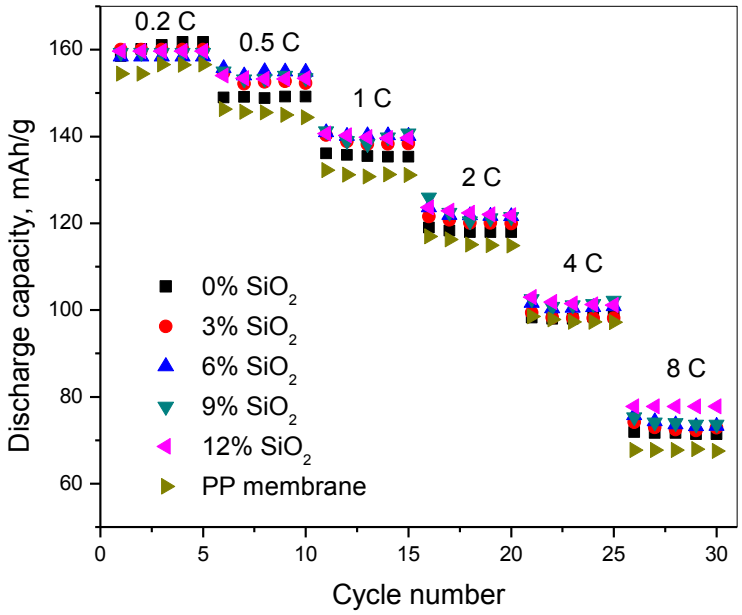

Figure 5.12 C-rate performance of Li/$LiFePO_4$ cells containing SiO_2/nylon 6,6 nanofiber membranes with different SiO_2 contents and micropous PP membrane.

It is known that although the electrode material and structure determine the maximum performance that lithium-ion cells can achieve, the measured C-rate performance of the cells is often affected by the ionic conductivity and interfacial resistance of liquid electrolyte-soaked membrane separators since they can influence the cell kinetics [19]. Hence, the superior rate capabilities of the cells containing SiO_2/nylon 6,6 nanofiber membranes can be ascribed to better interfacial properties and higher ionic conductivities of these membranes after uptaking liquid electrolyte.

5.4 Conclusion

SiO_2/nylon 6,6 nanofiber membranes were prepared by using electrospinning technique for use as thermally-stable Li-ion battery separator with good mechanical strength. Highly-porous nanofibrous structure was observed from SEM images. Experimental results showed that electrospun SiO_2/nylon 6,6 nanofiber membranes had better wettability, higher ionic conductivity, lower interfacial resistance and better thermal stability than microporous PP membrane. These membranes also showed superior mechanical properties. The cells containing SiO_2/nylon 6,6 nanofiber membrane separators with high SiO_2 contents showed excellent cycling and C-rate performance. It is, therefore, demonstrated that SiO_2/nylon 6,6 nanofiber membranes are promising separator candidate for high-performance Li-ion batteries.

REFERENCES

[1] M. Yanilmaz, C. Chen, X. Zhang, Fabrication and characterization of SiO2/PVDF composite nanofiber-coated PP nonwoven separators for lithium-ion batteries, Journal of Polymer Science Part B: Polymer Physics, 51 (2013) 1719-1726.

[2] M. Yanilmaz, Y. Lu, M. Dirican, K. Fu, X. Zhang, Nanoparticle-on-Nanofiber Hybrid Membrane Separators for Lithium-ion Batteries via Combining Electrospraying and Electrospinning Techniques, Journal of Membrane Science, 456 (2014) 57-65.

[3] X. Zhang, L. Ji, O. Toprakci, Y. Liang, M. Alcoutlabi, Electrospun nanofiber-based anodes, cathodes, and separators for advanced lithium-ion batteries, Polymer Reviews, 51 (2011) 239-264.

[4] H. Lee, M. Alcoutlabi, J.V. Watson, X. Zhang, Polyvinylidene fluoride-co-chlorotrifluoroethylene and polyvinylidene fluoride-co-hexafluoropropylene nanofiber-coated polypropylene microporous battery separator membranes, Journal of Polymer Science Part B: Polymer Physics, 51 (2013) 349-357.

[5] Y. Liang, Z. Lin, Y. Qiu, X. Zhang, Fabrication and characterization of LATP/PAN composite fiber-based lithium-ion battery separators, Electrochimica Acta, 56 (2011) 6474-6480.

[6] J. Song, M.-H. Ryou, B. Son, J.-N. Lee, D.J. Lee, Y.M. Lee, J.W. Choi, J.-K. Park, Co-polyimide-coated polyethylene separators for enhanced thermal stability of lithium ion batteries, Electrochimica Acta, 85 (2012) 524-530.

[7] M. Yanilmaz, F. Kalaoglu, H. Karakas, Investigation on the Effect of Process Variables on Polyurethane Nanofibre Diameter Using a Factorial Design, Fibres & Textıles in Eastern Europe, 21 (2013) 19-21.

[8] M. Yanilmaz, F. Kalaoglu, H. Karakas, Study on optimising the morphology of electrospun polyurethane nanofibers, Journal of Textile and Apparel, 22 (2012) 212-217.

[9] M. Yanilmaz, F. Kalaoglu, H. Karakas, A.S. Sarac, Preparation and characterization of electrospun polyurethane–polypyrrole nanofibers and films, Journal of Applied Polymer Science, 125 (2012) 4100-4108.

[10] R. Prasanth, V. Aravindan, M. Srinivasan, Novel polymer electrolyte based on cob-web electrospun multi component polymer blend of polyacrylonitrile/poly (methyl methacrylate)/polystyrene for lithium ion batteries—Preparation and electrochemical characterization, Journal of Power Sources, 202 (2012) 299-307.

[11] M. Yanilmaz, A.S. Sarac, A review: effect of conductive polymers on the conductivities of electrospun mats, Textile Research Journal, (2014) DOI 0040517513495943.

[12] H.-R. Jung, D.-H. Ju, W.-J. Lee, X. Zhang, R. Kotek, Electrospun hydrophilic fumed silica/polyacrylonitrile nanofiber-based composite electrolyte membranes, Electrochimica Acta, 54 (2009) 3630-3637.

[13] Y. Liang, S. Cheng, J. Zhao, C. Zhang, S. Sun, N. Zhou, Y. Qiu, X. Zhang, Heat treatment of electrospun PVDF fibrous membrane separators for rechargeable lithium-ion batteries, Journal of Power Sources, 240 (2013) 204-211.

[14] H. Lee, M. Alcoutlabi, J.V. Watson, X. Zhang, Electrospun nanofiber-coated separator membranes for lithium-ion rechargeable batteries, Journal of Applied Polymer Science, 129 (2013) 1939-1951.

[15] F. Zhang, X. Ma, C. Cao, J. Li, Y. Zhu, Poly (vinylidene fluoride)/SiO_2 composite membranes prepared by electrospinning and their excellent properties for nonwoven separators for lithium-ion batteries, Journal of Power Sources, 251 (2014) 423-431.

[16] X. Huang, J. Hitt, Lithium ion battery separators: Development and performance characterization of a composite membrane, Journal of Membrane Science, 97 (2001) 644-648.

[17] S. Chung, Y. Wang, L. Persi, F. Croce, S. Greenbaum, B. Scrosati, E. Plichta, Enhancement of ion transport in polymer electrolytes by addition of nanoscale inorganic oxides, Journal of Power Sources, 97 (2001) 644-648.

[18] Y. Liang, L. Ji, B. Guo, Z. Lin, Y. Yao, Y. Li, M. Alcoutlabi, Y. Qiu, X. Zhang, Preparation and electrochemical characterization of ionic-conducting lithium lanthanum titanate oxide/polyacrylonitrile submicron composite fiber-based lithium-ion battery separators, Journal of Power Sources, 196 (2011) 436-441.

[19] J. Cao, L. Wang, M. Fang, Y. Shang, L. Deng, J. Yang, J. Li, H. Chen, X. He, Interfacial compatibility of gel polymer electrolyte and electrode on performance of Li-ion battery, Electrochimica Acta, 114 (2013) 527-532.

CHAPTER 6. SIO_2/POLYACRYLONITRILE NANOFIBER MEMBRANES VIA CENTRIFUGAL SPINNING AS SEPARATOR FOR LI-ION BATTERIES

ABSTRACT

Centrifugal spinning is a fast, cost-effective and safe alternative to the electrospinning technique, which is commonly used for making fiber-based separator membranes. In this work, SiO_2/polyacrylonitrile (PAN) membranes were produced by using centrifugal spinning and they were characterized by using different electrochemical techniques for use as separators in Li-ion batteries. SiO_2/PAN membranes exhibited good wettability and high ionic conductivity due to their highly porous fibrous structure. Compared with commercial microporous polyolefin membranes, SiO_2/PAN membranes had larger liquid electrolyte uptake, higher electrochemical oxidation limit, and lower interfacial resistance with lithium. SiO_2/PAN membrane separators were assembled into lithium/lithium iron phosphate cells and these cells delivered high capacities and exhibited good cycling performance at room temperature. In addition, cells using SiO_2/PAN membranes showed superior C-rate performance compared to those using microporous PP membrane.

6.1 Introduction

Li-ion batteries have found applications in many electronics such as cellular phones, laptops, digital cameras, etc. due to their superior properties such as high energy density, high operational voltage, long cycle life, and low self-discharge rate. Although current Li-ion batteries have higher energy density than most other commercial rechargeable batteries, significant improvements are still needed in energy density, safety, durability and affordability to meet the long-term performance targets for electric vehicles and plug-in hybrid vehicles [1-3].

In Li-ion batteries, separators are placed between electrodes to prevent electronic contact and simultaneously they must allow Li-ion movements between electrodes. Microporous polyolefin membranes are commonly used in Li-ion batteries due to their good chemical stability and mechanical strength. However, their disadvantages such as low porosity and poor wettability with polar liquid electrolyte restrict cell performance. For example, these separators limit energy density and rate capability of rechargeable Li-ion batteries by affecting the cell resistance and kinetics [4].

Electrospinning technique is commonly used to produce continuous nano-sized polymer fibers by utilizing an electric field imposed on a polymer solution [5-8]. Electrospun nanofiber membranes can be used as separators in lithium-ion batteries due to their large porosity and unique pore structures. There are many studies that report enhanced electrochemical properties such as C-rate performance, cycling performance and lower cell resistances by using electrospun membranes [9-11]. However, this process has some serious disadvantages such as low spinning rate, poor safety, and high production cost [12].

Centrifugal spinning can be a fast, cost-effective, safe alternative to electrospinning for nanofiber production. In the centrifugal spinning technique, nanofibers are produced from polymer solutions by using a high speed rotary and perforated spinneret (Figure 6.1). In the process, high centrifugal force is generated on the polymer solution when the spinneret rotates. When the rotational speed is high enough to overcome the surface tension of the solution, liquid jets are ejected from nozzles. After stretching and solvent evaporation, fibers are deposited on the rod collectors [12]. The diameters of fibers can vary from several nanometers to micrometers [13]. The production rate of this simple centrifugal spinning process could be more than 500 times faster than conventional electrospinning, which significantly reduces the production cost of nanofiber membranes [12].

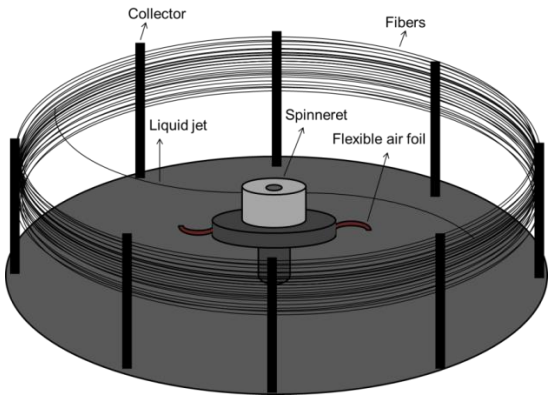

Figure 6.1 Schematic of centrifugal spinning process.

Here, we introduced centrifugal spinning technique as a fast, cost-effective and safe technique to fabricate high-performance fiber-based separators for Li-ion batteries. PAN was used to make the centrifugally-spun fibers because of its characteristics such as high room temperature ionic conductivity when it is electrolyte-soaked, good thermal stability, and

excellent resistance to oxidative degradation [14]. SiO_2 was added to PAN to further improve the electrochemical performance such as ionic conductivity and interfacial stability [9]. Electrochemical properties of these novel SiO_2/PAN membranes with various SiO_2 contents (0, 3, 6, 9 and 12%) were evaluated in detail. Experimental results showed that SiO_2/PAN membranes had higher ionic conductivities, lower interfacial resistances and better C-rate performance compared to microporous PP membranes. It is, therefore, demonstrated that these centrifugally-spun SiO_2/PAN membranes are promising separator candidate for high-performance Li-ion batteries.

6.2 Experimental

6.2.1 Chemicals

Polyacrylonitrile (PAN, M_w = 150000) was supplied from Pfaltz& Bauer Inc. N,N-dimethylformamide (DMF) and n-butanol were purchased from Sigma Aldrich. Hydrophilic pyrogenic SiO_2 (Aerosil 380, particle size = 7 nm, surface area = 380 m^2/g) was supplied from Evonic industries. Liquid electrolyte, 1 M lithium hexafluorophosphate ($LiPF_6$) in ethylene carbonate and ethyl methyl carbonate (EC+EMC, 1:1 by volume), was supplied from Ferro Corp. Celgard 2400 microporous monolayer polypropylene (PP) membrane with the thickness of 25 μm and the porosity of 41% was used for comparison. All chemicals were used as received without further purification.

6.2.2 Separator preparation

SiO_2/PAN membranes were prepared by using centrifugal spinning. PAN solution (17 wt.%) was prepared by dissolving PAN into DMF. SiO_2/PAN solutions were prepared by

adding different amounts of SiO_2 (3, 6, 9, and 12 wt.%) into the 17 wt.% PAN solution. All solutions were stirred mechanically overnight prior to centrifugal spinning.

The centrifugal spinning system was powered by a DC motor (115 v, Grainger) and the rotational speed was controlled by a speed controller (DART CONTROLS253G-200C). The rotational speed of the motor was controlled at 4000 rpm. The spinneret had a cylindrical shape with 2 cm in height, 1.5 cm in radius, and 0.3 mm in wall thickness. Two nozzles with inner diameter of 0.4 mm were located on the sidewall of the spinneret. The distance between the nozzle tip and the rod collector was set to 10 cm. All the spinning operations were conducted at room temperature.

6.2.3 Structure characterization

The morphology of centrifugally-spun SiO_2/PAN membranes was studied by using a JEOL JSM-6400F field-emission scanning electron microscope (FESEM). The fiber diameters were calculated by measuring 50 randomly-selected fibers in SEM images using Revolution 1.6 software for each sample.

The porosities of the membranes were determined by using n-butanol uptake tests. In a uptake test, the porosity was calculated by using the following equation:

$$Porosity\ (\%) = \frac{w_w - w_d}{\rho_b \times V} \quad (1)$$

where w_w and w_d are the weights of wet and dry membranes, respectively, ρ_b the density of n-butanol, and V the geometric volume of the membrane.

6.2.4 Performance evaluation

Liquid electrolyte uptakes were measured by soaking weighed membranes in the liquid electrolyte of 1M $LiPF_6$ in EC+EMC (1:1 in volume) for two hours at room temperature. The electrolyte uptake (*EU*) was calculated by:

$$EU\ (\%) = \frac{w_1 - w_0}{w_0} \times 100 \quad (2)$$

where w_0 and w_1 are the weights of dry and wet membranes, respectively.

The ionic conductivities of liquid electrolyte-soaked membranes were measured by electrochemical impedance spectroscopy (EIS) using Reference 600 Potentiostat/Galvanostat/ZRA (GAMRY). The impedance measurements were performed on liquid electrolyte-soaked membranes sandwiched between two stainless steel electrodes over a frequency range of 1 MHz to 1 Hz with AC amplitude of 10 mV and within a temperature range of 25 to 85 ^{o}C. The ionic conductivity was calculated by:

$$\sigma = \frac{d}{R_b \times S} \quad (3)$$

where d is the membrane thickness, S the cross-sectional area, and R_b the bulk resistance obtained at the high frequency intercept of the Nyquist plot on the real axis.

The electrochemical oxidation limits of liquid electrolyte-soaked membranes were determined by linear sweep voltammetry at room temperature. In these tests, electrochemical cells consisting of stainless steel working electrode and lithium metal counter electrode were used. The scan rate used was 10 mVs^{-1} and the potential range was 2.5 to 6.0 V.

The interfacial resistances between the liquid electrolyte-soaked membranes and lithium metal were investigated by measuring the impedances of symmetrical lithium cells. The frequency range used was 1 MHz to 1 Hz.

The charge-discharge tests of Li/$LiFePO_4$ cells containing liquid electrolyte-soaked membranes were conducted by using coin-type cells. The $LiFePO_4$ cathode was prepared by blending $LiFePO_4$ powder (80 wt%), carbon black conductor (10 wt%) and PVDF binder (10 wt%). Arbin automatic battery cycler was used with a potential range of 4.2 - 2.5 V at a current density of 0.2 C to evaluate the cycling performance. In order to evaluate C-rate performance, different C-rates (0.2C, 0.5C, 1C, 2C, 4C, and 8C) were applied to the cells.

6.3 Results and Discussion

6.3.1 Separator morphology

Figure 6.2 shows SEM images of SiO_2/PAN membranes with 0, 3, 6, 9, and 12 wt. % SiO_2. When the SiO_2 content was greater than 12 wt.%, fiber membranes were not obtained probably due to the severe particle aggregations. It is seen from Figure 6.2 that the introduction of SiO_2 fillers does not change the morphology of centrifugally-spun membranes significantly. However, the average fiber diameter of SiO_2/PAN membranes decreased slightly with increase in SiO_2 content. The average fiber diameters are 1.4, 1.3, 1.2, 0.9 and 0.8 μm, respectively, for 0, 3, 6, 9, and 12 wt.% SiO_2/PAN membranes. This decrease in fiber diameter may be contributed to the repulsive force of SiO_2 that minimizes the entanglement of polymer chains. Similar results were also reported for electrospun SiO_2/PAN membranes by Jung et al. [9] High membrane porosity helps absorb large amount of electrolyte and allows fast ion transportation between electrodes. Table 6.1 shows the porosities of SiO_2/PAN membranes with different SiO_2 contents. For comparison, the porosity of microporous PP membrane is also shown.

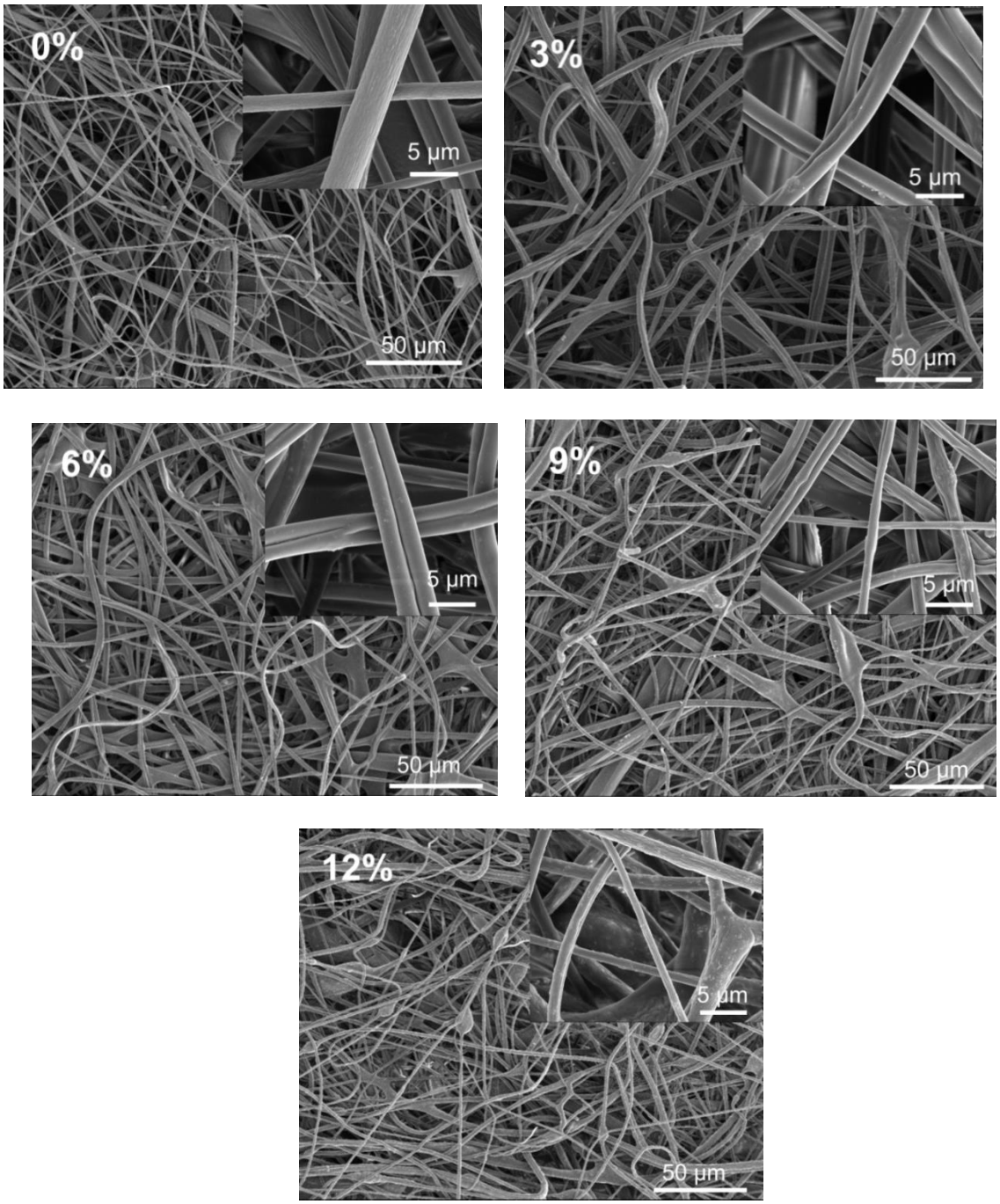

Figure 6.2 SEM images of SiO_2/PVDF membranes with different SiO_2 contents.

Table 6.1 Porosities, electrolyte uptakes and ionic conductivities of SiO_2/PAN membranes with different SiO_2 contents at room temperature.

	Porosity (%)	**Electrolyte uptake (%)**	**Ionic conductivity (mS/cm)**
0 wt.% SiO_2/PAN	68	270	2.8
3 wt.% SiO_2/PAN	69	278	3.0
6 wt.% SiO_2/PAN	70	290	3.2
9 wt.% SiO_2/PAN	71	295	3.4
12 wt.% SiO_2/PAN	72	310	3.6
Microporous PP membrane	41	158	0.8

It is seen that the porosities of 0, 3, 6, 9 and 12 wt.% SiO_2/PAN membranes are 68, 69, 70, 71 and 72%, respectively, which are significantly greater than that (41%) of microporous PP membrane. Fibrous morphology leads to high porosity since large void space is available between fibers. Furthermore, the introduction of SiO_2 nanoparticles further increases the porosity value. This is probably because the fiber diameter decreases with the presence of SiO_2 nanoparticles and the resultant thinner fibers are more loosely assembled during fiber deposition. In addition, SiO_2 nanoparticles may also contribute to the increased porosity by helping trap more liquid n-butanol during the porosity measurement. Similar results have also reported for SiO_2/PVDF membrane separators [15].

6.3.2 Liquid electrolyte uptake

The electrolyte uptake capacity of separators affects the ionic conductivity and cell resistance of Li-ion batteries. Electrolyte uptake capacities of SiO_2/PAN membranes with different SiO_2 contents are also shown in Table 6.1. The uptake capacities of 0, 3, 6, 9, and 12% SiO_2/PAN membrane are 270, 278, 290, 295 and 310%, respectively. These values are significantly higher than that (158%) of microporous PP membrane. The high uptake capacity of SiO_2/PAN membranes can be explained by high porosity value compared to microporous PP membrane. In addition, the introduction of SiO_2 nanoparticles increases the electrolyte uptake capacity by further increasing the porosity and offering high affinity to the electrolyte.

6.3.3 Ionic conductivity

The ionic conductivity of an electrolyte-soaked separator is determined by the porosity, tortuosity, and thickness of the separator and the resistivity of the electrolyte, and it affects the cell cycling and C-rate performance [16]. Table 6.1 shows the ionic conductivities of liquid electrolyte-soaked SiO_2/PAN membranes and microporous PP membrane at room temperature. The room-temperature conductivities of liquid electrolyte-soaked SiO_2/PAN membranes are significantly greater than that (0.8×10^{-3} S/cm) of liquid electrolyte-soaked microporous PP membrane since SiO_2/PAN membranes have higher porosity values and larger uptake capacities. The room-temperature conductivities are 2.8×10^{-3}, 3.0×10^{-3}, 3.2×10^{-3} 3.4×10^{-3} and 3.6×10^{-3} S/cm, respectively, for liquid electrolyte-soaked SiO_2/PAN membranes with 0, 3, 6, 9, and 12% SiO_2. For SiO_2/PAN membranes, an increase in SiO_2 content leads to high ionic conductivity due to increased porosity and electrolyte uptake. In

addition, it is known that inorganic particles could interact with electrolyte components and these interactions could also help to improve ionic conductivity [17]. Same trend on conductivity improvement was also reported for electrospun SiO_2/PAN membranes [9].

Figure 6.3 shows the temperature dependence of ionic conductivities of liquid electrolyte-soaked SiO_2/PAN membranes. The ionic conductivities of all membranes increase with increase in temperature. Ionic conductivity is dependent on the number of charge carriers and their mobility. Increasing temperature enhances the mobility of charge carriers, which in turn leads to increased conductivity [18]. From Figure 6.3, it is also seen that after soaking liquid electrolyte, SiO_2/PAN membranes exhibit higher ionic conductivities than microporous PP membrane at all temperatures and higher SiO_2 contents lead to higher ionic conductivities for SiO_2/PAN membranes.

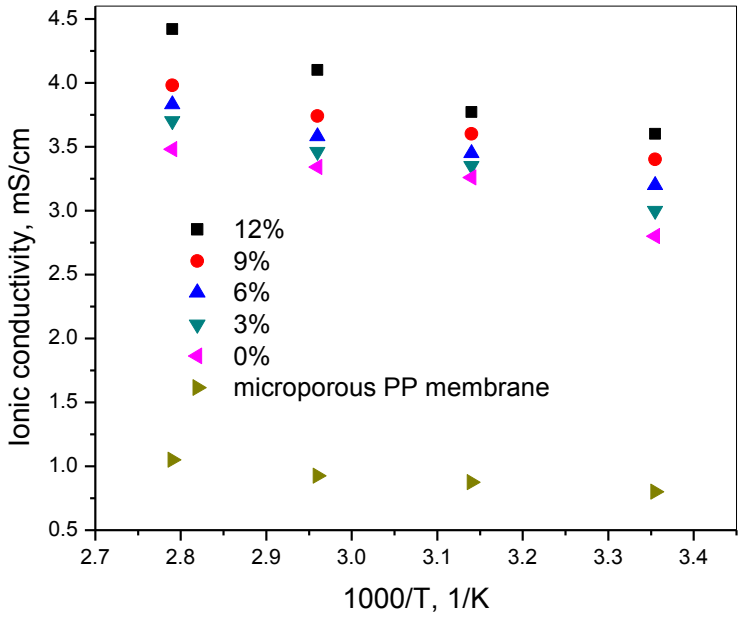

Figure 6.3 Ionic conductivities of SiO_2/PAN membranes with different SiO_2 contents and microporous PP membrane as a function of temperature.

6.3.4 Electrochemical oxidation limit

The electrochemical oxidation limits of liquid electrolyte-soaked membranes were evaluated by linear sweep voltammetry measurements (Figure 6.4). In these measurements, the rapid increase of the current can be observed when the electrolyte starts to decompose.

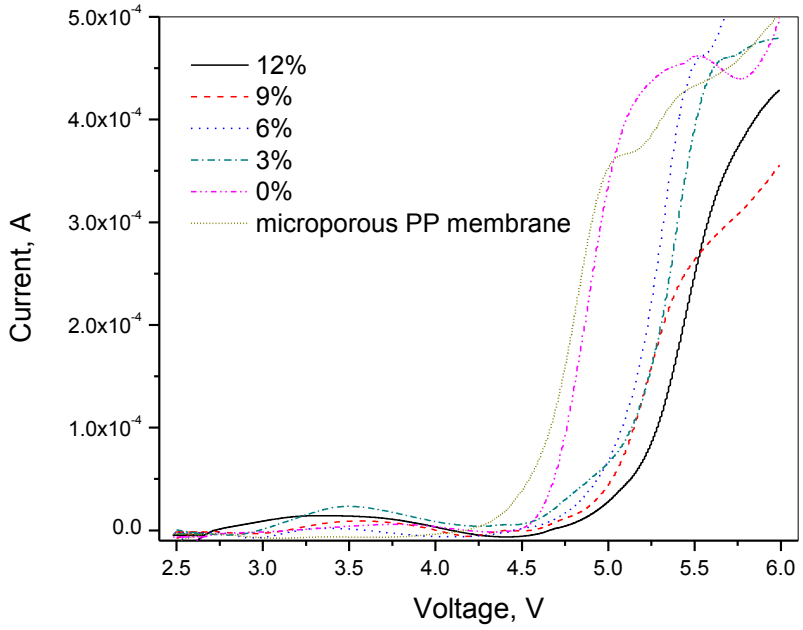

Figure 6.4 Electrochemical oxidation limits of SiO_2/PAN membranes with different SiO_2 contents and microporous PP membrane.

It is seen from Figure 6.4 that as compared to microporous PP membrane, the PAN membrane shows slightly higher electrochemical oxidation limit (4.5 V compared to 4.25 V). The introduction of SiO_2 further increases the electrochemical oxidation limit up to 4.75 V, which is achieved when the SiO_2 content is 12 wt.%. The improved electrochemical oxidation limit might be due to the excellent affinity of SiO_2 nanoparticles to the electrolyte and the stabilization effect of SiO_2 nanoparticles. It was reported that SiO_2 nanoparticles can

absorb impurities in the electrolyte and hence can help to stabilize the liquid electrolyte at high voltages [9, 15, 17].

6.3.5 Interfacial resistance

The compatibility of liquid electrolyte-soaked membranes with lithium metal was investigated by measuring electrochemical impedance spectra of Li/liquid electrolyte-soaked membrane/Li cells, and the results are shown in Figure 6.5.

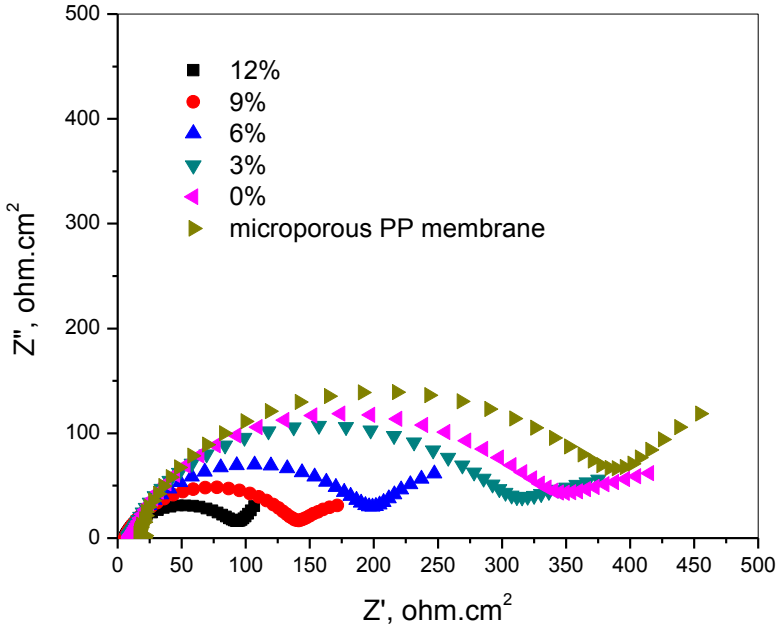

Figure 6.5 Electrochemical impedance spectra of SiO_2/PAN membranes with different SiO_2 contents and micropous PP membrane.

The diameters of semi-circles at the intermediate frequency region represent the interfacial resistances of liquid electrolyte-soaked membranes with Li metal. The PAN membrane exhibits lower interfacial resistance (350 ohm·cm^2) than that (400 ohm·cm^2) of microporous PP membrane. The introduction of SiO_2 further decreases the interfacial resistance down to

100 ohm·cm^2 when the SiO_2 content is 12 wt.%. It has also been reported in previous studies [17, 19] that adding ceramic fillers can improve the interfacial properties with the Li electrode because high-surface area nanoparticles can trap impurities and protect Li from corrosion.

6.3.6 Cycling performance

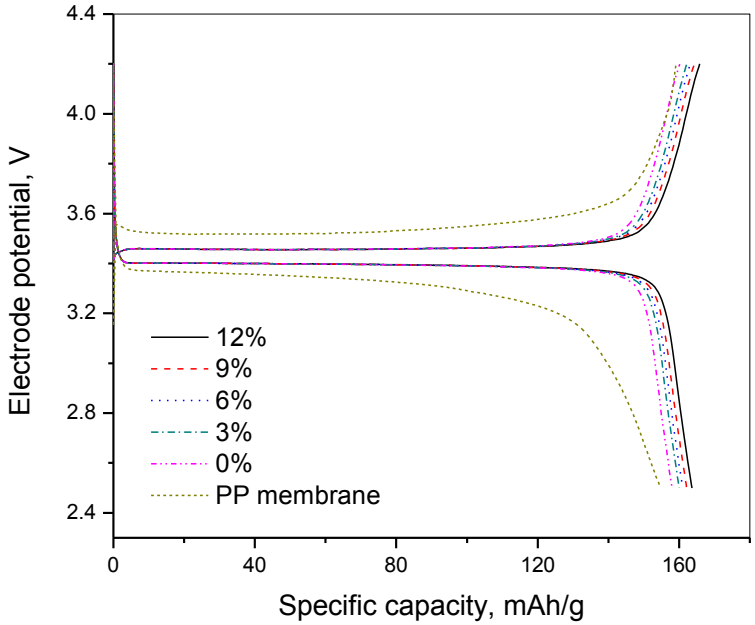

Figure 6.6 First-cycle charge-discharge curves of Li/$LiFePO_4$ cells containing SiO_2/PAN membranes with different SiO_2 contents and micropous PP membrane at 0.2 C.

The cycling performance of SiO_2/PAN membranes were investigated by using coin-type Li/$LiFePO_4$ cells. The first-cycle charge-discharge curves of Li/$LiFePO_4$ cells at 0.2 C are shown in Figure 6.6. The cell capacities are mainly determined by the type and structure

of the electrodes. However, it is known that the separator material and structure also play an important role in determining the overall cell performance since separators can affect the ion transportation between the two electrodes, which is important in regulating the cell kinetics [15]. As shown in Figure 6.6, the discharge capacity of the cell using microporous PP membrane is 154 mAh/g. The discharge capacities of cells containing 0, 3, 6, 9, and 12 wt.% SiO_2/PAN membranes are 158, 160, 161, 162, and 163 mAh/g, respectively. The cell containing 12 wt.% SiO_2/PAN membrane delivers the highest discharge capacity of 163 mAh/g. The high porosities and ionic conductivities of SiO_2/PAN membranes are the main reason for achieving improved capacity values in cells containing these membranes.

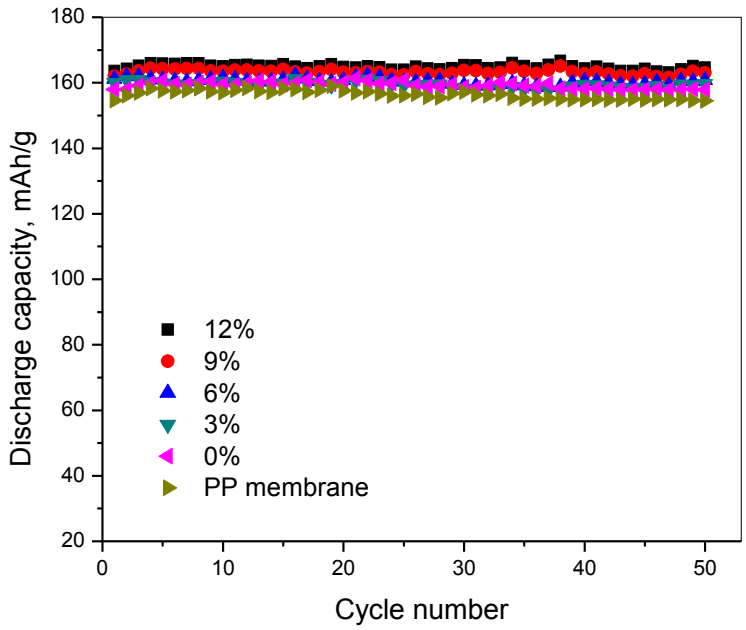

Figure 6.7 Cycling performance of Li/$LiFePO_4$ cells containing SiO_2/PAN nanofiber membranes with different SiO_2 contents and microporous PP membrane at 0.2 C.

Figure 6.7 shows the cycling performance of Li/$LiFePO_4$ cells containing 0, 3, 6, 9, and 12 wt.% SiO_2/PAN membranes and microporous PP membrane at 0.2 C. For all six cells, no apparent capacity loss is observed in 50 cycles at a low rate of 0.2 C.

6.3.7 C-rate performance

Figure 6.8 shows the C-rate performance of Li/$LiFePO_4$ cells containing 0, 3, 6, 9, and 12 wt.% SiO_2/PAN nanofiber membranes and microporous PP membrane. The cell containing microporous PP membrane has a relatively low discharge capacity of around 154 mAh/g at 0.2 C, which decreases to 67 mAh/g at 8 C. The cells containing SiO_2/PAN nanofiber membranes have higher discharge capacities (about 160 mAh/g) at 0.2 C and they exhibit less capacity fading as the C rate increases. The capacities at 8 C are 71, 75, 76, 80 and 85 mAh/g, respectively, for the cells containing 0, 3, 6, 9, and 12 wt.% SiO_2/PAN nanofiber membranes. It is known that although the electrode material and structure determine the maximum performance that lithium-ion cells can achieve, the measured C-rate performance of the cells is often affected by the ionic conductivity and interfacial resistance of liquid electrolyte-soaked membrane separators [20]. Hence, the superior rate capabilities of the cells containing SiO_2/PAN nanofiber membranes can be ascribed to higher ionic conductivities and better interfacial properties of these membranes after up-taking liquid electrolyte. These results confirm that centrifugally-spun SiO_2/PAN membranes are promising separator candidate for rechargeable Li-ion batteries.

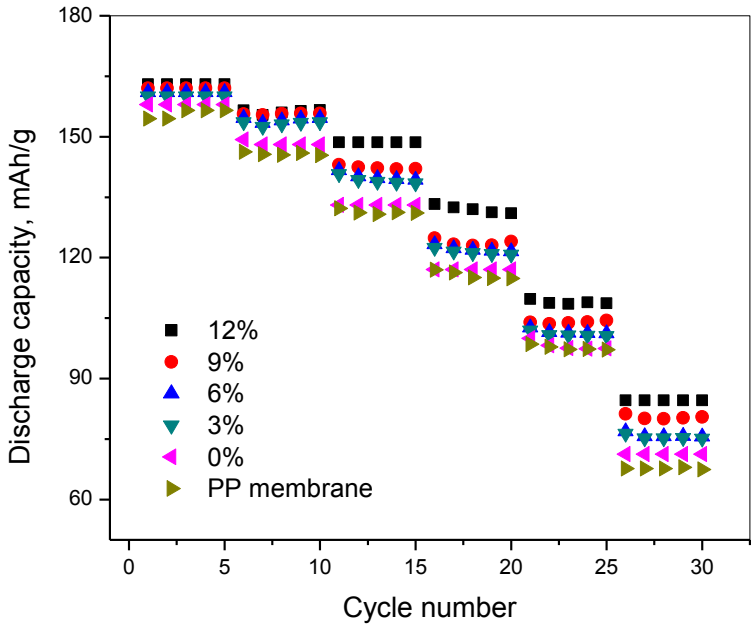

Figure 6.8 C-rate performance of Li/$LiFePO_4$ cells containing SiO_2/PAN membranes with different SiO_2 contents and micropous PP membrane.

6.4. Conclusion

Centrifugal spinning is introduced as a fast, cost-effective and safe technique to prepare fiber-based separator membranes. Centrifugally-spun SiO_2/PAN membranes were prepared and characterized for use as separator membranes in Li-ion batteries. Porosity, electrolyte uptake capacity, ionic conductivity, electrochemical oxidation limit, interfacial resistance, cycling performance, and C-rate performance were investigated and compared with a commercial microporous PP membrane. SiO_2/PAN membranes possessed better wettability, higher ionic conductivity, lower interfacial resistance and better cycling performance than microporous PP membrane. The cells containing SiO_2/PAN separators with high SiO_2 contents also showed excellent cycling and C-rate performance. Therefore,

centrifugal spinning is an alternative to electrospinning and centrifugally-spun SiO_2/PAN membranes are promising separator membranes for high-performance Li-ion batteries.

REFERENCES

[1] Y. Li, G. Xu, Y. Yao, L. Xue, M. Yanilmaz, H. Lee, X. Zhang, Solid State Ionics, 258 (2014) 67-73.

[2] M. Dirican, M. Yanilmaz, K. Fu, Y. Lu, H. Kizil, X. Zhang, Journal of Power Sources, 264 (2014) 240-247.

[3] K. Fu, Y. Lu, M. Dirican, C. Chen, M. Yanilmaz, Q. Shi, P.D. Bradford, X. Zhang, Nanoscale, (2014).

[4] X. Huang, Journal of Solid State Electrochemistry, 15 (2011) 649-662.

[5] M. Yanilmaz, F. Kalaoglu, H. Karakas, Fibres & Textiles in Eastern Europe, 21 (2013) 19-21.

[6] M. Yanilmaz, F. Kalaoglu, H. Karakas, Journal of Textile & Apparel, 22 (2012) 212-217.

[7] M. Yanilmaz, F. Kalaoglu, H. Karakas, A.S. Sarac, Journal of Applied Polymer Science, 125 (2012) 4100-4108.

[8] M. Yanilmaz, A.S. Sarac, Textile Research Journal, (2014).

[9] H.-R. Jung, D.-H. Ju, W.-J. Lee, X. Zhang, R. Kotek, Electrochimica Acta, 54 (2009) 3630-3637.

[10] Y. Liang, Z. Lin, Y. Qiu, X. Zhang, Electrochimica Acta, 56 (2011) 6474-6480.

[11] X. Zhang, L. Ji, O. Toprakci, Y. Liang, M. Alcoutlabi, Polymer Reviews, 51 (2011) 239-264.

[12] Y. Lu, Y. Li, S. Zhang, G. Xu, K. Fu, H. Lee, X. Zhang, European Polymer Journal, 49 (2013) 3834-3845.

[13] L.A. Mary, T. Senthilram, S. Suganya, L. Nagarajan, J. Venugopal, S. Ramakrishna, V. Dev, Express polymer letters, 7 (2013) 238-248.

[14] R. Prasanth, V. Aravindan, M. Srinivasan, Journal of Power Sources, 202 (2012) 299-307.

[15] M. Yanilmaz, Y. Lu, M. Dirican, K. Fu, X. Zhang, Journal of Membrane Science 456 (2014) 57-65.

[16] P. Arora, Z. Zhang, Chemical Reviews-Columbus, 104 (2004) 4419-4462.

[17] M. Yanilmaz, C. Chen, X. Zhang, Journal of Polymer Science Part B: Polymer Physics, (2013).

[18] P. Raghavan, X. Zhao, J.-K. Kim, J. Manuel, G.S. Chauhan, J.-H. Ahn, C. Nah, Electrochimica Acta, 54 (2008) 228-234.

[19] M. Yanilmaz, M. Dirican, X. Zhang, Electrochimica Acta 133 (2014) 501-508.

[20] J. Cao, L. Wang, M. Fang, Y. Shang, L. Deng, J. Yang, J. Li, H. Chen, X. He, Electrochimica Acta, 114 (2013) 527-532.

CHAPTER 7. POLYMETHYLMETHACRYLATE/POLYACRYLONITRILE BLEND NANOFIBER MEMBRANES VIA CENTRIFUGAL SPINNING AS SEPARATOR FOR LI-ION BATTERIES

ABSTRACT

Electrospun nanofiber membranes have been extensively studied as separators in Li-ion batteries due to their large porosity, unique pore structure, and high electrolyte uptake. However, the electrospinning process has some serious drawbacks such as low spinning rate and high production cost. Centrifugal spinning technique can be used as a fast, cost-effective and safe technique to fabricate high-performance fiber-based separators. In this work, polymethylmethacrylate (PMMA)/polyacrylonitrile (PAN) membranes with different blend ratios were produced via centrifugal spinning and characterized by using different electrochemical techniques for use as separators in Li-ion batteries. Compared with commercial microporous polyolefin membrane, centrifugally-spun PMMA/PAN membranes had larger ionic conductivity, higher electrochemical oxidation limit, and lower interfacial resistance with lithium. Centrifugally-spun PMMA/PAN membrane separators were assembled into Li/LiFePO4 cells and these cells delivered high capacities and exhibited good cycling performance at room temperature. In addition, cells using centrifugally-spun PMMA/PAN membrane separators showed superior C-rate performance compared to those using microporous PP membranes. It is, therefore, demonstrated that centrifugally-spun PMMA/PAN membranes are promising separator candidate for high-performance Li-ion batteries.

7.1. Introduction

Li-ion batteries have been widely used in many electronic devices including mobile phones, laptop computers and digital cameras because of their high energy density, large operational voltage, long cycling life, and low self-discharge rate [1,2]. In recent years, Li-ion batteries have found new application areas such as electric/hybrid vehicles and energy storage for smart grids. To meet the requirements of these new applications, designing new battery components with improved performance is critical [3-5].

In Li-ion batteries, the separator is placed between two electrodes, the anode and the cathode. It prevents the physical contact of electrodes while serving as the electrolyte reservoir to enable ionic transport. Although the separator does not directly participate in electrode reactions, its structure and properties affect battery performance, including cycle life, safety, energy density, and power density by regulating the cell resistance and kinetics [6,7]. Microporous polyolefin membranes are widely used in Li-ion batteries since they have good chemical stability and mechanical strength. However, low porosity and poor wettability of these membranes affect the cell resistance and kinetics negatively and restrict the cell performance, including energy density and rate capability [8].

Over the past 10 years, electrospun nanofiber membranes have been extensively studied as alternative separators for Li-ion batteries due to their large porosity and unique pore structure. In electrospinning technique, continuous nanosized polymer fibers are produced through the action of an external electric field imposed on a polymer solution [9-11]. Enhanced electrochemical properties such as higher C-rate capability, better cycling performance and lower cell resistance have been reported for Li-ion cells using electrospun nanofiber-based separators [12,13]. However, electrospinning process has some serious

drawbacks such as low spinning rate and high production cost, which hinder the practical use of electrospun nanofiber separators in Li-ion batteries [14]. Therefore, a new technique that can produce high-performance nanofiber separators at high speed and low cost is urgently needed.

Recently, centrifugal spinning has been studied as an alternative approach to fabricate nanofibers in a large-scale and low-cost fashion [14,15]. In this technique, a high speed rotary and perforated spinneret is used to fabricate nanofibers from polymer solutions (Figure 7.1).

Figure 7.1. Schematic of centrifugal spinning process.

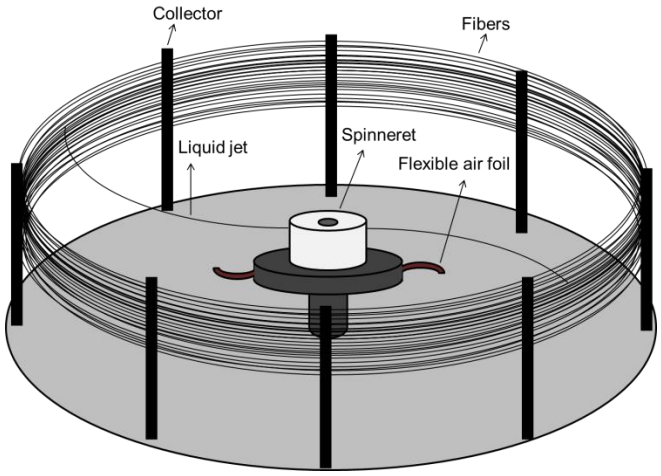

During fiber spinning, high centrifugal force is generated on the polymer solution by rotating the spinneret. When the spinneret reaches a critical rotational speed, the centrifugal force is able to overcome the surface tension of the solution and liquid jets are ejected from nozzles. Liquid jets are stretched by the centrifugal force, accompanied by solvent evaporation. The resultant solidified fibers are deposited on the rod collectors. The diameters

of fibers can vary from several nanometers to micrometers and the production rate of the centrifugal spinning process could be more than 500 times faster than conventional electrospinning technique [8,14].

Polyacrylonitrile (PAN) has been studied as a separator material and PAN-based separators show promising properties including high ionic conductivity, good thermal stability, high electrolyte uptake and good compatibility with Li metal [16]. Polymethylmethacrylate (PMMA) has also been used as a separator material due to its good compatibility with Li and high affinity to liquid electrolyte [17,18]. Blending PAN and PMMA can potentially lead to new separators with enhanced microstructure, porosity and electrochemical properties that cannot be achieved by single-component polymer membranes. Different blend separators including PVDF/PMMA-co-PEGMA microporous separators [19], PVDF-co-HFP/PAN microporous membranes [20], PVDF/PMMA microporous membranes [17,21], electrospun PVDF/PAN membranes [16], and electrospun PVDF-HFP/PMMA [22] have been reported so far, and results demonstrated that blend separators have the advantages of improved electrolyte uptake, ionic conductivity, and cycling performance. In this work, centrifugal spinning was utilized to produce PAN/PMMA blend membranes for use as high-performance separator for Li-ion batteries. The porosity, ionic conductivity, electrochemical oxidation limit and interfacial resistance of these membranes were investigated, and results showed that compared with commercial microporous polyolefin membranes, centrifugally-spun PMMA/PAN membranes had larger ionic conductivity, higher electrochemical oxidation limit, and lower interfacial resistance with lithium. Furthermore, PMMA/PAN membranes were assembled into Li/$LiFePO_4$ cells and these cells delivered high capacities and exhibited good cycling performance at room

temperature. In addition, cells using PMMA/PAN membranes showed superior C-rate performance compared to those using microporous PP membranes. It is, therefore, demonstrated that these centrifugally-spun PMMA/PAN membranes are promising separator candidate for high-performance Li-ion batteries.

7.2. Experimental Section

7.2.1 Materials

Polyacrylonitrile (PAN, Mw = 150000) was supplied from Pfaltz& Bauer Inc. Polymethylmethacrylate (PMMA, 300000) and N,N-dimethylformamide (DMF) were purchased from Sigma Aldrich. Celgard 2400 microporous monolayer polypropylene (PP) membrane with the thickness of 25 μm and the porosity of 41% was used for comparison. All chemicals were used as received.

7.2.2 Separator preparation

PMMA/PAN membranes were prepared by using centrifugal spinning. PMMA/PAN solutions with two blend ratios (75/25 and 50/50 w/w) were prepared by dissolving PMMA and PAN into DMF with a total polymer concentration of 17 wt. %. For comparison, a PMMA solution (17 wt. %) was also prepared. All solutions were stirred mechanically overnight prior to centrifugal spinning.

The centrifugal spinning system was powered by a DC motor (115 v, Grainger) and the rotational speed of the motor was controlled by a speed controller (DART CONTROLS253G-200C). The spinneret had a cylindrical shape with 2 cm in height, 1.5 cm in radius, and 0.3 cm in wall thickness. Two nozzles with inner diameter of 0.4 mm were located on the sidewall of the spinneret. The distance between the nozzle tip and the rod

collector was 10 cm. In this work, the spinning operations of PMMA and PMMA/PAN solutions were conducted with a rotational speed of 4000 rpm at room temperature.

7.2.3 Structure characterization

The morphology of centrifugally-spun PMMA and PMMA/PAN membranes was studied by using a JEOL JSM-6400F field-emission scanning electron microscope (FESEM). The fiber diameters were calculated by measuring 50 randomly-selected fibers in SEM images using Revolution 1.6 software for each sample. The porosities of the membranes were calculated by using the following equation:

$$Porosity\ (\%) = \left(1 - \frac{\rho_M}{\rho_P}\right) \times 100 \qquad (1)$$

where ρ_M is the apparent density of the separator, and ρ_P the density of the polymer.

7.2.4 Performance evaluation

Electrochemical performance was measured after soaking weighed membranes in the liquid electrolyte of 1M $LiPF_6$ in EC+DMC+DEC (1:1:1 in volume) for two hours at room temperature.

The ionic conductivities of liquid electrolyte-soaked membranes were measured by electrochemical impedance spectroscopy (EIS) using Reference 600 Potentiostat/Galvanostat/ZRA (GAMRY). The impedance measurements were performed on liquid electrolyte-soaked membranes sandwiched between two stainless steel electrodes over a frequency range of 1 MHz to 1 Hz with AC amplitude of 10 mV at room temperature. The ionic conductivity was calculated by:

$$\sigma = \frac{d}{R_b \times S} \qquad (2)$$

where d is the membrane thickness, S the cross-sectional area, and R_b the bulk resistance obtained at the high frequency intercept of the Nyquist plot on the real axis.

The electrochemical oxidation limits of liquid electrolyte-soaked membranes were determined by linear sweep voltammetry at room temperature. In these tests, electrochemical cells consisting of stainless steel working electrode and lithium metal counter electrode were used. The scan rate used was 10 mVs^{-1} and the potential range was 2.5 to 6.0 V.

The interfacial resistances between liquid electrolyte-soaked membranes and lithium metal were investigated by measuring the impedances of symmetrical lithium cells. The frequency range used was 1 MHz to 1 Hz.

The charge-discharge tests of Li/$LiFePO_4$ cells containing liquid electrolyte-soaked membranes were conducted by using coin-type cells. The $LiFePO_4$ cathode was prepared by blending $LiFePO_4$ powder (80 wt%), carbon black conductor (10 wt%) and PVDF binder (10 wt%). Arbin automatic battery cycler was used with a potential range of 4.2 - 2.5 V at a current density of 0.2 C to evaluate the cycling performance. In order to evaluate C-rate performance, different C-rates (0.2C, 0.5C, 1C, 2C, 4C, and 8C) were applied to the cells.

7.3. Results and Discussion

7.3.1 Separator morphology

The morphology of membrane separators affects the electrochemical properties of Li-ion cells by influencing the ion transport and conductivity behavior. Figure 7.2 shows SEM images of PMMA membrane and PMMA/PAN membranes with the blend ratios of 75/25 and 50/50.

Figure 7.2. SEM images of PMMA, PMMA/PAN (75/25), PMMA/PAN (50/50) membranes.

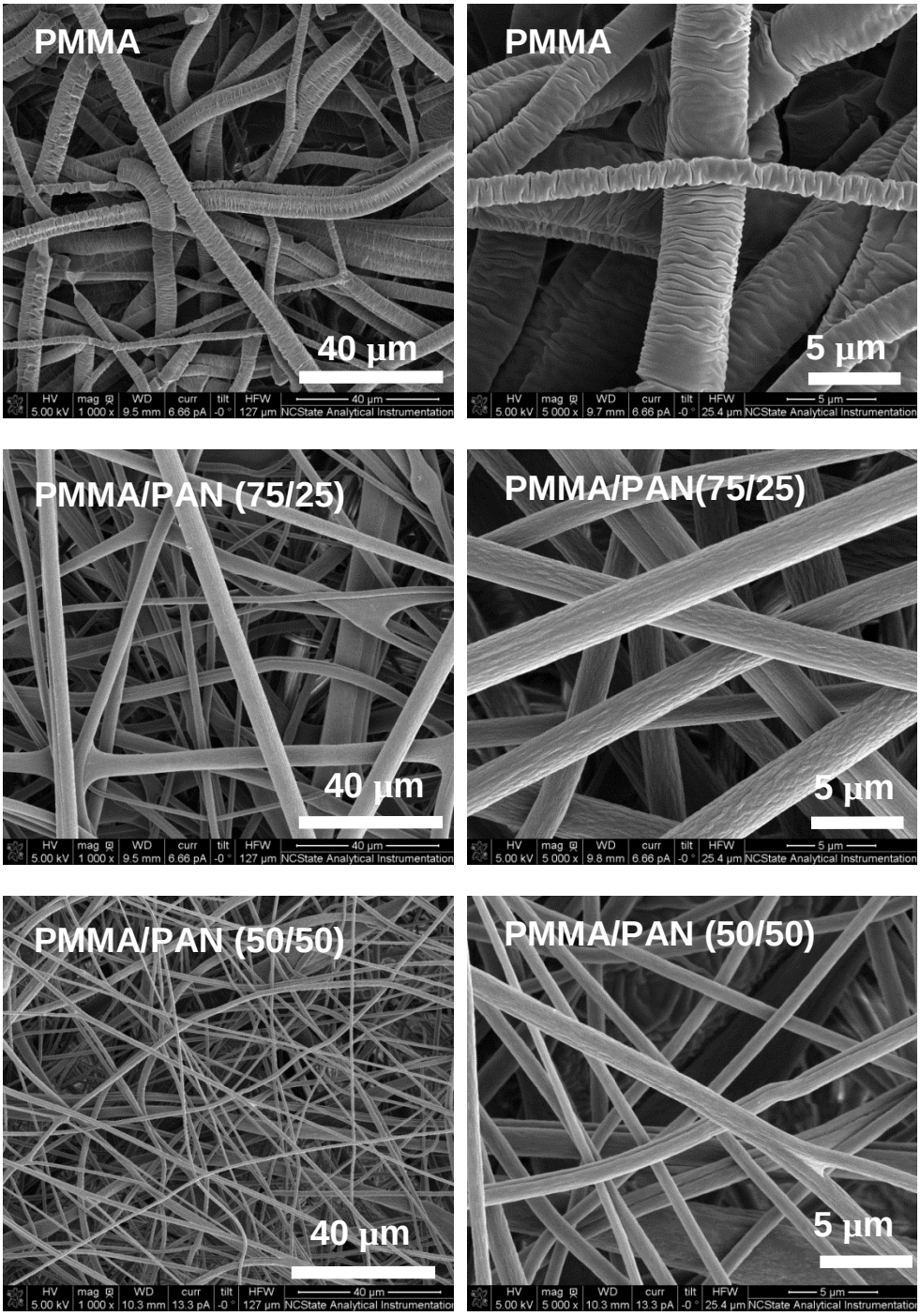

All three membranes have bead-free fibrous structure with a large number of pores. The average fiber diameters are 3.0, 1.8, and 0.7 μm, respectively, for PMMA, PMMA/PAN (75/25), and PMMA/PAN (50/50) membranes. With the introduction of PAN into PMMA membrane, the average fiber diameter decreases. The increase in the amount of low-molecular weight PAN leads to lower solution viscosity and less polymer chain entanglement during centrifugal spinning, which in turn causes reduced fiber diameter.

Table 7.1. Porosities and ionic conductivities of PMMA membrane, PMMA/PAN (75/25) membrane, PMMA/PAN (50:50) membrane, and microporous PP membrane at room temperature.

	Porosity (%)	**Ionic conductivity (mS/cm)**
PMMA membrane	57	2.8
PMMA/PAN (75/25) membrane	64	3.0
PMMA/PAN (50/50) membrane	73	3.2
Microporous PP membrane	41	0.8

It has been well established that high porosity is beneficial for membrane separators because it helps absorb large amount of liquid electrolyte and allows fast ion transportation between two electrodes [21]. Table 7.1 presents the porosities of PMMA, PMMA/PAN

(75/25), and PMMA/PAN (50/50) membranes. The porosity of microporous PP membrane (41%) is also shown for comparison. Centrifugally-spun PMMA and PMMA/PAN membranes have higher porosities than PP membrane due to their fibrous structure. The porosities of PMMA, PMMA/PAN (75/25) and PMMA/PAN (50:50) membranes are 57%, 64% and 73%, respectively. PMMA/PAN membranes present higher porosities compared to PMMA membrane owing to their lower average fiber diameters. From Table 1, it is also seen that the porosity increases with increasing PAN content, which may also be ascribed to the increasing average fiber diameter.

7.3.2 Ionic conductivity

Ionic conductivities of liquid electrolyte-soaked membranes influence cell resistance which in turn affects the cycling and C-rate performance of Li-ion batteries. Ionic conductivities of electrolyte-soaked PMMA and PMMA/PAN membranes are shown in Table 7.1. Ionic conductivities of electrolyte-soaked PMMA, PMMA/PAN (75/25) and PMMA/PAN (50/50) membranes are 2.8, 3.0 and 3.2 mS/cm, respectively. High ionic conductivities of electrolyte-soaked PMMA and PMMA/PAN membranes can be ascribed to highly porous structures of these membranes. In addition, with increase in PAN content, the ionic conductivity increases due to the increased membrane porosity, which allows higher electrolyte uptake.

7.3.3 Electrochemical oxidation limit

For practical battery applications, the electrochemical stability of the electrolyte-soaked separators must be within the operation voltage of the battery, which is typically between 1.5 V and 3.5 V vs. Li/Li^+. The electrochemical oxidation limits of liquid

electrolyte-soaked membranes can be evaluated by linear sweep voltammetry measurements. In these measurements, the rapid increase of the current can be observed when the electrolyte starts to decompose. Figure 7.3 demonstrates the electrochemical oxidation limits of PMMA, PMMA/PAN (75/25), PMMA/PAN (50/50), and microporous PP membranes.

Figure 7.3. Electrochemical oxidation limits of PMMA membrane, PMMA/PAN (75/25) membrane, PMMA/PAN (50/50) membrane, and microporous PP membrane.

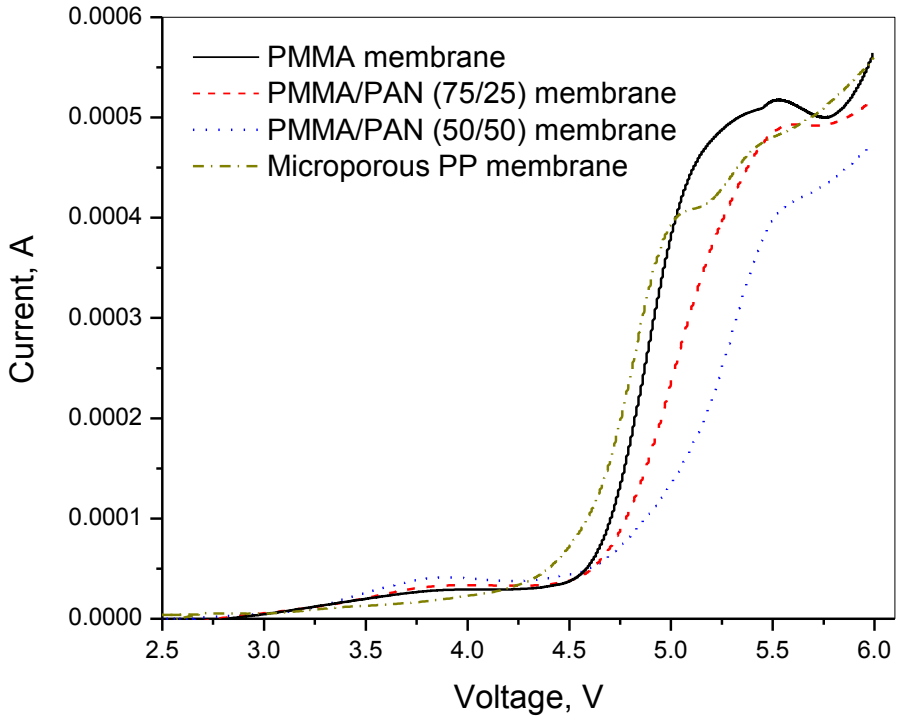

It is seen that PMMA and PMMA/PAN membranes exhibit the electrochemical oxidation limit of around 4.5 V while the electrochemical oxidation limit of the microporous PP membrane is 4.25 V. The electrochemical stability

window is affected by the interface between the electrolyte and the separator and it can be enhanced by improving affinity to the liquid electrolyte, increasing the specific surface area and decreasing the average fiber diameter of the electrolyte-soaked separators [21,23,24]. Hence, the improved electrochemical stability of PMMA and PMMA/PAN membranes could be attributed to the high affinity of PAN and PMMA to the liquid electrolyte. This result is also in agreement with earlier studies which reported that electrolyte-soaked PAN fibrous membranes had improved electrochemical stability due to the high affinity of these membranes to the liquid electrolyte [24,25].

7.3.4 Interfacial resistance

The electrochemical performance of Li-ion batteries is affected by the interfacial properties of electrolyte-soaked separators with Li metal [26]. The formation of stable solid electrolyte interface on the lithium metal helps not only conduct lithium ions freely but also prevents electrolyte decomposition [27]. The interfacial resistances between liquid electrolyte-soaked membranes and lithium metal were investigated by measuring electrochemical impedance spectra of Li/liquid electrolyte-soaked membrane/Li cells. Figure 7.4 shows the electrochemical impedance spectra of PMMA, PMMA/PAN and microporous PP membranes.

The diameters of semi-circles at the intermediate frequency region represent the interfacial resistances of liquid electrolyte-soaked membranes with Li metal. It is seen from Figure 7.4 that microporous PP membrane has an interfacial resistance of 400 ohm·cm^2. However, centrifugally-spun PMMA membrane exhibits a lower interfacial resistance compared to

microporous PP membrane, and the presence of PAN further decreases the interfacial resistance. The interfacial resistances are 300 ohm·cm^2, 280 ohm·cm^2, and 250 ohm·cm^2, respectively, for PMMA membrane, PMMA/PAN (75/25) membrane, and PMMA/PAN (50/50) membrane. Smaller average fiber diameters, higher porosities and good swelling abilities of PAN and PMMA are the main reasons for lower interfacial resistances of PMMA/PAN membranes. The high ionic conductivities, resulted from the highly porous fibrous structure, and the high affinity of PAN and PMMA to the liquid electrolyte also contribute to the lower interfacial resistances [23].

Figure 7.4. Electrochemical impedance spectra of PMMA membrane, PMMA/PAN (75/25) membrane, PMMA/PAN (50/50) membrane, and microporous PP membrane.

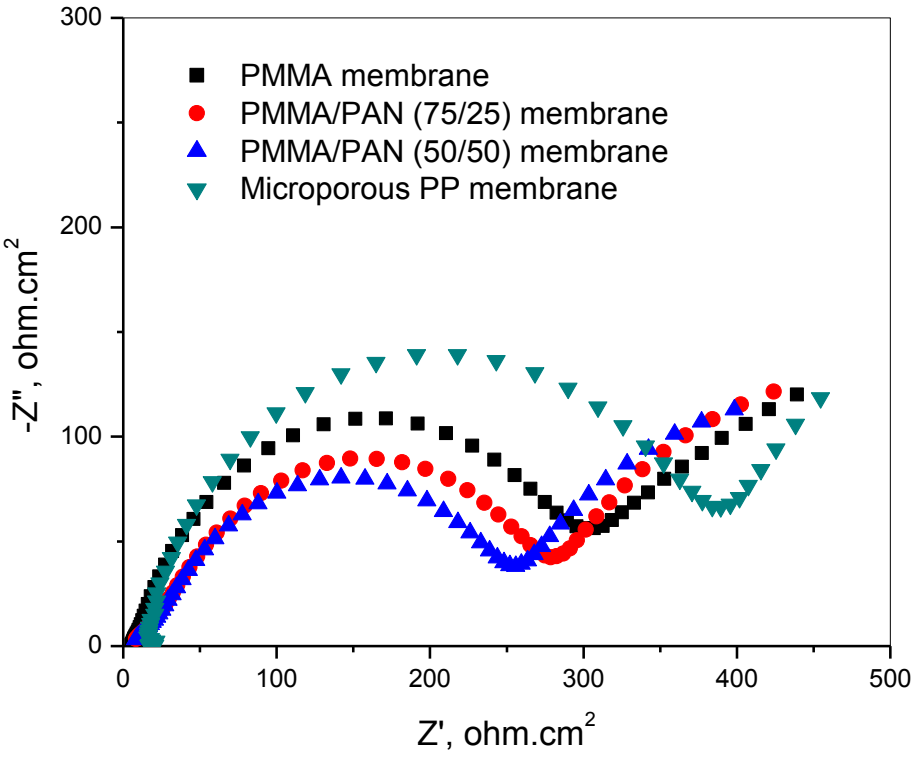

7.3.5 Cycling performance

In order to further examine the feasibility of using centrifugally-spun PMMA/PAN membranes as separators in rechargeable lithium-ion batteries, coin-type cells were fabricated with $LiFePO_4$ as the cathode and Li metal as the counter electrode. The first-cycle charge-discharge curves of $Li/LiFePO_4$ cells containing PMMA, PMMA/PAN and microporous PP membranes are shown in Figure 7.5.

Figure 7.5. First-cycle charge-discharge curves of $Li/LiFePO_4$ cells containing PMMA membrane, PMMA/PAN (75/25) membrane, PMMA/PAN (50/50) membrane, and microporous PP membrane at 0.2 C.

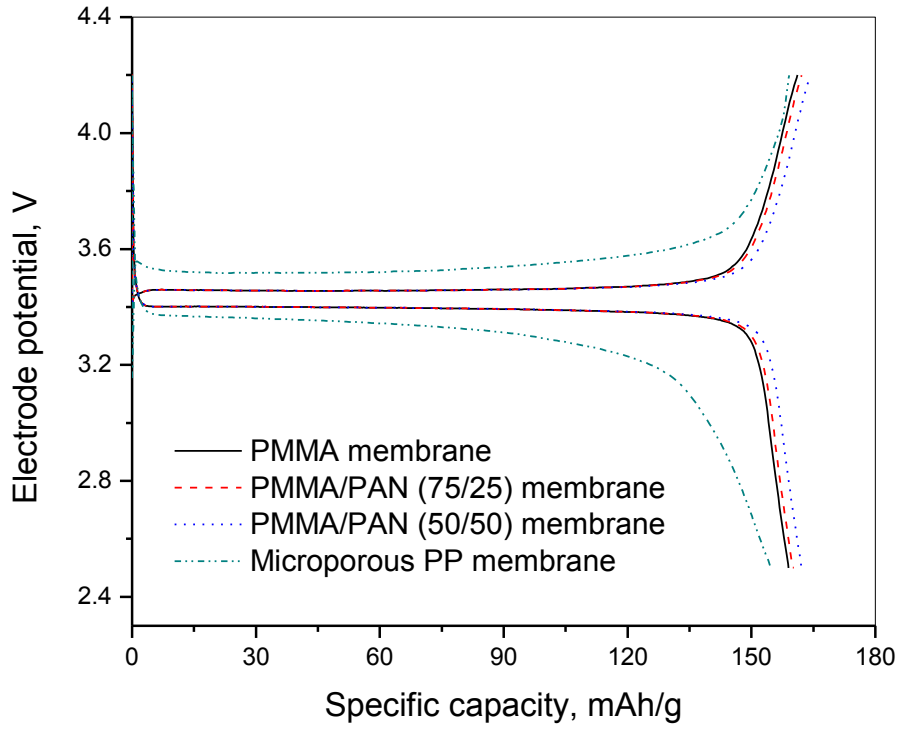

Figure 7.6. Cycling performance of Li/$LiFePO_4$ cells containing PMMA membrane, PMMA/PAN (75/25) membrane, PMMA/PAN (50/50) membrane, and microporous PP membrane at 0.2 C.

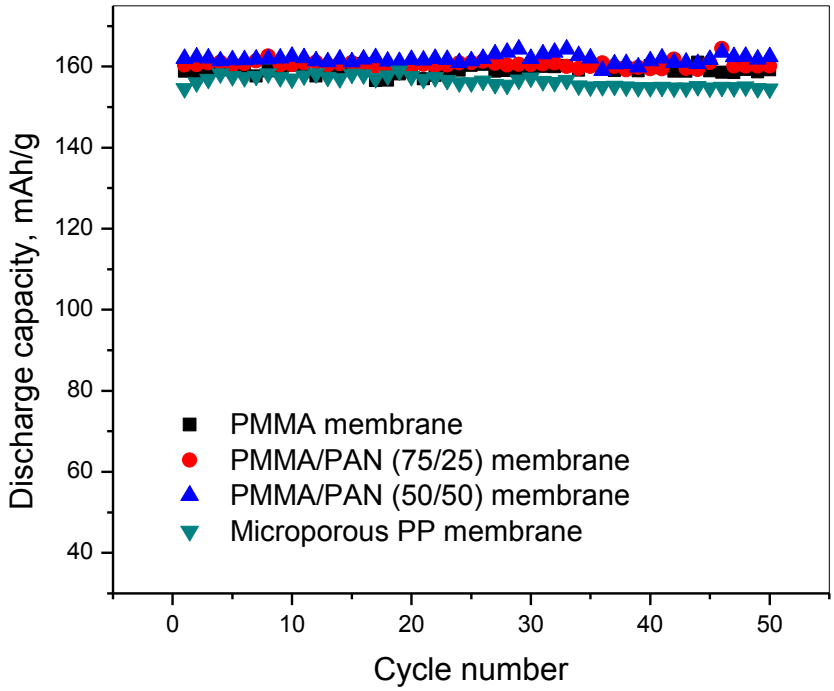

Separators do not directly participate in electrode reactions. However, it is known that the separator material and structure can influence the cell performance since separators affect the ion transportation between the electrodes, which is important in regulating the cell kinetics [6,8]. As shown in Figure 7.5, the discharge capacity of the cell using microporous PP membrane is 154 mAh/g. The discharge capacities of cells containing PMMA, PMMA/PAN (75/25) and PMMA/PAN (50/50) membranes are 159, 160 and 162 mAh/g, respectively. In addition, the highest discharge capacity is observed when PMMA/PAN

(50/50) membrane is used due to its highest ionic conductivity and lowest interfacial resistance, which are beneficial in enhancing the cell kinetics and help making the measured capacity to be closer to the theoretical value.

Figure 7.6 shows the cycling performance of Li/$LiFePO_4$ cells containing PMMA, PMMA/PAN and microporous PP membranes at 0.2 C. For all four cells, no apparent capacity loss is observed in 50 cycles at a low rate of 0.2 C.

7.3.6 C-rate performance

Figure 7.7. C-rate performance of Li/$LiFePO_4$ cells containing PMMA membrane, PMMA/PAN (75/25) membrane, PMMA/PAN (50/50) membrane, and microporous PP membrane.

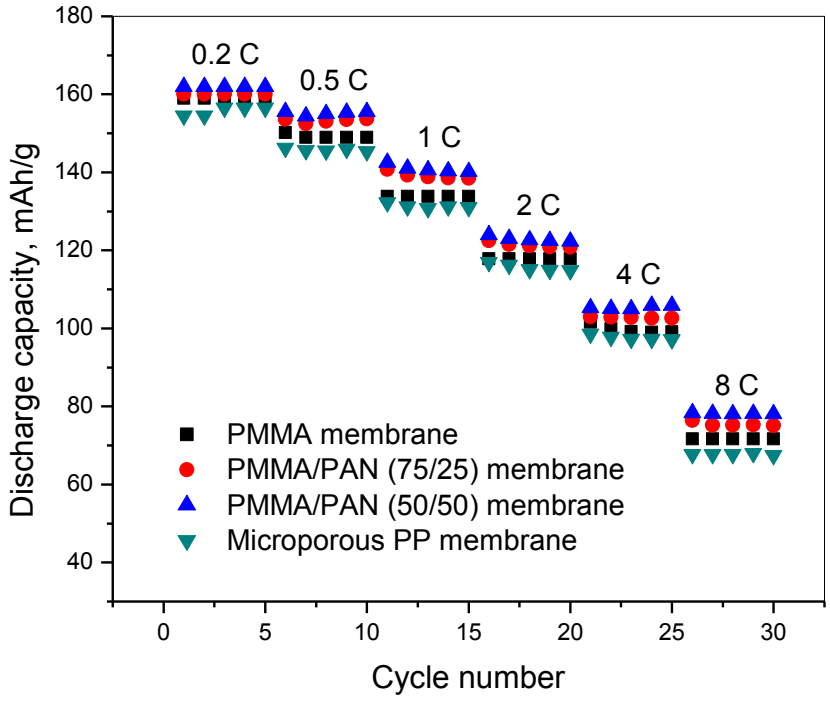

In order to evaluate the C-rate performance of $LiFePO_4$/Li cells containing PMMA and PMMA/PAN membranes, the cells were forced to charge and discharge at high rates and the results are presented in Figure 7.7. The cell containing microporous PP membrane is also shown and it has a relatively low discharge capacity of around 154 mAh/g at 0.2 C, which decreases to 67 mAh/g at 8 C.

The cells containing centrifugally-spun PMMA, PMMA/PAN (75/25) and PMMA/PAN (50/50) membranes have higher discharge capacities of 159, 160 and 162 mAh/g, respectively, at 0.2 C and they exhibit less capacity fading as the C-rate increases. For example, the capacities at 8 C are 71, 75 and 78 mAh/g, respectively, for the cells containing PMMA, PMMA/PAN (75/25) PMMA/PAN (50/50) membranes. It is known that the ionic conductivity and interfacial resistance of liquid electrolyte-soaked membrane separators affect C-rate performance [8,26,28-30]. The superior rate capabilities of the cells containing centrifugally-spun PMMA/PAN membranes could be resulted from higher ionic conductivities and better interfacial properties of these membranes after uptaking liquid electrolyte. These results confirm that centrifugally-spun PMMA/PAN membranes are promising separator candidate for rechargeable Li-ion batteries.

7.4. Conclusions

High-speed, low-cost centrifugal spinning technique was used to prepare fiber-based separator membranes for use as separators in Li-ion batteries. Porosity, ionic conductivity, electrochemical oxidation limit, interfacial resistance, cycling performance and C-rate performance were investigated and compared with a commercial microporous PP membrane. Centrifugally-spun PMMA/PAN membranes possessed higher ionic conductivity and lower

interfacial resistance than microporous PP membrane. Increasing the amount of PAN in PMMA/PAN membranes promoted their ionic conductivity after uptaking liquid electrolyte. Li/$LiFePO_4$ cells containing centrifugally-spun PMMA/PAN separators showed excellent cycling and C-rate performance. Therefore, centrifugally-spun PMMA/PAN membranes are demonstrated to be promising separator candidate for high-performance Li-ion batteries.

REFERENCES

[1] M. Yanilmaz, Y. Lu, M. Dirican, K. Fu, X. Zhang, Nanoparticle-on-Nanofiber Hybrid Membrane Separators for Lithium-ion Batteries via Combining Electrospraying and Electrospinning Techniques, Journal of Membrane Science, (2014).

[2] M. Dirican, M. Yanilmaz, K. Fu, Y. Lu, H. Kizil, X. Zhang, Carbon-enhanced electrodeposited SnO_2 carbon nanofiber composites as anode for lithium-ion batteries, Journal of Power Sources, (2014).

[3] Y. Li, G. Xu, Y. Yao, L. Xue, M. Yanilmaz, H. Lee, X. Zhang, Coaxial electrospun Si/C–C core–shell composite nanofibers as binder-free anodes for lithium-ion batteries, Solid State Ionics, 258 (2014) 67-73.

[4] K. Fu, Y. Lu, M. Dirican, C. Chen, M. Yanilmaz, Q. Shi, P.D. Bradford, X. Zhang, Chamber-Confined Silicon-Carbon Nanofiber Composites for Prolonged Cycling Life of Li-Ion Battery, Nanoscale, (2014).

[5] M. Dirican, M. Yanilmaz, K. Fu, O. Yildiz, H. Kizil, Y. Hu, X. Zhang, Carbon-Confined PVA-Derived Silicon/Silica/Carbon Nanofiber Composites as Anode for Lithium-Ion Batteries, journal of the Electrochemical Society, 161 (2014) A2197-A2203.

[6] H. Lee, M. Yanilmaz, O. Toprakci, K. Fu, X. Zhang, A review of recent developments in membrane separators for rechargeable lithium-ion batteries, Energy & Environmental Science, 7 (2014) 3857-3886.

[7] M. Yanilmaz, C. Chen, X. Zhang, Fabrication and characterization of SiO2/PVDF composite nanofiber-coated PP nonwoven separators for lithium-ion batteries, Journal of Polymer Science Part B: Polymer Physics, (2013).

[8] M. Yanilmaz, Y. Lu, Y. Li, X. Zhang, SiO< sub> 2</sub>/polyacrylonitrile membranes via centrifugal spinning as a separator for Li-ion batteries, Journal of Power Sources, 273 (2015) 1114-1119.

[9] M. Yanilmaz, F. Kalaoglu, H. Karakas, A.S. Sarac, Preparation and characterization of electrospun polyurethane–polypyrrole nanofibers and films, Journal of Applied Polymer Science, 125 (2012) 4100-4108.

[10] M. Yanilmaz, F. Kalaoglu, H. Karakas, Investigation on the Effect of Process Variables on Polyurethane Nanofibre Diameter Using a Factorial Design, FIBRES & TEXTILES IN EASTERN EUROPE, 21 (2013) 19-21.

[11] M. Yanilmaz, F. KALAOĞLU, H. KARAKAŞ, STUDY ON OPTIMISING THE MORPHOLOGY OF ELECTROSPUN POLYURETHANE NANOFIBERS, Journal of Textile & Apparel/Tekstil ve Konfeksiyon, 22 (2012).

[12] M. Yanilmaz, M. Dirican, X. Zhang, Evaluation of electrospun SiO2/nylon 6,6 nanofiber membranes as a thermally-stable separator for lithium-ion batteries, Electrochimica Acta, 133 (2014) 501-508.

[13] M. Yanilmaz, A.S. Sarac, A review: effect of conductive polymers on the conductivities of electrospun mats, Textile Research Journal, (2014) 0040517513495943.

[14] Y. Lu, K. Fu, S. Zhang, Y. Li, C. Chen, J. Zhu, M. Yanilmaz, M. Dirican, X. Zhang, Centrifugal spinning: A novel approach to fabricate porous carbon fibers as binder-free electrodes for electric double-layer capacitors, Journal of Power Sources, 273 (2015) 502-510.

[15] X. Zhang, Y. Lu, Centrifugal Spinning: An Alternative Approach to Fabricate Nanofibers at High Speed and Low Cost, Polymer Reviews, 54 (2014) 677-701.

[16] Y. Lu, Y. Li, S. Zhang, G. Xu, K. Fu, H. Lee, X. Zhang, Parameter study and characterization for polyacrylonitrile nanofibers fabricated via centrifugal spinning process, European Polymer Journal, 49 (2013) 3834-3845.

[17] S.S. Zhang, K. Xu, T.R. Jow, An inorganic composite membrane as the separator of Li-ion batteries, Journal of Power Sources, 140 (2005) 361-364.

[18] A.I. Gopalan, P. Santhosh, K.M. Manesh, J.H. Nho, S.H. Kim, C.-G. Hwang, K.-P. Lee, Development of electrospun PVdF–PAN membrane-based polymer electrolytes for lithium batteries, Journal of Membrane Science, 325 (2008) 683-690.

[19] X.H. Flora, M. Ulaganathan, R.S. Babu, S. Rajendran, Evaluation of lithium ion conduction in PAN/PMMA-based polymer blend electrolytes for Li-ion battery applications, Ionics, 18 (2012) 731-736.

[20] J.-Y. Sohn, J.-S. Im, J. Shin, Y.-C. Nho, PVDF-HFP/PMMA-coated PE separator for lithium ion battery, Journal of Solid State Electrochemistry, 16 (2012) 551-556.

[21] H. Li, C.-E. Lin, J.-L. Shi, X.-T. Ma, B.-K. Zhu, L.-P. Zhu, Preparation and characterization of safety PVDF/P (MMA-co-PEGMA) active separators by studying the liquid electrolyte distribution in this kind of membrane, Electrochimica Acta, 115 (2014) 317-325.

[22] A. Subramania, N. Sundaram, G.V. Kumar, Structural and electrochemical properties of micro-porous polymer blend electrolytes based on PVdF-< i> co</i>-HFP-PAN for Li-ion battery applications, Journal of Power Sources, 153 (2006) 177-182.

[23] T. Ma, Z. Cui, Y. Wu, S. Qin, H. Wang, F. Yan, N. Han, J. Li, Preparation of PVDF based blend microporous membranes for lithium ion batteries by thermally induced phase

separation: I. Effect of PMMA on the membrane formation process and the properties, Journal of Membrane Science, 444 (2013) 213-222.

[24] Y. Ding, P. Zhang, Z. Long, Y. Jiang, F. Xu, W. Di, The ionic conductivity and mechanical property of electrospun P (VdF-HFP)/PMMA membranes for lithium ion batteries, Journal of Membrane Science, 329 (2009) 56-59.

[25] C.K. Hong, K.S. Yang, S.H. Oh, J.H. Ahn, B.H. Cho, C. Nah, Effect of blend composition on the morphology development of electrospun fibres based on PAN/PMMA blends, Polymer International, 57 (2008) 1357-1362.

[26] H.-R. Jung, D.-H. Ju, W.-J. Lee, X. Zhang, R. Kotek, Electrospun hydrophilic fumed silica/polyacrylonitrile nanofiber-based composite electrolyte membranes, Electrochimica Acta, 54 (2009) 3630-3637.

[27] P. Raghavan, X. Zhao, C. Shin, D.-H. Baek, J.-W. Choi, J. Manuel, M.-Y. Heo, J.-H. Ahn, C. Nah, Preparation and electrochemical characterization of polymer electrolytes based on electrospun poly(vinylidene fluoride-co-hexafluoropropylene)/polyacrylonitrile blend/composite membranes for lithium batteries, Journal of Power Sources, 195 (2010) 6088-6094.

[28] S. Choi, J. Kim, S. Jo, W. Lee, Y.-R. Kim, Electrochemical and spectroscopic properties of electrospun PAN-based fibrous polymer electrolytes, journal of the Electrochemical Society, 152 (2005) A989-A995.

[29] M. Raja, N. Angulakshmi, S. Thomas, T.P. Kumar, A.M. Stephan, Thin, flexible and thermally stable ceramic membranes as separator for lithium-ion batteries, Journal of Membrane Science, 471 (2014) 103-109.

[30] N. Shubha, R. Prasanth, H.H. Hng, M. Srinivasan, Study on effect of poly (ethylene oxide) addition and in-situ porosity generation on poly (vinylidene fluoride)-glass ceramic composite membranes for lithium polymer batteries, Journal of Power Sources, 267 (2014) 48-57.

CHAPTER 8. SUMMARY AND CONCLUSIONS

This research focused on the fabrication and characterization of nanofiber-based membranes by electrospinning and centrifugal spinning of different polymers and nanoparticles. The major results and discussion of each chapter in this dissertation are summarized as follows.

(I) SiO_2/PVDF Composite Nanofiber-Coated PP Nonwoven Membranes as Separator for Lithium-Ion Batteries

SiO_2/PVDF nanofiber-coated PP nonwoven membranes were prepared by using electrospinning technique. The physical and electrochemical properties, such as porosity, mechanical strength, uptake capacity, lithium-ion conductivity, electrochemical oxidation limit, interfacial resistance and cycling performance were investigated.

Results showed these novel composite separators possessed good wettability, high ionic conductivity, sufficient electrochemical stability, low interfacial resistance and good cycling performance. Improved mechanical strengths, ionic conductivities, electrochemical stabilities and interfacial resistances were observed at high SiO_2 contents. The cells containing SiO_2/PVDF nanofiber-coated PP nonwoven separators with high SiO_2 contents also showed excellent cycling performance.

(II) Nanoparticle-on-Nanofiber Hybrid Membranes as Separator for Lithium-ion Batteries via Combining Electrospraying and Electrospinning Techniques

SiO_2/PVDF nanoparticle/nanofiber hybrid membranes were prepared by combining electrospraying and electrospinning techniques. Three-dimentional PVDF nanofibrous structure loaded with high amounts of SiO_2 nanoparticles on fiber surfaces was observed from SEM images. The physical and electrochemical properties, such as porosity, thermal

dimensional stability, electrolyte uptake capacity, ionic conductivity, electrochemical oxidation limit, interfacial resistance, cycling performance, and C-rate performance were investigated. Results show that these novel hybrid separators possessed better wettability, higher ionic conductivity, lower interfacial resistance and better cycling performance than both microporous PP membrane and pure PVDF nanofiber membrane. The cells containing SiO_2/PVDF hybrid separators with high SiO_2 contents also showed excellent cycling and C-rate performance.

(III) Electrospun SiO_2/Nylon 6,6 Nanofiber Membranes as Thermally-Stable Separator for Lithium-Ion Batteries

SiO_2/nylon 6,6 nanofiber membranes were prepared by using electrospinning technique for use as thermally-stable Li-ion battery separator with good mechanical strength. Highly-porous nanofibrous structure was observed from SEM images. Experimental results showed that electrospun SiO_2/nylon 6,6 nanofiber membranes had better wettability, higher ionic conductivity, lower interfacial resistance and better thermal stability than microporous PP membrane. These membranes also showed superior mechanical properties. The cells containing SiO_2/nylon 6,6 nanofiber membrane separators with high SiO_2 contents showed excellent cycling and C-rate performance.

(IV) SiO_2/Polyacrylonitrile Nanofiber Membranes via Centrifugal Spinning as Separator for Li-Ion Batteries

Centrifugally-spun SiO_2/PAN membranes were prepared and characterized for use as separator membranes in Li-ion batteries. Porosity, electrolyte uptake capacity, ionic conductivity, electrochemical oxidation limit, interfacial resistance, cycling performance, and C-rate performance were investigated and compared with a commercial microporous PP

membrane. SiO_2/PAN membranes possessed better wettability, higher ionic conductivity, lower interfacial resistance and better cycling performance than microporous PP membrane. The cells containing SiO_2/PAN separators with high SiO_2 contents also exhibited excellent cycling and C-rate performance.

(V) Polymethylmethacrylate/Polyacrylonitrile Blend Nanofiber Membranes via Centrifugal Spinning as Separator for Li-Ion Batteries

High-speed, low-cost centrifugal spinning technique was used to prepare fiber-based separator membranes for use as separators in Li-ion batteries. Centrifugally-spun PMMA/PAN membranes possessed higher ionic conductivity and lower interfacial resistance than microporous PP membrane. Increasing the amount of PAN in PMMA/PAN membranes promoted their ionic conductivity after uptaking liquid electrolyte. Li/$LiFePO_4$ cells containing centrifugally-spun PMMA/PAN separators showed excellent cycling and C-rate performance.

In summary, two different nanofiber production techniques, electrospinning and centrifugal spinning, and various polymers, PVDF, nylon 6,6, PAN, and PMMA, were employed to produce high-performance nanofiber membrane separators for lithium-ion batteries. In order to improve electrochemical properties, different approaches were utilized, including nanofiber-coating on nonwoven membranes, electrospraying of nanoparticles on nanofibers, fabrication of ceramic nanoparticle-incorporated nanofibers, and blending of different polymers. The physical and electrochemical properties of these nanofiber membrane separators are summarized in Table 8.1. It is seen that, all nanofiber membrane separators have large porosity and high electrolyte uptake, which lead to improved ionic conductivity and enhanced C-rate performance. In addition, the cells prepared with these

nanofiber membrane separators deliver higher capacity compared to the cells with PP membrane. Improved electrochemical performance of the separators was attributed to the enhanced morphology of the resultant nanofiber membrane separators and inorganic nanoparticle-containing composite structures.

Table 8.1 Physical and electrochemical properties of nanofiber membrane separators.

	Porosity (%)	**Electrolyte uptake (%)**	**Ionic conductivity (mS/cm)**	**Discharge capacities of Li/$LiFePO_4$ cells at 0.2C (mAh/g)**	**Discharge capacities of Li/$LiFePO_4$ cells at 8C (mAh/g)**
SiO_2/PVDF Composite Nanofiber-Coated PP Nonwoven Membrane	73	291	2.6	159	-
SiO_2/PVDF hybrid membrane	70	370	2.6	162	95
SiO_2/nylon 6,6 nanofiber membrane	77	360	3.8	161	78
Centrifugally-spun SiO_2/PAN nanofiber membrane	72	310	3.6	163	85
Centrifugally-spun PMMA/PAN blend nanofiber membrane	73	370	3.2	162	78
Microporous PP membrane	41	158	0.8	154	67

CHAPTER 9. RECOMMENDATION FOR FUTURE WORKS

The recommended future work includes but is not limited to:

(1) Preparation and characterization of nanofiber-based membranes using sol–gel method and centrifugal spinning as separator for Li-ion batteries

As demonstrated in Chapters 6 and 7, centrifugal spinning can be employed to produce nanofiber-based membranes. This technique has the benefits of fast production, low cost, high safety and good scalability. It is also well-known that introducing ceramic nanoparticles improves electrochemical performance of the separators. However, ceramic nanoparticles can easily aggregate and limit the performance. Moreover these pre-prepared nanoparticles change the solution properties including viscosity and electrical conductivity so that the content is limited when they are added directly into the polymer solutions. Hence, sol-gel technique could be used to obtain nanofiber membranes containing high amount of inorganic materials. This technique improves compatibility of inorganic materials with organic matrix by forming inorganic network in hybrid structures. When an organic polymer is mixed with a metal alkoxide, such as tetraethyl orthosilicate (TEOS, $Si(OCH_2CH_3)_4$), hydrolysis and polycondensation of TEOS occur and this technique allows us to fabricate organic-inorganic composite structures with high amount of inorganic particles. In order to obtain sol solution, TEOS, ethanol, hydrochloric acid and water can be mixed and be added to the polymer solution. As-prepared solution can then be directly used to produce nanofibers via centrifugal spinning. The resultant composite nanofiber membranes can potentially show improved thermal stability and electrochemical performance owing to high amount of inorganic particles in the structure.

(2) Preparation and characterization of centrifugally-spun PVDF nanofiber membranes as separator for advanced low-temperature Li-ion batteries.

Reduced performance of Li-ion cells at low temperatures is a serious problem for electric cars and many other applications. The reasons for the reduced performance at low temperatures are low electrolyte conductivity, sluggish kinetics of charge transfer, and increased resistance of solid electrolyte interphase. As demonstrated in Chapters 6 and 7, centrifugal spinning can be employed to produce highly porous nanofiber-based membranes. Centrifugally-spun nanofiber separators could improve cell kinetics because their highly porous structure can uptake more electrolyte and promote the cell kinetics at low temperatures. PVDF is one of the most studied polymers for separator applications owing to its high electrolyte uptake capacity. Centrifugal spinning technique could be employed to produce PVDF nanofiber membrane separators. Therefore, highly porous PVDF nanofiber separators could be prepared by using centrifugal spinning as separator for advanced low-temperature Li-ion batteries. In order to obtain centrifugally-spun PVDF membranes, PVDF solution can be prepared by dissolving the polymer in DMF. After centrifugal spinning process, SEM and porosity test can be performed for structure characterization. To evaluate the low-temperature performance of the resultant separators, liquid electrolyte uptake test, electrochemical impedance spectroscopy, linear sweep voltammetry and charge-discharge tests can be done at low temperatures.

(3) Preparation and characterization of electrospun nylon 6,6 nanofiber membranes containing different inorganic nanoparticles as thermally-stable separator for lithium-ion batteries.

Electrospinning technique can be used to produce nanofiber membranes with large porosity, and inorganic nanoparticles can also be employed to further improve their electrochemical performance. As demonstrated in Chapter 5, SiO_2/nylon 6,6 nanofiber membranes have superior thermal stability and mechanical strength with highly porous structure. Enhanced electrochemical properties are also obtained for these nanofiber membranes due to their high porosity values. Hence, different inorganic particles including SiO_2, Al_2O_3 and TiO_2 could be employed to investigate the effect of inorganic particles on the morphology and electrochemical properties. In order to obtain nylon 6,6 nanofiber membranes containing different inorganic nanoparticles, ceramic nanoparticle-containing nylon 6,6 solution can be prepared by dissolving the polymer in formic acid and adding different nanoparticles to this solution. After electrospinning process, SEM and porosity test can be performed for structure characterization of the separators. To evaluate the performance of the resultant separators, different electrochemical tests including liquid electrolyte uptake test, electrochemical impedance spectroscopy, linear sweep voltammetry and charge-discharge tests can be done.